Charles University in Prague

Faculty of Science

PhD program: Molecular and Cell biology, Genetics and Virology

Mgr. Bohumil Fafílek

Adjusting Wnt signaling

new regulatory mechanisms of the Wnt pathway

Dissertation Thesis

Supervisor: RNDr. Vladimír Kořínek, CSc.

Prague 2012

I declare I wrote this doctoral thesis by myself and all the informational sources and literature are properly cited. The thesis has not been submitted, either in whole or in part, for a degree at this or any other university.

Prague, October 31, 2012

Mgr. Bohumil Fafílek

Acknowledgement

I would like to thank all the people that made creation of this thesis possible. At the first place I thank my wife for her understanding for my work that frequently occupied my private life. I thank my children for their passion for weekend visits of the laboratory. I thank my parents for their distant support and my collaborators in the lab for their immediate support and valuable discussions. Lastly, my special thanks go to my supervisor Vladimír Kořínek.

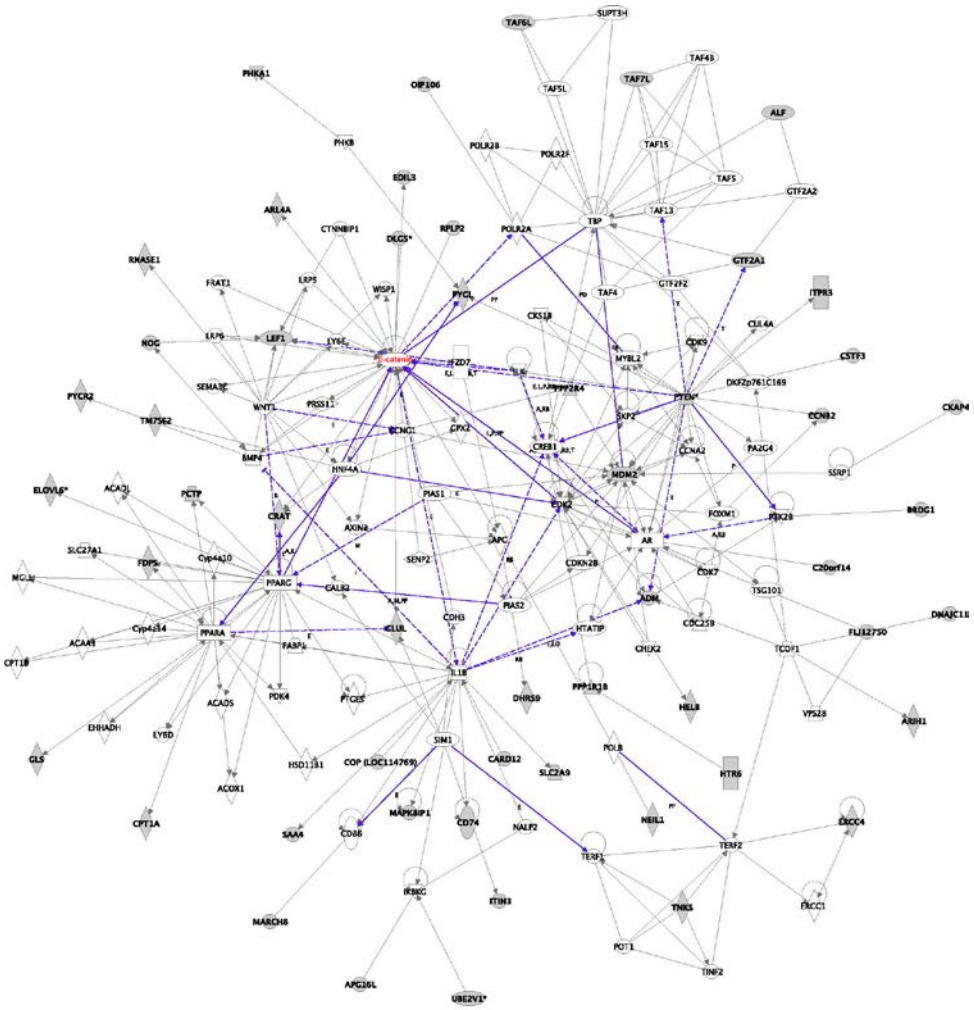

"All mankind is of one author, and is one volume; when one man dies, one chapter is not torn out of the book, but translated into a better language; and every chapter must be so translated...As therefore the bell that rings to a sermon, calls not upon the preacher only, but upon the congregation to come: so this bell calls us all: but how much more me, who am brought so near the door by this sickness....No man is an island, entire of itself...any man's death diminishes me, because I am involved in mankind; and therefore never send to know for whom the bell tolls; it tolls for thee."

John Donne

The picture depicts protein interactions within the cellular signaling network. β-catenin is highlighted in red. Adapted from reference[1].

Contents

List of abbreviations

aa	amino acid
AMER1	APC membrane recruitment protein 1
APC	Adenomatous Polyposis Coli
Ascl2	Achaete scute-like 2
Axin	Axis Inhibition protein
Bmi1	B lymphoma Mo-MLV insertion region 1
BTP/POZ	Broad-Complex, Tramtrack, Bric à brac/Pox virus and Zinc finger
β-TrCP	β-Transducin repeat-Containing Protein
CBC	Crypt Base Columnar cell, fast cycling $Lgr5^+$ intestinal stem cell
CBP	CREB binding protein
C/EBP	CCAAT-enhancer-binding protein
CRD	Cystein Rich Domain
CREB	cyclic adenosine monophosphate responsive element binding protein
CtBP	C-terminal Binding Protein
Dazap2	Deleted in Azoospermia Associated Protein 2
Dkk	Dickkopf
DNA	DeoxyriboNucleic Acid
Dvl	Dishevelled
EDAR	Ectodysplasin-A receptor
Evi	Evenness interrupted
Fer	Feline Encephalitis virus-Related kinase
Fz	Frizzled
GSK-3	Glycogen Synthase Kinase-3β
HIC1	Hypermethylated In Cancer 1
HIF1α	Hypoxia Induced Factor 1α
HIPK	Homeodomain-Interacting Protein Kinase
HMG	High Mobility Group
HSPGs	Heparan Sulphate Proteoglycans
int1	integration1
JNK	c-Jun N-terminal Kinase
Krm	Kremen
LDL	Low Density Lipoprotein
LEF	Lymphoid Enhancer-binding Factor
LGR	Leucine-rich repeat-containing G-protein coupled Receptor
LRP	Low density lipoprotein Related Protein
LTα	Lymphotoxin α
MMTV	Mouse Mammary Tumor Virus
Tert	telomerase reverse transcriptase
NES	Nuclear Export Signal
NgR1	Nogo-66 Receptor 1
NLS	Nuclear Localization Signal
PKA	Protein Kinase A
Porc	Porcupine
Postn	Periostin
PTK7	receptors of the tyrosine kinase-7
ROR	Receptor tyrosine kinase-like Orphan Receptor

Rspo	R-spondin
Ryk	related to tyrosine kinase
sFRP	secreted Frizzled Related Proteins
SOST	Sclerostin
Srt	Sprinter
TBP	TATA binding protein
TCF	T Cell-specific transcription Factor
TLE	Transducin Like Enhancer
TROY	Tumor necrosis factor Receptor family member ubiquitously expressed in the whOle embrYo
Wg	wingless
Wif	Wnt inhibitory factor
WISE	context-dependent activator and inhibitor of Wnt signaling protein
Wls	Wntless
WRE	Wnt responsive element

Preface

Human beings likewise living cells are in a close contact with their environment. They absorb signals which tell them whether they should change their behavior or location, whether they should work more or less, or whether it is a right time to produce offspring. In contrast to humans, however, cells perceive a signal from the surrounding environment by simple receptors, which can recognize mostly one specific signaling molecule. Nevertheless, cell response to any signal can be extremely variable, depending on the cell type, its inner state and on the additional incoming signals. This variability in cell response is caused by "batteries" of various proteins which are available at the moment of signal perception; the modulators and "fine-tuners" of the cellular signaling pathways.

This work is focused on protein components of one such signaling pathway, the Wnt signaling cascade. It includes four publications, each dealing with a different aspect of Wnt pathway adjustment:

Troy, a Tumor Necrosis Factor Receptor Family Member, Interacts with Lgr5 to Inhibit Wnt Signaling in Intestinal Stem Cells
Fafilek B, Krausova M, Vojtechova M, Tumova L, Pospichalova V, Sloncova E, Huranova M, Chmelikova J, Sedlacek R, Luksan O, Oliverius M, Voska L, Jirsa M, Paces J, Kolar M, Krivjanska M, Klimesova K, Tlaskalova-Hogenova H, Korinek V.
Gastroenterology 2012, accepted for publication

Fatty acid modification of Wnt1 and Wnt3a at serine is prerequisite for lipidation at cysteine and is essential for Wnt signalling.
Doubravska L, Krausova M, Gradl D, Vojtechova M, Tumova L, Lukas J, Valenta T, Pospichalova V, **Fafilek B**, Plachy J, Sebesta O, Korinek V.
Cell Signal. 2011 May;23(5):837-48. Epub 2011 Jan 16.

Generation of two modified mouse alleles of the Hic1 tumor suppressor gene.
Pospichalova V, Tureckova J, **Fafilek B**, Vojtechova M, Krausova M, Lukas J, Sloncova E, Takacova S, Divoky V, Leprince D, Plachy J, Korinek V.
Genesis. 2011 Mar;49(3):142-51. doi: 10.1002/dvg.20719.

Dazap2 modulates transcription driven by the Wnt effector TCF-4.
Lukas J, Mazna P, Valenta T, Doubravska L, Pospichalova V, Vojtechova M, **Fafilek B**, Ivanek R, Plachy J, Novak J, Korinek V.
Nucleic Acids Res. 2009 May;37(9):3007-20. Epub 2009 Mar 20.

Abstract

The Wnt pathway is one of the major signaling cascades contributing to multiple cellular processes during embryogenesis, and adult tissue homeostasis and regeneration. Moreover, aberrant activation of the Wnt signaling pathway is connected with development of neoplasia, notably colorectal cancer.

The aim of the thesis was to identify new ways of the Wnt pathway regulation to understand better physiological as well as non-physiological mechanisms of Wnt signaling. The results are summarized in four publications.

The first article deals with TROY, a member of tumor necrosis factor receptor family. We identified *TROY* as a Wnt target gene during our search for Wnt responsive genes in colorectal cancer cell lines. Additionally, we detected expression of *Troy* in tumors of two mouse models of intestinal cancer. In the healthy gut, Troy is produced in fast cycling intestinal stem cells where negatively regulates the Wnt pathway.

The second study focuses on processing and posttranslational modification of murine Wnt1 and Wnt3a. Wnts are glycosylated and double acetylated by lipid adducts and our results revealed that O-linked acylation of serine is required for the subsequent S-palmitoylation of cysteine. Moreover, acylation of Wnts is connected with their signaling activity which is related to Wnt1 and Wnt3a ability to associate with the extracellular matrix.

The third report describes the generation of conditional knock-out and citrine-reporter alleles of the gene Hic1, a tumor suppressor gene which was previously described in our laboratory as a negative regulator of the Wnt signaling pathway.

Finally, protein Dazap2 a small, evolutionary conserved, ubiquitously expressed gene was identified as an interacting partner of the TCF proteins. We detected Dazap2 modulates the affinity of TCF4 for its DNA recognition motif and thus enhance the expression of the Wnt signaling target genes.

Overview of the literature

The signaling pathway initiated by the extracellular ligands Wnts (wingless in *Drosophila*) is one of several evolutionarily-conserved signal transduction pathways found in all metazoan ranking from Hydra to humans[2-5]. Wnt signals control myriads of processes in animal development, tissue regeneration, stem cell maintenance, synaptic plasticity and neurotransmission[6, 7]. Additionally, aberrant Wnt signaling is linked to cancer initiation and progression[8, 9].

Studies in *Drosophila* and vertebrates have shown that Wnt signals are transduced in at least two distinct ways; first, a well-established 'canonical' or the Wnt/β-catenin pathway which eventually changes gene expression, and, secondly, β-catenin independent or noncanonical pathways which are known to affect cellular shape and motility and do not alter gene expression. Since all publications that are part of the thesis deal with a transcriptional regulation of Wnt signaling only the canonical Wnt/β-catenin branch will be discussed further.

Basic mechanisms of canonical Wnt signaling

The Wnt pathway is initiated by binding of Wnt proteins to the Frizzled (Fz)/low density lipoprotein (LDL) receptor-related protein (LRP) receptor complex at the cell surface. These receptors transduce the signal to protein complex which comprise several intracellular proteins, including Dishevelled (Dvl), glycogen synthase kinase-3β (GSK-3β), axis inhibition protein (Axin), Adenomatous Polyposis Coli (APC), and the key protein of the canonical Wnt pathway, β-catenin. The cellular level of β-catenin is in absence of Wnt signal kept low by continuous proteasome-mediated degradation. This process is controlled by the aforementioned protein complex and the E3 ubiquitin ligase β-transducin repeat-containing protein (β-TrCP; Figure 1). When cells receive Wnt signals, the degradation is inhibited, and, consequently, β-catenin accumulates in the cytoplasm and enters nucleus. Nuclear β-catenin interacts with transcription factors of the T cell-specific transcription factor/lymphoid enhancer-binding factor (TCF/LEF) family (hereafter referred to as TCFs), which are in unstimulated cells bound by Groucho transcription repressors, however in complex β-catenin activate transcription of Wnt signaling target genes.

The most notable Wnt target genes include: components of the Wnt pathway itself as *Axin2*[10-12], which provides a negative feedback control; cell cycle progression related genes as *c-Myc*[13]; and stem cell markers as leucine-rich repeat-containing G-protein coupled receptor (*Lgr*) *5*[14].

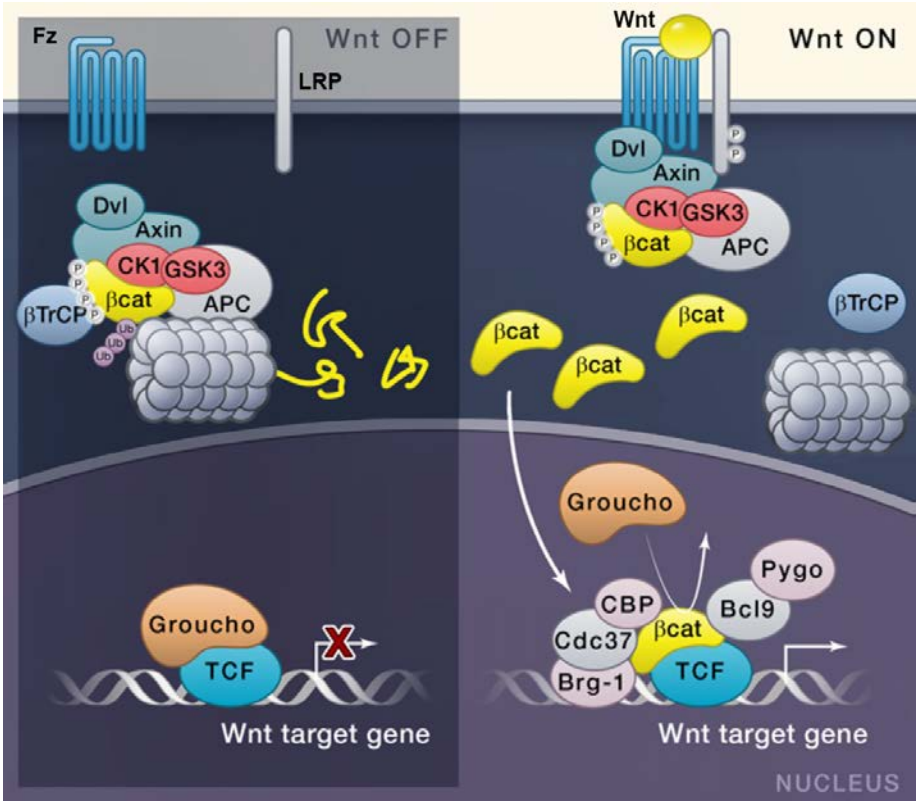

Figure 1: A simplified scheme of canonical Wnt signaling. In the absence of Wnt, the β-catenin destruction complex comprising scaffolding proteins Axin and APC, kinases CK1 and GSK3, and protein Dvl continuously binds, phosphorylates, and mediates ubiquitination of β-catenin by β-TrCP. The proteasome instantly recognizes and degrades such modified β-catenin. Wnt induces the association of the entire complex with phosphorylated LRP trough proteins Dvl and Axin, while β-TrCP dissociate. After binding to LRP, the destruction complex saturates with phosphorylated, but not ubiquitinated, β-catenin and newly synthesized β-catenin accumulates in the cytoplasm and enters the cell nucleus. In there, it displaces the Groucho transcriptional repressors from Wnt target gene regulatory elements occupied by TCF transcription factors, and recruits the transcriptional coactivators instead. Modified from the reference[7].

Extracellular and membrane components of the Wnt pathway

Wnt ligands

The word Wnt [wĭnt], which gave the name to the signaling pathway, is a compound of two words *wingless* and *integration1*. These original names were given by two independent research groups to the first discovered gene of the pathway encoding a ligand currently known as *Wnt1*. *Integration1* locus (*int1*) was reported to induce cancer of mouse mammary gland due to non-physiological overexpression caused by integration of mouse mammary tumor virus (MMTV) in proximity of the *int1* gene transcription start site[15]. Further studies revealed an intriguing similarity of *int1* to *Drosophila* segment polarity gene *wingless* (Wg), which was identified previously as a mutant allele leading to a loss of wing tissue[16].

Subsequent studies revealed another 18 members of the Wnt family in mammals and 6 others in *Drosophila*. Although the sequence homology of different Wnt ligands is rather low, all Wnts display conserved tertiary structure. All Wnts share homology in N-terminal signal sequence that targets them to the secretory pathway and, also, in high number of well-conserved cysteine residues that are thought to form disulphide bonds crucial for correct folding of the protein[17, 18].

The common feature of most of the Wnt proteins is the post-translational modification by N-glycosylations and lipid adducts[19-21]. These alteration make them highly hydrophobic and "sticky" to cell membranes and the extracellular matrix[22]. Acylation by palmitoyl and palmitoleoyl fatty acids is mediated by membrane-bound O-acyltransferase Porcupine (Porc)[23, 24], which is believed to be necessary for the Wnt secretion and signaling activity[25].

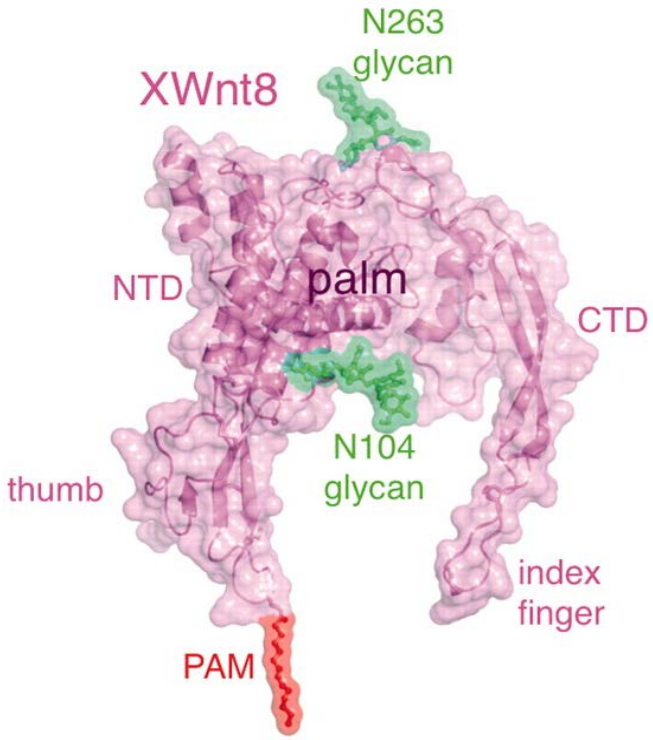

Figure 2: A crystal structure of *Xenopus* Wnt8 (XWnt8). An unusual two-domain Wnt structure, not obviously related to any known protein folds, resembles a "hand" with "thumb" and "index" finger extended to grasp receptor at two distinct binding sites. One site is dominated by the palmitoleic acid lipid group (PAM) at the tip of the Wnt's thumb, the second binding site, the conserved tip of Wnt's "index finger" forms hydrophobic amino acid contacts with a depression on the opposite side of the Fz cystein-rich domain. Glycosylations are depicted in green; NTD, N-terminal domain; CTD, C-terminal domain. Adapted from reference[26].

Function of the glycosylation in Wnt biology is not that clear. Whereas some studies found glycosylation to be dispensable for the secretion and activity of Wnts[27], others found that certain Wnts were no longer secreted upon mutation of their glycosylation sites[21, 28]. Another reports suggested that lipid modification is linked to Wnt N-glykosylation. One study proposed that palmitoylation mediated by Porc stimulated N-glycosylation of Wg[20], whereas another article presented contradictory result showing that N-glycosylation of Wnt3a is required for its palmitoylation[28]. Thus, a distinct relationship between these two Wnt posttranslational modifications has to be specified.

One of the best insights into the role of Wnt lipidation provided recent study revealing that palmitoleic acid lipid group of Xenopus Wnt8 fits into a deep hydrophobic groove of the Wnt receptor Fz8, thus confirming the necessity of fatty acid attachment for proper Wnt signaling (Figure 2)[26].

Although highly hydrophobic, Wnts may act at long distances. Wg is produced only by a thin line of cells in the wing imaginal disk of *Drosophila* but as a part of lipoprotein particles it spreads throughout the tissue. Consequently, expression of various genes can be triggered by Wnt,

depending on the local concentration of this morphogen[29, 30]. However, this long range signaling is rather rare. More evidence implies Wnts as short-range signaling molecules acting predominantly between cells that are close to each other[31-34].

For secretion of most of the Wnt ligands, a protein Wntless (Wls, also known as Evenness interrupted [Evi] or Sprinter [Srt]) is required[35-40]. Wls is located in all compartments of the exo/endocytic pathway – the endoplasmatic reticulum, Golgi network, endosomes and the plasma membrane – and directs Wnts through it to the cell exterior. After the Wnt release, Wls is recycled back to the trans-Golgi by a retromer complex[25, 41, 42].

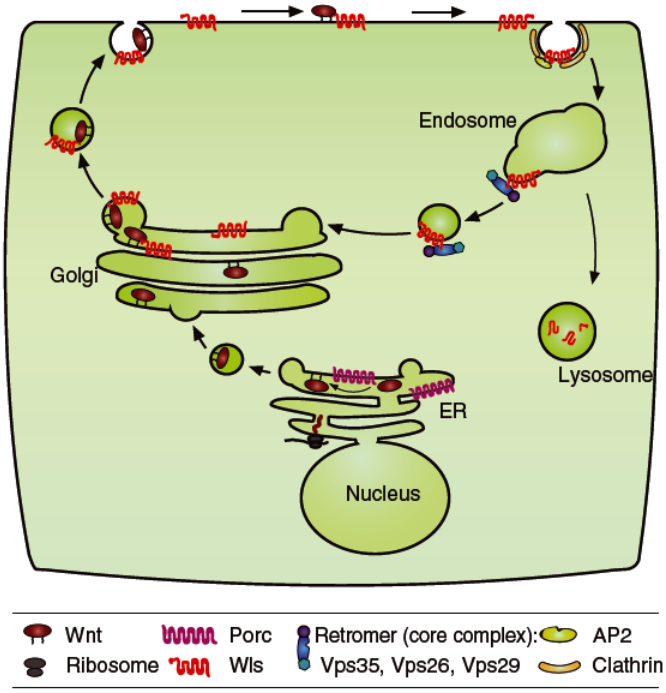

Figure 3: Proteins involved in an uneasy journey of the Wnt ligands out of the cell. In the endoplasmatic reticulum, Wnts are lipid modified by the acetyltransferase Porc. Lipid bound Wnts are transported to the Golgi complex, where they encounter Wls. Wls supports transport of Wnts from the trans-Golgi network to the plasma membrane, where Wnt is released to initiate autocrine or paracrine signaling. Free Wls is taken up by the clathrin-mediated endocytosis, and with assistance of retromer complex it undergoes retrograde trafficking back to the trans-Golgi network. Adapted from reference[17].

All these steps of the Wnt processing in fact govern and modulate the level of the Wnt ligands activity and thus the signaling output. Moreover, binding of Wnts to various extracellular proteins further extends the complexity of the regulation. Secreted Wnts can interact with heparan sulphate proteoglycans (HSPGs)[43] and periostin (Postn)[44] to increase their signaling activity. On the other hand, secreted Frizzled related proteins (sFRPs)[45, 46] and Wnt inhibitory factors (Wifs)[47, 48] restrain Wnts and so diminish their activating function. Additionally, recently identified transmembrane protease Tiki1 cleaved eight amino-terminal residues of a Wnt proteins, resulting in oxidized Wnt oligomers with reduced receptor-binding capacity[49].

Wnt receptors

Fz/LRP heteroreceptor

To initiate canonical Wnt signaling, Wnt proteins bind a heterodimeric receptor complex, consisting of the Fz and an LRP5/6 protein[50, 51]. Ten mammalian Fz proteins share structural homology of seven-transmembrane receptors related to G-protein coupled receptors family[52]. Fzs contain large extracellular N-terminal cysteine-rich domains (CRD)[53] that provide a primary platform for Wnt binding[26, 54]. Unlike Fz, which can also function as an inducer of the non-canonical Wnt pathways, LRP (arrow in *Drosophila*) proteins appear to be specifically required for Wnt/β-catenin signaling[55, 56]. LRPs consist of a large extracellular domain (~1400 aa), single pass transmembrane domain and small (~200 aa) proline-serine rich intracellular part, which is essential for the Wnt pathway activation (see below)[57, 58].

The Wnt-Fz interaction is not selective, thus a single Wnt can bind multiple Fz proteins and *vice versa*[26, 53]. Moreover, LRP6 coreceptor can also distinguish between different classes of Wnt proteins and thus enhance or reduce the signaling input[59].

Binding of Wnt to its dimeric receptors induces a conformational change of the receptors leading to phosphorylation of the LRP tail by kinases, GSK3-β and CK1γ[58, 60], which halts the process of β-catenin degradation by restraining Axin to the cytoplasmic tail of LRP[61]. Subsequently, GSK3-β phosphorylates serine in the PPPSP motif found in LRPs[62]. CK1γ, which is anchored in the membrane by its palmitoylated C terminus, rapidly phosphorylates LRPs on residues in close proximity to the PPPSP motif[63].

Important protein relying the signal from the Fz receptor, yet with not completely understood function, is Dvl. Dvl is possibly not a permanent component of the Fz/LRP receptor complex but it associates with the Wnt receptors after Wnt binding[64-66] and through the interaction with both Axin and Fz, it may facilitate binding of Axin to LRP[67-69].

The action of the Wnt ligands can be also regulated on the surface of the signal receiving cell. Inhibitory proteins of the Dickkopf (Dkk) and WISE/SOST families induce disruption of the Fz/LRP complex formation thus interfere the Wnt signaling[70-73].

Additional Wnt-related receptors and ligands

Fzs/LRPs are not the only receptors for the Wnt ligands. Also, receptor tyrosine kinase-like orphan receptor (ROR) proteins can recognize Wnts but the outcome of their signaling is rather ambiguous. According to the cellular context, they can either activate or repress transcription of the Wnt target genes, or simply sequester Wnt ligands and thus modulate Wnt signaling[74]. Other Wnt receptors, protein tyrosine kinase-7 (PTK7)[75] and related to tyrosine kinase (Ryk)[76], activate only

non-canonical pathways which might in turn interfere with canonical Wnt signaling[75]. An alternative ligand for the Fz4/LRP5 receptor complex is a cysteine-knot protein Norrin which activates Wnt/β-catenin signaling[77] essential for retina vascularization[78-81].

Finally, a family of small secreted proteins defined by two N-terminal furin domains and a thrombospondin domain, R-spondin (Rspo) proteins, was found to promote the canonical Wnt pathway both *in vivo*[82, 83] and *in vitro*[84]. Expression of *Rspos* overlaps with expression of *Wnt* proteins during mouse development[85-88] and knock-out studies suggested their importance in Wnt-dependent developmental processes[88-90]. Rspo proteins do not have capacity to activate Wnt signaling by themselves, they rather enhance the signal at low-dose of Wnt[91]. Rspos signal through the LGR receptors (LGR4-6), a small family of seven-pass transmembrane receptors, related to the G-protein-coupled receptors, which physically reside within Fz/LRP receptor complexes[91-93]. Although, exact mechanism of signal transduction from these receptors is not known, current evidence indicates that they do not utilize G proteins[91, 92]. Out of the three Rspo receptors, *Lgr4* could be regarded as a major one as it is expressed in many tissues and its ablation leads to the most severe phenotype[94-97]. On the other hand, *Lgr5* and *Lgr6* expression seem to be more interesting since their expression is restricted to adult stem cells. Whereas Lgr5 marks the stem cells in a number of actively self-renewing organs, including the intestinal tract and the hair follicle[98-100], Lgr6 is expressed in rare primitive stem cells that generates all lineages of the skin[101].

Cytoplasmic and nuclear components of the Wnt pathway

The β-catenin destruction complex

As β-catenin is the key molecule in canonical Wnt signaling, then the destruction complex regulating its stability is the key-holder protecting the cell from uncontrolled β-catenin/TCF signaling. Mutations impairing the function of the β-catenin destruction complex result in cancer, most notably of the colon[102-106].

A backbone of the complex is constituted by the tumor suppressor protein Axin which binds β-catenin, other tumor suppressor proteins APC and APC membrane recruitment protein 1 (AMER1), and two constitutively active serine-threonine kinases CK1α/δ and GSK3α/β[107-112].

Second major component is APC, a large multidomain protein which participates in stabilization of the destruction complex by bringing PP1 and PP2A, phosphatases participating in the regulation of the Axin1 and β-catenin stability[113, 114]. Apart from being involved in degradation of β-catenin, APC promotes export of β-catenin from the nucleus[115] and acts as a chromatin-associated suppressor of β-catenin-activated genes[116]. In addition, APC is essential for many other

cellular processes including intercellular adhesion[117], cytoskeleton stabilization[118], cell cycle regulation[119], apoptosis[120] and DNA repair[121].

Another tumor suppressor protein involved in the function of the destruction complex is AMER1[111]. Exact mechanism of its function is not known but it was suggested that Amer1 directly interacts with the armadillo repeats of β-catenin and assembles the β-catenin destruction complex at the plasma membrane. By recruiting β-catenin, APC and Axin, Amer1 links the complex with phosphorylated LRP trough binding APC[122].

The primary function of the complex, i.e. targeting β-catenin for degradation, is executed by two kinases, CK1 and GSK3-β. These enzymes sequentially phosphorylate Axin-bound β-catenin at a series of regularly spaced N-terminal Ser/Thr residues. Such prosphorylated β-catenin is then recognized by the F box/WD repeat protein β-TrCP, an essential component of the E3 ubiquitin ligase complex, and marked by ubiquitin. As consequence, ubiquitinated β-catenin is targeted for rapid destruction by the proteasome, thus preventing activation of TCF/β-catenin target genes in the nucleus[123]. Upon receptor activation by Wnt ligands, Axin is recruited to the phosphorylated tail of LRP. Recent data show that, through this relocalization, β-TrCP dissociates from the degradation complex, which leads to accumulation of phosphorylated, but not ubiquitinated, β-catenin. Subsequently, the complex becomes saturated by such modified β-catenin and newly synthesized β-catenin then accumulates and translocates to the nucleus to activate target genes of the pathway[124].

β-catenin

β-catenin (armadillo in *Drosophila*) is a crucial protein of canonical Wnt signaling. Apart from that, it also contributes to cell adhesion by linking E-cadherins to cytoskeletal structures[125]. β-catenin is able to perform both tasks largely due to its central region comprising 12 imperfect Armadillo repeats (Figure 4). The repeats form a superhelix featuring a long positively charged groove that provides a binding region for three most important interactors: E-cadherin (the main partner in adherent junctions), APC (the main partner in the destruction complex), and TCF/LEF

Figure 4: Crystal structure of β-catenin armadillo repeats interacting with N-terminal part TCF3 protein. Adopted from reference[126].

(the main partner in the nucleus)[126-130]. Various cellular roles of β-catenin and its processing are summarized in Figure 5.

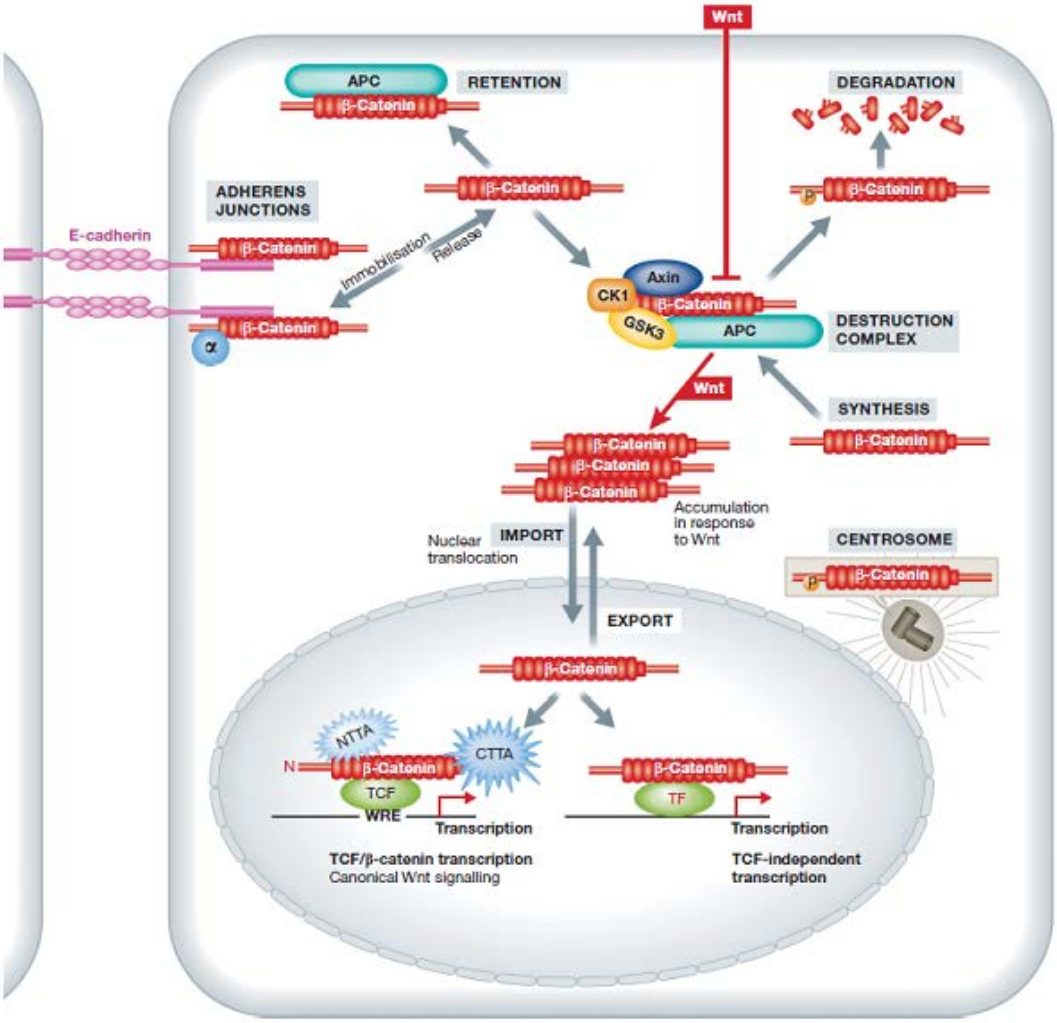

Figure 5: Lifecycle of β-catenin. Newly synthesized β-catenin is either immediately immobilized by E-cadherin to form adherens junctions or phosphorylated by the destruction complex and thus marked for subsequent degradation. Phosphorylation by protein kinases or downregulation of the E-cadherin levels results in release of β-catenin from the adherens junctions; this free pool of β-catenin can be kept in the cytoplasm protected by APC. Wnt signaling blocks the activity of the destruction complex which leads to increasement of cytoplasmic β-catenin and its translocation to the nucleus. In the nucleus, β-catenin binds TCF/LEF transcription factors and drives transcription of Wnt/β-catenin target genes. Other factors can also provide β-catenin with DNA binding domains, often counteracting canonical Wnt signaling. The activity of β-catenin in the nucleus can be regulated by posttranslational modifications or by modulation of its nuclear import/export. β-catenin may also play an important function in the centrosome. CTTA, C-Terminal Transcriptional Activators, NTTA, N-Terminal Transcriptional Activators. Adapted from reference[131].

Although β-catenin has only one binding site for all its interacting partners, its adhesive and signaling properties seem to be independent[132]. This notion is further supported by finding that close relative of β-catenin, γ-catenin (plakoglobin), may in certain cases compensate for the loss of the β-catenin structural function but not for its signaling role[133, 134]. Moreover, in *C. elegans*, the

adhesive and signaling functions of β-catenin are performed by two different β-catenin homologs[135].

Surprisingly, not all β-catenin phosphorylated by GSK3 undergoes degradation. A fraction of N-terminally phosphorylated β-catenin was detected in centrosomes, where it contributes to centrosomal cohesion and separation at the beginning of mitotic spindle formation[136]. APC and Axin were found to be an important regulator of centrosomes too, suggesting a new role for these components of the β-catenin destruction complex in centrosomal maintenance and separation[137].

Phosphorylation of β-catenin at multiple sites governs the balance between its structural and signaling functions. Phosphorylation at Y142 by Src-like kinase Fyn, feline encephalitis virus-related kinase (Fer), or the receptor tyrosine kinase c-Met significantly reduces α-catenin binding and thus impairs the adhesive function of β-catenin[138-140]. A similar effect is achieved upon Y654 phosphorylation by receptor tyrosine kinases (e.g. EGFR) or c-src kinase, which dramatically reduces the binding to cadherin thus enhances β-catenin-driven transcription[141-143]. Additionally, phosphorylation on Y654 evokes a conformational change which promotes further phosphorylation by protein kinase A (PKA) on S675 which strongly potentiates the signaling activity of β-catenin by increased recruitment of transcriptional co-activators such as CREB binding protein (CBP) or TATA binding protein (TBP)[142, 144].

Additional phosphorylation, mediated by JNK2 and promoted by the small GTPase Rac1, was found to be important for β-catenin nuclear accumulation[145], however the exact function of this phosphorylation, less so the mechanism of β-catenin nuclear entry, was not revealed yet[115, 146]. The classical nuclear import mediated by the importin-karyopterin complex is probably not utilized because polypeptide sequence of β-catenin contains no obvious nuclear localization or nuclear export signal (NLS or NES, respectively)[147]. Instead, β-catenin can directly interact with nuclear pore complex proteins, or other proteins like FoxM1, which may assist its entry to the nucleus[148-151].

The C terminus of β-catenin acts as a transcriptional activation domain which binds histone modifiers such as CBP/p300 and Brg-1, and mediators of RNA polymerase II interaction Parafibromin/Hyrax/Cdc73[146, 152, 153]. Furthermore, CBP can acetylate β-catenin at K49 and p300 at K345. Point mutations that block K49 acetylation are often found in various cancers and result in ectopic transcriptional activation of the gene *c-Myc*, an effect that seems to be specific to this Wnt signaling target gene, since other known target genes remains unaffected[154]. In contrast, modification of K345 by p300 has a broader effect and increases the affinity of β-catenin for TCFs; β-catenin acetylated at K345 was found strongly enriched in colon cancer cells with hyperactivated Wnt/β-catenin transcription[155]. Since β-catenin does not possess a DNA binding domain it needs DNA binding partners to bring it to the promoters of its target genes[127, 156]. TCF/LEF transcription factors serve as the main nuclear partners of β-catenin guiding it to specific DNA loci. However, additional DNA binding proteins like hypoxia induced factor (HIF) 1α[157], androgen receptor[158, 159] and forkhead transcription factor FOXO[160] were reported to interact with and sequester β-catenin at

the expense of TCF transcription factors. However, in terms of canonical Wnt signaling, TCFs are responsible for the vast majority of Wnt/β-catenin signaling outputs.

TCF/LEF transcription factors – nuclear partners of β-catenin

Transcription factors of TCF/LEF family are encoded by a single *TCF* gene in *D. melanogaster* and *C. elegans* and four *TCF* genes in mammals[161]. In mammals, *TCF7* produces TCF1 protein, LEF1 is produced from the *LEF1* gene, and TCF3 and TCF4 are encoded by TCF7 like 1 (*TCF7L1*) and TCF7 like 2 (*TCF7L2*) genes, respectively.

The N-terminal part of TCFs (aa 1-50) is highly similar between orthologs and binds β-catenin[126]. The second part of the proteins contains NLS and remarkably conserved high mobility group (HMG) box which recognizes a specific motif (CCTTTGAT(G/C) in the minor groove of target DNA, called Wnt responsive element (WRE)[152, 162]. The C-terminal part is, especially in vertebrates, often alternatively spliced, thus producing numerous variants with different DNA binding affinity and specificity[161, 163, 164]. For example, such splicing can generate a TCF variant containing a cysteine-rich domain known as the C-clamp, which can bind to so-called helper sequences and thus enhance the association of TCFs with target sequences[165, 166]. Moreover, usage of alternative promoters and multiple splicing variants affecting the entire transcript has been documented for each *TCF*, which further increase the Wnt signaling pathway complexity[167-169].

Although the highly conserved HMG box makes all TCFs recognize an identical DNA motif, function of individual TCF proteins seems to be distinct. Whereas Tcf3 seems to act preferentially as a transcriptional repressor[170], Lef1, together with β-catenin, behaves more like an activator. Tcf4 and Tcf1 fulfill both modes of action (i.e. transcriptional activation or repression) depending on the spatial and temporal context of their binding site in corresponding promoter[163, 171]. But still, there is some redundancy among TCFs. Knocking out *Tcf1*, for example, impairs thymocyte differentiation[172] and loss of *Lef1* results in postnatal mortality with no obvious defects in lymphoid cell populations at birth[173]. However, a combined *Lef1/Tcf1* double null mice exhibit defects in paraxial mesoderm leading to the formation of additional neural tubes[174]. Moreover, these phenotypes were identical to those reported for *Wnt3a*-deficient mice thus confirming role of TCFs in Wnt signaling. Further evidence for involvement of TCF/β-catenin in the Wnt pathway was presented in mice harboring synthetic TCF-specific transcriptional reporters. The activity of the reporters correlated with those of β-catenin, which was determined by loss- and gain-of-function mutations in the gene for β-catenin[134, 175, 176].

Without β-catenin, TCFs act as transcriptional repressors by forming a complex with Groucho/Transducin Like Enhancer (TLE) repressors[177, 178]. The binding of β-catenin physically displaces Groucho/TLE and converts TCFs into transcriptional activators, translating the Wnt signal into transcription of specific target genes[177, 179].

The TCF/β-catenin interaction can be modulated by phosphorylation, acetylation, sumoylation, and ubiquitination-mediated degradation to enhance, repress, or switch off β-catenin-mediated transcription[180-182]. TCF phosphorylation mediated by homeodomain-interacting protein kinases (HIPKs) has both positive and negative effects depending on the cell context[183-185]. Traf2 and Nck-Interacting Kinase (TNIK) protein kinase was found as direct interaction partners of both TCF4 and β-catenin, positively affecting TCF/β-catenin-mediated transcription in mammalian cells; the association seems to be especially important for intestinal progenitor development[186]. Additionally, SUMO E3 ligase PIASy has been shown to modify different TCFs with various consequences on TCF/β-catenin signaling output: whereas sumoylation of Lef1 leads to its immobilization in nuclear bodies where it cannot interact with β-catenin[187], sumoylation of TCF4 enhances β-catenin binding and thus increases TCF/β-catenin mediated transcription[188, 189].

Binding of β-catenin to TCFs can be also restricted by additional proteins, such as inhibitor of β-catenin and TCF (ICAT) and hypermethylated in cancer 1 (HIC1). While ICAT interacts with the central armadillo repeat of β-catenin, thereby blocking the access to TCFs[190], HIC1 attenuates Wnt signaling by restraining TCF/β-catenin from its target sequences[191].

Two other coactivators of the TCF/β-catenin complex, Bcl9/Legless and Pygopus bind unusually the N-terminus of β-catenin[192-194]. However, these proteins seem to be crucial for Wnt signaling only in *Drosophila*, since their ablation in mice results in no severe phenotype[195, 196].

Although β-catenin has been mainly described as an activator of gene transcription, it is becoming increasingly clear that it can also repress transcription of some Wnt target genes. A direct repression has been reported for *E-cadherin* in keratinocytes or $p16^{INK4a}$ in melanomas[197, 198]. Another example of β-catenin-mediated transcriptional repression was shown in *Drosophila* cells, where dTCF/β-catenin-mediated repression was surprisingly related to WREs dramatically different from the TCF consensus, suggesting existence of alternative TCF-repressive DNA motifs[199].

Wnt/β-catenin target genes

Wnt/β-catenin signaling regulates expression of genes involved in proliferation, fate specification, differentiation during various developmental stages and in adult tissue homeostasis. Interestingly, Wnt signaling also regulates the expression of many genes encoding the components of the pathway itself. Induction of negative regulators *Axin2*, *DKK1*, and *Naked* (a Dvl antagonist) and suppression of *Fz* and *LRP6* constitute negative feedback loops that attenuate Wnt signaling[6, 180]. On contrary, Wnt induction of *Rspo* and *TCF* genes constitutes positive feed forward circuits that reinforce Wnt signaling, a feature that has been misused during colon carcinogenesis[161, 182].

These Wnt pathway self-regulatory loops are mostly utilized in a cell-specific manner, bringing additional complexity in controlling amplitude and duration of the Wnt response. Nevertheless, the *Axin2* and *Drosophila Naked* genes seem to represent a few universal Wnt/Wg-induced target genes[6, 10]. Among other Wnt target genes, *c-MYC* deserves being highlighted since it is critical for intestinal homeostasis and transformation[13, 200]. *c-Myc* encodes a "promiscuous" transcription factor that is believed to bind promoters and regulate expression of up to 15% of the human genes[201, 202]. c-Myc importance for conversion of intestinal tissue to neoplasia was revealed in mice. Deletion of *Apc* in murine small intestine, which normally causes massive onset of intestinal cancer, was rescued by a simultaneous deletion of *c-Myc*, as double negative cells gave rise to intestinal epithelia comparable to wild-type tissue[203].

Other target genes are subject to a complex, context-dependent regulation and are expressed in a tissue-specific or temporally restricted manner[204, 205]. A comprehensive updated list of the Wnt target genes can be found at: http://wnt.stanford.edu.

Role of Wnt signaling in adult tissue homeostasis

Apart from being involved in the crucial developmental processes, such as gastrulation[206], body axis formation[206, 207], neural tube establishment[208, 209] and limb development[174], Wnt signaling also contributes to adult tissue maintenance and regeneration[210].

Wnt signaling has been reported to participate in hematopoiesis[211], bone mass and cartilage maintenace[212, 213], adipogenesis[214], liver zonation[215] and many other processes. Nevertheless, probably the most important function of Wnt signaling is the stem cell-driven maintenance of the epithelia.

Stem cell maintenance

The stem cells properties, the self-renewing capacity and the ability to produce numerous specialized cells, are given by the signals produced by the niche stem cells reside in[216]. Although many stem cell-sustaining signals are known, such as proteins from the BMP, Hedgehog, and Delta/Notch families, the Wnt signals stand out because of their widespread activity. The role of Wnt/β-catenin signaling in stem cell maintenance has been well documented in the intestine[217-219], mammary gland[220], hair follicles and in the skin[221-223]. Blocking Wnt signaling by overexpression of the Wnt antagonist *Dkk* eliminates hair follicles and mammary gland in a way that indicate that the tissue-specific stem cells were primarily affected[224]. Conversely, activating Wnt signaling by the use of mutant forms of β-catenin causes expansion of stem cells in both hematopoietic and hair follicle systems[225]. Similarly, Wnt proteins can increase the number of clonogenic cells from the

mammary gland, with preservation of the developmental potential of the cells when transplanted back into animals[226]. Despite all these examples, it should be emphasized that there are clear cases in which there is no obvious role for Wnt-dependent stem cell maintenance, like in male and female germlines of *Drosophila*[216].

On the other hand, the Wnt pathway has been proposed to be essential for maintenance of mouse embryonic stem cell pluripotency[227]. Indeed, several genes important for cell "stemness", like *Oct4*, *Nanog*, *Sox9* and *Fz7*, have been found to be regulated by Wnt signaling[171, 228-231]. The last two named genes were also found to be expressed in intestinal stem cells, an intensively studied adult body stem cells compartment.

Wnt signaling in intestinal stem cells (ISCs)

Intestinal stem cells reside at the most bottom part of the intestinal crypt, far from the ingested toxins and protected by antibacterial agents-producing Paneth cells (Figure 6). Inhere, supplied by various niche factors, they divide rapidly to completely renew the intestinal epithelia every 3-5 days. Considering that typical surface area of human intestine is about two hundreds square meters, such extensive self-renewal makes the intestinal epithelium the most dynamic tissue in mammalian body[232]. Several findings implicate a tight connection between the self-renewing process and the Wnt signaling pathway. Firstly, inactivating mutations in mouse *Tcf4* lead to a loss of intestinal stem cells and subsequent breakdown of the tissue[233]. Secondly, germinal mutations in the *APC* gene promote development of the Familial Adenomatous Polyposis (FAP) syndrome, a disorder characterized by multiple colorectal polyps[234]. Lastly, injection of the Wnt agonist RSPO1 into mouse bloodstream induced a rapid onset of crypt cells proliferation[82]. The fact, that perturbations of Wnt signaling are often manifested in the intestine is the reason why many research laboratories focus on the intestinal tissue. Moreover, the crypt niche produces Wnt3, Wnt6, Wnt9b and Fz5, which further underlines the role of Wnt signaling in the intestinal stem cell proliferation and the proper epithelial turnover [235, 236]. However, it is not clear, which cells at the crypt bottom are genuine ISC at what are the unique markers of these cells. Long-term lineage tracing experiments have identified Lgr5[14], B lymphoma Mo-MLV insertion region 1 (Bmi1)[237], telomerase reverse transcriptase (Tert)[238], and homeodomain-only protein homeobox (Hopx)[239] as bona fide ISC markers, since cells expressing any of these genes are able to give rise to all cell lineages of the intestinal epithelium. Whereas Lgr5 marks a distinctive, highly proliferative population of small intestinal and colonic stem cells (also known as crypt base columnar cells [CBC], red stem cells in Fig. 6), $Bmi1^+$ and $Tert^+$ cells reside at position of the fourth cell (blue stem cells in Fig. 6) from the crypt base and are mostly quiescent[240, 241]. Interestingly, it has been recently shown that $Bmi1^+$ cells are insensitive to perturbations of Wnt signaling, contribute weakly to homeostatic regeneration, and are resistant to high-dose radiation injury[242]. Upon

irradiation, Bmi1^{+} ISCs dramatically proliferate to repopulate multiple neighboring crypts and villi and replenish the eliminated Lgr5^{+} CBC cells[242, 243].

The above findings support the model for existence of proliferative, Lgr5^{+} Wnt-dependent ISCs, which are responsible for regular intestinal tissue maintenance, and reserve Bmi1^{+} stem cell population, which is used occasionally and in emergency. Such a hierarchy is not unprecedented, since similar principle is also applied in other tissues like hair follicle[244] and the haematopoietic system[245].

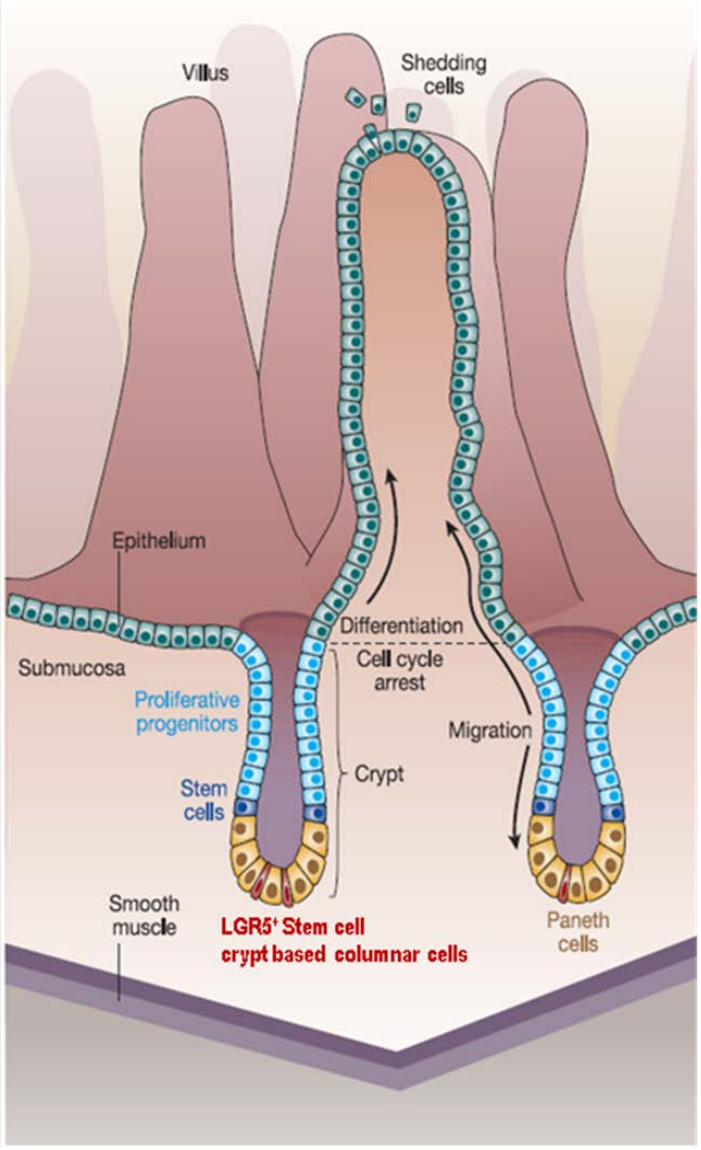

Figure 6: The epithelium of the small intestine. The scheme represents a crypt/villus unit in the adult mouse small intestine. Active proliferation of stem cells, residing at the bottom of the crypts, feeds an upward compartment of transit-amplifying progenitor cells. On migrating up, cells terminally differentiate in specialized cell types to fulfill their absorptive/secretory function. When reaching the top of the villi, the cells are shed out and die. There are at least two populations of intestinal stem cells. The stem cells were originally placed at the "+4 position," i.e. four cell diameters from the crypt base (depicted in blue). New paradigm suggests existence of additional cell population, characterized by the expression of the *Lgr5* gene. The Lgr5^{+} cells are interspaced between Paneth cells and are called crypt base columnar cells (CBC). Adapted from[246].

In the rapidly proliferating ISCs, Wnt signaling drives expression of the specific genes required for their maintenance. The known factors include Lgr5 and basic helix-loop-helix transcription factor Achaete scute-like 2 (Ascl2). Whereas Lgr5 is a part of regulatory loop, it can augment Wnt signaling by binding the Wnt agonist Rspo[91-93], Ascl2 controls ISC fate; forced expression of Ascl2 in the intestinal epithelia induces crypt hyperplasia and ectopic crypt on villi[247]. Moreover, Lgr5 is a direct target gene of Ascl2 and ablation of any of these two genes leads to the elimination of Lgr5^{+} stem cells[91, 247]. The loss of Lgr5^{+} ISC population is not permanent

because new Lgr5^{+} cells reappears soon as the offspring of unaffected CBC or Bmi1^{+} cell. This example illustrates the complexity of stem cell fate regulation. Many regulatory mechanism are involved to compensate imbalance caused by loss of any of them. Recently, two functional homologues of membranous zinc and ring finger E3 ubiquitin ligases important for managing ISC signaling input were identified. Both genes had to be eliminated from the gut to get the hyperproliferative crypt phenotype indicated hyperactivation of the Wnt pathway. On the other hand, ISC can be cultured *in vitro*[84] to form spheroids called organoids. The technology of organoid cultures helps to reveal the role of genes which would otherwise stay hidden behind their functional homologues in whole body system. In such a way it has been discovered that Paneth cells are the source of Wnt3[248] and constitute the niche for the fast cycling ISCs[249]. It should be noted, however, that ablation of Paneth cell from the mouse intestine has no impact on fast cycling Lgr5^{+} ISCs[250].

Wnt signaling and intestinal cancer

Cancer is regarded as a stem cells disease[251-253]. Direct evidence that a single mutation in a stem cell can cause immediate formation of neoplasia has been demonstrated in case of the intestinal cancer. Hyperactivation of the Wnt pathway in the ISCs, initiated either by homozygous disruption of the *Apc* gene[99] or expression of stabilized β-catenin[237], were revealed to be the cancer inducing event. In contrast, mutation in proliferative progenitor or terminally differentiated cell are rarely manifest in tumor growth. Since these cells are short-lived, they have only a limited opportunity to accumulate multiple mutations in critical genes required for tumor progression[99, 254, 255]. The Wnt pathway is the most frequently mutated pathways in colorectal carcinogenesis and intestinal tumors often display elevated expression of ASCL2 or LGR5, i.e. markers of fast cycling ISCs[103, 256-259]. Recently, one study identified LGR5^{+} cells as so-called cancer stem cells; i.e. the cells that initiate and sustain malignant growth and give rise to the phenotypic heterogeneity observed in the tumors[260].

Aims of the study

Although we know a lot about how signal represented by Wnt ligand is relayed inside the cell, there still remain many questions to be answered. For example, it is unknown whether and how posttranslational modifications of Wnt ligand contribute to Wnt affinity for particular Fz receptor. Additionally, multiple proteins interact with Fz/LRP receptors[91-93], which may further modulate their affinity for various Wnt ligands and so increase the complexity of the signaling output. The activity of other components of the Wnt pathway can be also regulated by various proteins, which presence or absence might be dependent on the cells type and cell cycle stage. These putative regulators might be primarily involved in different signaling pathways, thus their involvement in the Wnt pathway may create a complex network of signaling regulation. Additionally, we still do not know which genes are in specific cell type targets Wnt/β-catenin signaling and how is the expression of these genes beneficial for these cells.

The specific aims in deciphering the complexity of Wnt signaling thus were:

1) To reveal new target genes of the Wnt pathway by chromatin immunoprecipitation combined with microarray technology (ChIP-on-chip) and to determine what might be the function of these genes.

2) To clarify differences between Wnt ligands, namely how are these proteins postranslationaly modificated and how these modifications regulate secretion and signaling activity of these morphogenes.

3) To identify new interacting proteins for nuclear components of the Wnt pathway, specifically for the Tcf4protein. To elucidate how these proteins might contribute to the canonical Wnt pathway regulation

4) To get use the knowledge of the Wnt pathway interacting proteins, i.e. Hic1, to prepare genetics tool to reveal a role of this proteins in various body compartments *in vivo.*

Results

Troy, a Tumor Necrosis Factor Receptor Family Member, Interacts with Lgr5 to Inhibit Wnt Signaling in Intestinal Stem Cells

The fact that aberrant Wnt signaling is linked do development of colorectal cancer is very well known[8, 246]. However, the exact mechanism how Wnt target genes drive cells towards cancer, is still uncertain. To clarify this issue, we performed ChIP-on-chip experiment, to identify Wnt/β-catenin target genes in colorectal cancer cells.

Among the identified genes we found *TROY,* a member of tumor necrosis factor receptor family, previously described as a target of Wnt signaling in the developing mouse somites[261]. *Troy* expression was elevated in distinct β-catenin dependent models of mouse intestinal cancer confirming its status as a genuine Wnt/β-catenin target gene. However, in sporadic human colorectal cancer samples, we did not find any significant enrichment of *TROY* mRNA.

Troy expression in adult mice had an intriguing pattern. It was expressed in intestinal stem cells and potentially in stem cells of the hair follicle. We further focused on the well characterized intestinal stem cells population namely those marked by expression of another Wnt target gene, the Rspo receptor *Lgr5*[14]. We demonstrated that expression of Troy is confined to these stem cells. Additionally, we proved that TROY interacted with LGR5 and limited the level of canonical Wnt signaling. In conclusion, Troy function is to adjust the proper level of the Wnt pathway activity in the stem-cell compartment of the intestine.

My contribution to this work: I participated in writing of the manuscript and I generated the vast majority of all the experimental data.

Troy, a Tumor Necrosis Factor Receptor Family Member, Interacts with Lgr5 to Inhibit Wnt Signaling in Intestinal Stem Cells

Bohumil Fafilek[*], Michaela Krausova[*], Martina Vojtechova[*], Vendula Pospichalova[*], Lucie Tumova[*], Eva Sloncova[*], Martina Huranova[*], Jitka Stancikova[*], Adela Hlavata[*], Jiri Svec[*,#], Radislav Sedlacek[*], Ondrej Luksan[‡], Martin Oliverius[‡], Ludek Voska[‡], Milan Jirsa[‡], Jan Paces[*], Michal Kolar[*], Maria Krivjanska[‖], Klara Klimesova[§], Helena Tlaskalova-Hogenova[§] and Vladimir Korinek[*,¶]

Short Title: TROY inhibits Wnt signaling in the intestine

[*]*Institute of Molecular Genetics, Academy of Sciences of the Czech Republic, Videnska 1083, 142 20 Prague 4, Czech Republic*

[#]*Second Department of Internal Medicine, Third Faculty of Medicine, Charles University, Prague, Šrobárova 50, 100 34 Prague 10, Czech Republic*

[‡]*Institute for Clinical and Experimental Medicine, Vídenska 1958/9, 140 21 Prague 4, Czech Republic*

[‖]*Central European Biosystems Ltd., Nad Safinou II 365,252 42 Vestec u Prahy, Czech Republic*

[§]*Institute of Microbiology, Academy of Sciences of the Czech Republic, Videnska 1083, 142 20 Prague, Czech Republic*

[¶]**corresponding author:**

Vladimir Korinek

Institute of Molecular Genetics AS CR

Videnska 1083

142 20 Prague 4, Czech Republic

Tel: (+420) 241063146

FAX: (+420) 244472282

e-mail: korinek@img.cas.cz

Funding: This work was supported by qChIP/chip06 project from the Ministry of Education, Youth and Sports of the Czech Republic (grant number B06077); Grant Agency of the Czech Republic (P305/11/1780, P304/11/1252 and 204/09/H058); Grant Agency of Charles University in Prague (43-251452) and the institutional grant from the Academy of Sciences of the Czech Republic [(ASCR); RVO 68378050]. J.S. was supported by the Third Faculty of Medicine, Charles University in Prague research project UNCE204010; R.S by the project BIOCEV (CZ.1.05/1.1.00/02.0109); M.H. was supported by ASCR (KAN200520801); O.L., M.O. and M.J. were supported by the IKEM MZO 00023001 grant.

Authors' contribution: B.F. and V.K. conceived and designed the experiments; B.F., A. H., M.K., M.V., L.T., V.P., E.S., M.H., J.S. and V. K. performed the experiments; K.Kli., M.Kri., R.S., and H.T.-H. contributed reagents, materials and analysis tools; O.L., M.J., L.V. and M.O. provided clinical samples and performed their mutation analysis; J.S. provided clinical samples of premalignant lesions and participated in expression analysis; J.P. and M.Kol. performed the bioinformatics and statistical analyses; B.F., M.Kra. and V.K. wrote the manuscript.

Conflicts of interest: There are no conflicts of interest to disclose.

Abbreviations used in this paper: AOM, azoxymethane; APC, adenomatous polyposis coli; Axin, axis inhibition protein; BAC, bacterial artificial chromosome; CBC cells, crypt base columnar cells; Cp, crossing point; CRC, colorectal cancer; ChIP, chromatin immunoprecipitation; DS, dextran sulfate; FRET, fluorescence resonance energy transfer; IHC, immunohistochemistry; ISH, in situ hybridization; LacZ, β-galactosidase; Lef, lymphoid enhancer-binding factor; Lgr, leucine-rich-repeat containing G-protein coupled receptor; Lrp, low-density lipoprotein receptor-related protein; LTα, lymphotoxin-α; Min, multiple intestinal neoplasia; Nkd, naked cuticle homolog; Rspo, R-spondin; RT-qPCR, reverse transcription-quantitative polymerase chain reaction; siRNA, small inhibitory RNA; TA cells, transit amplifying cells; TCF, T-cell factor; TNFRSF, tumor necrosis factor receptor superfamily.

Abstract

***Background & Aims*:** The Wnt signaling pathway is required for maintenance of the intestinal epithelia; blocking this pathway reduces the proliferative capacity of the intestinal stem cells. However, aberrant Wnt signaling leads to intestinal cancer. We investigated the roles of the Wnt pathway in intestinal epithelium homeostasis and during malignant transformation in human cells and mice.

***Methods*:** We performed chromatin immunoprecipitation with DNA microarray analysis (ChIP-on-chip) to identify genes regulated by Wnt signaling in human colorectal cancer (CRC) cells Colo320, DLD1, LS174T, and SW480. Intestinal tumor formation was induced in C57BL/6J mice using azoxymethane and dextran sulphate. Intestine tissues from these mice, as well as $Apc^{+/Min}$ and $Apc^{CKO/CKO}$/Lgr5-EGFP-IRES-CreERT2 mice, were analyzed by immunohistochemisty and in situ hybridization.

***Results*:** We identified promoter regions of 960 genes that interacted with the Wnt pathway nuclear effector T-cell factor 4 in four different human CRC-derived cell lines; 18 of these promoters were present in all chromatin precipitates. Wnt signaling upregulated a member of the tumor necrosis factor receptor superfamily called TROY. Levels of TROY mRNA were increased in human cells with deficiencies in the adenomatous polyposis coli (*APC*) gene and in cells stimulated with the Wnt3a ligand. Troy expression was significantly upregulated in neoplastic tissues from mice during intestinal tumorigenesis. Lineage-tracing experiments revealed that Troy is produced specifically by fast-cycling intestinal stem cells. TROY associated with a unique marker of these cells, leucine-rich-repeat containing G-protein coupled receptor (LGR) 5. In organoids established from the intestinal crypts, Troy suppressed signaling by R-spondin, a Wnt agonist.

***Conclusions*:** TROY is upregulated in human colorectal cancer cell lines and in intestinal tumors in mice. It functions as a negative modulator of the Wnt pathway in LGR5-positive stem cells.

***Key words*:** mouse model of colon cancer; β-catenin; TCF; Tnfrsf19; transcription

Introduction

Development of neoplasia is a multi-step process requiring sequential acquisition of mutational events for its completion. In human colorectal carcinomas, the inheritance of a single mutation inactivating the *APC* gene can result in a significant predisposition to tumor formation and cancer. Moreover, mutations of the *APC* tumor suppressor are frequently found in sporadic colorectal carcinoma.[1] It has been well established that *APC*-deficient cells lose control over β-catenin turnover and display constitutive activation of the Wnt pathway.[2]

The central feature of the canonical Wnt pathway – also known as Wnt/β-catenin signaling - is the post-transcriptional control of the β-catenin protein stability (reviewed in[3]). In the absence of the Wnt ligand, the cytoplasmic level of free β-catenin is low due to the activity of a β-catenin degradation complex that includes Apc, axis inhibition protein (Axin), glycogen synthase kinase (GSK) 3β and casein kinase (CK) 1α. β-catenin is phosphorylated and subsequently destroyed in the ubiquitin-proteasome pathway. The binding of Wnt to the receptor Frizzled (Fz) and the Wnt co-receptor low-density lipoprotein receptor-related protein (Lrp) leads to disruption of the β-catenin degradation complex. Consequently, β-catenin accumulates in the cytoplasm and nucleus, where it associates with members of the lymphoid enhancer-binding factor (Lef)/T cell factor (Tcf) family of transcriptional factors (further referred to as Tcfs). Tcf/β-catenin heterocomplexes function as transcriptional activators of Wnt-responsive genes such as *Axin2*, *c-myc*, *Cyclin D1* and *naked cuticle homolog* (*Nkd*) *1*.

The gastrointestinal epithelia represent the most rapidly self-renewing tissue in the adult mammalian body and completely renew approximately every five days (reviewed in[4]). The single-layer epithelium of the small intestine is ordered into invaginations called crypts and microscopic projections called villi. Each crypt contains several long-lived stem cells. The progenitors [transit-amplifying (TA) cells] generated from these stem cells frequently divide and move upwards from the crypt. TA cells that have reached the edge of the crypts start to differentiate. When the differentiated cells arrive at the top of the villus (in the small intestine) or to the luminal surface (in the colon), they

undergo apoptosis and are shed to the intestinal lumen. Paneth cells of the small intestine are the only exception to this scheme. These antibacterial agent-producing cells stay at the crypt base, where they persist for approximately three to six weeks. Two types of intestinal stem cells have been described based on their markers, cycling rate and location in the crypt. *Lgr5*-positive fast-cycling stem cells [also known as crypt base columnar (CBC) cells] are interspersed among the Paneth cells.[5] The second pool consists of *Bmi1*-expressing cells. These relatively slowly dividing cells represent the reserve stem population and reside several cell diameters from the bottom of the crypt.[6] The physiological role of Wnt signaling in the gut was revealed by gene targeting experiments in mice. Disruption of the Wnt signaling pathway components *Tcf4* or *β-catenin* resulted in the terminal differentiation of stem cells followed by complete loss of the intestinal proliferative compartments of the crypts.[7, 8]

To investigate the role of the Wnt pathway in the intestine, we employed ChIP-on-chip on chromatin isolated from human CRC cells. We identified TROY [alternative names *the tumor necrosis factor receptor superfamily, member 19* (TNFRSF19) or TAJ],[9] as a target of canonical Wnt signaling. In addition, we showed that Troy is produced in fast-cycling stem cells of the small intestine and interacts with LGR5, a recently described receptor for the Wnt agonists R-spondins (Rspos).[10, 11] Interestingly, multicellular structures called organoids established from the intestinal crypts of Troy-deficient mice could be propagated at remarkably lower concentrations of exogenous Rspo ligand than organoids derived from the wild-type mice. This observation was in concordance with results showing that TROY inhibits signaling induced by Wnt and Rspo ligands. In conclusion, Troy represents a membrane modulator of the Wnt pathway that tunes the levels of the signaling in the signal-receiving cell.

Materials and Methods

Cell and Organoid Culture, Chip-on-chip, Biochemistry and Microscopy

All cell lines were purchased from ATCC. Isolated crypts were cultured according to Sato et al.[12] ChIP-on-chip on formaldehyde-crosslinked chromatin isolated from approximately $2x10^9$ Colo320, DLD1, SW480 and LS174T cells was processed as described previously[13] and immunoprecipitated using an anti-human TCF4 rabbit polyclonal antibody or anti-EGFP polyclonal antibody (negative control). Immunoprecipitated DNA was processed onto Human RefSeq Promoter Arrays (4226 HG18; Nimblegen) covering 2000 bps upstream and 500 bps downstream of the putative transcription start sites of all known human genes. Complementary DNAs (cDNAs) encoding human and mouse Troy, human LGR5 and Ectodysplasin A receptor (EDAR) were purchased from Open Biosystems. Two small inhibitory RNA (siRNA) targeting *β-CATENIN* (s437 and s438; Ambion) and two *TROY*-specific siRNAs (Dharmacon siGENOME SMART pool; Ambion) were used and gave similar results. *LGR5*-specific (siGENOME SMART pool) and control non-silencing siRNAs were purchased from Dharmacon. Western blotting, co-immunoprecipitations, RNA purification and reverse transcription-quantitative polymerase chain reaction (RT-qPCR) were performed as described previously.[13] Mouse Wnt3a ligand was isolated from the culture medium of Wnt3a-producing L cells according to the detailed protocol of Willert[14]. Wnt3a and/or mouse Rspo1 (R&D; final concentration 250 ng/ml) stimulations lasted 18 hours. Control stimulations were performed by "empty" ligand buffers. Fluorescence resonance energy transfer (FRET) was measured by the acceptor photobleaching method[15] using a Leica SP5 confocal microscope. Additional information is given in Supplemental Methods. The primers are listed in Supplemental Table S1.

Animal Manipulations

$Apc^{+/Min}$, Lgr5-EGFP-IRES-CreERT2 and Rosa26 "reporter" (Rosa 26R) mice were purchased from the Jackson Laboratory; $Apc^{CKO/CKO}$ mice were obtained from the Mouse Repository (NCI, Frederick, US); $Troy^{-/-}$ mice[16] were obtained from MMRRC (University of California, Davis, US). Animals were housed and handled according to guidelines approved by the Institutional committee.

Tamoxifen (Sigma) was administrated by a single intraperitoneal injection (1 mg dissolved in 0.1 ml of corn oil). β-galactosidase (LacZ) staining was performed as described elsewhere;[5] *in situ* hybridization (ISH) and immunohistochemistry (IHC) were performed as described in detail previously.[17] Tumor induction, generation of transgenic mice, sequences of antisense RNA probes and antibodies for IHC are described in Supplemental Methods.

Human Tumor Analysis

Ethical approval was obtained from the Institute for Clinical and Experimental Medicine (ICEM) and the Thomayer University Hospital Research Ethics Committee and the Ethics Committee of the Third Faculty of Medicine, Charles University. A cohort of 35 patients with precancerous colorectal lesions and 20 non-consecutive patients with primary colorectal cancer were enrolled into the study. Additional information is given in Supplemental Methods.

Results

TROY is a Wnt/β-catenin target gene in APC-deficient cancer cells

ChIP-on-chip was performed using chromatin isolated from human DLD1, SW480, Colo320 and LS174T cells. These CRC cells produce distinct truncated versions of the APC protein; LS174T cells are the only exception as they harbor wild-type *APC*, but carry instead an oncogenic mutation in *β-catenin*.[18] Subsequent analysis revealed that promoter regions of 960 genes were retained on the anti-TCF4 antibody-coupled beads; promoters of only 18 genes were positive in all four cell lines tested (Table 1, Supplemental Figure S1 and Supplemental Table S8). Among these putative TCF target genes we identified *TROY*. The gene encodes a type I transmembrane protein from the TNFRSF family that was described previously as a Wnt target in dermomyotome of mouse embryos.[19] In contrast to some other putative Wnt/β-catenin-activated genes, the *TROY* promoter (containing multiple consensus Tcf binding sites) was precipitated reproducibly with the TCF4-specific antibody (Figure 1*A*). A subsequent RT-qPCR analysis showed that *TROY* mRNA is abundant mainly in *APC*-deficient cells (Colo320, DLD1, SW480), although its expression in cells with intact *APC* (but harboring *β-CATENIN* activating mutation: LS174T, HCT116) was still detected (Figure 1*B*). In addition, we observed robust downregulation of *TROY* mRNA upon *β-CATENIN* knockdown (Figure 1*C*). Interestingly, when different mammalian cells were stimulated with recombinant Wnt3a, the *TROY* gene was – contrary to the "general" Wnt signaling target gene *Axin2* - upregulated only in cells of human origin [HEK293, U2OS, primary human intestinal epithelial cells (HIEC)] and not in mouse cells [3T3, C57MG, (Figure 1*D*)]. Taken together, these results indicated that *TROY* is a tissue-specific target of canonical Wnt signaling.

Troy is a tumor marker in mouse intestinal neoplasia

Next, we analyzed *Troy* expression in tumors in multiple intestinal neoplasia (Min) mice (further referred to as the $Apc^{+/Min}$ strain) and in neoplastic tissue generated in wild-type animals upon treatment with azoxymethane (AOM) and dextran sulphate (DS). $Apc^{+/Min}$ animals carry a truncation

mutation in one allele of the *Apc* gene and all adult individuals eventually develop large amounts of intestinal polyps and die of cancer.[20] Although AOM/DS treatment induces tumors displaying aberrant Wnt signaling[21], these tumors (in contrast to $Apc^{+/Min}$ animals that suffer mainly from the neoplasia of the small intestine) are localized in the distal colon and rectum. We observed a substantial increase in *Troy* mRNA and protein in tumor tissue in both cancer models (Figure 2*AB*). The same expression pattern was noted for another Wnt signaling target gene, *Nkd1*. The analysis of some additional genes regulated by the Wnt/β-catenin pathway was less conclusive. Whereas mRNAs encoding *Axin2* and *Lgr5* were more abundant in the small intestinal lesions of $Apc^{+/Min}$ animals, another Wnt target gene, *Sp5*, was expressed predominantly in the large intestine tumors induced by AOM/DS (Figure 2*A*). Subsequently, we performed ISH using the *Troy*-specific antisense RNA probe. Similarly as *Axin2*, *Troy* expression was detected through the tumor mass, although the signal was less intense. Interestingly, the positive staining was detected not only in tumors but also in the crypts of healthy mucosa of the small intestine (Figure 2*C* and Supplemental Figure S4*A*).

Recently, Lgr5 was established as a specific marker of the intestinal epithelium stem cells. Moreover, knock-in mice designated Lgr5-EGFP-IRES-CreERT2 expressing a tamoxifen-regulated variant of Cre recombinase from the *Lgr5* locus were produced.[5] To evaluate the Troy expression at early stages of tumor development we intercrossed Lgr5-EGFP-IRES-CreERT2 mice with animals carrying the conditional alleles (*CKO*) of the *Apc* gene. The Cre-mediated excision of the floxed exon 14 in the *CKO* allele results in production of the truncated non-functional Apc polypeptide.[22] Multiple β-catenin-positive dysplastic lesions were observed in $Apc^{CKO/CKO}$/Lgr5-EGFP-IRES-CreERT2 mice as early as 5 days after tamoxifen injection. These microadenomas were also positive for *Axin2* and *Troy* mRNA (Figure 2*D*). To confirm our assumption that Troy possibly represents a reliable marker of the neoplastic growth related to non-physiological Wnt signaling, we performed *TROY* expression analysis in sporadic human colorectal specimens. Both in early and advanced stages of tumor progression, the presence of the inactivating *APC* mutations was positively correlated with increased expression levels of *AXIN2* (Supplemental Figure S2 and Supplemental Table S6). In comparison, the increased expression of the intestinal stem cell marker *LGR5* was related to the *APC* mutation status only at the early, but not the late, stages of tumorigenesis. Contrary to mouse tumors, *TROY*

transcription in human carcinomas did not follow the expected pattern, and no correlation between the levels of *TROY* mRNA and the mutation status of *APC* was observed. In addition, the analysis of *TROY* expression in thirty-five polyps of the colon showed a decrease in *TROY* mRNA in the majority of these premalignant lesions (compared to healthy mucosa; Supplemental Figure S3 and Supplemental Table S7).

Taken together, these data indicate that in contrast to mouse neoplasia in human sporadic lesions the TROY expression is governed possibly by a more complex regulatory mechanism.

Troy is produced in Lgr5-positivive intestinal stem cells

Using ISH, we noted a *Troy* localization in the lower part of the crypt compartments (Figure 2*C*, bottom right panels; Supplemental Figure S4*A*). Since the colocalization of *Troy* and EGFP (a surrogate marker of $Lgr5^{+}$ CBC cells), using a combination of ISH and IHC, was not conclusive (Supplemental Figure S4*A*), we prepared crypts from Lgr5-EGFP-IRES-CreERT2 knock-in mice and sorted the isolated cells according to the EGFP production (Supplemental Figure S4*B*). *Troy* mRNA was detected mainly in cells with high GFP signal (GFP^{high}) and not in cell populations with low or no GPF expression (GFP^{low} and $GFP^{negative}$, respectively). The same expression pattern was recorded for *Lgr5* but not for *Bmi1* (Figure 3*A*). In a complementary approach, neither *Troy* nor *Lgr5* were enriched in sorted Paneth cells (Supplemental Figure S4*C*). To study the identity of the Troy-producing cells in detail we used BAC carrying the mouse *Troy* locus to generate transgenic mice (designated Troy-CreERT2) expressing tamoxifen-inducible Cre enzyme inserted in frame at the translation initiation codon of the *Troy* gene (Supplemental Figure S5*ABC*). Then we performed the lineage-tracing experiments in the intestinal tissue. We intercrossed Troy-CreERT2 with Rosa26R mice. Rosa26R animals produce bacterial *LacZ* mRNA from the ubiquitously active *Rosa26* allele.[23] The mRNA is not translated (and the enzyme produced) unless a transcriptional stop signal flanked by a pair of loxP sites is removed from the genome by Cre-mediated excision. Adult Troy-$CreERT2^{+}$/Rosa26R mice were injected with a single dose of tamoxifen and sacrificed at several time points later. Interestingly, Cre-mediated recombination was the most efficient in the proximal part of small intestine (duodenum, jejunum) and much less effective in the ileum or colon (Figure 3*B* and Supplemental Figure S5*D*). As

shown in Figure 3*C* and Supplemental Figure S5*F*, one day after the induction of Cre, LacZ-expressing cells were located at the crypt bottom of the small intestine. At later time points, "blue" cell clones were moving upwards from the crypt and reached the top of the villus. The labeled cells persisted in the gut for more than two months (Figure 3*C* and Supplemental Figure S5*G*) and also descendants of *Troy*-expressing cells differentiated into all major cell lineages of the intestinal epithelium (Figure 3*D*). The labeling of Cre-expressing cells in the colon – although less efficient – displayed a similar pattern (see Supplemental Results for details). These data indicated that Troy-positive cells are capable of long-term renewal of the epithelium and correspond to CBC cells. Our conclusion that Troy is a novel marker of CBC stem cells was in concurrence with a recently published analysis of expression profiling of these cells.[24, 25]

TROY interacts with LGR5

Next, we visualized the cellular localization of TROY and LGR5 in HeLa cells transfected with TROY and LGR5 expression constructs using confocal microscopy. Interestingly, a clear colocalization of TROY with LGR5 was noted (Figure 4*A*). The possible interaction of TROY with LGR5 was further analyzed using co-immunoprecipitation. Experiments involving tagged variants of TROY and LGR5 demonstrated that MYC-tagged LGR5 could be co-isolated with FLAG-tagged TROY by an anti-FLAG antibody. Conversely, TROY was present in the anti-GFP precipitates when TROY-FLAG and LGR5-EGFP were co-produced in the same cell (Figure 4*B*). To confirm TROY association with LGR5, we employed the FRET acceptor photobleaching approach in HeLa cells expressing various combinations of TROY and LGR5 fused to fluorescent protein at their C-termini. EDAR, a TNFRSF member related to TROY known for its homodimerization, was used as a control.[26] Indeed, a high FRET signal was measured in cells co-expressing EDAR-EYFP (acceptor) and EDAR-ECFP (donor). Moreover, the signal was also detected in cells producing TROY-EYFP and LGR5-ECFP, confirming the results obtained by co-immunoprecipitation (Fig 4*C*). Virtually no energy transfer was recorded between EDAR and TROY; however, we noted FRET between EDAR and LGR5. This implied a possible association of these two molecules which was verified subsequently by co-immunoprecipitation of EDAR with LGR5 in HEK293 cells (Supplemental Figure S6).

TROY functions as a negative regulator of Wnt signaling

Recently, several studies have shown that Rspos, the secreted agonists of Wnt signaling, bind to Lgr5 and this interaction augments the action of Wnt ligands.[10, 11, 27] To examine whether TROY affects the Rspo function, we performed a reporter gene assay and a RT-qPCR analysis in HEK293 cells treated with siRNA specific for TROY. We found that the *TROY* mRNA level was reduced to 15-20% upon transfection with two different TROY siRNAs (Figure 5*A* and data not shown). Interestingly, TROY knockdown elevated the Wnt-dependent transcription not only in the cells treated with a combination of Wnt3 and Rspo1, but also in cells stimulated with the Wnt3a ligand only. In a parallel control experiment, cells were transfected with LGR5-specific siRNA and the potentiating effect of Rspo1 on Wnt signaling was partly abolished (Figure 5*A*). Of note, although the *LGR5* mRNA level was reduced to 16% on average (SD=1.1), the effect of the knockdown on the activity of pTOPFLASH reporter in cells stimulated with Wnt3a/Rspo1 was moderate (reduction to 59% in comparison to cells treated with non-silencing siRNA). Nevertheless, since HEK293 cells produce an additional Rspo receptor, LGR4, this observation was in concordance with previously published data indicating partial redundancy of LGR4 and LGR5 proteins.[27] Importantly, TROY knockdown had no effect on the transcription from the negative-control reporter pFOPFLASH (not shown) and, furthermore, the TROY downregulation did not potentiate TCF/β-catenin-mediated transcription in human CRC cells with aberrant Wnt signaling (Supplemental Figure S7*A*). The latter finding indicated that TROY functions at the level or upstream of the β-catenin degradation complex. In cells with inducible expression of TROY, only minor effects on transcription of Wnt signaling target genes were recorded (Supplementary Figure S7*B*). Nevertheless, we observed that binding of Rspo1 to LGR5 was not eradicated by the TROY presence (Supplemental Figure S8). We further focused on the signaling downstream of Wnt and Rspo ligands. Interestingly, although Dvl phoshorylation was not changed by TROY knockdown, the treatment of HEK293 cells with TROY siRNA increased phosphorylation and cellular levels of the Wnt co-receptor LRP6 (Supplemental Figure S8*B* and Figure 5*B*). We concluded that TROY might block specific modifications of LRP6 which in turn can change LRP6 stability and/or function. However, western blots with antibodies recognizing phospho-Ser1490 andphospo-Thr1572 of LRP6 protein did not show differential modification of these residues in control and

TROY siRNA-treated cells (Figure 5*B* and data not shown). Thus, the putative phoshorylation site(s) remains to be determined. Finally, we functionally tested the role of Troy in defined primary cultures of the intestinal crypts. Troy$^{-/-}$organoids – in contrast to organoids derived from the wild-type mice – retained cell proliferation even in the absence of exogenous Rspo1 (Figure 6*AB*). However, growth of these "miniguts" ceased 48 hours after Rspo1 withdrawal (Supplemental Figure S9). This prompted us to test the organoid culture at decreasing concentrations of Rspo1. Strikingly, *Troy*$^{-/-}$ organoids could be propagated for many weeks in culture medium supplemented with Rspo1 at the concentration 15 ng/ml. Contrary to that, at the same Rspo1 concentration the growth of intestinal organoids established from wild-type mice was arrested (Figure 6*C*). These results convincingly confirmed the possible inhibitory role of Troy on Wnt/Rspo signaling.

Discussion

In the present study, we identified TROY as the Wnt/β-catenin pathway target gene in human CRC cells and in mouse tumors. Using expression profiling, ISH and lineage-tracing experiments in the mouse we demonstrated that in the healthy small intestine, Troy marks the fast-cycling CBC stem cells. In addition, we showed that TROY interacts with LGR5 and inhibits canonical Wnt signaling.

In mouse neoplasia, Troy behaved as a reliable marker of tumors with active Wnt signaling. Of note, although expression analyses of mouse and human tissues or cell lines included several well-defined Wnt/β-catenin signaling target genes, we never observed a "hundred percent" correlation between the expression of the analyzed genes and (hyper)active Wnt signaling. Even *Axin2*, considered to be a "universal" target of the canonical Wnt pathway, was not (significantly) upregulated in AOM/DS-induced neoplasia (Figures 1BC and 2A). These data indicate that the transcription of the tested genes is regulated by complex mechanisms and cannot be solely related to the status of the Wnt pathway. Contrary to mouse tumors, *TROY* expression in human sporadic colorectal cancer did not correlate with the mutation status of *APC* (Supplemental Figure S2). Moreover, TROY mRNA was decreased in the majority of human premalignant lesions. These observations preclude the usage of TROY as a marker of the Wnt pathway activity status in human colorectal cancer and/or TROY targeting in therapeutic applications.

The ISH indicated that *Troy* mRNA is uniformly expressed throughout tumor tissues (Figure 2*B*). This result was somehow contradictory to the lineage-tracing experiments in Troy-CreERT2^{+}/Rosa26R/Apc$^{+/Min}$ that showed "patches" of the LacZ-positive cells in tumor tissues (Figure 3*E*). As Cre-mediated recombination displayed different efficiency in distinct parts of the intestine, we suppose that the observed variability in LacZ staining was caused by the inefficient recombination of the "floxed" transcriptional stop signal rather than by the heterogeneous expression of *Troy* (or its surrogate marker Cre) in tumor tissue.

Troy expression was described in the adult central nervous system, the developing hair follicle and embryonic skin.[26] In postnatal neurons, Troy interacts with the Nogo-66 receptor 1 (NgR1) and

activates RhoA signaling.[28] Moreover, in glial tumor or HEK293 cells, TROY participates in the Rac1 and JNK pathways, respectively.[29, 30] Recently, a study of Hashimoto and colleagues revealed that the cytokine lymphotoxin-α (LTα) binds to Troy and triggers NFκB signaling.[31] All these results suggest a complex and pleiotropic role of Troy in various cellular contexts.

According to our data, TROY interacts with LGR5 and limits the level of canonical Wnt signaling. Importantly, active Wnt/Rspo signaling could not be completely compensated by Troy deficiency and Troy$^{-/-}$ organoids arrested their growth upon withdrawal of exogenous Rspo (Figure 6 and Supplementary Figure S9). This result indicated that Troy-mediated inhibition of the Wnt pathway is indirect. In agreement with this conclusion, we observed that Troy knockdown increased the levels and phosphorylation of LRP6 (Figure 5*BC*). Recently, zinc and ring finger (ZNRF) 3 and ring finger (RNF) 43 transmembrane ubiquitin ligases were identified as negative regulators of Wnt signaling.[32] These related ligases decrease the stability of the Wnt receptor FZ through ubiquitin-mediated degradation. Interestingly, Rspo associates with both ZNRF3 and LGR and promotes removal of ZNRF3 from the plasma membrane. Consequently, the levels of FZ and also Wnt co-receptor LRP are increased, which leads to the enhanced Wnt response. However, the relationship between Troy and ZNRF3/RNF43 ligases and Troy involvement in LRP6 phosphorylation and stability remains to be determined.

Troy-deficient mice are viable and fertile with no apparent defects in the gut tissue.[16, 31] This fact is rather unexpected considering the increased proliferation rate and decreased dependence on Rspo1 observed by the Troy-deficient organoids. Very recently, Farin and colleagues described a similar discrepancy between the requirement of Wnt3 for growth of intestinal organoids and dispensability of Wnt3 in living animals.[33] These data implicate that cultured crypt organoids do not entirely recapitulate the complex situation involving interaction of multiple cell types present in intestinal tissue. Alternatively, the Troy absence results in a relatively subtle with survival-compatible phenotype that was not noted during the primary analysis of Troy$^{-/-}$ animals. Finally, Troy$^{-/-}$ mice must be “challenged” in some way to reveal any functional outcomes of the Troy absence.

Acknowledgments

We thank A. Abo, L. Andera, V. Bryja, and M. Klima for the constructs, J.F. Beaulieu for HIEC cells and Z. Kozmik for Rosa26R mice. We are grateful to the staff of the Transgenic Unit for generation of the transgenic mice. We further thank S. Takacova and T. O'Hearn, II for reading the manuscript.

Figure and Table Legends

Table 1. List of the genes bound by TCF4 in chromatin isolated from all four CRC cell lines tested. The left columns indicate the fold change of the signal obtained using the anti-TCF4 antibody vs. negative control antibody. The statistical significance of the results (p-value) was evaluated by the chi-square test (see Supplemental Methods for details). The genes are listed according to the signal intensity recorded in the ChIP-on-chip analysis of Colo320 cells. A region was scored as "TCF4-bound" if the ratio of the signal obtained by ChIP with the anti-TCF4 antibody vs. control antibody was ≥ 1.5. The table includes previously identified TCF/β-catenin target genes *AXIN2*, *LGR5*, *NKD1* and *SP5* (listed below the dashed line), although none of these genes fulfilled completely the selection criterion. The base numbering of chromosomal DNA corresponds to the human genome annotation HG18. For comparison, genes identified by the screen of Hatzis and colleagues[34] are shown in the right column.

Figure 1. *TROY* is a Wnt/β-catenin target gene. (*A*) ChIP analysis in human CRC cells. Genomic DNA including promoter regions of the presumptive Wnt signaling target genes *LGR5*, *NKD1*, *SP5*, *TROY* were immunoprecipitated from chromatin isolated from the indicated cells. The promoter sequences of the *β-ACTIN* gene and 3' untranslated region (UTR) of *c-MYC* were used as negative controls. Bars represent enrichment of the tested DNA elements in precipitates obtained with the TCF4-specific versus control antibody. (*B*) *Troy* expression is abundant in *APC*-deficient cells. Results of the RT-qPCR analysis of mRNA isolated from indicated CRC cells. Crossing point (Cp) values were normalized to the *β-ACTIN* expression levels (Cp=16.5). The Wnt/β-catenin non-responsive gene *AXIN1* was also included in the test. (*C*) *β-CATENIN* knockdown reduces *TROY* expression. (*D*) In human cells, *TROY* acts as a Wnt responsive gene. Cells of human (HEK293, HIEC, U2OS) or mouse (C57MG, 3T3) origin were stimulated using Wnt3a or Wnt storage buffer (vehicle) and assayed in RT-qPCR. All experiments were performed in triplicates and repeated three times. Histograms

represent mean values of a representative experiment with the corresponding standard deviations (SDs). Missing bars stand for unexpressed gene (normalized Cp≥35).

Figure 2. *Troy* mRNA is enriched in mouse intestinal tumors. (*A*) RT-qPCR analysis of 19 tumors dissected from colons of 12 AOM/DS-treated mice and 23 small intestinal tumors from 9 $Apc^{+/Min}$ animals. Control RNA samples were isolated from matched healthy tissue. (*B*) Western blot analysis of 3 tumors isolated from $Apc^{+/Min}$ mice. Intact mucosa adjacent to the corresponding neoplasia was used as a control; α-tubulin, loading control. (*C*) Left, ISH of *Troy* and *Axin2* mRNAs in tumors (red arrowheads) developing in $Apc^{+/Min}$ mice. Right, in the healthy intestinal tissue both genes are expressed in the lower parts of the crypts (black arrowheads; the image was taken from the duodenum). The enlarged crypt base is shown in the bottom right of the image (one *Troy*-positive CBC cell was outlined by a dashed line). (*D*) Immunohistochemical detection of β-catenin (left panel; counterstained with hematoxylin) and ISH of *Axin2* and *Troy* (right panels) in the microadenomas developed 5 days after Cre-mediated ablation of the *Apc* gene in Lgr5-EGFP-IRES-CreERT2/$Apc^{CKO/CKO}$ animals. Notice that the neoplastic lesions (black arrows in the right image) produce increased amounts of β-catenin and are also positive for *Axin2* and *Troy* (red arrowheads). Original magnification for panels: (*C*) 100 × (the bottom right image 600 ×); (*D*) 200 ×.

Figure 3. *Troy* expression is confined to the Lgr5-positive cells in the intestinal crypts. (*A*) Expression profiling of GFP^{high} and GFP^{low} cells isolated from the intestinal crypts of 10 Lgr5-EGFP-IRES-CreERT2 knock-in mice (details are given in Supplemental Figure S4*B*). (*B-E*) Lineage tracing in the intestinal epithelium of Troy-$CreERT2^{+}$/Rosa26R mice. (*B*) Upper image, whole-mount staining of LacZ in different parts of the intestine 1 day after tamoxifen administration. Lower image, whole-mount staining of the jejunum 3 days after tamoxifen administration. Duo, duodenum; Ile, ileum; Jej, jejunum; Col, colon. (*C*) Histochemical detection of the LacZ activity in the duodenum 1 day, 3 days and 60 days after tamoxifen administration. Notice that one-day induction generates LacZ-positive cells located at the crypt base (black arrowheads). (*D*) Double-labeling demonstrates that LacZ-

expressing (“blue”) clones produce markers of differentiated cell lineages (arrows) including Paneth, goblet and enteroendocrine cells. Lys, lysozyme; ChrA, chromogranin A; PAS, periodic acid Schiff. (*E*) The tumor-associated LacZ activity (red arrowhead) developed in the small intestine of Troy-CreERT2^{+}/Rosa26R/Apc$^{+/Min}$ mice. The tissue was analyzed 1 day after tamoxifen administration using whole-mount (left panel) or histochemical staining (right). Counterstain: nuclear red. Original magnification: (*B*) upper panel 1.5 ×, lower panel 7 ×; (*C*) 100 ×; (*D*) 600 ×; (*E*) left panel 7 ×, right panel 100 ×.

Figure 4. TROY interacts with the marker of intestinal CBC cells LGR5. (*A*) Colocalization of ectopically expressed LGR5-MYC and TROY-FLAG in HeLa cells stained with rabbit anti-MYC and mouse anti-FLAG monoclonal antibodies. The panel at the right shows the overlap of fluorescence intensity peaks along the profile as indicated in the merged micrograph. (*B*) Co-immunoprecipitation of TROY and LGR5. IP, immunoprecipitation; IB, immunoblotting. (*C*) Detection of TROY binding to LGR5 using FRET microscopy. Fluorescently tagged LGR5, TROY and EDAR proteins were co-expressed in HeLa cells and visualized as indicated under the histogram. EYFP was photo bleached in a selected area of the cytoplasmic membrane and FRET efficiency measured as an increase of ECFP fluorescence upon EYFP photo destruction. The bars indicate the relative FRET efficiency calculated from the given cell numbers (n); $^{**}p<0.01$ (Student's t-test).

Figure 5. TROY inhibits Wnt signaling. (*A*) Downregulation of TROY potentiates the responsiveness of HEK293 cells to Wnt3a and Rspo1 stimulation. Left, results of the reporter gene assay using the Wnt/β-catenin reporter pTOPFLASH. Right, RT-qPCR analysis of HEK293 cells treated as indicated. The blot in the inset demonstrates the efficiency of TROY knockdown. The reporter gene activity (left diagram) or expression level of a given gene (right diagram) in cells transfected with control non-silencing siRNA and treated with vehicle (Wnt storage buffer) was arbitrarily set to 1. (*B*) TROY influences cellular levels and phosphorylation of LRP6. The western

blot of whole-cell extracts prepared from HEK293 cells treated with non-silencing or TROY siRNA and further stimulated as indicated. The immunoblotting was performed with antibodies recognizing the total cellular pool of LRP6 (bottom panel) or its form phosphorylated at Ser1490 (p-LRP; upper panel). Notice that TROY siRNA increased the amount and phosphorylation of LRP6 (the putative phosphoprotein with changed mobility is marked by red asterisk) but, other residue than Ser1490 is modified. Moreover, TROY siRNA induced stabilization of β-CATENIN including the N-terminally non-phosphorylated form of the protein. (*C*) A possible model of TROY action. The absence of TROY increases levels and phosphorylation of LRP at specific residue (indicated by "P" in red circle). This potentiates the outcome of Wnt/Rspo signaling and leads to β-catenin accumulation.

Figure 6. Proliferation of intestinal organoids derived from Troy$^{-/-}$ mice is less dependent on exogenous Rspo than the growth of organoids established from wild-type mice. (*A*) Confocal microscopy images of organoids derived from Troy$^{+/+}$and Troy$^{-/-}$small intestinal crypts. The organoids were grown for 2 days with or without Rspo1 and stained using an anti-E-cadherin (E-cad) antibody (red) and DAPI nuclear stain (blue); proliferating cells were visualized by EdU incorporation (green). (*B*) Proliferation assay of organoids. *p<0.05; **p<0.01. (*C*) Stereomicroscopic images of the intestinal organoids propagated at various concentrations of Rspo1. The images were taken for 6 consecutive days as indicated. Original magnification: (*A*) 400 ×; (*C*) 20 ×.

References

1. Kinzler KW, Vogelstein B. Lessons from hereditary colorectal cancer. Cell 1996;87:159-70.
2. Korinek V, Barker N, Morin PJ, et al. Constitutive transcriptional activation by a beta-catenin-Tcf complex in APC-/- colon carcinoma. Science 1997;275:1784-7.
3. Cadigan KM, Peifer M. Wnt signaling from development to disease: insights from model systems. Cold Spring Harbor perspectives in biology 2009;1:a002881.
4. Marshman E, Booth C, Potten CS. The intestinal epithelial stem cell. BioEssays 2002;24:91-8.
5. Barker N, van Es JH, Kuipers J, et al. Identification of stem cells in small intestine and colon by marker gene Lgr5. Nature 2007;449:1003-7.
6. Tian H, Biehs B, Warming S, et al. A reserve stem cell population in small intestine renders Lgr5-positive cells dispensable. Nature 2011;478:255-9.
7. Fevr T, Robine S, Louvard D, et al. Wnt/beta-catenin is essential for intestinal homeostasis and maintenance of intestinal stem cells. Molecular and cellular biology 2007;27:7551-9.
8. Korinek V, Barker N, Moerer P, et al. Depletion of epithelial stem-cell compartments in the small intestine of mice lacking Tcf-4. Nat Genet 1998;19:379-83.
9. Hisaoka T, Morikawa Y, Kitamura T, et al. Expression of a member of tumor necrosis factor receptor superfamily, TROY, in the developing mouse brain. Brain Res Dev Brain Res 2003;143:105-9.
10. de Lau W, Barker N, Low TY, et al. Lgr5 homologues associate with Wnt receptors and mediate R-spondin signalling. Nature 2011;476:293-7.
11. Glinka A, Dolde C, Kirsch N, et al. LGR4 and LGR5 are R-spondin receptors mediating Wnt/beta-catenin and Wnt/PCP signalling. EMBO Rep 2011;12:1055-61.
12. Sato T, Vries RG, Snippert HJ, et al. Single Lgr5 stem cells build crypt-villus structures in vitro without a mesenchymal niche. Nature 2009;459:262-5.
13. Lukas J, Mazna P, Valenta T, et al. Dazap2 modulates transcription driven by the Wnt effector TCF-4. Nucleic Acids Res 2009;37:3007-20.
14. Willert K, Brown JD, Danenberg E, et al. Wnt proteins are lipid-modified and can act as stem cell growth factors. Nature 2003;423:448-52.
15. Huranova M, Jablonski JA, Benda A, et al. In vivo detection of RNA-binding protein interactions with cognate RNA sequences by fluorescence resonance energy transfer. RNA 2009;15:2063-71.
16. Pispa J, Pummila M, Barker PA, et al. Edar and Troy signalling pathways act redundantly to regulate initiation of hair follicle development. Hum Mol Genet 2008;17:3380-91.
17. Pospichalova V, Tureckova J, Fafilek B, et al. Generation of two modified mouse alleles of the Hic1 tumor suppressor gene. Genesis 2011;49:142-51.
18. Rosin-Arbesfeld R, Cliffe A, Brabletz T, et al. Nuclear export of the APC tumour suppressor controls beta-catenin function in transcription. Embo J 2003;22:1101-13.
19. Buttitta L, Tanaka TS, Chen AE, et al. Microarray analysis of somitogenesis reveals novel targets of different WNT signaling pathways in the somitic mesoderm. Dev Biol 2003;258:91-104.
20. Su LK, Kinzler KW, Vogelstein B, et al. Multiple intestinal neoplasia caused by a mutation in the murine homolog of the APC gene. Science 1992;256:668-70.
21. Tanaka T, Kohno H, Suzuki R, et al. Dextran sodium sulfate strongly promotes colorectal carcinogenesis in Apc(Min/+) mice: inflammatory stimuli by dextran sodium sulfate results in development of multiple colonic neoplasms. International journal of cancer 2006;118:25-34.
22. Kuraguchi M, Wang XP, Bronson RT, et al. Adenomatous polyposis coli (APC) is required for normal development of skin and thymus. PLoS Genet 2006;2:e146.
23. Soriano P. Generalized lacZ expression with the ROSA26 Cre reporter strain. Nature genetics 1999;21:70-1.
24. van der Flier LG, van Gijn ME, Hatzis P, et al. Transcription factor achaete scute-like 2 controls intestinal stem cell fate. Cell 2009;136:903-12.
25. Sato T, van Es JH, Snippert HJ, et al. Paneth cells constitute the niche for Lgr5 stem cells in intestinal crypts. Nature 2011;469:415-8.

26. Kojima T, Morikawa Y, Copeland NG, et al. TROY, a newly identified member of the tumor necrosis factor receptor superfamily, exhibits a homology with Edar and is expressed in embryonic skin and hair follicles. The Journal of biological chemistry 2000;275:20742-7.
27. Carmon KS, Gong X, Lin Q, et al. R-spondins function as ligands of the orphan receptors LGR4 and LGR5 to regulate Wnt/beta-catenin signaling. Proc Natl Acad Sci U S A 2011;108:11452-7.
28. Shao Z, Browning JL, Lee X, et al. TAJ/TROY, an orphan TNF receptor family member, binds Nogo-66 receptor 1 and regulates axonal regeneration. Neuron 2005;45:353-9.
29. Eby MT, Jasmin A, Kumar A, et al. TAJ, a novel member of the tumor necrosis factor receptor family, activates the c-Jun N-terminal kinase pathway and mediates caspase-independent cell death. The Journal of biological chemistry 2000;275:15336-42.
30. Paulino VM, Yang Z, Kloss J, et al. TROY (TNFRSF19) is overexpressed in advanced glial tumors and promotes glioblastoma cell invasion via Pyk2-Rac1 signaling. Mol Cancer Res 2010;8:1558-67.
31. Hashimoto T, Schlessinger D, Cui CY. Troy binding to lymphotoxin-alpha activates NF kappa B mediated transcription. Cell cycle (Georgetown, Tex 2008;7:106-11.
32. Hao HX, Xie Y, Zhang Y, et al. ZNRF3 promotes Wnt receptor turnover in an R-spondin-sensitive manner. Nature 2012;485:195-200.
33. Farin HF, Van Es JH, Clevers H. Redundant Sources of Wnt Regulate Intestinal Stem Cells and Promote Formation of Paneth Cells. Gastroenterology 2012.
34. Hatzis P, van der Flier LG, van Driel MA, et al. Genome-wide pattern of TCF7L2/TCF4 chromatin occupancy in colorectal cancer cells. Mol Cell Biol 2008;28:2732-44.

Table 1

Cell line:	**Colo320**		**DLD1**		**LS174T**		**SW480**			
Gene	fold change	p-value	fold change	p-value	fold change	p-value	fold change	p-value	peak position	Gene identified by Hatzis et al.[33]
LEF1	4.45	1.08E-09	3.73	1.57E-09	2.11	6.78E-10	3.62	9.87E-10	chr4: 109310227-109310282	+
TROY	4.03	1.08E-09	3.56	1.57E-09	2.69	6.78E-10	3.16	9.87E-10	chr13: 23042725-23042786	+
RPS27	3.91	7.58E-08	3.4	1.01E-07	2.75	5.25E-08	2.43	7.05E-08	chr1: 152229752-152229801	-
MOBKL3	3.37	1.08E-09	2.88	1.57E-09	2.24	6.78E-10	2.78	9.87E-10	chr2: 198088264-198088315	-
GGH	2.45	3.16E-07	3.36	1.57E-09	2.6	5.95E-09	2.84	9.87E-10	chr8: 64114840-64114890	-
C12orf35	3.45	7.58E-08	2.26	2.51E-06	2.33	2.24E-07	2.78	4.14E-07	chr12: 32002831-32002889	-
NT5C2	2.21	1.10E-06	3.98	1.57E-09	1.72	7.98E-07	2.21	3.51E-08	chr10: 104943406-104943455	-
SUPT4H1	2.9	1.08E-09	3.09	1.57E-09	1.59	2.56E-08	2.05	9.87E-10	chr17: 53785562-53785611	+
C9orf103	2.88	2.66E-06	2.26	3.34E-06	1.52	1.98E-06	2.87	7.05E-08	chr9: 85426185-85426234	-
SYMPK	2.65	7.58E-08	3.22	1.57E-09	1.7	2.24E-07	1.77	2.51E-06	chr19: 51057357-51057406	-
PCTK2	2.33	3.16E-07	2.58	4.14E-07	2.08	2.24E-07	2.32	8.48E-06	chr12: 95319254-95319303	-
CBWD3	2.46	6.42E-07	2	6.79E-06	2.67	4.23E-06	2.02	5.23E-06	chr9: 70047011-70047060	-
TOM1L1	1.69	1.08E-09	2.79	5.16E-08	2.22	7.98E-07	2.44	9.87E-10	chr17: 50332402-50332451	-
KLF5	2.94	1.08E-09	2.49	1.25E-08	1.77	2.24E-07	1.83	3.51E-08	chr13: 72530342-72530396	+
CBWD5	2.42	2.66E-06	1.83	6.79E-06	2.4	4.68E-07	2.05	6.03E-07	chr9: 69729627-69729676	-
DACH1	2.72	7.58E-08	2.53	3.34E-06	1.57	1.98E-06	1.87	2.51E-06	chr13: 71340031-71340087	+
CBWD2	2.59	5.51E-06	1.92	6.79E-06	2.37	4.23E-06	1.76	5.23E-06	chr2: 113912252-113912301	-
IFRD1	1.5	3.16E-07	2.73	3.16E-07	2.04	8.31E-09	1.65	4.14E-07	chr7: 111876650-111876702	-
AXIN2	3.52	6.42E-07	3.04	8.23E-07	1.49	4.68-07	2.17	8.31E-09	chr17: 60988928-60988982	+
LGR5	NA	NA	1.69	4.13E-07	1.59	5.94E-09	0.79	2.61E-02	chr12: 70119080-70119131	+
NKD1	2.22	7.57E-08	1.60	1.56E-09	0.83	4.16E-04	2.42	2.50E-06	chr16: 49137941-49137998	+
SP5	1.3	3.81E-03	2.72	1.75E-02	1.45	1.56E-08	1.08	2.18E-03	chr2: 171279606-171280055	+

Figure 1
Click here to download high resolution image

Figure 1

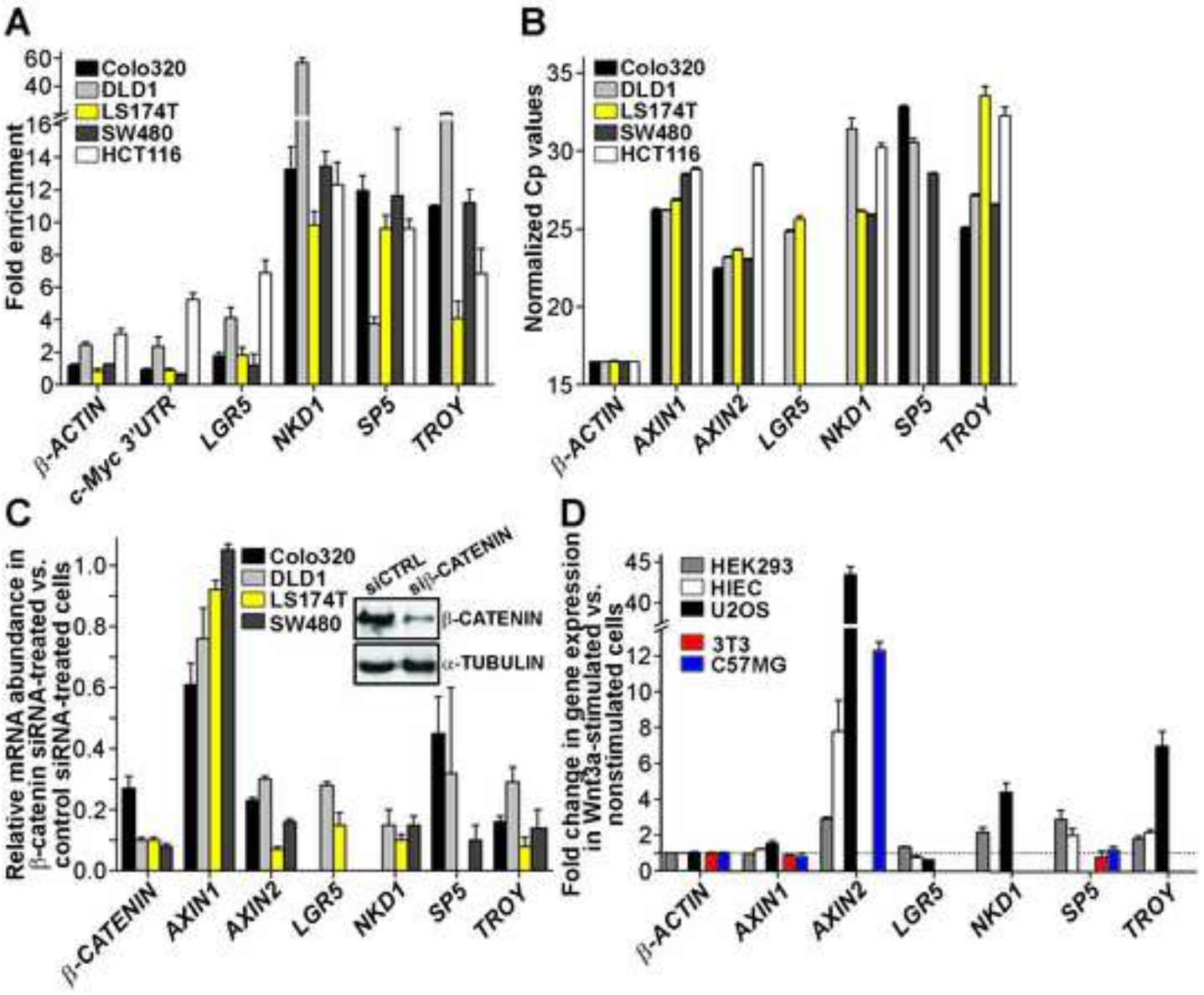

Figure 2
Click here to download high resolution image

Figure 2

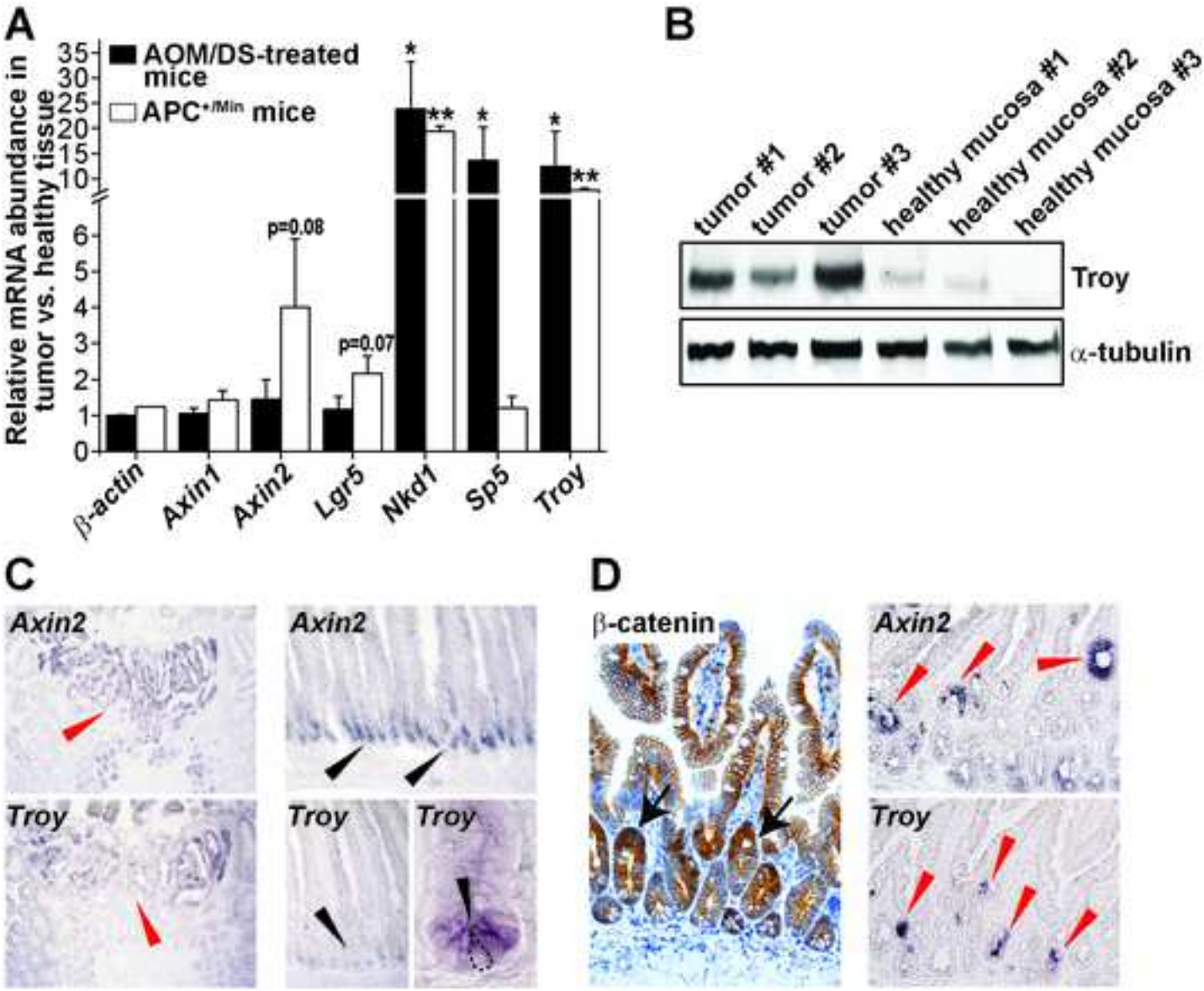

Figure 3
Click here to download high resolution image

Figure 3

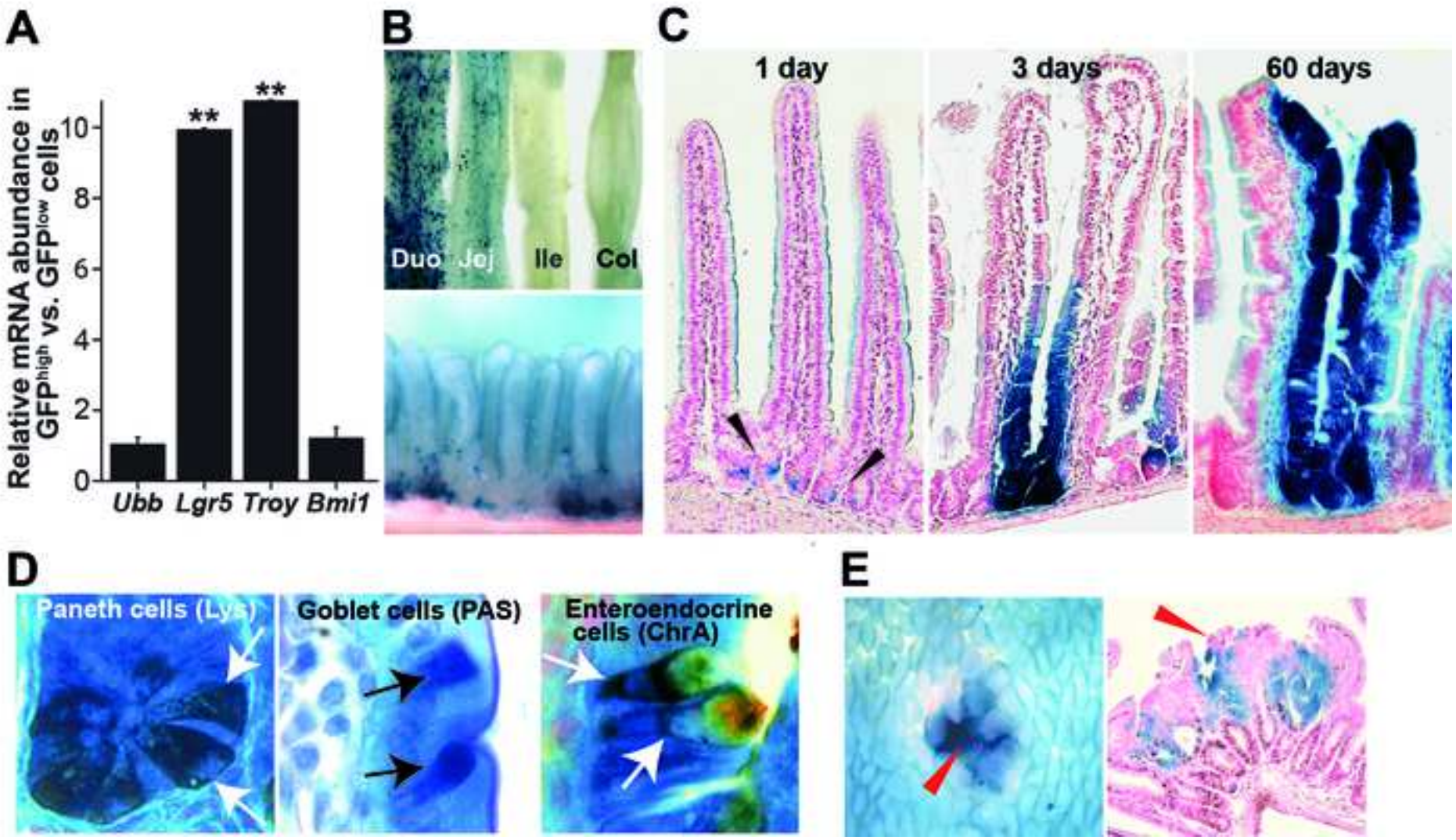

Figure 4
Click here to download high resolution image

Figure 4

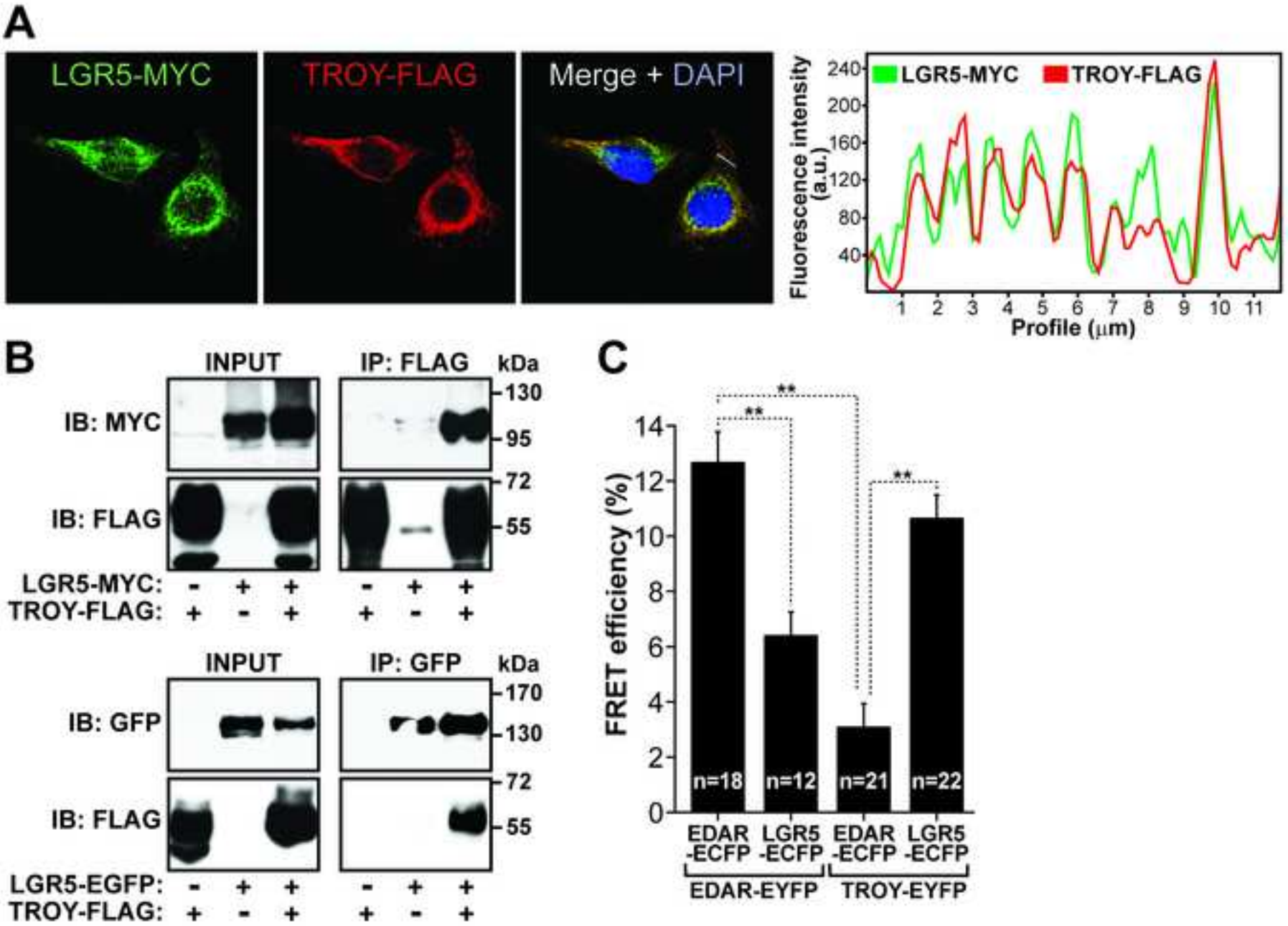

Figure 5
Click here to download high resolution image

Figure 5

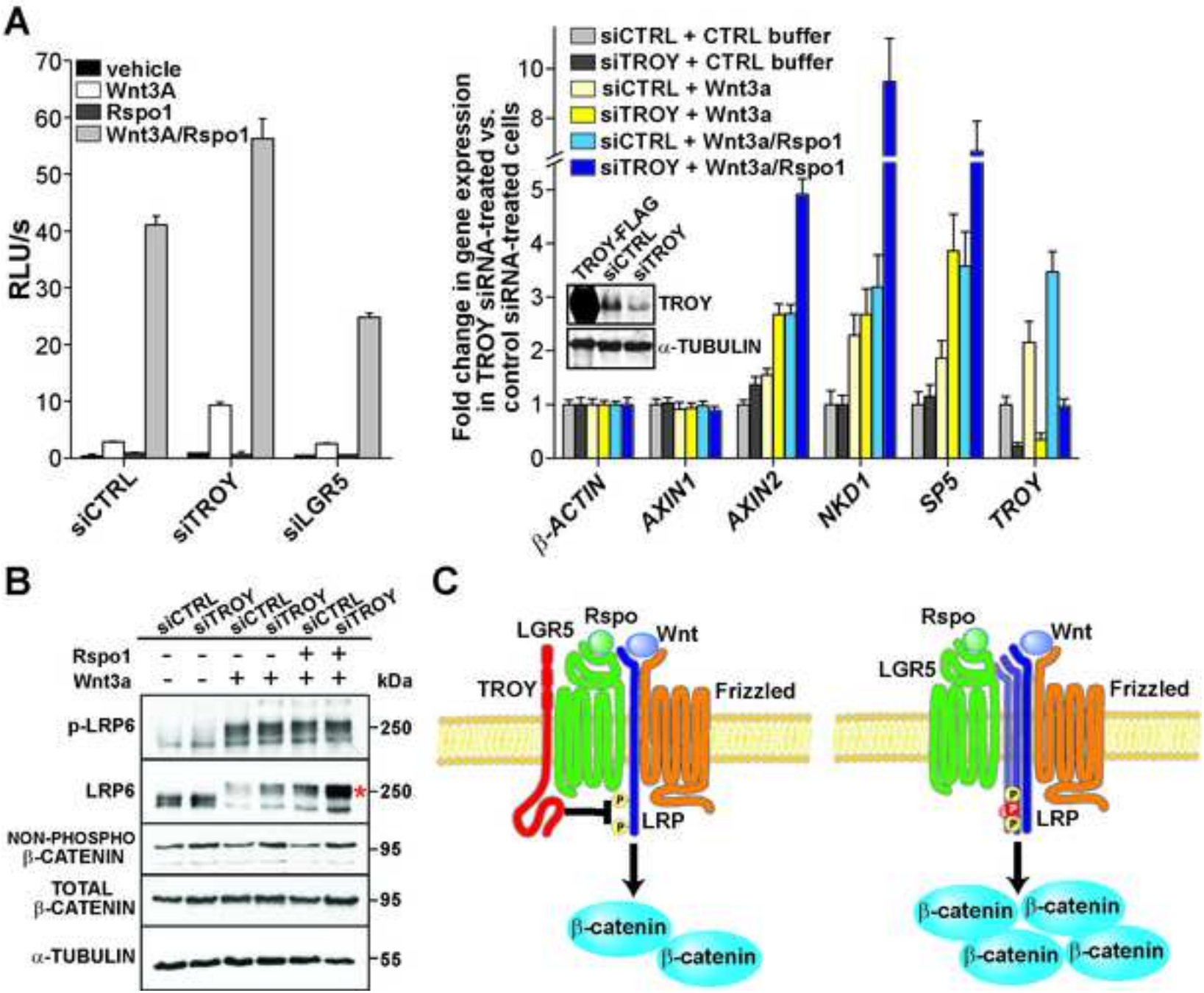

Figure 6
Click here to download high resolution image

Figure 6

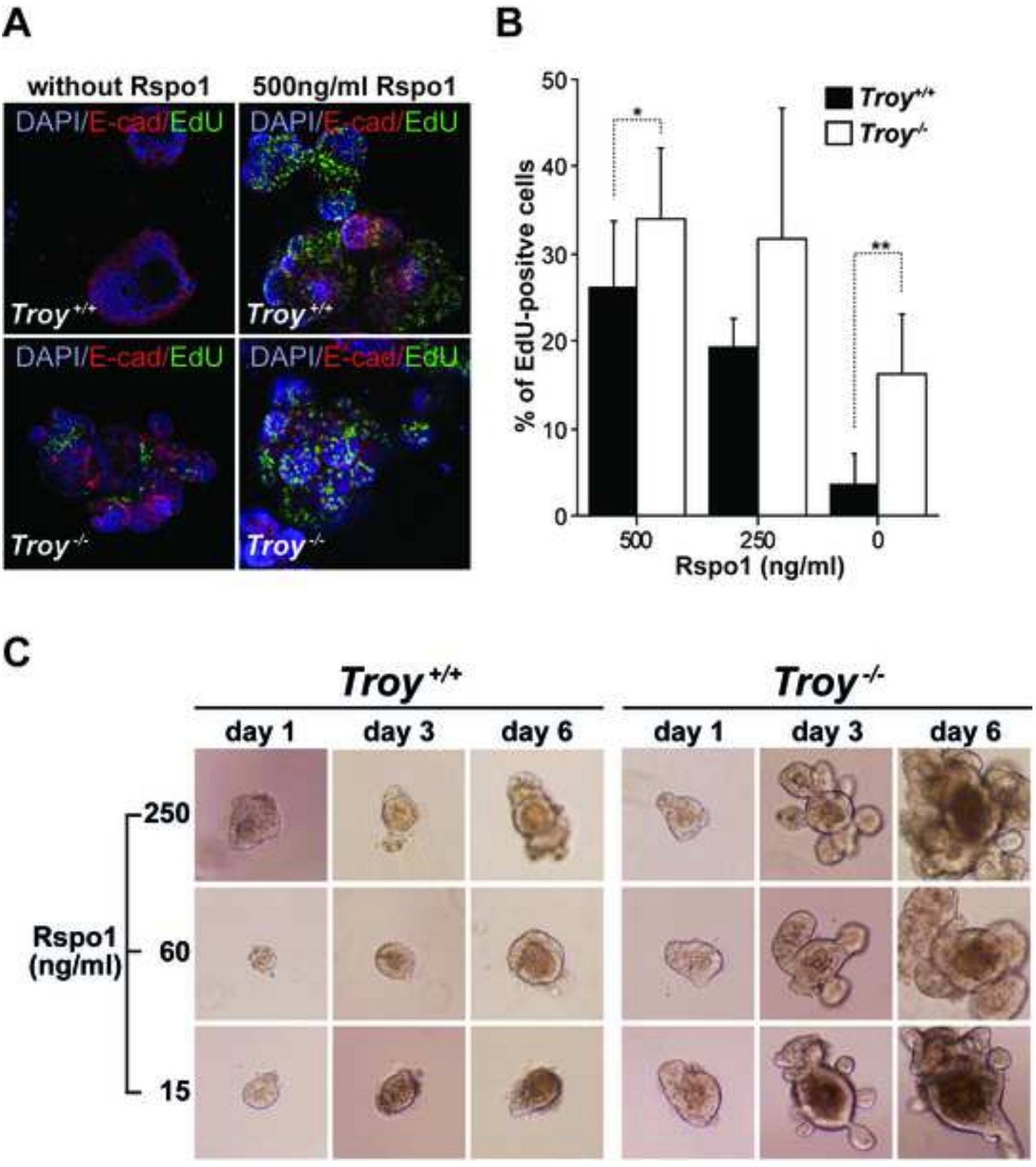

Supplemental Material

Supplemental Methods

Cell Lines and Transfections

Human HEK293, Colo320, DLD1, HCT116, HeLa, LS174T, SW480, U2OS cells and mouse 3T3, C57MG and Wnt3a-producing L cells were used for the experiments. All cell lines were maintained in Dulbecco's modified Eagle's medium [(DMEM); purchased from Sigma)] supplemented with 10% fetal bovine serum (Gibco), penicillin, streptomycin and gentamicin (Invitrogen). Transfections were performed using Lipofectamine RNAiMAX or Lipofectamine 2000 reagent (Invitrogen).

ChIP-on-chip Data Analysis

The results of hybridizations were obtained in a gff file format (Nimblegen). The fluorescent intensity peaks in corresponding areas of the microarray were identified by "triangle shape model" described by Kim and colleagues.[1] The peaks were used to define the threshold for "positive" probes. Enrichment of positive probes was then calculated using chi-square of the actual number compared to the expected number of positive probes in a given window.[2] The p-value listed in Table 1 and Supplementary Table S8 is the best (=smallest) p-value assigned to a probe located in the peak region.

Plasmids and Constructs

Proteins with a C-terminal FLAG or MYC tag were produced from pCMV-FLAG/MYC vector (Sigma). Fluorescently tagged proteins were generated in pECFP-N, pEGFP-N, pEYFP-N (Clontech) and pTaqBFP (Evrogen) vectors. The construct encoding the N-terminally truncated variant of human LRP6 protein (LRP6ΔN)[3] in the pCS2 vector was kindly provided by V. Bryja.

Coimmunoprecipitations and Western Blotting

The following antibodies were used: mouse anti-β-catenin, (clone E5; Santa Cruz); rabbit anti non-phospho-β-catenin/S33/S37/T41 (polyclonal; Santa Cruz); rabbit anti-Dvl2 (30D2; Cell Signaling); mouse anti-FLAG (M2; Sigma); mouse anti-GFP (JL-8; Clontech); goat anti-GFP (polyclonal; a gift of D. Stanek); mouse anti-MYC (9E10; Roche); rabbit anti-MYC (71D10; Cell Signaling); rabbit anti-LRP6 (C5C7; Cell Signaling); rabbit anti-phospho-LRP6/Ser1490 (polyclonal; Cell Signaling); rabbit anti-phospho-LRP6/T1572 (polyclonal; Millipore); mouse anti-TROY (ab55043, Abcam); mouse anti-α-tubulin (TU-01; Exbio CZ).

FRET

HeLa cells were transfected with the corresponding constructs. Twenty-four hours after transfection the cells were fixed in 4% (w/v) paraformaldehyde/PIPES buffer (10 min, at room temperature). After rinsing with PBS and distilled water, cells were embedded in glycerol containing DABCO (Sigma). Intensities of ECFP (excited by 405 nm laser set to 5-10% of maximum power) and EYFP (excited by 514 nm laser line set to 2-10% of maximum power) fluorescence were recorded. Subsequently, EYFP was bleached in the region of interest by four intensive (80% maximum power) pulses of 514 nm laser beam and ECFP- and EYFP-emitted fluorescence was measured again. The apparent FRET efficiency was calculated according to the equation: FRET efficiency {%} = (ECFP after -ECFP before) × 100/ECFP after. Unbleached regions of the same cell were used as negative control.

Rspo Binding Assay

Human U2OS or HeLa cells were transiently co-transfected with a combination of LGR5-EYFP and TROY-TagBFP or with LGR5-EYFP and "empty" pTagBFP vector. The next day, cells were incubated (1 hour, 37^{o}C) with conditioned medium containing recombinant mouse Rspo1 containing the constant region of the mouse immunoglobulin G2a heavy chain (IgG2a).[4] In control staining, the cells were incubated with recombinant IgG2a alone. Conditioned media were harvested from HEK293 cells transiently transfected with constructs encoding mouse Rspo1-IgG2a or IgG2a proteins (the constructs were kindly provided by V. Bryja; media were harvested 3 days upon transfection). The presence of recombinant proteins in culture media was verified by Western blotting using the goat anti mouse secondary antibodies (BIO-RAD). Cells were washed twice with PBS and fixed for 10 min in 4% (w/v) paraformaldehyde in PBS. Rspo1-IgG2a or IgG2a retained on the cell surface was visualized by a goat anti-mouse IgG2a Alexa Fluor 594 secondary antibody (Life Sciences; 1:900 dilution, 1 hour at room temperature). Nuclei were counterstained with Draq5 stain (Biostatus Limited).

Generation of Stable Cell Lines

To obtain cells with inducible expression of human TROY, the Lenti-X Tet-On Advanced Inducible Expression System (Clontech) was used. HEK293 cells were transduced with recombinant lentiviruses producing the tetracycline-controlled transcription activator (rtTA) and selected without subcloning using G418 (Enzo Life Sciences; 0.5 mg/ml). Resistant cells were further transduced with lentivirus pLVX-Tight-Puro encoding full-length human *TROY* with the C-terminal FLAG tag. HEK293/TROY cells were selected and maintained in puromycin (Alexis; 2 μg/ml) and G418 (0.2 mg/ml).

Reporter Gene Assays

To test the effect of TROY on the Wnt-dependent transcription, TROY expression was induced in HEK293/TROY by doxycycline (Sigma; 1μg/ml). The cells were stimulated simultaneously with doxycycline, Wnt3a and/or human Rspo1 and analyzed 18 hours later. Reporter gene assays in siRNA-treated HEK 293 cells were performed in an analogous manner. To ensure effective downregulation of TROY, two days after the first transfection with TROY or control non-silencing siRNA the cells were lipofected with the same siRNA together with pTOPFLASH/pFOPFLASH and *Renilla* luciferase expression plasmid. Twenty-four hours upon the second transfection, Wnt3a and Rspo1 ligands were added to culture medium (separately or in combination). The cells were stimulated for an additional 18 hours, then harvested and analyzed.

AOM/DS Treatment

Tumors of the colon and rectum were collected from adult C57BL/6J mice five weeks after a single subcutaneous injection of AOM (10 mg/kg; Sigma) followed by a 5-day DS treatment in drinking water [3% (w/v) DS; MW 36-50 kDa; MP Biomedicals].

Generation of Troy-CreERT2 Transgenic Mice

The TROY-CreERT2 bacterial artificial chromosome (BAC) transgenic construct was generated using homologous recombination in bacteria according to the previously published protocol.[5] A BAC clone RP23-166C22 was purchased from imaGenes (Berlin, Germany); a construct containing CreERT2 cDNA was kindly provided by M. Cepko via Addgene. The adapters "a" (5'-CCTCTCGTCTTTGACTTGCATCCTTCAGGAATAAACACGTTT GGTGAGAGCCatgtccaatttactgaccgtac - 3'; the *Troy*-specific sequence is highlighted in capital letters, the part complementary to the CreERT2 expression cassette is given in small caps) and "b" (5'-TGATAGGAGTTCTTTCCCCATATTCATATGAAAGAGAAGAGGCAACTTACgccgctctaga actagtggatc - 3') were derived from the sequence of the exon containing the translation start site or from the flanking intron, respectively (Supplemental Fig. S5*A*). The adapters were employed for the PCR amplification, the product was purified from agarose gel and electroporated into the *E. coli* strain EL250 harboring the BAC clone RP23-166C22. Bacterial clones containing correctly recombined BACs were verified by PCR. Isolated recombinant BAC DNA was linearized and used for pronuclear injection of fertilized eggs (C57Bl/6J background). Three TROY-CreERT2 transgenic founder lines were produced using the service of the Transgenic Unit of the Institute of Molecular Genetics. All three lines exhibited a virtually identical pattern of the Cre recombinase activity.

RNA Probes and IHC

Antisense RNA probes were derived from the following regions of the analyzed genes: *Axin2* (NM_015732.4), nucleotides 2069-2938; *Lgr5* (NM_010195.2), nucleotides 373-887, *Troy* (NM_013869.5), nucleotides 763-1924. Antibodies for IHC: mouse monoclonal anti-β-catenin antibody (E5; Santa Cruz); anti-Chromogranin A (Abcam) and anti-Lysozyme (DAKO) rabbit polyclonal antibodies.

Processing of Specimens of Human Sporadic Colorectal Carcinomas and Precancerous Colorectal Lesions

Samples of the following macroscopically distinguishable tissue segments were taken from fresh colectomy specimens: (1) the center (stroma) of the tumor without, if any present, ulcerated luminal portion and the least necrotic parts of the lesion were preferred, and, (2) healthy surrounding mucosa were collected in the distance of a maximum of 5 cm from the primary tumor site. Pathological and morphological criteria included tumor location, pTNM classification, histological subtype, grade of differentiation and presence of vessel invasion (a summary is given in Supplemental Table S2). RNA was isolated from biological replicates of distinct tumor segments and healthy mucosa. Sporadic precancerous colorectal lesions were obtained during colonoscopies carried out at the Second Department of Internal Medicine, Third Faculty of Medicine, Charles University in Prague. Collection of each polyp was accompanied by two biopsies of normal mucosa from the rectosigmoideum region.

Histopathology of the lesions was evaluated on hematoxylin and eosin stained sections by two pathologists (a summary is given in Supplemental Table S3). Tissue samples were homogenized in RNA Blue reagent (TopBio, Czech Republic) using a T8 Ultra Turrax disperser (IKA). Total RNAs were extracted according to the manufacturer's protocol and subjected to RNA integrity number (RIN) analysis (Agilent 2100 Bioanalyzer; samples with RIN > 8 were used). Reverse transcription was performed using the RevertAid H Minus reverse transcriptase (Fermentas) with1.5 μg of total RNA using random hexanucleotide primers (Invitrogen). Negative controls were represented by input RNA processed in the absence of reverse transcriptase. PCR reactions were run in parallel triplicates for each primer set in Light Cycler 480 (Roche Applied Science). Two housekeeping genes, *UBIQUITIN B* (*UBB*) and *β-ACTIN* were used as internal controls. Primer sequences are listed in Supplemental Table S1.

The APC Mutation Analysis

Genomic DNA was extracted from deep-frozen samples of tumor tissue and healthy surrounding mucosa using the DNeasy Blood & Tissue Kit (Qiagen). Seven PCR fragments partially

covering the sequence of human *APC* exon 18 and two fragments corresponding to *β-CATENIN* (*CTNNB1)* exons 3 and 4, including intron-exon boundaries, were amplified using gene-specific primers (Supplemental Table S4) containing overhangs recognized by T7 (5'-TAATACGACTCACTATAG - 3') and RP (5'-TGAAACAGCTATGACCATG - 3') universal sequencing primers. PCR was performed in 38 cycles with 30 second primer annealing at 60°C and 45 second extension at 71°C. Each fragment was directly sequenced from both sides using the BigDye® Terminator v3.1 cycle sequencing kit and ABI 3130 Genetic Analyzer (Applied Biosystems).

Statistical Analysis of RT-qPCR Data of Colorectal Cancer Samples

RNA isolated from each specimen (biological replicate) of tumor or healthy mucosa was subjected to the RT-qPCR analysis; the PCR reactions were performed in triplicates. In each technical replicate, Cp's were normalized using *β-ACTIN* as a reference gene to obtain ΔCp's and averaged. Principal component analysis (PCA) on ΔCp's of biological replicates identified one outlying patient. All samples of this patient were removed and the remaining 76 samples of 19 patients were used in downstream statistical analyses. To detect differences in expression, we applied Wilcoxon's rank-sum test. To account for different genetic background of the patients, we further fitted a linear model (REML) described by the formula ΔCp ~ patient + tissue/(stage * mutation), with biological replicates treated by a random effect and all healthy mucosa samples treated as a single group and validated the results. No correction of multiple testing was applied. Statistical significance was estimated at the level of 0.05 (or 0.01 and 0.001) and marked by asterisk (or ** and ***) in Supplemental Figure S2. All analyses were performed in R language/environment.

Statistical Analysis of RT-qPCR Data of Precancerous Lesions

Messenger RNA obtained from 35 samples of precancerous lesions of the colon and matching healthy mucosa was subjected to RT-qPCR analysis. Cp´s of individual technical triplicates were normalized by geometric average of internal control genes *β-ACTIN*, *AXIN1* and *UBB* and averaged (ΔCp). PCA revealed that specimens of one patient were deemed outlying and were consequently omitted from further statistical analyses. Differential expression was evaluated as described for colorectal cancer samples.

Bisulfite Analysis of Cytosine Methylation

Genomic DNA (0.5 μg) isolated from tumor center and matched healthy surrounding mucosa was subjected to bisulfite conversion using the EZ DNA Methylation™ Kit (Zymo Research). Bisulfite-treated DNA was amplified by nested PCR using the following primers: for primary amplification oligonucleotides 5´-ATTTTATTGGTGGAAAAGTATTTTAT-3´ [forward; priming on nucleotides (nt) -672 to -647 upstream from the *TROY* genes transcription start (according to sequence

NM_001204458.1)], and 5′-AACTTACTCTACAACTAAATTCTTTAA-3′ (reverse; nt -163 to -137). The PCR product was re-amplified using primers 5′-TTTTTTTAGTAAAATTGTTTAGTGAGTTTT -3′ (forward; nt -629 to -600) and 5′-AATAAATATAAAACTAACTAAAAACTTAAAAATA-3′ (reverse; nt -225 to -193). Cytosines (not included in CpG dinucleotides) were changed to T or A in forward and reverse primers, respectively. Amplification products were cloned into the pGEM-T-Easy vector (Promega) and sequenced. Nine to twelve independent PCR clones with at least 95% conversion of cytosine outside of CpG dinucleotides were analyzed.

Paneth Cells Sorting

Single cells from crypts were obtained as in reference[6]. Cells were stained with phycoerythrin (PE)-conjugated anti-CD24 antibody (eBioscience), allophycocyanin (APC)-conjugated anti-Epcam antibody (eBioscience) and FITC-conjugated anti-CD45 antibody (ExBio) for 30 min at 4°C, and sorted by Influx cell sorter (BD Biosciences).

Organoid Proliferation Assay

Freshly isolated crypts were cultured for 6 days in crypt culture medium containing Rspo1 (250 ng/ml). Crypt-derived multicellular organoids were removed from Matrigel (BD Biosciences), mechanically dissociated and then transferred to fresh Matrigel and medium (split ratio 1:4) containing various concentrations (0 to 500 ng/ml) of Rspo1. Cell proliferation was visualized by a Click-iT™ EdU Imaging Kit (10 μM EdU incorporation for 1 hour at 37°C) according to manufacturer's instructions (Invitrogen). Organoids were further stained with an anti-E-cadherin antibody (Zymed) and DAPI and imaged using a Leica Sp5 confocal microscope. The proliferation rate was determined by counting of EdU-positive vs. DAPI-positive cells; at least 10 organoids were evaluated per each genotype and Rspo1 concentration. The organoids prepared from 3 mice of corresponding genotype were grown in quadruplicates for each concentration of Rspo1. Statistical significance was estimated by the Student's t-test.

Supplemental Results

Troy expression in the mouse colon

To detect Troy expression in the colon two experimental approaches were used. First, *in situ* hybridization was performed; however, our attempts to visualize *Troy* mRNA were not successful. Secondly, Troy-CreERT2^{+}/Rosa26R mice were used to detect Cre/LacZ-expressing cells in the colonic tissue. Recombined (i.e. blue) cells were observed – although at lower frequency than in the small intestine – at the bottom of the colonic crypts one day after the induction of Cre. Lately, the labeled cell clones spread to the luminal surface and persisted in the colon for several months (Supplemental Figure S5*G*). This result indicated that similarly to the small intestine epithelium, Troy-positive cells are self-renewing stem cells. The low frequency of the blue clones in the colon was rather unexpected as endogenous *Troy* expression (similar to the *CreERT2* production from the transgene) is abundant in the colon (Supplemental Figure 5*E*). A similar phenomenon was observed by Powel and colleagues in Lgr5-EGFP-IRES-CreERT2 mice.[7] Interestingly, in the same study induction of a remarkably greater number of labeled colonic crypts (compared to the Lgr5-CreERT2 mice) was observed in Leucine-rich repeats and immunoglobulin-like domains (Lrig) 1-CreERT2 reporter mice. Since Lrig1 marks noncycling, long-lived stem cells, these data indicate that the recombination of the transcription "roadblock" cassette is inefficient in highly proliferative Lgr5- or Troy-positive cells of the colon.

TROY expression profiling in sporadic colorectal carcinoma and premalignant lesions

Two biological replicates of both tumor and healthy tissue were obtained from each individual and used for sequence analysis of the *APC* gene. The analyses encompassed the somatic mutation cluster region of *APC* as well as flanking regulatory sequences encoding elements required for the β-CATENIN interaction and downregulation [nucleotides 1959 to 4945 (numbering was taken from the sequence NM_000038.5)].[8] Putatively inactivating mutations of *APC* were found in 11 out of 20 patients (55%), which is in concordance with published data.[9] Of note, since the mutational analysis was covering only a "hot spot" of the *APC* gene, we cannot exclude that not all mutations in the *APC* sequence have been detected. No oncogenic mutations were detected in the somatic hotspot regions of exons 3 and 4 of *β-CATENIN* (summary of the *APC* mutations can be found in Supplemental Table S5).

To analyze differences in the expression of *AXIN2*, *LGR5* and *TROY* genes in tumor tissue versus healthy mucosa, we applied non-parametric Wilcoxon's test. In addition, to account for

histopathological variations in specimens obtained from different patients we used a linear model (REML). Both statistical analyses clearly showed significant correlation between the presence of the inactivating *APC* mutations and expression levels of the *AXIN2* gene (Supplemental Figure S2*A*; p- and other values are indicated in Supplemental Table S6). This result was in agreement with previously published data.[10] On the other hand, *LGR5* mRNA was increased in tumor tissues irrespective of the *APC* status. The *TROY* expression levels did not follow any conclusive expression pattern, moreover we detected a decrease in *TROY* expression in the majority of tumors. To study a molecular mechanism of possible *TROY* silencing in tumor tissue, genomic DNA isolated from specimens with elevated and decreased *TROY* expression was subjected to the cytosine methylation analysis. The analysis of the sequence containing 35 CpG doublets located in the proximity of the *TROY* transcription start (see Supplemental Methods for details) in two carcinomas with reduced *TROY* expression revealed that only 2 and 14% of analyzed CpG dinucleotides were methylated (Supplemental Fig. S2*B*). This implied that the observed reduction in *TROY* expression is not related to changes in the DNA methylation status. In addition, the analysis of *TROY* expression in thirty-five premalignant lesions of the colon was performed. In polyps, *AXIN2* and *LGR5* displayed a significant increase in mRNA levels (compared to healthy mucosa tissue). Expression of both genes strongly correlated with the grade of the neoplastic tissues showing elevated expression in more progressed lesions. These results were in good concordance with published data.[11] In contrast, *TROY* mRNA was decreased in the majority of premalignant lesions irrespective of their histological category (Supplemental Figure S3 and Supplemental Table S7).

Supplemental Acknowledgments

We thank J. Dobes and J. Tureckova for help with sorting and RT-qPCR analysis of Paneth cells. We also thank O. Sebesta for help with microscopy.

Supplemental Figure and Table Legends

Supplemental Figure S1. Summary of the ChIP-on-chip analysis. Venn diagram depicts the numbers of promoter regions bound by TCF4 in each cell line (the selection criterion is defined in the Table 1 legend). Of 960 genes identified, 18 genes scored positive in all four cell lines.

Supplemental Figure S2. *TROY* expression does not correlate with the *APC* status in human colorectal cancer. (*A*) Comparison of relative expression levels of *AXIN2*, *LGR5* and *TROY* genes in sporadic colorectal tumors (T) compared to surrounding healthy mucosa (HM) samples. Individual Cp values were normalized to the level of the housekeeping gene *β-ACTIN* to obtain a log of relative expression levels (-ΔCp) and averaged. Tumors were assigned to four distinct subgroups with respect to the *APC* mutation status (WT, wild-type *APC*; MUT, *APC* mutated) and disease stage. Stage grouping: the "early stage" encompasses tumors classified 0 to IIC according to the 7th Edition of the American Joint Committee on Cancer (AJCC) Cancer Staging Manual. Stages of advanced colorectal disease (IIIA-IV) constitute the subgroup designated as the "advanced stage". Median of ΔCp values for each respective subgroup is indicated by the red line. The differences in the expression levels of a selected gene in the given groups and their statistical significance were tested by Wilcoxon's rank-sum test (solid line) and a linear model (REML, dashed line), which accounted for tissue type, *APC* status, stage and biological background of the patients. *, $p < 0.05$; **, $p < 0.01$; ***, $p < 0.001$. Data accompanying this figure can be found in Supplemental Table S6. (*B*) Cytosine methylation analysis of the CpG island located upstream of the *TROY* promoter. The analysis was performed on genomic DNA isolated from tumors with "high" (normalized Cp<25.5) or "low" (Cp> 31) *TROY* expression. Both early and advanced stage tumors were assayed as indicated. Open circles mark unmethylated CpG dinucleotides, while closed circles indicate methylated CpGs. Tumor samples (T) are depicted in red, matched healthy surrounding mucosa (HM) in black.

Supplemental Figure S3. *TROY* expression is decreased in precancerous lesions of the human colon. Comparison of relative expression levels of *AXIN2*, *LGR5* and *TROY* genes in sporadic premalignant lesions (P) of human colon and matching healthy mucosa (HM) samples. Based on prevailing microscopic appearance, lesions were subdivided to three histological categories: hyperplasia (H), low grade dysplasia (LGD) and high grade dysplasia (HGD). Median of ΔCp values in individual subgroups is indicated by the red line. Statistical significance of differences in expression levels was examined by nonparametric Wilcoxon´s rank-sum test (solid line). Moreover, a linear model (REML; dashed line) encompassing tissue type, histology and individual biological background

of the patients was applied. *, $p < 0.05$; **, $p < 0.01$; ***, $p < 0.001$. Data accompanying this figure can be found in Supplemental Table S7.

Supplemental Figure S4. Analysis of Troy expression in the small intestine using ISH and fluorescence-activated cell sorting (FACS). (*A*) Left, ISH of *Troy* mRNAs in jejunum showing expression in the lower parts of the crypts (black arrowheads). Right, colocalization of Troy-expressing and CBC cells in the intestine. Frozen sections prepared from Lgr5-EGFP-IRES-CreERT2 mice were stained using ISH for *Troy* mRNA (black arrowhead). The slides were mounted in glycerol and the results recorded. Next, the cover slips were removed and the CBC cells were visualized in the same specimen using IHC detection of GFP protein (brown arrowheads). (*B*) FACS of $Lgr5^{+}$ cells. Left, fresh isolates of the crypts from the small intestine of Lgr5-EGFP-IRES-CreERT2 mice. A detailed confocal image of one crypt stained with DAPI nuclear stain is shown in bottom panel. The putative CBC stem cells located at the base of each crypt are marked by EGFP expression. Right, diagrams of the cell-sorting procedure. Three cell populations (GFP^{high}, GFP^{low}, $GFP^{negative}$) were obtained from the crypts of Lgr5-EGFP-IRES-CreERT2 mice. GFP^{high} and GFP^{low} cells, which are not present in the intestine of control wild-type (WT) mice, were used for the subsequent RT-qPCR analysis. The crypt isolations were performed as described in the reference.[12] (*C*) Cell sorting of Paneth cells. Left, FACS plots of dissociated single cells from small intestinal crypts of wild-type mice. Viable single cells were gated by forward scatter, side scatter, pulse-width parameter and negative staining for Hoechst 33258. Epithelial cells ($CD45^{-}Epcam^{+}$) were sorted in three gates. Two CD24 bright populations differed by side-scatter (SSC) pattern. Sorted $CD24^{high}SSC^{low}$ population (Gate 1) corresponds to enteroendocrine cells and $CD24^{high}SSC^{high}$ cells are Paneth cells (Sort 2 gate). Right, RT-qPCR from sorted cells, Sort 2 vs. Sort 3 gate ($CD24^{low}$) illustrates that *Troy* (and *Lgr5*), unlike the Paneth cell markers *Lysozyme (Lys)* and *Defensin α 20 (Defa20)*, is not enriched in Paneth cells. Original magnification: (*A*) left panel 100 ×, right panel 400 ×; (*B*) upper panel 200 ×, lower panel 400 ×.

Supplemental Figure S5. Tracking the Troy expression using the *Troy-CreERT2* BAC transgenic allele. (*A*) CreERT2 was inserted in frame into the first coding exon of the mouse *Troy* gene. The non-coding or translated regions are depicted by empty and black boxes, respectively. *a,b*, Troy sequences employed for the homologous recombination into the BAC clone RP23-166C22. *RGB poly A*, a poly A signal derived from the rabbit *β-globulin* gene; Kan^{r}, the *kanamycin* resistance gene; *pBla*, *β-lactamase* promoter. Prior to pronuclear injection, the bacterial resistance cassette was excised from recombinant BAC using Flp recombinase and FRT sites (black semicircles) flanking the cassette. (*B*) The whole-mount hybridization of wild-type mouse embryo at embryonic day (E) 14.5 using an antisense probe against *Troy*. (*C*) The activity of CreERT2 recombinase produced from the Troy-CreERT2 BAC transgene was visualized at E 14.5 in embryos derived from crossing of Troy-

CreERT2 and Rosa26R mice. Tamoxifen was injected intraperitoneally into pregnant females. The animals were sacrificed one day later; embryos were removed and used to stain the LacZ-expressing tissues. The CreERT2 expression pattern visualized by the X-gal substrate phenocopies the sites of expression of endogenous *Troy* mRNA and its localization is also in concordance with the *Troy* expression pattern described previously.[13, 14] cb, cerebral plate; drg, dorsal root ganglion; e, ear; ma, maxilla; mg, mammary gland primordium; v, vibrissae. (*D*) Frequency of Cre-mediated recombination in different anatomical parts of the intestine of Troy-CreERT2^{+}/Rosa26R mice. Three mice were injected with tamoxifen and sacrificed 60 days later. Percentage of positive (i.e. blue) crypts in duodenum (Duo), jejunum (Jej), ileum (Ile) and colon (Col) is indicated with given SD in parentheses. Notice that the image was taken from Figure 3*B*. (*E*) RT-qPCR profiling of the *CreERT2* and *Troy* genes in intestinal mucosa dissected from different parts of the gastrointestinal system. The tissues were obtained from four Troy-CreERT2 transgenic mice or from their wild-type littermates (n=4). (*F*) Localization of LacZ-positive cells in the crypts of Troy-CreERT2^{+}/Rosa26R mice 1 day after tamoxifen administration. The diagram depicts frequency of occurrence of blue cells at specific positions in the crypt; the positions are indicated in the scheme in the inset. Four hundred crypts from the proximal part of the small intestine of two mice were counted. Results are depicted as means with SDs. Most of the LacZ-expressing cells occurred in the bottom part of the crypt, whereas less than 6% of these cells were observed at the +5 position or higher. (*G*) Cell lineage tracing in the colon of Troy-CreERT2^{+}/Rosa26R mice 1 day and 60 days after tamoxifen administration. Black arrowheads indicate LacZ-positive cells emerging 1 day upon induction. Original magnification: 100 ×.

Supplemental Figure S6. LGR5 interacts with the TROY-related receptor EDAR. Co-immunoprecipitation of MYC-tagged EDAR or MYC-tagged TROY with LGR5-FLAG. In panels indicated as ”INPUT”, 20% of the total lysate used for one immunoprecipitation was loaded. AB, the precipitation was performed without cell lysates; NT, lysate from non-transfected cells was precipitated; IP, immunoprecipitation; IB, immunoblotting.

Supplemental Figure S7. (*A*) Downregulation of TROY does not potentiate TCF/β-catenin-mediated transcription in human CRC cells. Results of the RT-qPCR analysis of indicated genes in TROY siRNA-treated vs. control siRNA-treated cells. The Wnt/β-catenin non-responsive gene *AXIN1* was also included in the test. Cp values were normalized to the *β-ACTIN* expression levels (Cp=16.5). The histogram represents mean Cp values of a representative experiment performed in triplicates (repeated twice). The expression level of a given gene in cells transfected with control non-silencing siRNA and treated with vehicle was arbitrarily set to 1. Missing bars stand for unexpressed gene (normalized Cp>35). (*B*) The effect of ectopic TROY was tested in HEK293/TROY cells with doxycycline-

inducible expression of TROY transgene. RT-qPCR analysis of cells grown with or without doxycycline (DOX) and stimulated with Wnt3a and/or Rspo1 ligands.

Supplemental Figure S8. The most proximal events triggered by Wnt or Rspo ligand are not influenced by TROY. (*A*) TROY does not interfere with binding of Rspo1 to LGR5. Laser scanning confocal microscopy images of U2OS cells transfected with equimolar amounts of constructs expressing LGR5-EYFP (green) and TagBFP (pseudocolored in red; upper panels) or LGR5-EYFP and TROY-TagBFP (lower panels). Cells grown on cover slips were incubated with conditioned medium containing Rspo1-IgG2a fusion protein. The cell surface binding of Rspo1-IgG2a to its receptor LGR5 was detected using Alexa Fluor 594 anti-IgG2a antibody (gray). Recombinant IgG2a alone did not display any nonspecific binding to the cells (not shown). Nuclear counterstain Draq5 (gray) is omitted from the overlay images for clarity. (*B*) Colocalization analysis of LGR5 with its ligand Rspo1 in the presence of TagBFP (left panel) or TROY-TagBFP (right), respectively. The analysis was performed using the intensity correlation analysis (ICA) plug-in for ImageJ image processing program.[15] Areas displaying colocalization of the proteins were pseudocolored in white; the areas with non-overlapping localization are shown in black. Original magnification: 1000 ×. (*C*) Dvl phosphorylation is not affected by *TROY* knockdown. The western blot of whole-cell extracts prepared from HEK293 cells treated with non-silencing or TROY siRNA and further stimulated as indicated. The putative phosphorylated form of Dvl with changed mobility in the gel is marked by arrow.

Supplemental Figure S9. Stereomicroscopic images of the intestinal organoids derived from wild-type or *Troy*$^{-/-}$ mice. Organoids grown for 6 days in complete crypt culture medium were mechanically dissociated and then transferred to Matrigel and fresh medium with or without Rspo1 ligand. The images of the same organoids were taken for 5 consecutive days as indicated. Original magnification: 20 ×.

Supplemental Table S1. Sequences of primers used for ChIP and RT-qPCR analyses. The sequence of the forward primer is given in the upper line with the corresponding reverse primer in the lower line, respectively.

Supplemental Table S2. Clinical and histopathological features of colorectal cancer patients. Tumors were classified according to the 7th edition of AJCC Cancer Staging Manual.

Supplemental Table S3. Clinical and histopathological characteristics of patients with precancerous lesions of the colon. Polyps were classified according to the Vienna Classification of gastrointestinal epithelial neoplasia.[16]

Supplemental Table S4. Sequences of primers utilized to amplify selected *APC* and *β-CATENIN* exons. The sequence-specific portion of the primer is highlighted in capital letters; the T7 and RP adaptor primers are in small caps. [1)] Exon and nucleotide numbering according to NM_000038.5; [2)] primer sequence situated in intron 55 bps upstream of exon 18; [3)] primer sequence situated in intron 134 bps upstream of exon 3; [4)] primer sequence situated in intron 172 bps downstream of exon 3; [5)] primer sequence situated in intron 111 bps upstream of exon 4; [6)] primer sequence situated in intron 84 bps downstream of exon 4.

Supplemental Table S5. Summary of detected *APC* mutations in samples of sporadic human colorectal carcinomas. The sequenced region of the *APC* exon 18 encompasses c.1959-c.4945 (NM_000038.5) including the exon 18´s 5´ intron-exon boundary. [1)] Mutation identifiers: "c" syntax indicates the type and localization of the mutation in the *APC* cDNA coding sequence (CDS; NM_000038.5); "p" syntax indicates the position and change in the protein; see the reference Forbes et al., 2010 for details[17]; [2)] according to PolyPhen prediction analysis[18] this substitution is scored as possibly damaging (it is supposed to affect the protein function or structure; PSIC score difference: 1.773); [3)] according to PolyPhen prediction analysis, this substitution is considered benign (no evidence for damaging effect is seen; PSIC score difference: 1.386); [4)]the presence of single nucleotide polymorphism (SNP) at *APC* c.4479 (G/A; rs41115) indicated that heterozygosity status in a tumor sample was preserved (wt; patients #20 and #14) or lost (LOH; patients #1, #2 and #18). In the absence of *APC* c.4479 polymorphism (c.4479 A/A; patients #15 and #6), the information concerning zygosity status of the *APC* locus is not available (n.a.). [5)] In cases of carcinomas that display a reduction to homozygosity at c.4479 (patients #2 and #18), the presence of the *APC* inactivating mutations is presumed although it was not detected (n.d.) in the analyzed region (see reference[19] for additional information). All tumors listed in Supplemental Table S5 constitute the subgroup of the APC-deficient tumors [designated as "APC mut" in downstream statistical analyses (Supplemental Figure S2 and Supplemental Table S6)].

Supplemental Table S6. Statistical analysis of tumor expression profiles (data accompanying Supplemental Figure S2). Individual Cp values were normalized to the expression level of the *β-ACTIN* housekeeping gene to obtain relative expression levels (-ΔCp) and averaged. Biological replicates were further treated by a random effect and all HM treated as a single group (ΔΔCp). FC, fold change.

Supplemental Table S7. Statistical analysis of expression profiles of precancerous lesions of human colon (data accompanying Supplemental Figure S3). Individual Cp values were normalized using geometric average of three housekeeping genes (*β-ACTIN*, *AXIN1* and *UBB*) to obtain relative expression levels (-ΔCp) and averaged. All healthy mucosae were treated as a single group (ΔΔCp). FC, fold change.

Supplemental Table S8. A complete list of genes identified by Chip-on-chip using the TCF4-specific antibody and chromatin isolated from Colo320, DLD1, LS174T and SW480 CRC cells.

Supplemental References

1. Kim TH, Barrera LO, Zheng M, et al. A high-resolution map of active promoters in the human genome. Nature 2005;436:876-80.
2. Scacheri PC, Crawford GE, Davis S. Statistics for ChIP-chip and DNase hypersensitivity experiments on NimbleGen arrays. Methods Enzymol 2006;411:270-82.
3. Tamai K, Zeng X, Liu C, et al. A mechanism for Wnt coreceptor activation. Mol Cell 2004;13:149-56.
4. Ootani A, Li X, Sangiorgi E, et al. Sustained in vitro intestinal epithelial culture within a Wnt-dependent stem cell niche. Nature medicine 2009;15:701-6.
5. Yang XW, Model P, Heintz N. Homologous recombination based modification in Escherichia coli and germline transmission in transgenic mice of a bacterial artificial chromosome. Nature biotechnology 1997;15:859-65.
6. Sato T, van Es JH, Snippert HJ, et al. Paneth cells constitute the niche for Lgr5 stem cells in intestinal crypts. Nature 2011;469:415-8.
7. Powell AE, Wang Y, Li Y, et al. The pan-ErbB negative regulator Lrig1 is an intestinal stem cell marker that functions as a tumor suppressor. Cell 2012;149:146-58.
8. Miyoshi Y, Nagase H, Ando H, et al. Somatic mutations of the APC gene in colorectal tumors: mutation cluster region in the APC gene. Human molecular genetics 1992;1:229-33.
9. Smith G, Carey FA, Beattie J, et al. Mutations in APC, Kirsten-ras, and p53--alternative genetic pathways to colorectal cancer. Proc Natl Acad Sci U S A 2002;99:9433-8.
10. Lustig B, Jerchow B, Sachs M, et al. Negative feedback loop of Wnt signaling through upregulation of conductin/axin2 in colorectal and liver tumors. Mol Cell Biol 2002;22:1184-93.
11. Cattaneo E, Laczko E, Buffoli F, et al. Preinvasive colorectal lesion transcriptomes correlate with endoscopic morphology (polypoid vs. nonpolypoid). EMBO Mol Med 2011;3:334-47.
12. Sato T, Vries RG, Snippert HJ, et al. Single Lgr5 stem cells build crypt-villus structures in vitro without a mesenchymal niche. Nature 2009;459:262-5.
13. Kojima T, Morikawa Y, Copeland NG, et al. TROY, a newly identified member of the tumor necrosis factor receptor superfamily, exhibits a homology with Edar and is expressed in embryonic skin and hair follicles. The Journal of biological chemistry 2000;275:20742-7.
14. Pispa J, Mikkola ML, Mustonen T, et al. Ectodysplasin, Edar and TNFRSF19 are expressed in complementary and overlapping patterns during mouse embryogenesis. Gene expression patterns 2003;3:675-9.
15. Li Q, Lau A, Morris TJ, et al. A syntaxin 1, Galpha(o), and N-type calcium channel complex at a presynaptic nerve terminal: analysis by quantitative immunocolocalization. The Journal of neuroscience : the official journal of the Society for Neuroscience 2004;24:4070-81.
16. Schlemper RJ, Riddell RH, Kato Y, et al. The Vienna classification of gastrointestinal epithelial neoplasia. Gut 2000;47:251-5.
17. Forbes SA, Tang G, Bindal N, et al. COSMIC (the Catalogue of Somatic Mutations in Cancer): a resource to investigate acquired mutations in human cancer. Nucleic acids research 2010;38:D652-7.
18. Ramensky V, Bork P, Sunyaev S. Human non-synonymous SNPs: server and survey. Nucleic acids research 2002;30:3894-900.
19. Segditsas S, Rowan AJ, Howarth K, et al. APC and the three-hit hypothesis. Oncogene 2009;28:146-55.

Supplemental Figure S1

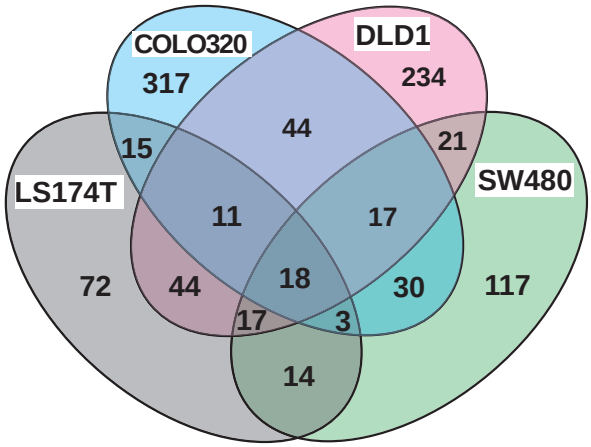

Supplemental Figure S2

A

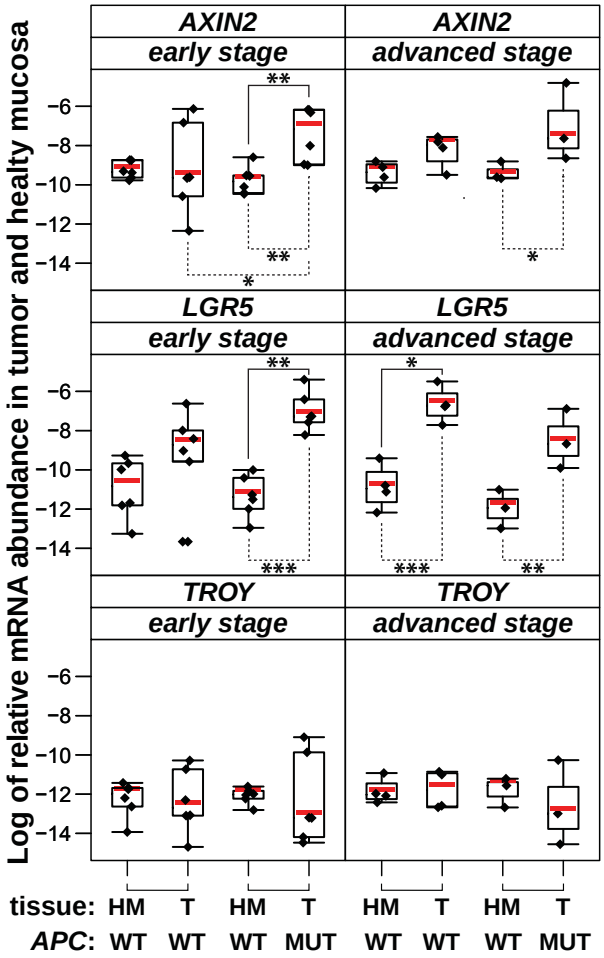

B

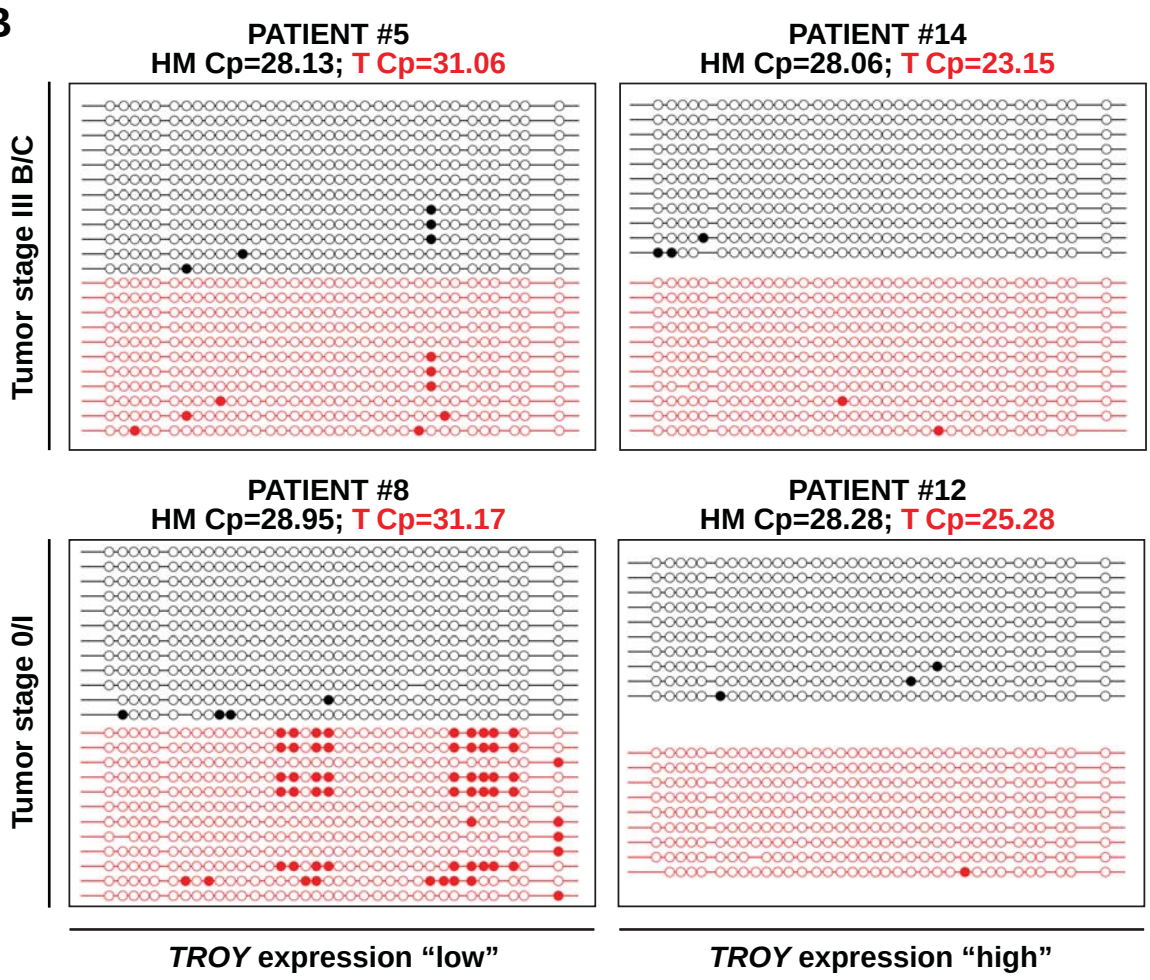

Supplemental Figure S3

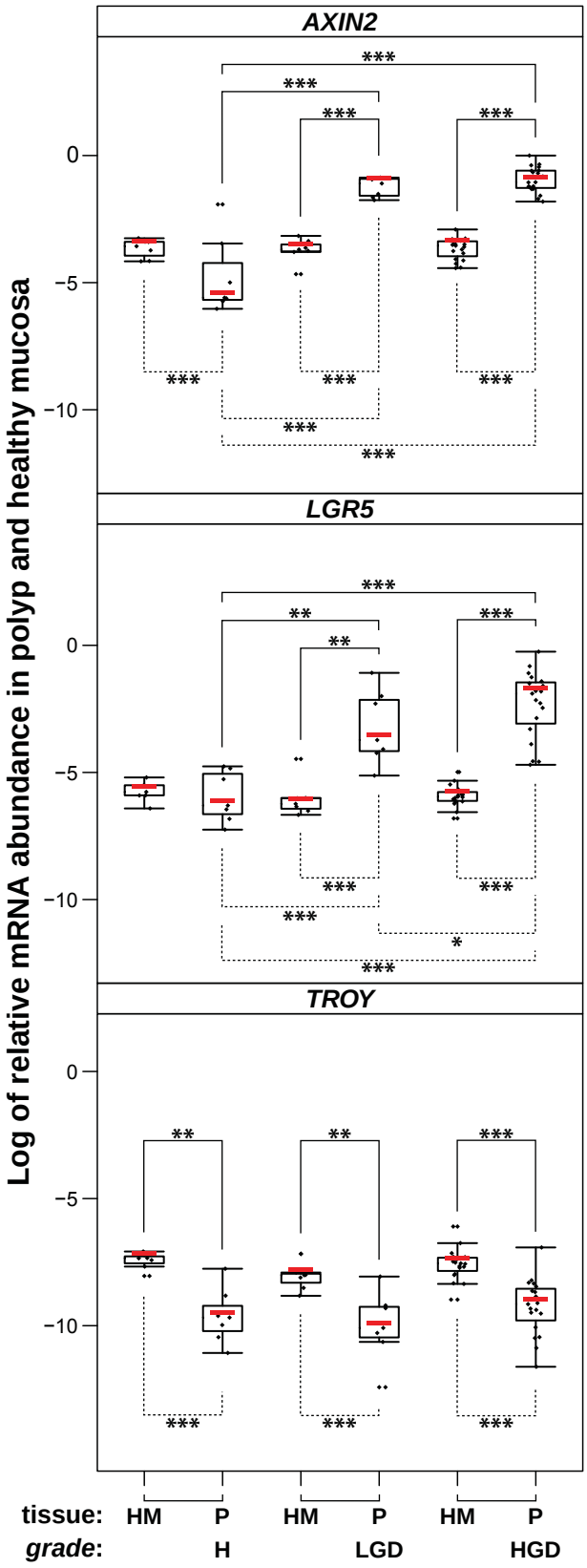

Supplemental Figure S4

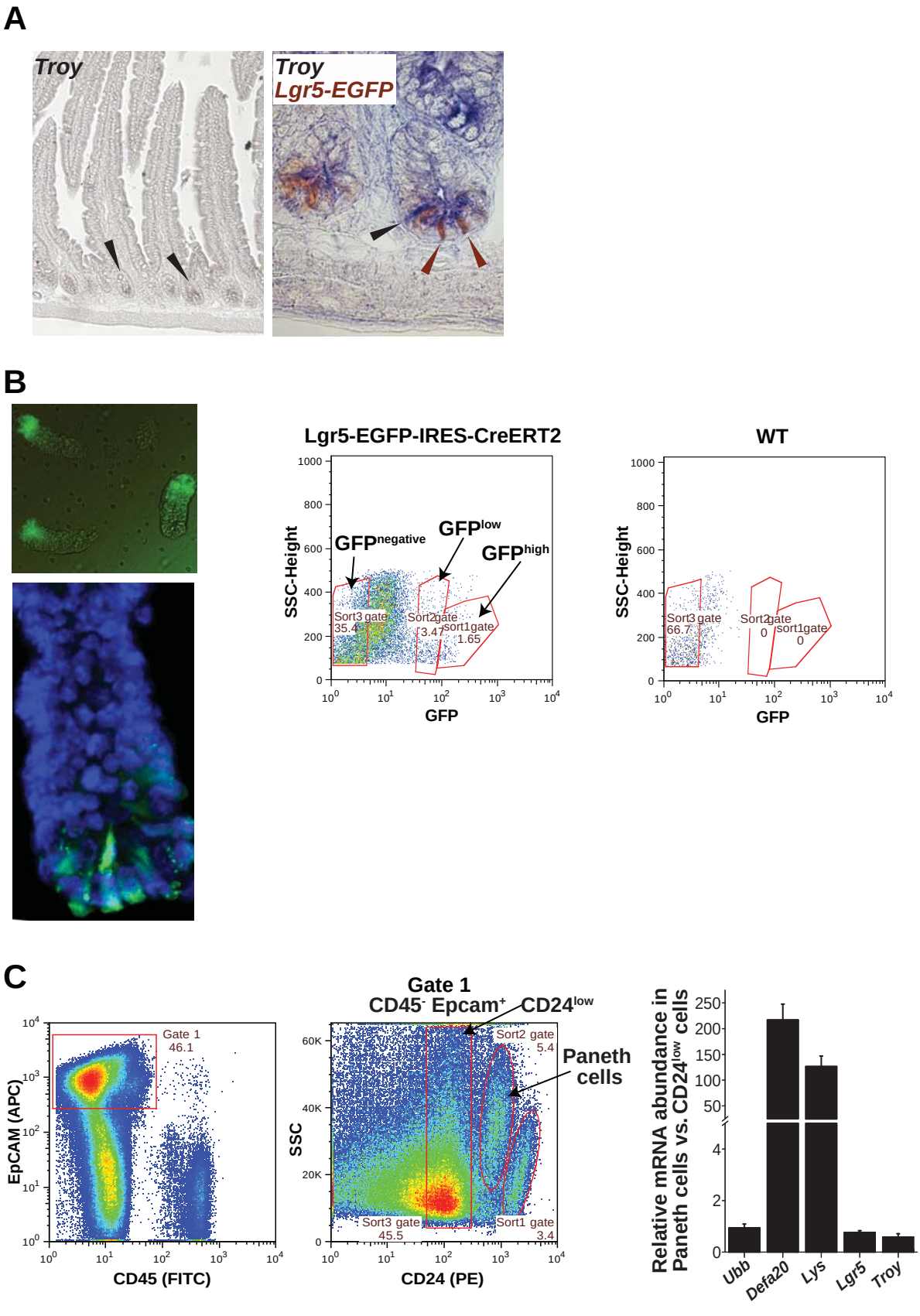

Supplemental Figure S5

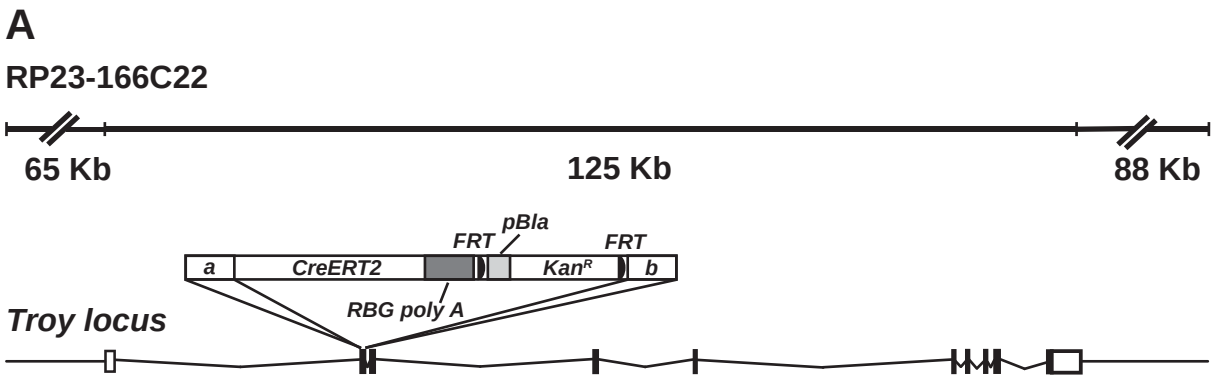

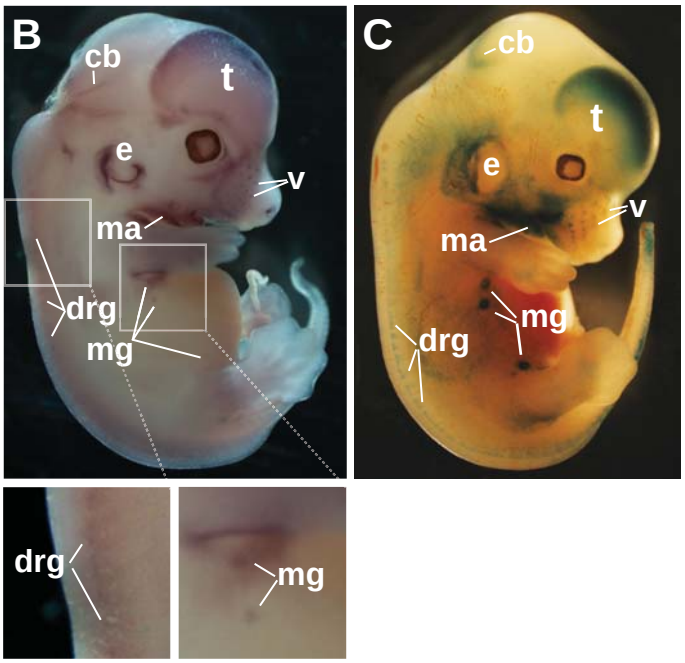

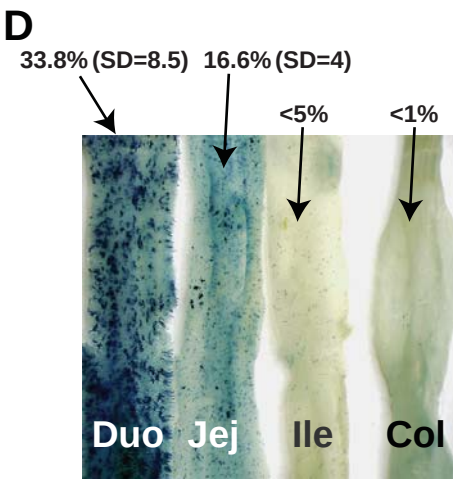

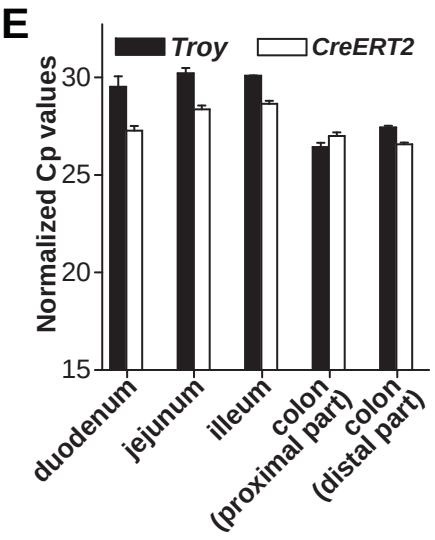

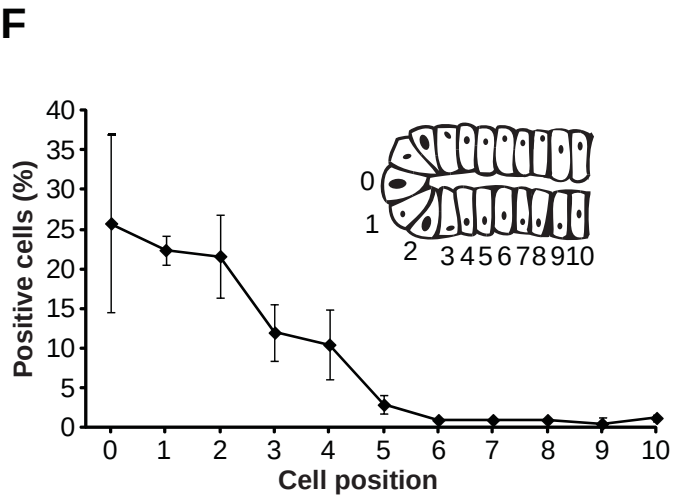

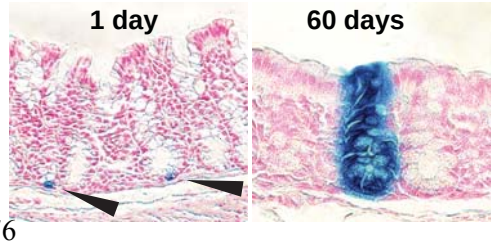

Supplemental Figure S6

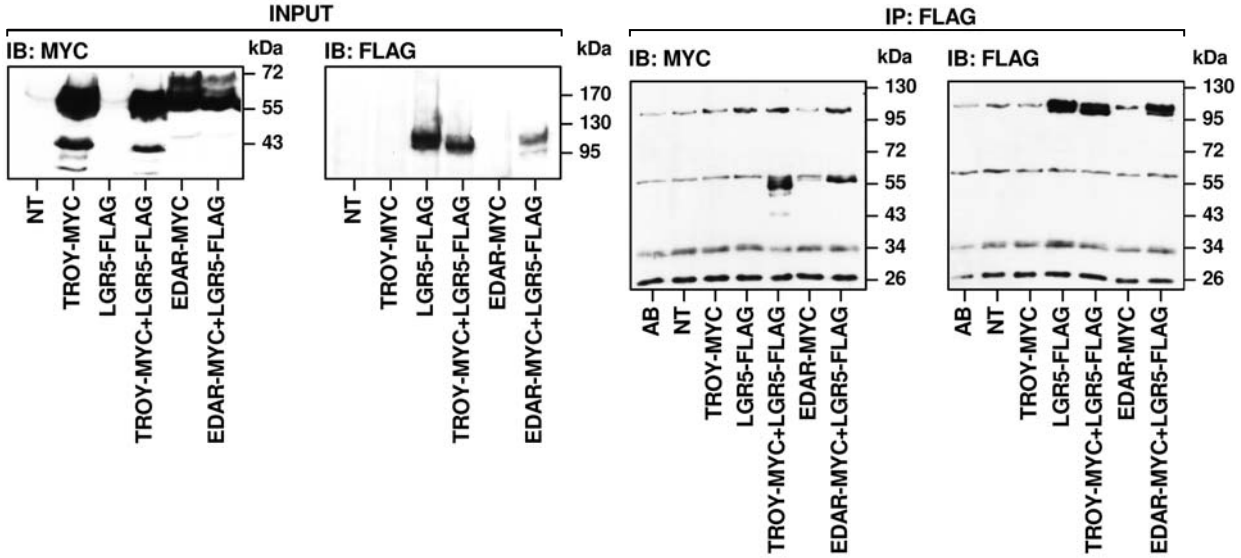

Supplemental Figure S7

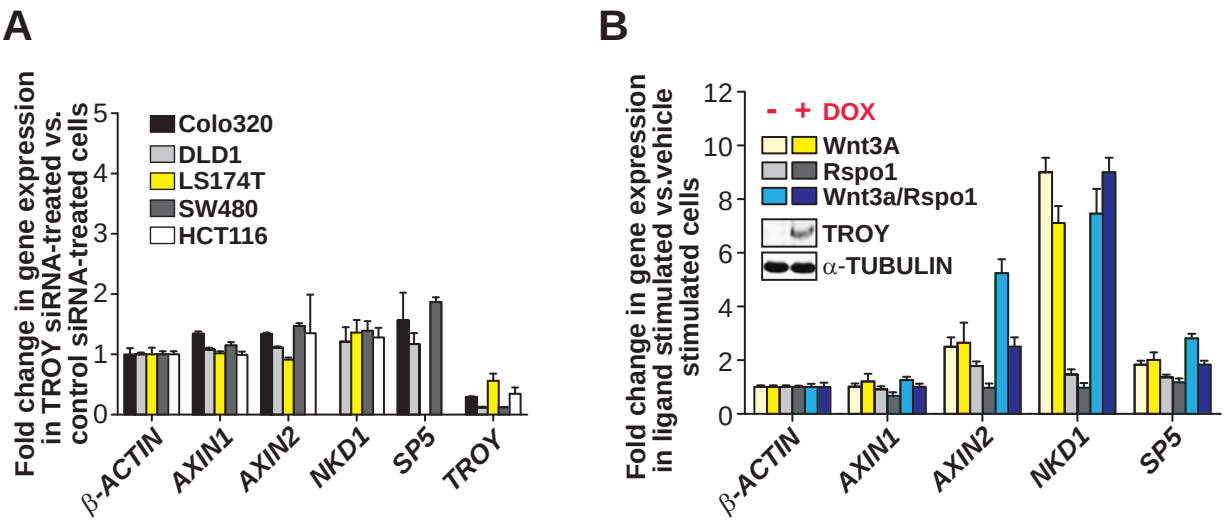

Supplemental Figure S8

A

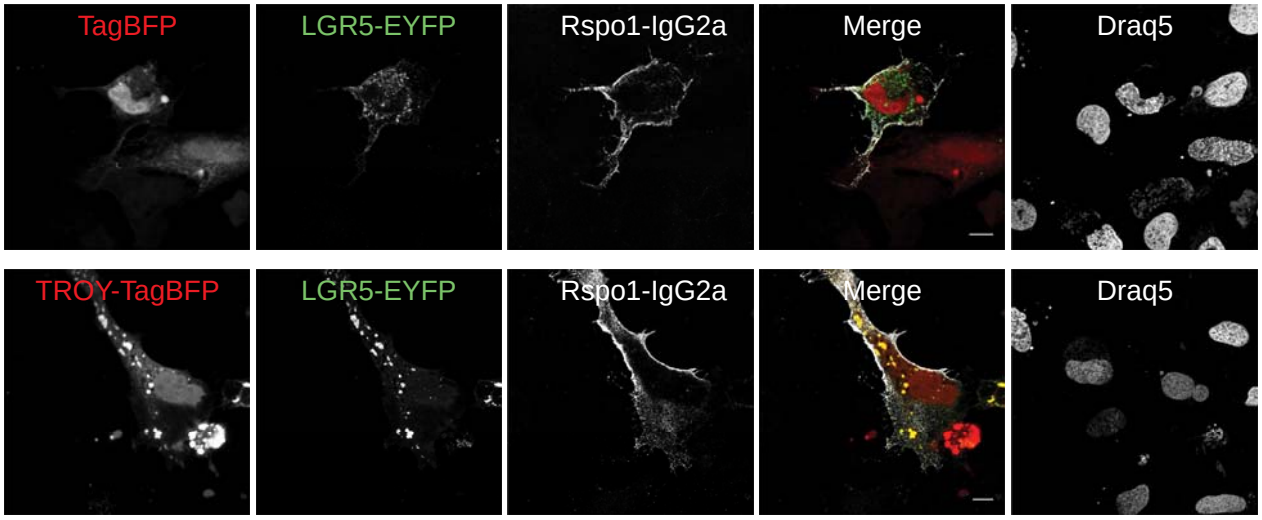

B

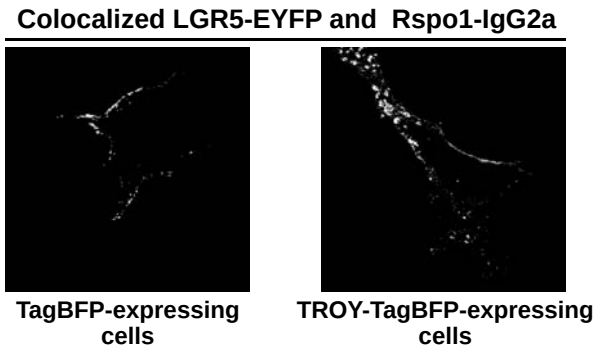

C

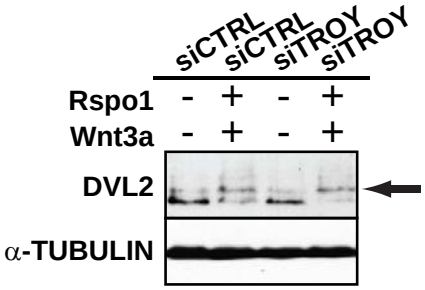

Supplemental Figure S9

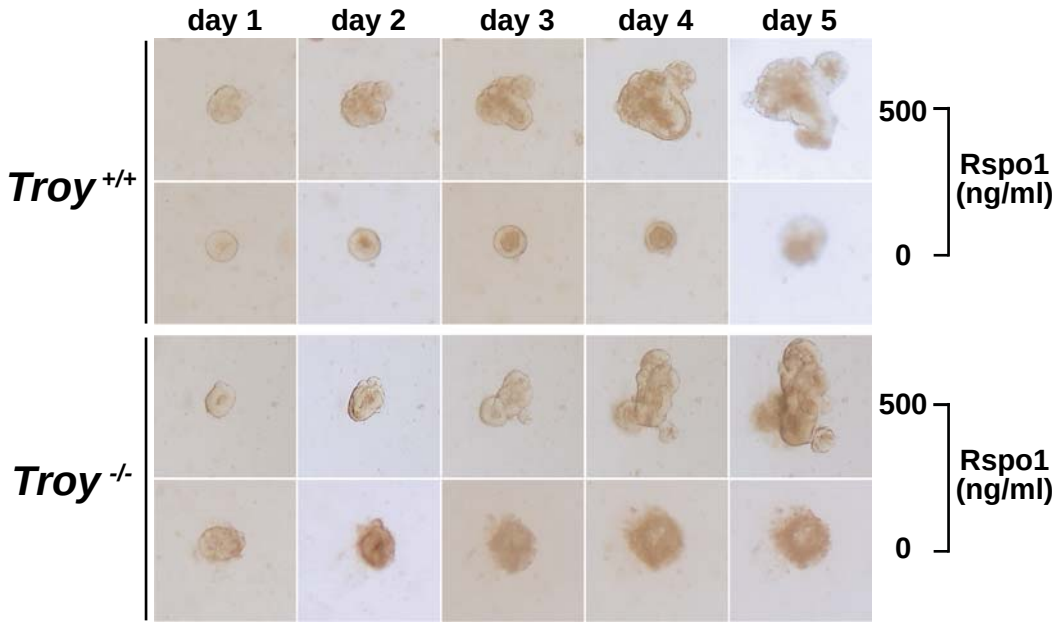

Supplemental Table S1

Gene	Organism	Sequence	Application
β-ACTIN	Human	GGCATCCTCACCCTGAAGTA AGGTGTGGTGCCAGATTTTC	qRT PCR/ChIP
β-Actin	Mouse	GATCTGGCACCACACCTTCT GGGGTGTTGAAGGTCTCAAA	qRT PCR
β-catenin	Human	TTCCAGACACGCTATCATGC AATCCACTGGTGAACCAAGC	qRT PCR
AXIN1	Human	GAAGGTGAGGACGGCGATCCAT AGGCACCTGGCACCTCGGTGC	qRT PCR
Axin1	Mouse	ACCCAGTACCACAGAGGACG CTGCTTCCTCAACCCAGAAG	qRT PCR
AXIN2	Human	CTGGCTTTGGTGAACTGTTG AGTTGCTCACAGCCAAGACA	qRT PCR
Axin2	Mouse	GGGGGAAAACACAGCTTACA TCTTCATTCAAGGTGGGGAG	qRT PCR
Bmi1	Mouse	TGTGTCCTGTGTGGAGGGTA TTGAAAAGCCCTGGGACTAA	qRT PCR
Cre	P1 phage	GCACTGATTTCGACCAGGTT GCTAACCAGCGTTTTCGTTC	qRT PCR/genotyping
c-MYC	Human	CTCCTGGCAAAAGGTCAGAG TCGGTTGTTGCTGATCTGTC	ChIP
Defensin α 20	Mouse	TGGGACCTGCTCAGGACGACT TCATCTGCATGTTCAGTGGCGG	qRT PCR
LGR5	Human	CTCTTCCTCAAACCGTCTGC GATCGGAGGCTAAGCAACTG	qRT PCR
LGR5	Human	GTGAAGGAAAAGGGTGTCCA ATGTGCCTTCCTTCATGTCC	ChIP
Lgr5	Mouse	CCTGTCCAGGCTTTCAGAAG CTGTGGAGTCCATCAAAGCA	qRT PCR
Lysozyme	Mouse	CCTGACTCTGGGACTCCTCCTGCT CTAAACACACCCAGTCGGCCAGGC	qRT PCR
NKD1	Human	CGCCGGGATAGAAAACTACA CTGGAGCTCTGAGACCTTGG	qRT PCR
NKD1	Human	GACCTCCCCAGACAAAACAA TCAGCCAGTCTCTGGGATCT	ChIP
Nkd1	Mouse	AGGACGACTTCCCCCTAGAA TGCAGCAAGCTGGTAATGTC	qRT PCR
SP5	Human	ACTTTGCGCAGTACCAGAGC ACGTCTTCCCGTACACCTTG	qRT PCR
SP5	Human	TCCAGACCAACAAACACACC GCTTCAGGATCACCTCCAAG	ChIP
Sp5	Mouse	ACTCACTGCAGGCCTTCCT TCCAAGGGTGGAAAAGTCTG	qRT PCR
TROY	Human	CTATGGGGAGGATGCACAGT TCTCCACAAGGCACACACTC	qRT PCR
TROY	Human	TTTCATCTCCCTGCTCGTCT TGCGAAAAATGCAGTGAAAG	ChIP
Troy	Mouse	GCTCAGGATGCTCAAAGGAC CCAGACACCAAGACTGCTCA	qRT PCR
Troy locus	Mouse	TTGCATGCTGTGCAGAGACG CACCTCAGTGTGGCATCGAC	qRT PCR/genotyping
UBB	Human	GCTTTGTTGGGTGAGCTTGT TCACGAAGATCTGCATTTTGA	qRT PCR
Ubb	Mouse	ATGTGAAGGCCAAGATCCAG TAATAGCCACCCCTCAGACG	qRT PCR

Supplemental Table S2

Clinical and histopathological features of colorectal cancer patients (*n=20*)	
	Total N (%)
No. of patients	20
Primary tumor duplicity	1 (5)
Total No. of tumors included in the study	21
Gender	
Male/Female	17/3
Age, Years	
Median	64
Range	45-86
≥ 65 years	9 (45)
Primary tumor location	
left-sided	10 (50)
right-sided	10 (50)
Metastatic disease	
Synchronous	8 (40)
Location of metastasis	
Liver	5 (25)
lymph nodes	8 (25)
Other	1 (5)
Histological differentiation level	
G1	2 (10)
G2-3	19 (90)

Supplemental Table S3

Clinical and histopathological features of patients with precancerous lesions (*n=35*)	
	Total N (%)
Total no. of lesions included in the study	35
Gender	
Male/Female	35/0
Age, Years	
Median	66
Range	38-83
≥ 65 years	21 (60)
Colon segment involved	
left-sided	29 (83)
right-sided	6 (17)
Histological examination	
Hyperplasia (H)	7 (20)
Low grade dysplasia (LGD)	12 (34)
High grade dysplasia (HGD)	16 (46)

Supplemental Table S4

Gene-specific primers			
Primer ID	Primer sequence	Product size (nucleotides)	Amplified region
APCex18/1T7 APCex18/1RP	taatacgactcactatagTGTTACTGCATACACATTGTGACC tgaaacagctatgaccatgTGACCTATTATCATCATGTCGATTG	567	APC, exon 18 c.1959-55bp[2] – c.2433[1]
APCex18/2T7 APCex18/2RP	taatacgactcactatagTCCCAAGGCATCTCATCGTAG tgaaacagctatgaccatgTGTATTCTAATTTGGCATAAGGCATAG	567	APC, exon 18 c.2340 – c.2869[1]
APCex18/3T7 APCex18/3RP	taatacgactcactatagTGCCCATACACATTCAAACAC tgaaacagctatgaccatgCACATTCCTGCTGTCCAAAATG	552	APC, exon 18 c.2781 – c.3295[1]
APCex18/4T7 APCex18/4RP	taatacgactcactatagAAAGTGAGCAAAGACAATCAAGG tgaaacagctatgaccatgCCTTTTGAGGCTGACCACTTC	589	APC, exon 18 c.3185 – c.3736[1]
APCex18/5T7 APCex18/5RP	taatacgactcactatagCCGAACATATGTCTTCAAGCAGTG tgaaacagctatgaccatgACATAGTGTTCAGGTGGACTTTTGG	545	APC, exon 18 c.3623 - c.4130[1]
APCex18/6T7 APCex18/6RP	taatacgactcactatagATCAGCCAGGCACAAAGC tgaaacagctatgaccatgAAATGGCTCATCGAGGCTCAG	548	APC, exon 18 c.4035 - c.4545[1]
APCex18/7T7 APCex18/7RP	taatacgactcactatagAGAGGGTCCAGGTTCTTCCAG tgaaacagctatgaccatgAGGTGTCCCTTCAACACAATAC	552	APC, exon 18 c.4430 - c.4944[1]
CTNNB1ex3T7 CTNNB1ex3RP	taatacgactcactatagTGCTTTTCTTGGCTGTCTTTCAG tgaaacagctatgaccatgTCCACAGTTCAGCATTTACCTAAG	571	CTNNB1, exon 3 including intron-exon boundaries; c.1-134bp[3] – c.241+172bp[4]
CTNNB1ex4T7 CTNNB1ex4RP	taatacgactcactatagTTGTGGTGAAGAAAAGAGAGTAATAGC tgaaacagctatgaccatgTGGTATTGGGTAGACATTCTGAAAC	486	CTNNB1, exon 4 including intron-exon boundaries; c.242-111bp[5] – c.495+84bp[6]

Supplemental Table S5

Mutation analysis of *APC* in human sporadic colorectal carcinomas							
Stage	**Patient No.**	**Mutation in genomic DNA[1]**	**Change in APC protein**	**Mutation type**	**Mutation in genomic DNA[1]**	**Change in APC protein**	**Mutation type**
0	8	c.4666_4667insA	p.T1556fs*3	Insertion - Frameshift	c.3095C>T	p. S1032L[2]	Substitution - Missense
	10	c.2956_2963delTATTCTGA	p.Y986fs*2	Deletion - Frameshift	c.4474_4475insT	p.A1492fs*22	Insertion - Frameshift
I	12	c.3183_3187delACAAA	p.Q1062fs*1	Deletion - Frameshift	c.4326T>A	p.Pro1442=	Substitution - Silent
	15	c.3910delA	p.I1303fs*1	Deletion - Frameshift	c.4479 A/A (n.a.)[4]	---	---
	20	c.4666_4667insA	p.T1556fs*3	Insertion - Frameshift	c.4479 G/A (wt)[4]	---	---
II	1	c.4926T>A	p.Y1642*	Substitution - Nonsense	c.4479 G/A>A/A (LOH)[4]	---	---
	6	c.3095C>T	p. S1032L[2]	Substitution - Missense	c.4479 A/A (n.a.)[4]	---	---
III	2	n.d.[5]	---	---	c.4479 G/A>A/A (LOH)[4,5]	---	---
	5	c.3340C>T	p. R1114*	Substitution - Nonsense	c.3961A>G	p. S1321G[3]	Substitution - Missense
	18	n.d.[5]	---	---	c.4479 G/A>A/A (LOH)[4,5]	---	---
	14	c.4348C>T	p.R1450*	Substitution - Nonsense	c.4479 G/A (wt)[4]	---	---

Supplemental Table S6

Linear model *ΔCp ~ patient + tissue / (stage * mutation)*					**Wilcoxon's rank-sum test**	
Early stage cancer					***Early stage cances***	
Gene	**ΔΔCp**	**FC**	**mean ΔCp**	**p-value**	**Gene**	**p-value**
APC wt tumor vs. healthy surrounding mucosa						
LGR5	-1.8	3.48	9.36	0.032	*LGR5*	0.09
TROY	0.07	0.95	11.92	0.91	*TROY*	0.82
AXIN2	-0.07	1.05	8.71	0.91	*AXIN2*	0.70
APC mut tumor vs. healthy surrounding mucosa						
LGR5	-4.33	20.05	9.36	< 0.0001	*LGR5*	0.0022
AXIN2	-2.35	5.09	8.71	0.002	*AXIN2*	0.0087
TROY	0.27	0.83	11.92	0.68	*TROY*	0.39
APC mut tumor vs. APC wt tumor						
AXIN2	-2.27	4.83	8.71	0.027	*AXIN2*	0.18
LGR5	-2.53	5.77	9.36	0.032	*LGR5*	0.041
TROY	0.19	0.87	11.92	0.83	*TROY*	0.82
Advanced stage cancer					***Advanced stage cancer***	
Gene	**ΔΔCp**	**□C**	**mean ΔCp**	**p-value**	**Gene**	**p-value**
APC wt tumor vs. healthy surrounding mucosa						
LGR5	-4.13	17.47	9.36	0.00072	*LGR5*	0.029
AXIN2	-1.17	2.26	8.71	0.22	*AXIN2*	0.11
TROY	0.26	0.83	11.92	0.77	*TROY*	0.89
APC mut tumor vs. healthy surrounding mucosa						
LGR5	-3.47	11.05	9.36	0.0049	*LGR5*	0.10
AXIN2	-2.34	5.06	8.71	0.024	*AXIN2*	0.10
TROY	0.76	0.59	11.92	0.41	*TROY*	0.70
APC mut tumor vs. APC wt tumor						
AXIN2	-1.16	2.24	8.71	0.4	*AXIN2*	0.63
LGR5	0.66	0.63	9.36	0.68	*LGR5*	0.11
TROY	0.5	0.71	11.92	0.7	*TROY*	0.63

Supplemental Table S7

Linear model $\Delta Cp \sim tissue\_stage + patient$					Wilcoxon´s rank-sum test	
Precancerous lesions of the colon						
Gene	**ΔΔCp**	**FC**	**mean ΔCp**	**p-value**	**Gene**	**p-value**
Polyp hyperplasia vs. healthy mucosa						
TROY	1.98	0.25	8.58	< 0.0001	*TROY*	0.0012
AXIN2	1.09	0.47	2.75	< 0.0001	*AXIN2*	0.097
LGR5	0.05	0.97	4.60	0.91	*LGR5*	0.71
Polyp low grade dysplasia vs. healthy mucosa						
AXIN2	-2.45	5.47	2.75	< 0.0001	*AXIN2*	0.00058
LGR5	-2.69	6.46	4.60	< 0.0001	*LGR5*	0.0012
TROY	2.31	0.20	8.58	< 0.0001	*TROY*	0.0041
Polyp high grade dysplasia vs. healthy mucosa						
AXIN2	-2.73	6.63	2.75	< 0.0001	*AXIN2*	< 0.0001
LGR5	-3.59	12.00	4.60	< 0.0001	*LGR5*	< 0.0001
TROY	1.60	0.33	8.58	< 0.0001	*TROY*	< 0.0001
Polyp low grade dysplasia vs. polyp hyperplasia						
AXIN2	-3.54	11.62	2.75	< 0.0001	*AXIN2*	0.00058
LGR5	-2.74	6.67	4.60	< 0.0001	*LGR5*	0.0023
TROY	0.33	0.80	8.58	0.50	*TROY*	0.71
Polyp high grade dysplasia vs. polyp hyperplasia						
AXIN2	-3.82	14.10	2.75	< 0.0001	*AXIN2*	< 0.0001
LGR5	-3.63	12.39	4.60	< 0.0001	*LGR5*	< 0.0001
TROY	-0.38	1.30	8.58	0.35	*TROY*	0.33
Polyp high grade dysplasia vs. polyp low grade dysplasia						
LGR5	-0.89	1.86	4.60	0.044	*LGR5*	0.19
TROY	-0.71	1.63	8.58	0.087	*TROY*	0.25
AXIN2	-0.28	1.21	2.75	0.29	*AXIN2*	0.21

Fatty acid modification of Wnt1 and Wnt3a at serine is prerequisite for lipidation at cysteine and is essential for Wnt signaling

Wnt ligands are posttranslationally modified by adding sugar or lipid residues. The exact role of these modification is still unknown – yet the debates continue weather one modification is a prerequisite for the other, or *vice versa*[20, 28]. Nevertheless, lipid adducts, palmitoylation of the most amino-terminally conserved cysteine[19] and highly conserved serine palmitoleoylation in the central part of the protein[262], were shown to be important for proper signaling activity of Wnts[19, 21, 26, 28] and their secretion[35, 262].

To shed a light on the function of the Wnt modifications, we prepared various mutants of murine Wnt1 and Wnt3a with impaired acylation/glycosylation sites.

We found that acylation at serine precedes and conditions acylation at cysteine and that Wnt activity relies on these lipid modifications. Because we did not find any non-functional lipid-mutant deposited on the extracellular matrix, we concluded that lipid adducts are important for association with extracellular matrix, a feature which is connected to their signaling activity. Importantly, secretion of any "lipid-less" mutant was not disrupted.

Although Wnt1 and Wnt3a are partially redundant[208], the function of their N-glycosylations is probably different. Whereas unglycosylated form of Wnt1 is normally secreted and can induce the pathway even more efficiently than wild type ligand, the secretion of unglycosylated Wnt3a is impaired, as well as its signaling properties.

In conclusion, N-glycosylation precedes and conditions Wnts for efficient acylation. Acyl modification on the conserved serine in the central part of the protein is added first and it is required for the palmitoylation of the N-terminal conserved cysteine.

My contribution to this work: I performed part of the qRT PCR analysis used in Figure 4.

Cellular Signalling 23 (2011) 837–848

Contents lists available at ScienceDirect

Cellular Signalling

journal homepage: www.elsevier.com/locate/cellsig

Fatty acid modification of Wnt1 and Wnt3a at serine is prerequisite for lipidation at cysteine and is essential for Wnt signalling

Lenka Doubravska [a,1], Michaela Krausova [a,1], Dietmar Gradl [b], Martina Vojtechova [a], Lucie Tumova [a], Jan Lukas [a], Tomas Valenta [a], Vendula Pospichalova [a], Bohumil Fafilek [a], Jiri Plachy [a], Ondrej Sebesta [c], Vladimir Korinek [a,*]

[a] Institute of Molecular Genetics, Academy of Sciences of the Czech Republic, Videnska 1083, 142 20 Prague 4, Czech Republic
[b] Zoologisches Institut II, Universität Karlsruhe, Kaiserstrasse 12, 76131 Karlsruhe, Germany
[c] Department of Genetics and Microbiology, Faculty of Science, Charles University in Prague, Vinicna 7, 128 43 Prague 2, Czech Republic

ARTICLE INFO

Article history:
Received 9 November 2010
Received in revised form 27 December 2010
Accepted 10 January 2011
Available online 16 January 2011

Keywords:
Wnt signalling
Post-translational modification
Acylation
N-glycosylation
Double axis formation
TCF/β-catenin transcription

ABSTRACT

The Wnt family of proteins is a group of extracellular signalling molecules that regulate cell-fate decisions in developing and adult tissues. It is presumed that all 19 mammalian Wnt family members contain two types of post-translational modification: the covalent attachment of fatty acids at two distinct positions, and the N-glycosylation of multiple asparagines. We examined how these modifications contribute to the secretion, extracellular movement and signalling activity of mouse Wnt1 and Wnt3a ligands. We revealed that O-linked acylation of serine is required for the subsequent S-palmitoylation of cysteine. As such, mutant proteins that lack the crucial serine residue are not lipidated. Interestingly, although double-acylation of Wnt1 was indispensable for signalling in mammalian cells, in *Xenopus* embryos the S-palmitoyl-deficient form retained the signalling activity. In the case of Wnt3a, the functional duality of the attached acyls was less prominent, since the ligand lacking S-linked palmitate was still capable of signalling in various cellular contexts. Finally, we show that the signalling competency of both Wnt1 and Wnt3a is related to their ability to associate with the extracellular matrix.

1. Introduction

The body of a multi-cellular organism is a highly organized structure of cells, tissues and organs. A handful of evolutionarily conserved cell signalling pathways is responsible for generating this structural complexity, both during development and its maintenance in adulthood. The Wnt pathway, initiated by secreted Wnt proteins, controls a remarkably diverse array of processes that include cell proliferation, differentiation, cell migration and cell polarity. Deregulation of Wnt signalling is implicated in a number of human disorders and cancer (reviewed in [1–4]). Currently, several different modes of the pathway have been recognized, with the majority of Wnt-dependent cascades requiring the seven-pass transmembrane Wnt receptor, Frizzled (Fz), the co-receptor low-density lipoprotein receptor-related protein (Lrp) and cytoplasmic protein, Dishevelled (Dvl). In canonical Wnt signalling the association of Wnt ligand with its corresponding receptors leads to the stabilization and accumulation of β-catenin protein via Dvl-dependent inhibition of the Axin, glycogen synthase kinase 3 (Gsk-3), and adenomatous polyposis coli (Apc) multi-protein complex. Subsequently, β-catenin enters the cell nucleus and together with the T-cell factor (Tcf)/Lymphoid Enhancer Factor (Lef) transcriptional regulators activates the expression of Wnt target genes [5] (a detailed summary on Wnt signalling can be found at the Wnt homepage http://www.stanford.edu/~rnusse/wntwindow.html).

The mammalian genome encodes 19 Wnt proteins of approximately 350–400 amino acids in length that contain an invariant pattern of 23–24 cysteines. It is presumed that many of these cysteine residues participate in the formation of intra-molecular disulphide bonds that stabilize proper folding of the polypeptide [6]. Although the degree of sequence identity between some Wnt family members is only 18%, it is thought that all Wnt proteins form a similar three-dimensional structure [7].

Mouse Wnt3a is post-translationally acylated by the attachment of two fatty acid adducts [8,9]. The modification by palmitic acid occurs at the first cysteine residue (C77) of the mature secreted protein, whilst the linkage of palmitoleic acid occurs at serine 209. In many Wnt ligands, the regions containing the acylated amino acids are homologous; thus it is thought that the majority of Wnt proteins are doubly-acyl-modified (reviewed in [10,11]). Indeed, S-acylation at the corresponding "prototype" C77 in Wnt3a was experimentally verified

* Corresponding author. Institute of Molecular Genetics, AS CR, Videnska 1083, 142 20 Prague 4, Czech Republic. Tel.: +420 241063146; fax: +420 244472282.
E-mail address: korinek@img.cas.cz (V. Korinek).
[1] These authors contributed equally to this work.

0898-6568/$ – see front matter © 2011 Elsevier Inc. All rights reserved.
doi:10.1016/j.cellsig.2011.01.007

in chicken Wnt1 and Wnt3a, mouse Wnt5a, *Drosophila* Wingless (Wg; the Wnt1 orthologue) and Wnt8 [9,12–14]. The presence of the O-acyl moiety at positions homologous to S209 in Wnt3a has been studied in less detail; however, it was confirmed in Wg and chicken Wnt1 [12,15]. To date, *Drosophila* WntD is the only known non-lipidated member of the Wnt family [16]. Another common biochemical feature of Wnt ligands is N-linked glycosylation. The N-glycosylation status of approximately 11 different Wnts has been examined with all proteins displaying a distinct pattern of N-linked oligosaccharide attachment at multiple positions [6,17–20].

It has been well documented in both *Drosophila* and *C. elegans* that Wnts act as morphogens, initiating specific responses in relation to the amount of a particular Wnt protein in the extracellular space [21,22]. Thus, within a given tissue, the concentration of Wnt molecules can provide positional information to cells influencing their developmental fate. The effect of each post-translational modification on the Wnt "morphogenic" behaviour is rather elusive (reviewed in [23]). Interestingly, ectopically expressed mammalian Wnts are not easily diffusible and remain tightly associated with the cell surface [18,24,25]. It was suggested that the fatty acid moieties are responsible for this "stickiness" and limit Wnt long-range signalling [11]. However, the concentration gradient of Wg can be mediated by membranous exovehicles, so-called argosomes [26], or by lipoprotein particles [27]. These findings would rather support a positive role of lipid adducts in long-range signalling of Wg in *Drosophila* tissues.

In cultured mammalian cells, Wnt3a lacking the palmitic adduct is normally secreted, but its signalling activity is considerably perturbed [9,12,17]. This reduction is caused by a decreased affinity for the receptors, Frizzled or Lrp [17,28]. Similar results were obtained using corresponding mutants of Wnt5a and Wg [13,15]. However, the same Wg mutant was not functional in the *Drosophila* wing imaginal disc as it was retained in the endoplasmic reticulum [15]. Other discrepancies were also observed in studies involving O-acyl-linked and N-glycosylated modifications. For example, mutation of the acylated S209 residue of Wnt3a resulted in an inefficiently secreted protein, whereas the equivalent mutation (S239A) in Wg was released from *Drosophila* S2 cells with the same efficiency as wild-type ligand [8,15]. In Wnt1, the absence of N-linked oligosaccharide chains did not impair its activity and was properly secreted and induced transformation of Wnt-sensitive mouse mammary epithelial cells [19,25,29]. In contrast, N-glycosylation of Wnt3a and Wnt5a ligands was necessary for their efficient secretion. Finally, purified and subsequently enzymatically deglycosylated Wnt5a preserved its activity, but a non-glycosylated mutant form of Wnt3a was less active than its wild-type counterpart [13,17,30].

In the present study, we thoroughly examined the N-glycosylation and acylation status of mouse Wnt1 and Wnt3a ligands to determine how these post-translational modifications affect the secretion and signalling activities of these polypeptides. The activity tests included secondary axis formation in *Xenopus* embryos, reporter gene assays and real-time quantitative RT-PCR (qRT-PCR) analysis. Additionally, β-catenin stabilization, the hallmark of canonical Wnt signalling, was visualized by confocal microscopy in Wnt-producing cells. We demonstrated that fatty acid modification at the serine residue precedes and conditions subsequent palmitoylation of cysteine. Wnt ligands without any lipidic adducts were still N-glycosylated and secreted. In contrast, non-N-glycosylated Wnts displayed a decreased rate of secretion. This phenomenon could account for the lower activity of non-N-glycosylated ligands in paracrine signalling. Although we observed some discrepancies between the outcome of the experiments performed in *Xenopus* embryos and in cultured cells, both testing systems showed that the non-lipidated Wnts were completely inactive. In addition, our studies revealed functional and biochemical differences between Wnt1 and Wnt3a proteins. Particularly, the relationship between fatty acid content and activity was less stringent in Wnt3a since S-acyl-deficient ligand [Wnt3a(C77A)] – contrary to the corresponding Wnt1 variant [Wnt1(C93A)] – retained a substantial signalling activity. Moreover, Wnt3a(C77A) was deposited on the extracellular matrix (ECM) and released to culture medium with the same efficiency as the wild-type polypeptide. Interestingly, we never detected any Wnt1 in cell supernatants, which indicates that the majority of the extracellular protein binds to the cell surface or ECM. However, the ability of acyl-deficient Wnt1 mutants to adhere to ECM was severely impaired.

2. Materials and methods

2.1. Plasmids and lentiviral constructs

Constructs encoding mouse wild-type and mutant Wnt1 [31] and Wnt3a (kindly provided by O. Machon) proteins were generated in the mammalian lentiviral vector, pCDH1 (System Biosciences). Single or multiple amino acid substitutions were introduced into corresponding cDNA using a site-directed mutagenesis kit (Stratagene). Wnt1 and Wnt3a lacking the signal peptide (ΔNWnt1 and ΔNWnt3a, respectively) were generated by PCR and cloned into the pCDH1 vector [31]. PCR amplification steps were performed with Phusion High-Fidelity DNA Polymerase (Finnzymes). The truncated proteins were fused at the N-terminus to the Myc-tag (ΔNWnt1) or HA-tag (ΔNWnt3a). EGFP-tagged mouse Frizzled (Fz) 4, cloned into the pCS2 vector, was obtained from V. Bryja. The expression construct encoding Flag-tagged mouse Lrp5 was a kind gift from M. Semenov and X. He [32]. PCR-derived constructs were verified by sequencing; details of plasmid constructs are available on request.

2.2. Software and statistical analysis of data

Protein sequence alignments were performed using the MegAlign program (DNASTAR Lasergene 7). Signalling peptides and N-glycosylation sites were predicted using the Expert Protein Analysis System (ExPASy) at http://www.expasy.ch. Fisher's exact test was used to analyse the statistical significance of the results of the double axis formation assay. Data sets obtained in the gene reporter and qRT-PCR analyses were evaluated by Student's t-test.

2.3. Cell culture, transfections and generation of stable cell lines

Human HeLa, human embryonic kidney (HEK) 293, mouse L_{TK^-}, mouse 3T3 and mouse Wnt3a-producing L cells were purchased from ATCC. Rat2 and mouse Wnt1-transduced Rat2 fibroblasts (Rat2Wnt1) were kindly provided by A. Brown [33]. Rat2 cells producing wild-type mouse Wnt3a were described previously [34]. HEK 293 FT cells utilized for packaging lentiviral stocks were purchased from Invitrogen. Super-TOPFLASH HEK 293 (STF 293) cells containing the genome-integrated Wnt/β-catenin-responsive luciferase reporter, SuperTOPFLASH [35] were obtained from Q. Xu and J. Nathans. All cell lines were maintained in Dulbecco's modified Eagle's medium [(DMEM; purchased from Biochrom AG)] supplemented with 10% fetal bovine serum (Hyclone), penicillin, streptomycin and gentamicin (Invitrogen). Transient transfections were performed using Fugene HD (Roche). Lentiviruses were prepared using the Trans-Lentiviral Packaging System (Open Biosystems). Rat2 cells transduced with the corresponding recombinant lentiviruses were selected without subcloning using puromycin (Alexis; 5 μg/ml).

2.4. Antibodies, co-immunoprecipitations, western blotting and tunicamycin treatment

cDNAs encoding N-terminally His-tagged mouse Wnt1 [amino acids (aa) 225–370] and Wnt3a (aa 190–355) were subcloned into the pET28b vector (Novagen). Recombinant proteins were purified from bacterial [*E. coli*, strain BL-21 (DE3)] cell lysates by TALON affinity

resins (Clontech) and utilized for immunizing rabbits or chickens. The preparation of rabbit anti-EGFP polyclonal antibody was described previously [36]. For co-immunoprecipitation experiments, HEK 293 FT cells were transfected overnight with an appropriate combination of constructs. The cells were harvested, washed with ice-cold phosphate-buffered saline (PBS) and disrupted in lysis buffer [1% NP-40, 20 mM Tris (pH 7.5), 100 mM NaCl, 10 mM EDTA, protease inhibitor cocktail Complete (Roche)] for 30 min on ice. The samples were centrifuged (16,000×*g*, 10 min, 4 °C) and the resulting supernatants transferred to fresh tubes and incubated for 3 h at 4 °C with Wnt1 or Wnt3a rabbit polyclonal antibodies bound to protein A/G Sepharose beads (Pierce). The beads were washed three times using lysis buffer and the retained proteins were eluted in Laemmli sample buffer [37] and immunoblotted. A detailed protocol describing the immunoblotting procedure can be found elsewhere [38]. To detect immunoprecipitated Wnt proteins, Wnt-specific polyclonal antisera from chickens were utilized. The following commercially available rabbit polyclonal and mouse and rabbit monoclonal antibodies were used: anti-α-tubulin (TU-01; Exbio), anti-β-catenin (610154; BD Transduction Laboratories and EM-22; Exbio), anti-Flag (M2; Sigma), anti-GFP (JL8; Clontech), and anti-Wnt3a (C64F2; Cell Signalling Technology). Peroxidase-conjugated anti-chicken, anti-mouse or anti-rabbit secondary antibodies were purchased from Sigma. Tunicamycin (Sigma) treatment was performed overnight at a final concentration of 1 μg/ml.

2.5. Metabolic labelling with [^{3}H] palmitate

HEK 293 cells grown on a 15 cm culture dish were transfected with the relevant Wnt-expression constructs. The next day cells were starved for 1 h in serum-free DMEM and incubated for an additional 3 h in DMEM supplemented with 5% dialysed foetal bovine serum and [^{3}H] palmitate (Perkin Elmer, final concentration 0.5 mCi/ml). Cell lysates were immunoprecipitated using rabbit anti-Wnt1 or anti-Wnt3a polyclonal antibodies. Precipitated proteins were separated in two SDS-PAGE gels. One gel was blotted and stained with chicken anti-Wnt1 or anti-Wnt3a polyclonal antisera. The second gel replica was fixed, soaked in Amplify Solution (Amersham Biosciences) and subsequently dried and exposed to Hyperfilm MP (Amersham Biosciences) for up to 3 months at −80 °C.

2.6. Immunofluorescent microscopy

For immunofluorescence studies, Wnt1- and Wnt3a-specific rabbit polyclonal antibodies were purified by affinity chromatography using Glutathione S-transferase (GST)-Wnt1 or GST-Wnt3a proteins coupled to glutathione Sepharose 4B (Amersham Pharmacia Biotech) [39]. The recombinant GST-fusion proteins (same sequences of Wnt1 or Wnt3a used for immunizations) were expressed from the pET42b vector (Novagen) in the bacteria *E. coli* BL-21/DE3. To distinguish extracellular and intracellular pools of Wnt proteins mammalian cells grown on coverslips were transfected with the relevant Wnt-expression construct. The next day antigen-purified anti-Wnt1 or anti-Wnt3a antibody was added to the culture medium. After 30 min at 37 °C, the cells were washed three times with PBS and fixed (10 min at 4 °C) in 4% (w/v) paraformaldehyde (Electron Microscopy Sciences) solution made in PBS. The samples were subsequently permeabilized in 0.2% Triton X-100/PBS solution (5 min, 4 °C), rinsed 3 times with PBS and stained for 1 h using a goat anti-rabbit antibody conjugated with the Alexa 488 dye (Molecular Probes). After another round of excessive washing using PBS, the specimens were incubated (1 h, 4 °C) with the same Wnt1- or Wnt3a-specific rabbit antibody. The coverslips were washed with PBS and stained using the Alexa 594 dye conjugated to a goat anti-rabbit antibody (Molecular Probes). For double staining of mouse L and 3T3 cells, the specimens were washed three times with PBS and fixed (10 min at 4 °C) in 4% paraformaldehyde. The samples were subsequently permeabilized in a 0.2% Triton X-100/PBS solution (5 min, 4 °C), rinsed 3 times with PBS and incubated consecutively with Wnt antibodies (1 h, 4 °C) and with an anti-β-catenin monoclonal antibody (additional 12 h, 4 °C). The coverslips were washed with PBS and stained using the Alexa 594 dye conjugated to a goat anti-rabbit antibody and Alexa 647 goat anti-mouse antibody (Molecular Probes). Finally, the samples were washed three times in PBS, incubated with DAPI nuclear stain (Molecular Probes; 1 min, room temperature, final concentration 1 μM), washed and mounted in MOWIOL (Calbiochem). Immunofluorescence was visualized using a confocal laser scanning microscope (TCS SP5; Leica) and analysed by ImageJ software (NIH freeware). Rat2 fibroblasts stably expressing various Wnt proteins were seeded on coverslips and processed as described for transiently transfected cells, except that the same secondary antibody (Alexa 488 conjugated to a goat anti-rabbit antibody) was used to visualize both the natively labelled and fixed pool of Wnt protein.

2.7. Double axis formation assay

cDNAs encoding wild-type, lipid- or N-glycosylation-deficient Wnt1 and Wnt3a proteins were subcloned into the pCS2 vector (Addgene). Capped mRNAs were synthesized from the Not I restriction-linearized constructs using the mMessage mMachine kit (Ambion). Eggs obtained from *Xenopus laevis* were fertilized by a standard method [40]. Twenty pg (in 4 nl) of each mRNA was microinjected into the marginal zone of the ventral blastomeres of 4-cell stage embryos. Embryos were kept as described previously [41] and at the neurulae stage scored for the double axis phenotype.

2.8. RNA purification and qRT-PCR

Total RNAs were isolated from cells using the Trizol reagent (Invitrogen). A detailed description of the qRT-PCR procedure was given previously [38]. All primers were calculated using the Primer 3 computer service at http://frodo.wi.mit.edu/. Two housekeeping genes, *Glyceraldehyde-3-phosphate dehydrogenase* (*GAPDH*) and *Ubiquitin b* (*Ubb*) were used as internal control genes to standardize the quality of different cDNA preparations [42]. cDNAs were produced from at least two independent RNA isolations and the PCR reactions were performed in triplicate for each primer set. The primers are written in the 5′ to 3′ direction; the first primer is derived from the plus and the second primer from the minus DNA strand:

rAxin1, ACCCAGTACCACAGAGGATG, CTGCTTCCTCATCCCAGAAG;
rAxin2, GCTGGAGAAGCTGAAACTGG, GACAGGTGGTCGTCCAAGAT;
rGAPDH, AAACCCATCACCATCTTCCA, GTGGTTCACACCCATCACAA;
rUbb, TCTTCGTGAAGACCCTGACC, CAGGTGCAGGGTTGACTCTT;
mWnt1, ATCGATT TTGGTCGCCTCTT, CTTGGCGCATCTCAGAGAAC;
mWnt3a, GCGGCTGTAGTGAGG ACATT, GCACTTGAGGTGCATGTGAC.

2.9. Autocrine and paracrine reporter gene assays

A detailed protocol of the reporter gene assay was described previously [38]. Briefly, to assay autocrine Wnt signalling, HEK 293 and 3T3 cells were transfected with firefly luciferase TOPFLASH and FOPFLASH reporters containing either multiple copies of the optimal Tcf motif GATCAAAGG or multiple copies of mutant motif GGCCAAAGG, respectively [43]. DNA mixtures further included the particular Wnt expression construct and as an internal control, *Renilla* pRL-SV40 plasmid (Promega). STF 293 cells that contain an integrated TCF-dependent reporter, SuperTOPFLASH [35,44], were lipofected with *Renilla* and Wnt-expressing plasmids only. Cells were harvested 24 and 48 h after transfection. To assess paracrine signalling, STF 293 cells were transfected “in batch” with the *Renilla*-expressing plasmid. The next day the cells were mixed at a ratio of 1:1 with either parental

Rat2 cells or Rat2 cells stably expressing wild-type or mutant Wnts. Twenty-four and 48 h later the activity of firefly and *Renilla* luciferase in cell lysates was determined using the Dual-Glo Luciferase Assay System (Promega) and EnVision 2100 Multilabel Reader (Perkin Elmer). Reporter gene activities were normalized against the activity of *Renilla* luciferase. All reporter gene assays were performed in triplicate. The results of a representative experiment from three in total are presented.

2.10. Recombinant Wnt3a purification

Mouse Wnt3a ligand was isolated from the culture medium of Wnt3a-producing L cells without the heparin purification step according to a detailed protocol of Willert and colleagues [9].

2.11. Density gradient ultracentrifugation

The plasma membranes of Rat2 fibroblasts stably expressing wild-type or mutant forms of Wnt1 or Wnt3a proteins were solubilized on ice in membrane lysis buffer (1% Brij 98; 20 mM Tris (pH 8.2), 100 mM NaCl, 10 mM EDTA, 50 mM NaF, 1 mM Na_3VO_4, Complete protease inhibitor cocktail) for 30 min. Lysates were then mixed at a 1:1 ratio with ice-cold 80% (w/v) sucrose diluted in membrane lysis buffer. The samples were transferred into 5 ml ultracentrifugation tubes and overlaid initially with 3.5 ml of ice-cold 30% sucrose diluted in membrane lysis buffer and then 0.5 ml of membrane lysis buffer. Fractions were collected upon centrifugation (268,000×*g*, 20 h at 4 °C) in the MLS-50 rotor (Beckman Coulter) from the top to the bottom of the tubes. Prior to Western blotting, proteins were precipitated by chloroform and methanol [45].

2.12. Isolation of the ECM and plasma membranes

Cells grown in 10 cm culture dishes for 72 h to 90% confluence were washed twice in Ca^{2+}, Mg^{2+}-free PBS and incubated for 10 min at 37 °C in Ca^{2+}, Mg^{2+}-free PBS supplemented with 5 mM EGTA. Cells were detached by gentle pipetting and the cell-free surfaces of the culture dishes were subsequently washed three times using ice-cold Ca^{2+}, Mg^{2+}-free PBS and once with distilled water. The ECM was then harvested by scraping the surface of the dish in Laemmli sample buffer. To isolate plasma membranes, the detached cells were washed twice in ice-cold PBS and resuspended in hypotonic buffer [10 mM Hepes (pH 7.5), 10 mM KCl, 10 mM $MgCl_2$, Complete protease inhibitor cocktail]. Cells were disrupted by passing them 10 times through a 25 gauge needle. Nuclei were removed from lysates by centrifugation (400×*g*, 5 min, 4 °C). Supernatants were transferred to fresh tubes and centrifuged at 18,000×*g* (10 min, 4 °C) to pellet the plasma membranes. To prepare whole-cell lysates (WCL), cells grown in one 10 cm culture dish were washed twice in PBS and subsequently harvested in Laemmli sample buffer.

3. Results

3.1. N-glycosylation and fatty acid modification of Wnt1 and Wnt3a ligands

To investigate the possible function of N-glycosylation or lipidation of Wnt proteins, we generated mutant Wnt1 and Wnt3a polypeptides containing single or multiple amino acid substitutions at the putative modification position(s) (Fig. 1A). Four or two asparagine residues were mutated to glutamine in mouse Wnt1 and Wnt3a, respectively. Expression constructs encoding wild-type or mutant proteins were lipofected into HEK 293 cells; the resulting cells were then treated either with the N-glycosylation inhibitor, tunicamycin or vehicle alone. Cell lysates were prepared and subjected to immunoblotting using an anti-Wnt1 or Wnt3a antibody. As shown in Fig. 1B, wild-type Wnt1 migrates in SDS-PAGE gels as a quadruplet, whilst Wnt3a was detected as a double band. Tunicamycin-treated cells expressed only one protein species, indicating that Wnt1 is N-glycosylated at three and Wnt3a at two residues. Further analysis of each mutant ligand revealed that Wnt1 is N-glycosylated at asparagine residues 29, 316 and 359, whilst Wnt3a is N-glycosylated at asparagine 87 and 298 [(Fig. 1B); (the numbering accounts for the signalling peptide)].

In addition to N-glycosylation, Wnt3a is palmitoylated on cysteine 77 and the palmitoleoyl modification occurs at serine 209 [8,9].The aforementioned amino acids and the homologous residues in Wnt1 (cysteine 93 and serine 224, respectively; see Fig. 1A) were mutated to alanines. The acylation status of wild-type and mutant polypeptides were tested in cells metabolically labelled with tritiated palmitate. Interestingly, substitution at the critical serine residue resulted in the expression of an entirely non-acylated form (Fig. 2).

3.2. Non-acylated Wnts do not induce ectopic axis in developing Xenopus embryos

We next compared the ability of wild-type and mutant Wnt proteins to dorsalize *Xenopus* embryos. Equal amounts of capped mRNA encoding different variants of Wnt1 or Wnt3a were injected into ventral blastomeres. Each embryo was then scored for the formation of the secondary axis. The analysis (results are summarized in Fig. 3) demonstrated that whilst Wnt1 and Wnt3a ligands display some similarities, there are also quite striking differences. For instance, the putative non-acylated forms of Wnt1(S224A), Wnt1 (C93,S224A), ΔNWnt1, Wnt3a(S209A) and Wnt3a(C77,S209A) failed to induce double axis. However, Wnt1(N29,316,359Q) lacking any N-glycosylation sites appeared to be the most potent Wnt. Interestingly, Wnt1(C93A) retained approximately two thirds of the activity of wild-type Wnt1, whilst the equivalent mutant Wnt3a(C77A) functioned as its wild-type Wnt3a counterpart. Finally, Wnt3a(N87,298Q) ligand lacking N-glycosylated residues displayed a significantly reduced ability (approximately one third) to produce *Xenopus* embryos with two body axes.

3.3. Mutant Wnts lacking the lipid-modified cysteine residue display decreased functionality in mammalian cells

We examined the effect of N-glycosylation or fatty acid modification on the signalling properties of Wnt ligands in mammalian cells. Expression constructs encoding wild-type or N-glycosylation/acylation mutants of Wnt1 and Wnt3a were introduced into SuperTOPFLASH 293 (STF 293) cells. These HEK 293-derived cells can be used as a sensitive cellular system to quantify Wnt signalling as they contain the genome-integrated TCF/β-catenin-dependent luciferase reporter, SuperTOPFLASH [35,46]. Constructs encoding Wnt1 and Wnt3a without a signalling peptide (ΔNWnt1 and ΔNWn3a) were used as negative controls in this and subsequent assays as these truncated forms remain intracellular (see e.g. Fig. 5B and C). In a parallel experiment, parental HEK 293 cells were transfected with the corresponding Wnt construct together with the "original" TCF/β-catenin-reporter, TOPFLASH [43]. Twenty-four hours post-transfection the cells were harvested and luciferase activities were determined in cell lysates. Contrary to our findings in the *Xenopus* embryo readout, the single-acyl mutant Wnt3a (C77A) was less stimulatory than wild-type Wnt3a. Moreover, the luciferase activities in STF 293 cells transfected with the expression constructs encoding analogous Wnt1(C93A) ligand or the acyl-deficient Wnt1 variants [Wnt1(S224A), Wnt1(C93, S224A)] were as low as in control cells transfected with the "empty" vector. Thus, we concluded that all theses mutant proteins appeared to be "signalling-dead". In agreement with the results of the double axis formation assay, non-N-glycosylated Wnt1(N29,316,359Q) was more functional than wild-type Wnt1; however, N-glycosylation-depleted Wnt3a(N87,298Q) protein

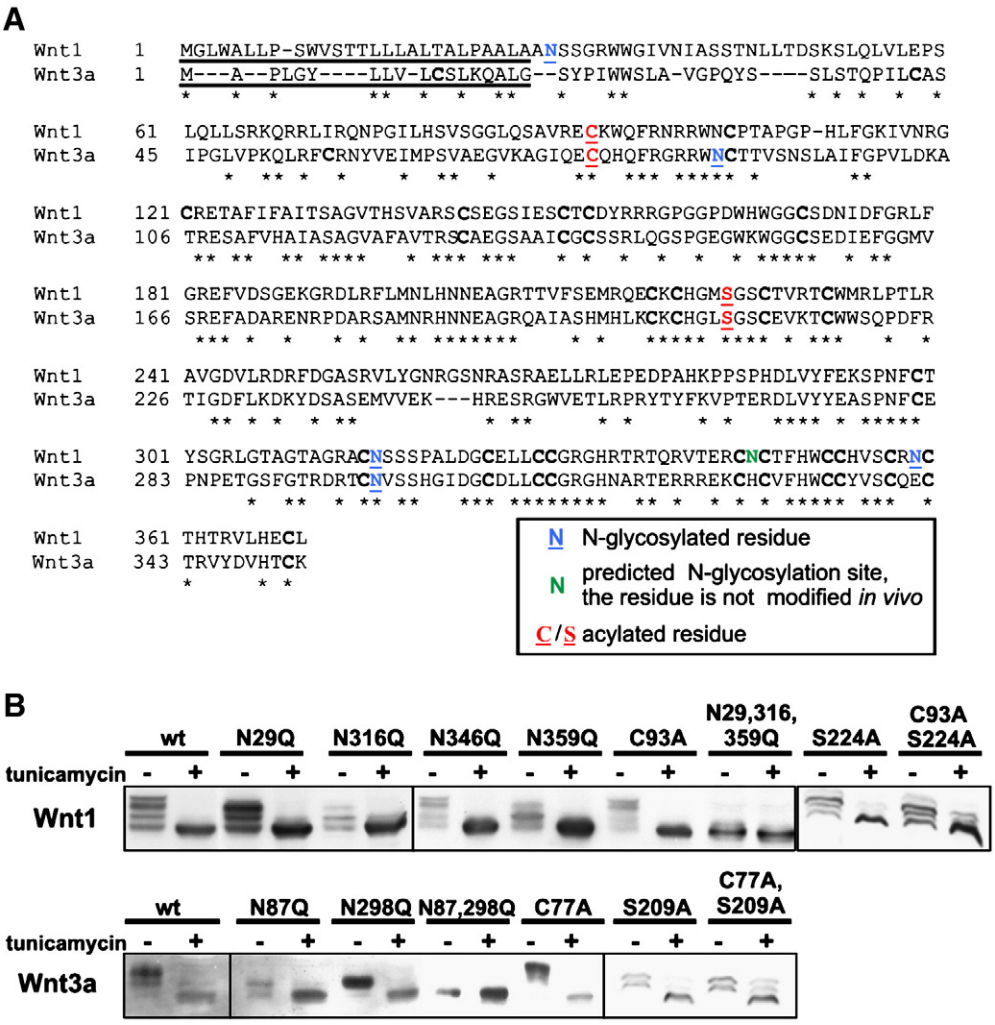

Fig. 1. N-glycosylation of Wnt1 and Wnt3a proteins. (A) Comparison of mouse Wnt1 and Wnt3a polypeptide sequences displaying the predicted and experimentally confirmed N-glycosylation sites. The putative signal peptides are underlined. The amino acid residues conserved in both Wnt1 and Wnt3a are marked by asterisks. The acylated cysteine and serine residues are also highlighted and the unmodified cysteines are typed in bold. (B) N-glycosylation status of Wnt1 and Wnt3a proteins. Human HEK 293 cells were transfected with constructs encoding either wild-type (wt) or mutant Wnt1 or Wnt3a polypeptides. Mutations were made at the putative N-glycosylated asparagines [(N); replaced by glutamine (Q)] or acylated cysteine (C) or serine (S) [both replaced by alanine (A)] residues. Eight hours post transfection either the N-glycosylation inhibitor, tunicamycin (1 μg/ml final concentration) or vehicle (DMSO) was added to cells. Cultures were incubated for an additional 18 h before being harvested and lysates prepared. Cell lysates were subjected to immunoblotting using either anti-Wnt1 or anti-Wnt3a antibodies.

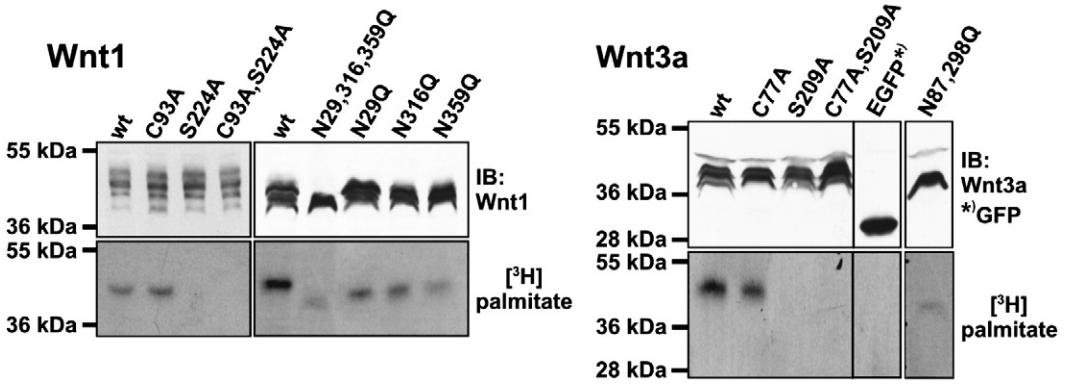

Fig. 2. In both Wnt1 and Wnt3a, fatty acid modification of serine is essential and precedes palmitoylation at the cysteine residue. HEK 293 cells metabolically labelled with [^{3}H] palmitate were transfected with the indicated Wnt1 or Wnt3a expression constructs or negative control EGFP-producing plasmid. The ectopic proteins were immunoprecipitated from cell lysates 20 h post-transfection using the corresponding rabbit polyclonal antisera. The precipitates were resolved in two SDS-PAGE gels. One of these gel replicas was dried and exposed directly to Hyperfilm MP (bottom panels); the second gel was blotted and stained with chicken anti-Wnt1 or anti-Wnt3a polyclonal antibodies or with a mouse anti-GFP monoclonal antibody (upper panels). IB, immunoblotting.

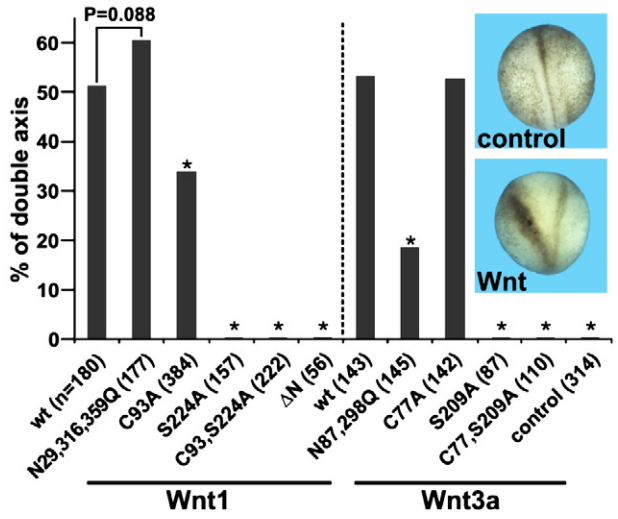

Fig. 3. Wnt1 and Wnt3a without fatty acyl adducts do not induce double axis formation in *Xenopus* embryos. Embryos at the 4-cell stage were microinjected with 20 pg of the indicated mRNA in the marginal zone of ventral blastomeres and scored for secondary axis induction at the neurulae stage (see the inset). Differences between wild-type and mutant ligands were compared by the Fisher exact probability test. *$P<0.001$. ΔN, truncated Wnt1 lacking signalling peptide; control, non-injected embryos.

showed a remarkably reduced ability to stimulate Wnt-responsive reporters (Fig. 4A; only results for STF cells are shown). We attempted to elucidate the observed discrepancies between the outcome of the tests performed in *Xenopus* embryos and in mammalian cells. At first, we injected decreased amounts of Wnt-encoding mRNAs into ventral blastomeres and scored for the formation of the secondary axis. Next, we extended the reporter gene assay and measured the luciferase activities in lysates of transfected cells 48 h post-transfection. Nevertheless, in these experiments all Wnt variants performed in a similar way as in the previous setup, confirming the initial results (Fig. 4A). Importantly, in all cellular backgrounds tested, the negative control reporter FOPFLASH never responded to any of the expressed Wnt proteins (not shown).

Subsequently, an analogous study was conducted in Wnt-responsive Rat2 fibroblasts [34]. In this study, lentiviral vectors were utilized to generate a pool of polyclonal Rat2 cell cultures that stably expressed either wild-type or mutant Wnt ligands. Although we did not succeed in preparation of Rat2 cells producing ΔNWnt1 and Wnt1(C93A,S209A) in levels comparable to the other forms (Fig. 6A and Supplementary Fig. S1), we used all types of transduced cells for following analyses. Total RNAs isolated from these Rat2 cells were utilized to examine the effect of each Wnt1 or Wnt3a variant on the transcription of the endogenous Wnt signalling target gene, *Axin2*. As a negative control, the Wnt-insensitive *Axin1* was analysed. In addition, mRNA levels of two housekeeping genes, *GAPDH* and *Ubb*, were assessed. The data generated from our qRT-PCR analysis agreed well with the results obtained in our reporter gene assay (Fig. 4B). *Axin2* mRNA was strongly up-regulated by wild-type proteins and the Wnt1(N29,316,359Q) mutant. Wnt3a(C77A) and Wnt3a(N87,298Q) were less stimulatory whilst the non-acylated forms of Wnt were not functional. Interestingly, Wnt1(C93A) showed a small level of activity in Rat2 fibroblasts (Fig. 4B).

Given that the previous experiments were unable to differentiate between autocrine and paracrine Wnt signalling, we decided to assess paracrine signalling only by co-culturing two different (one emitting and the other receiving the Wnt signal) cell types. We mixed "reporter" STF 293 cells with Rat2 fibroblasts stably expressing Wnt1 and Wnt3a variants. Cells were harvested 24 and 48 h after plating and SuperTOPFLASH activities were determined in cell lysates. Remarkably, "N-glycosylation-minus" Wnt1(N29,316,359Q) displayed reduced signalling capacity when paracrine only signalling was measured versus when both autocrine and paracrine signalling was determined (Fig. 4C).

To verify the results of the reporter gene assays we searched for a suitable cellular system that would allow us to directly visualize Wnt signalling. We noted that, in contrast to the majority of cells of human origin, mouse 3T3 and L cells robustly stabilize β-catenin upon addition of recombinant Wnt3a and accumulate β-catenin in the nuclei of stimulated cells (Fig. 5A). As such, constructs expressing Wnt1 or Wnt3a variants were lipofected into L or 3T3 cells grown on coverslips. The cells were fixed 24 h later and stained with anti-β-catenin and Wnt-specific antibodies (Fig. 5B and C; only data for L cells are shown). By visualizing the stabilization of β-catenin, we could detect Wnt signalling affected by wild-type, N-glycosylation-deficient and "single-acyl" mutant Wnt3a(C77A) proteins. In contrast, S-acyl-deficient Wnt1(C93A), non-acylated Wnt3a(S209A) and Wnt1 (S224A) and signalling peptide-devoid forms (ΔNWnt1, ΔNWnt3a) were inactive. Interestingly, the control ΔNWnt1 protein was localized to the cell nucleus [Fig. 5B; see also Supplementary Fig. S2C, panels o, o′]. We do not have any plausible explanation for this rather peculiar behaviour.

3.4. Non-functional Wnt proteins are secreted

An obvious explanation for the limited functionality of mutant Wnt proteins is their impaired secretion due to possible misfolding and retention within an intracellular compartment. To capture the extracellular pool of individual Wnt, relevant Wnt1- or Wnt3a-expression constructs were transfected into HEK 293, HeLa, 3T3 and L cells grown on coverslips. Twenty-four hours post-transfection, growing cells were briefly incubated with an anti-Wnt1 or anti-Wnt3a antibody. To visualize extracellular and membrane-associated Wnt (further referred to as "surface" Wnt) the cells were washed, fixed, permeabilized and the retained anti-Wnt immunoglobulins were directly stained with a fluorescently-conjugated secondary antibody. To detect intracellular Wnt, the samples were further subjected to another round of staining using the same primary antibody in combination with a differentially-labelled secondary antibody. The second staining also detected surface Wnt molecules whose epitopes were not fully saturated with the first-round staining [Supplementary Figs. S2A, panels l, l′; S2B, panels p, p′]. Approximately 20 cells of each cell type expressing particular Wnt were scanned using a confocal microscope. Virtually identical results were obtained for all utilized cell types (Supplementary Fig. S2). Importantly, we never observed surface labelling of intracellular ΔNWnt1 and ΔNWnt3a mutant proteins [Supplementary Fig. S2C, panel n]. Typically, single- or double-acyl-deficient ligands displayed a similar cell surface and intracellular distribution as wild-type Wnts. A somewhat different picture was observed for proteins lacking N-glycosylation. The surface localization of Wnt1(N29,316,359Q) was reduced whilst extracellular Wnt3a(N87,298Q) was almost undetectable. Nevertheless, the results from these assays exclude the possibility that limited secretion can explain the lack of activity demonstrated by the acyl-deficient Wnt proteins.

This observation led us to test the distribution of wild-type and mutated Wnt1 and Wnt3a in Rat2 cells stably expressing Wnt proteins. The cells (grown to 90% confluence in 10 cm dish) were detached by EGTA-treatment, and the surface of each dish was thoroughly washed and SDS-PAGE sample buffer used to yield any proteins associated with the ECM. To obtain the plasma membrane fractions, the detached cells were harvested, washed and disrupted under hypotonic conditions. Finally, whole-cell lysates (WCL) were obtained by direct lysis of cells growing in a parallel "replica" dish using SDS-PAGE sample buffer. Analysis of the ECM, membrane and WCL samples by immunoblotting revealed that wild-type and non-glycosylated polypeptides have a strong affinity for the ECM. The same biochemical feature was

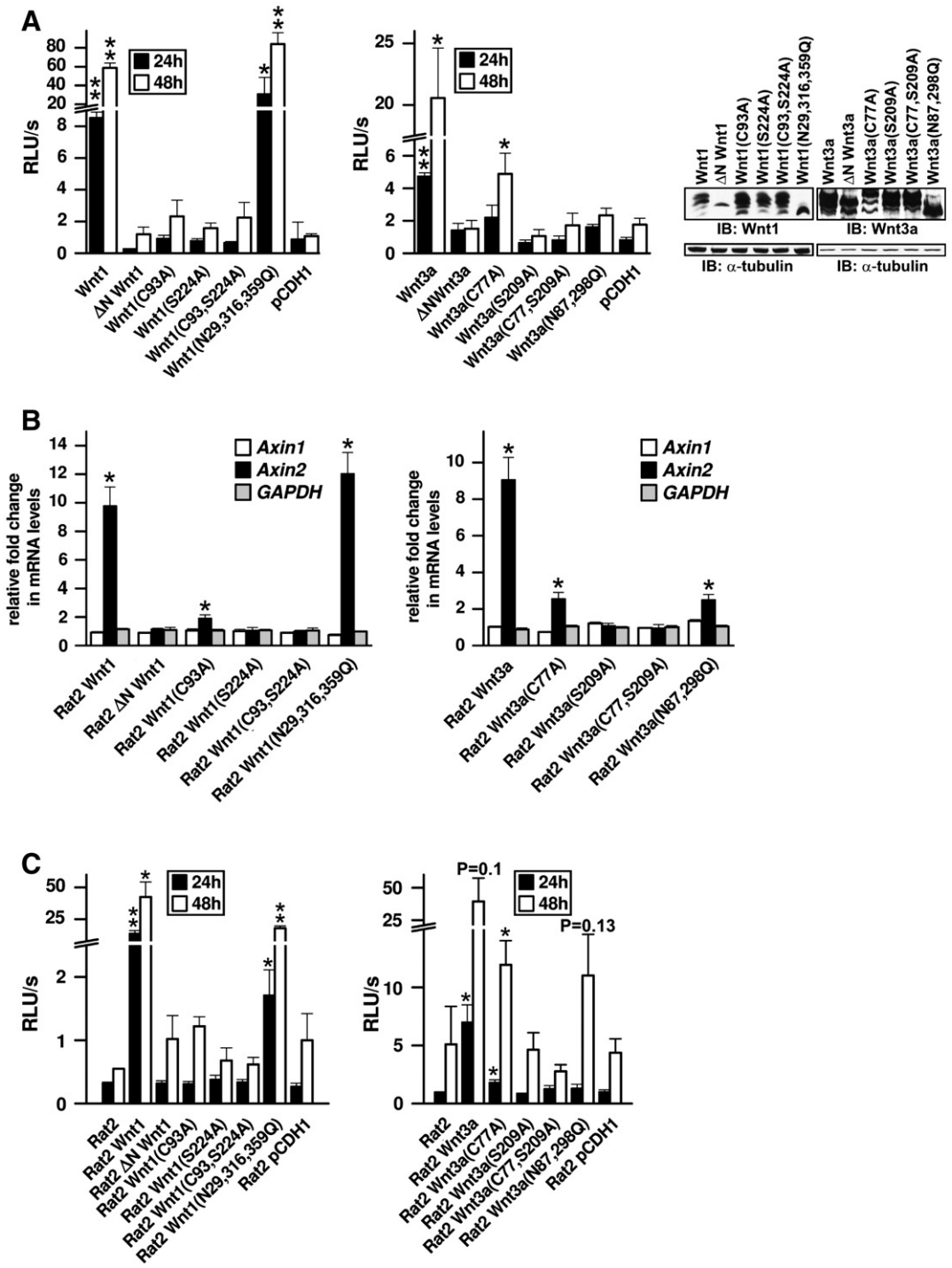

Fig. 4. Wnt3a lacking the palmitoylated cysteine residue retains the capacity to activate Wnt-dependent transcription in mammalian cells. (A) Activation of Wnt signalling in transiently transfected cells. HEK 293 cells containing the integrated reporter, SuperTOPFLASH (STF 293 cells), were transfected with constructs expressing wild-type or mutated variants of mouse Wnt1 (the left panel) or Wnt3a (the right panel) proteins. pCDH1 denotes cells transfected with an "empty" vector. Cells were harvested 24 or 48 h later and luciferase activities were determined in cell lysates. The histograms represent average luciferase light units per second (RLU/s) of a triplicate corrected for the efficiency of transfection using the internal control *Renilla* luciferase expression construct. SDs are shown by error bars. The results from one representative experiment out of three in total are shown. Western blots of whole-cell extracts prepared from STF 293 cells 24 h post-transfection are shown at the right. Blots were probed with anti-Wnt1, anti-Wnt3a or anti-α-tubulin [used as a "loading" control] antibodies. (B) qRT-PCR analysis of mRNAs isolated from Rat2 fibroblasts with retroviral constructs expressing wild-type or mutant Wnt1 or Wnt3a ligands. The resulting cells were used in triplicate experiments to determine the expression levels of *Axin2* (a Wnt signalling target gene), *Axin1* (negative control) and *Gapdh* (a "housekeeping" gene). The relative abundance of corresponding mRNAs was derived from the average CT values after normalizing to the levels of *ubiquitin B* (*Ubb*). The expression level of the genes in Rat2 cells transduced with the empty retroviral vector was set as 1. (C) Reduced activity of non-glycosylated Wnt1 protein in the paracrine signalling assay. STF 293 cells transfected with the *Renilla* luciferase expression construct were plated together with control cells [parental Rat2 fibroblasts or cells transduced with the empty lentivirus (denoted Rat2 pCDH1)] or with Rat2 cells stably producing the indicated Wnt constructs. The cells were harvested and lysed 24 or 48 h after plating. The average luciferase activities determined in cell lysates upon normalization to the *Renilla* levels are given. Results of three independent experiments performed in triplicates were combined to the final diagrams. Differences in values obtained in cells transfected/transduced with empty vector and in cells expressing given Wnt ligand was calculated by Student's t-test. $^{*}P<0.05$; $^{**}P<0.01$.

displayed by Wnt3a(C77A). The other ligands with reduced acyl content or completely without lipidation behaved differently and were preferentially co-isolated with membranes (Fig. 6A). Moreover, we attempted to evaluate how different forms of Wnt ligands are released from cells to culture medium (CM). We directly precipitated the proteins from CM using corresponding antibodies or, alternatively, we employed the purification protocol including Blue-Sepharose beads (see Materials and methods). The isolation was insensitive to any type of modification since all Wnt1 and Wnt3a variants could be quantitatively isolated from cell lysates (Fig. 6A). None of the Wnt1 forms was detected in CM. This was in stark contrast to Wnt3a, where all signalling-competent ligands were released to CM (Fig. 6A and data not shown).

Additionally, we examined the possible deposition of Wnt proteins on the ECM directly by confocal microscopy. Since the Wnt3a-specific signal was too low to obtain a good quality images, we used Rat2 cells expressing wild-type Wnt1 and Wnt1(C93A). The cells were seeded at low density onto coverslips and allowed to grow for 72 h. The specimens were stained using a protocol to capture both native extracellular/membrane-associated and intracellular Wnt (see Materials and methods). Strikingly, only wild-type Wnt1 displayed a remarkable deposition on the surface of the slip. This "deposit" was absent in the cells expressing mutated Wnt1(C93A), where the distribution of the proteins was localized to the membrane and intracellular compartments (Fig. 6B).

3.5. Non-acylated Wnt1 and Wnt3a are targeted to membrane microdomains and interact with the Frizzled receptor and Lrp co-receptor

Many palmitoylated proteins are associated with specialized detergent-resistant membrane microdomains (DRMs). These domains, also called lipid rafts, are thought to possibly serve as assembly sites for membrane signalling complexes [47]. Interestingly, it was previously shown that Wg is associated with DRMs and that ligands produced in cells grown in the presence of 2-bromopalmitate (an inhibitor of O-acyltransferases) lose their localization with lipid rafts [14]. We isolated membranes from cells transiently or stably expressing wild-type or mutant Wnt1 or Wnt3a. Cells were fractionated by ultracentrifugation according to density in a sucrose concentration gradient. Interestingly, all Wnts were located in the caveolin-containing, low-density fractions (presumable DRMs; Supplementary Fig. S3). This observation indicates that the presence of Wnts in lipid rafts is not dependent on their fatty acid content (or level of N-glycosylation). Furthermore, these results imply that there is no functional connection between Wnt signalling and the association of Wnt ligands with DRMs.

Finally, these results prompted us to examine the ability of wild-type and mutant Wnts to bind to their receptor, Fz, and co-receptor, Lrp. We performed a series of co-immunoprecipitation assays that showed no significant differences between the abilities of wild-type or signalling-deficient Wnt proteins to associate with both Fz4 and Lrp5 (Supplementary Fig. S4). In summary, although we noted that the signalling function of the tested Wnt ligands is related to their capacity to adhere to the ECM, the other biochemical features, including receptor complex binding and membrane distribution to lipid rafts, do not differ between wild-type and non-functional Wnt1 and Wnt3a proteins.

4. Discussion

Mouse Wnt1 and Wnt3a are two mammalian members of the Wnt family of extracellular signalling proteins that are modified post-translationally by N-glycosylation and fatty acid addition. The aim of this study was to define the relationship between post-translational modification and the signalling activities of these proteins. We demonstrated that for signalling in mammalian cells, the attachment of two fatty acid moieties is crucial. Originally it was presumed that the lipidic adducts mediate a tighter association of the ligand with the cell surface. However, our results reveal that the opposite is true and acylation promotes Wnt release into the extracellular space.

In agreement with previously published results [17,19], Wnt1 is modified at three out of the four predicted N-linked oligosaccharide sites, whilst Wnt3a is modified twice (Fig. 1A and B). As both Wnts showed a similar pattern of N-glycosylation in human, rodent and *Xenopus* cells (Supplementary Fig. S5), it seems that the positions of the N-glycosylated residues are invariant and independent of the cellular context [17,19,20,48]. Analogous to Wnt3a, the Wnt1 polypeptide includes two acyl additions located at different positions (Fig. 1). Strikingly, mutations preventing the attachment of O-linked fatty acid in both Wnt1 and Wn3a completely abolished palmitoylation at the N-terminal cysteine residue (Fig. 2). This implies that the initial lipidation of serine is essential for subsequent fatty acid modification. Such a conclusion is supported by the recent characterization of WntD. This *Drosophila* Wnt lacks the conserved serine that is contained in other Wnt ligands subjected to the acyl modification. Although WntD contains the potentially S-acylated site, the mature protein does not carry any lipidic adducts [16].

Fatty acid-deficient Wnts were still fully N-glycosylated, indicating that such modifications are not influenced by the presence or absence of fatty acyl moieties. The attachment of acyl adducts to Wnt molecules is presumably catalysed by O-acyltransferase Porcupine (Porc) [12,14,49]. Interestingly, the ectopic expression of Porc increased N-glycosylation of Wg and of several other mouse Wnt ligands [6,50]. Nevertheless, Wnt3a N-glycosylation is not affected in cells treated with Porc-specific siRNAs [8]. Interestingly, N-glycosylation-deficient Wnts displayed apparently reduced acyl content (Fig. 2). This would imply that N-glycosylation precedes and conditions Wnts for efficient acylation.

To compare the signalling properties of wild-type and post-translationally modified-deficient Wnts, several Wnt activity tests were performed. These tests included double axis formation in *Xenopus*, a reporter gene assay, qRT-PCR analysis and direct β-catenin staining in Wnt-responsive mammalian cells. In each assay performed, the acyl-deficient forms of Wnt1 [Wnt1(S224A), Wnt1(C93A, S224A)] and Wnt3a [Wnt3a(S209A), Wnt3a(C77, S209A)] were not able to function, implying that the presence of O-linked fatty acids is indispensable for correct signalling. Interestingly, we noted that non-palmitoylated Wnt1(C93A) and Wnt3a(C77A) exhibited different signalling capabilities depending upon the testing system used. In

Fig. 5. β-catenin stabilization test in mammalian cells. (A) Wnt signalling induces robust accumulation of β-catenin in mouse L cells. Laser scanning confocal microscopy images of L cells treated for 24 h either with recombinant Wnt3a or Wnt storage buffer. The cells were stained with an anti-β-catenin monoclonal antibody (red channel) or DAPI nuclear stain (blue channel). (B) The signalling properties of Wnt1 variants in L cells. Cells (grown on coverslips) were transfected with the indicated Wnt1-expression construct. Twenty-four hours later the cells were fixed, permeabilized and washed with PBS. Subsequently, the specimens were incubated with rabbit anti-Wnt1 polyclonal and mouse anti-β-catenin monoclonal antibodies. Rabbit immunoglobulins were detected using the ALEXA 488 dye conjugated to a goat anti-rabbit antibody [shown in greyscale in panels b, f, j, n, r; or depicted in green in the merged images (d, h, l, p, t)]. β-catenin-specific staining was visualized with the ALEXA 594 dye conjugated to a goat anti-mouse antibody [panels c, g, k, o, s; or red in the merged images]. The merged pictures were generated by overlaying the corresponding images gained in each appropriate input channel with the image obtained in the blue channel to capture DAPI nuclear staining [shown in greyscale in panels a, e, i, m, q; in blue in the merged images]. Boxed areas in (d), (h), (l), (p) and (t) are magnified in (d′), (h′), (l′), (p′), and (t′), respectively. (C) The β-catenin stabilizing activity of Wnt3a and its variants. L cells transfected with Wnt3a constructs were processed as in panel B using antigen-purified anti-Wnt3a polyclonal antiserum and anti-β-catenin monoclonal antibodies. Bar, 10 μm.

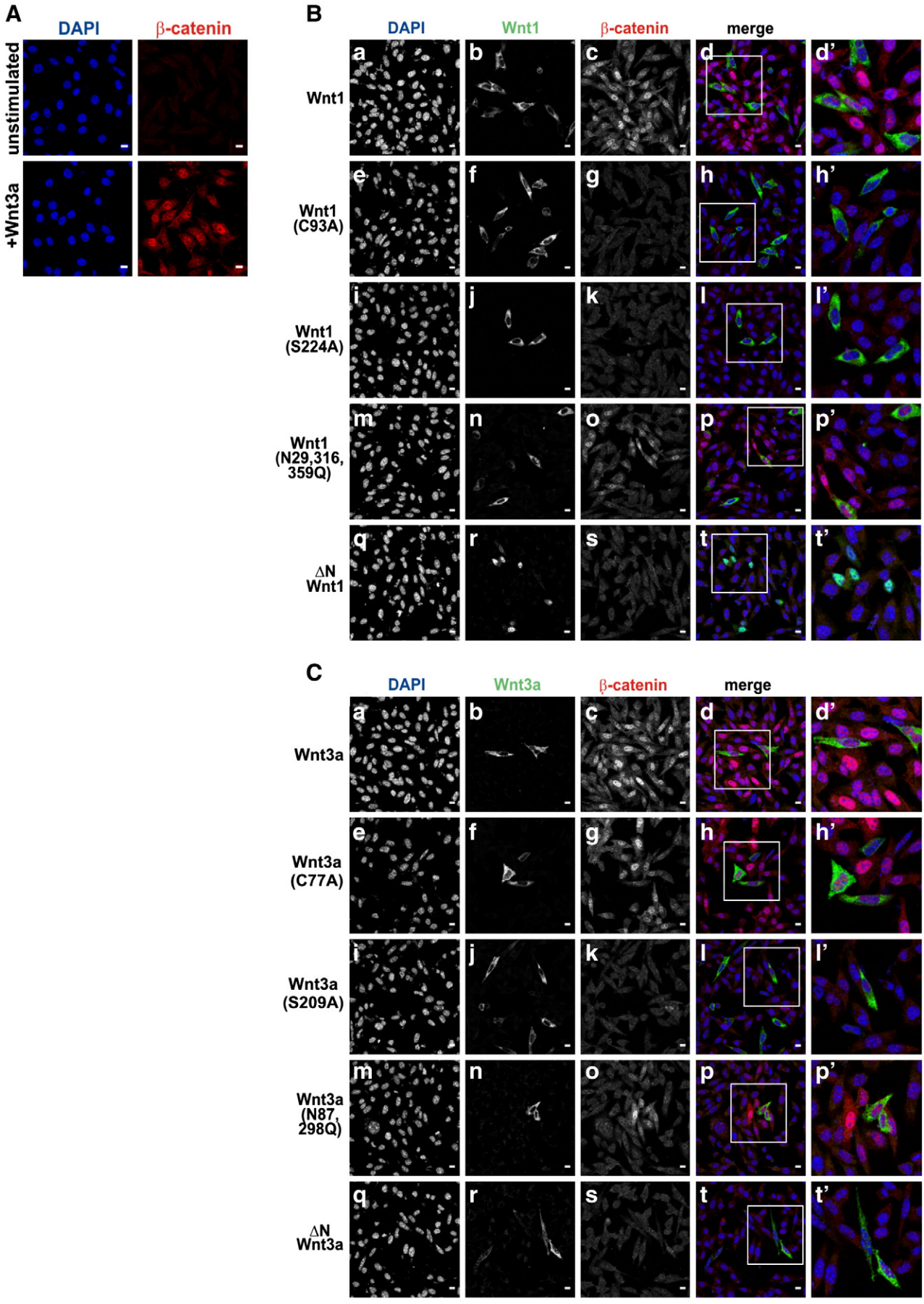
A
DAPI
β-catenin
unstimulated
+Wnt3a
B
DAPI
Wnt1
β-catenin
merge
Wnt1
Wnt1 (C93A)
Wnt1 (S224A)
Wnt1 (N29,316, 359Q)
ΔN Wnt1
C
DAPI
Wnt3a
β-catenin
merge
Wnt3a
Wnt3a (C77A)
Wnt3a (S209A)
Wnt3a (N87, 298Q)
ΔN Wnt3a

Xenopus embryos Wnt3a(C77A) was active as wild-type ligand and related Wnt1(C93A) retained approximately one third of the signalling capacity of wild-type Wnt1 (Fig. 3). On the other hand, in mammalian cells, the relationship between lipidation and function is apparently more stringent as we observed only limited signalling from single-acylated Wnt3a(C77A) and Wnt1(C93A) (Figs. 4 and 5). In the double axis formation assay the exogenous proteins function in the presumably complex cellular environment of developing embryo that contains various endogenous Wnt ligands and Wnt signalling inhibitors. The resulting phenotype (secondary axis) is generated by interplay among these proteins. Therefore, in the case that mutant Wnt retains some capacity to bind and block the inhibitors, the secondary axis might be induced even by signalling-deficient ligand. Alternatively, *Xenopus* cells can produce a different set of the Frizzled receptors than mammalian cells that can be effectively stimulated even by S-acyl-deficient Wnt1 or Wnt3a.

We observed that non-glycosylated Wnt3a was always less active than its wild-type counterpart (Figs. 3 and 4). This observation is consistent with the slower rate of secretion of non-glycosylated Wnt3a (Supplementary Fig. 2B). Similarly, N-glycosylation-deficient Wnt1 displayed decreased surface expression and reduced paracrine signalling (Fig. 4C and Supplementary Fig. S2A and C). Paradoxically, Wnt1(N29,316,359Q) was the best performing Wnt in all tests that included autocrine signalling (e.g. formation of artificial body axis).

Our results demonstrate that for intracellular transport to the cellular surface, fatty acid modification is not essential. Interestingly, the absence of lipidic adducts does not influence Wnt targeting to DRMs (lipid rafts; Supplementary Fig. S3). This observation is contradictory to the previous finding of Zhai and colleagues [14]. These researchers showed that 2-bromopalmitate, a systemic inhibitor of O-acyltransferase activity, abolishes the fractionation of Wg with DRMs. To our knowledge, the localization of these mutant Wnt

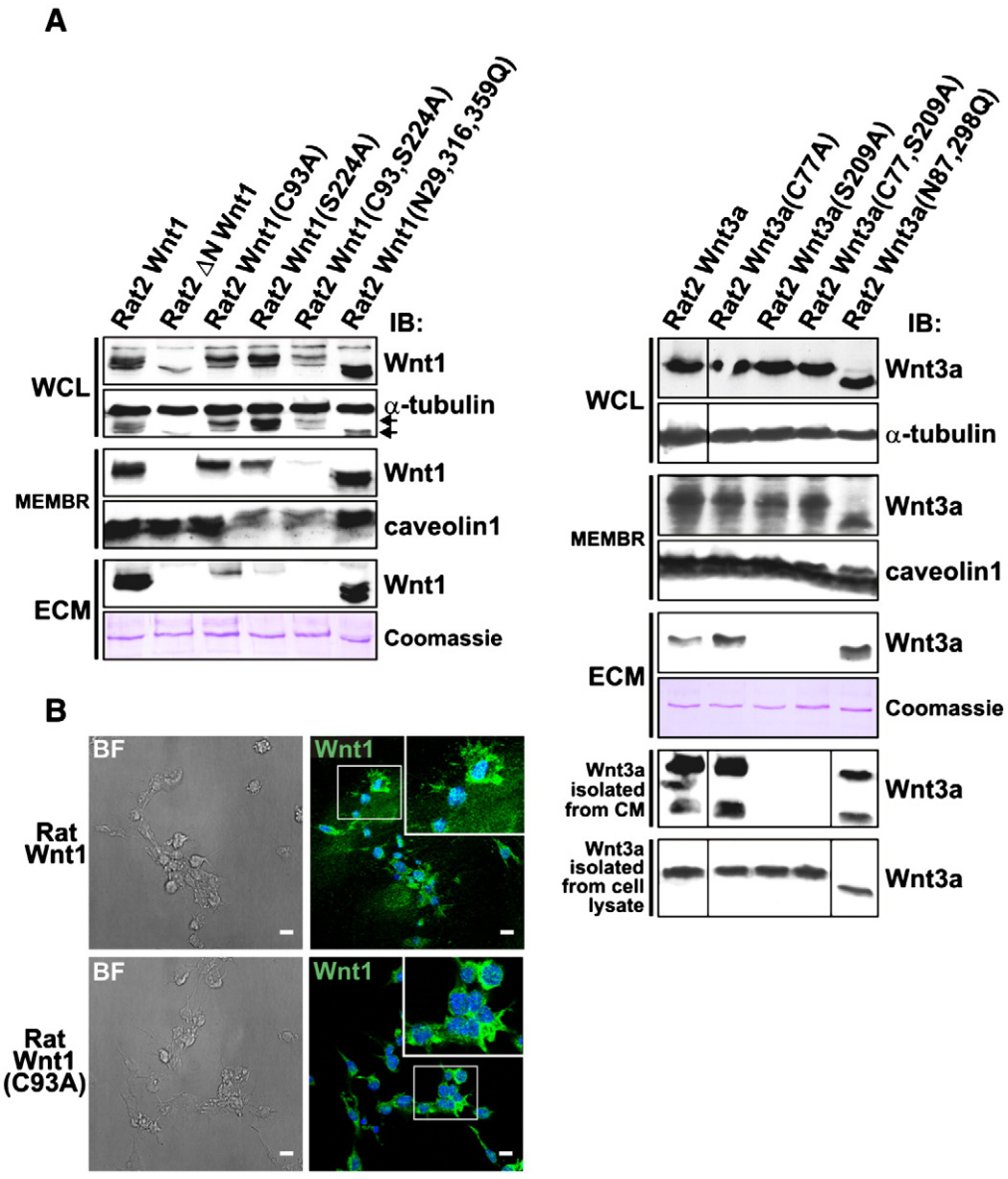

Fig. 6. Acylation promotes deposition of Wnt1 and Wnt3a on the ECM. (A) Cellular distribution of Wnt1 and Wnt3a variants expressed in Rat2 fibroblasts. Western blot analysis of indicated Wnt proteins present in whole-cell lysates (WCL) or co-isolated with plasma membranes (MEMBR) or the ECM. As loading controls, blots were re-probed with anti-α-tubulin and anti-caveolin1 antibodies, or the gel replicas were stained with Coomassie Brilliant Blue (Coomassie). Notice the remnants of the Wnt1 signal on the anti-α-tubulin-stained blot (arrows).The bottom two panels on the right show immunoblots of Wnt3a purified from conditioned media (CM) or cell lysates using Blue Sepharose. (B) Laser scanning confocal microscopy images of Rat2 fibroblasts stably producing wild-type Wnt1 or Wnt1(C93A) mutant polypeptides. Right, both extracellular and intracellular Wnt1 were stained using a rabbit anti-Wnt1 antibody followed by a goat anti-rabbit ALEXA 488 dye-conjugated secondary antibody. Bright field (BF) images are shown on the left. Bar, 10 μm.

proteins to lipid rafts has not been tested. Thus, we suggest that the association of Wnts with DRMs might be mediated via a protein–protein interaction that is not dependent on the presence of any acyl modification. In favour of this theory, protein targeting to DRMs via this mechanism was recently proposed for a variant of the SHP-1 protein phosphatase [51]. Further, we have shown that the interaction of Wnts with the Fz receptor or Lrp co-receptor is independent of the acylation or N-glycosylation status of Wnts (Supplementary Fig. S4). This result is somewhat controversial, as two previous publications indicated that Wnt3a containing no S-linked acyl moiety is unable to bind to Lrp or Fz [17,28]. Both studies, however, demonstrated this phenomenon via pull-down assays that utilized Wnt3a interacting with only recombinant fragments of Fz and Lrp, rather than co-immunoprecipitations using full-length proteins. Therefore, the variation in experimental procedure may explain the different outcomes.

Finally, we tested the distribution of wild-type and mutated Wnt1 and Wnt3a in Rat2 cells stably expressing Wnt proteins. In contrast to Wnt3a, we have never observed the release of any form of Wnt1 into culture medium. This is in agreement with previous studies demonstrating that only a minimal portion of biosynthetically labelled Wnt1 can be detected in cell supernatants [18,25]. Strikingly, we noted that only wild-type Wnt1 and non-glycosylated Wnt1 (N29,316,359Q) protein strongly associate with the ECM. This association was dramatically reduced by the absence of the S-acyl group and was almost completely abolished in acyl-deficient ligand. Instead, both these mutant proteins were preferentially co-isolated with the membrane fraction (Fig. 6A). This observation is consistent with previous findings that indicated that the interaction of Wg with extracellular matrix proteins helps it to spread in the extracellular milieu [52]. The nature of the deposits visualized by staining of native Wnt1 ligand (Fig. 6B), possible involvement of heparan sulfate proteoglycans (HSPGs) in Wnt1/Wnt3a movement, and the mechanisms mediating the Wnt1 (and Wnt3a) interaction to the ECM or plastic surface of the culture dish are unclear. Since the non-glycosylated forms of both Wnt1 and Wnt3a are signalling-competent and display similar biochemical features as wild-type protein, it would seem that N-glycosylation is less important than acylation for the transport of Wnts into the extracellular space. Interestingly, all Wnt3a variants that displayed signalling activity [wild-type Wnt3a, Wnt3a(C77A), Wnt3a(N87,298Q)] were not only deposited on the ECM, but they were also found in culture supernatants. Recently, Neumann and colleagues have discovered that Wnt3a is released from mammalian cells as lipoprotein particles. Wnt3a lacking its palmitate moiety is still secreted; nevertheless, its activity is reduced [53]. Remarkably, liposomal packaging of recombinant Wnt3a using exogenous lipids potentiates its signalling function [54]. In conclusion, the role of the N-terminal palmitate is to mediate lipoprotein packaging that subsequently enhances the action of Wnt3a ligand. Very recently, Coombs and co-authors reported that Wnt3a binding to the carrier protein wntless (WLS) requires lipid modification of Wnt3a at serine 209 [30]. Since acyl-deficient Wnts still reach the cell surface, we presume that mutant Wnts, similarly to non-lipidated WntD, might utilize yet another route of secretion that is not dependent on WLS. Given the results outlined above, we wonder why acylation is essential for Wnt activity. One plausible explanation recently proposed by Bazan and de Sauvage would be that only lipidated Wnt can productively engage with the Fz receptor [55].

Despite a number of revealing facts about the role of acylation and N-glycosylation for Wnt signalling, our study still raises a number of important questions. We still do not know whether differential acylation of Wnt ligands can regulate their gradients in various tissues. Further, although it was thought that Wnt1 and Wnt3a were redundant in the mouse [56], we observed their distinct features in some of our biochemical and functionality tests. Clearly more studies are needed to answer these and other critical questions regarding the intriguing role of Wnt signalling in living organisms.

Acknowledgements

We thank V. Bryja, X. He, and M. Semenov for the constructs; we are grateful to J. Nathans and Q. Xu for cell lines used in the study. We further thank A. Corlett and S. Takacova for critically reading the manuscript. This work was supported by the Grant Agency of the Czech Republic [grant numbers 204/07/1567 and 204/09/H058] and by the project Centre of Molecular and Cellular Immunology [1M0506] from the Ministry of Education, Youth and Sports of the Czech Republic. The Institute of Molecular Genetics is supported by an institutional grant from the Academy of Sciences of the Czech Republic [AV0Z50520514].

Appendix A. Supplementary data

Supplementary data to this article can be found online at doi:10.1016/j.cellsig.2011.01.007.

References

[1] K.M. Cadigan, Y.I. Liu, J. Cell Sci. 119 (2006) 395.
[2] R. van Amerongen, R. Nusse, Development 136 (2009) 3205.
[3] T. Reya, H. Clevers, Nature 434 (2005) 843.
[4] K.M. Cadigan, Curr. Biol. 18 (2008) R943.
[5] A. Weise, K. Bruser, S. Elfert, B. Wallmen, Y. Wittel, S. Wohrle, A. Hecht, Nucleic Acids Res. 38 (2010) 1964.
[6] K. Tanaka, Y. Kitagawa, T. Kadowaki, J. Biol. Chem. 277 (2002) 12816.
[7] K.M. Cadigan, R. Nusse, Genes Dev. 11 (1997) 3286.
[8] R. Takada, Y. Satomi, T. Kurata, N. Ueno, S. Norioka, H. Kondoh, T. Takao, S. Takada, Dev. Cell 11 (2006) 791.
[9] K. Willert, J.D. Brown, E. Danenberg, A.W. Duncan, I.L. Weissman, T. Reya, J.R. Yates III, R. Nusse, Nature 423 (2003) 448.
[10] F. Port, K. Basler, Traffic 11 (2010) 1265.
[11] M.J. Lorenowicz, H.C. Korswagen, Exp. Cell Res. 315 (2009) 2683.
[12] L.M. Galli, T.L. Barnes, S.S. Secrest, T. Kadowaki, L.W. Burrus, Development 134 (2007) 3339.
[13] M. Kurayoshi, H. Yamamoto, S. Izumi, A. Kikuchi, Biochem. J. 402 (2007) 515.
[14] L. Zhai, D. Chaturvedi, S. Cumberledge, J. Biol. Chem. 279 (2004) 33220.
[15] X. Franch-Marro, F. Wendler, J. Griffith, M.M. Maurice, J.P. Vincent, J. Cell Sci. 121 (2008) 1587.
[16] W. Ching, H.C. Hang, R. Nusse, J. Biol. Chem. 283 (2008) 17092.
[17] H. Komekado, H. Yamamoto, T. Chiba, A. Kikuchi, Genes Cells 12 (2007) 521.
[18] L.W. Burrus, A.P. McMahon, Exp. Cell Res. 220 (1995) 363.
[19] J. Papkoff, A.M. Brown, H.E. Varmus, Mol. Cell. Biol. 7 (1987) 3978.
[20] A.M. Brown, J. Papkoff, Y.K. Fung, G.M. Shackleford, H.E. Varmus, Mol. Cell. Biol. 7 (1987) 3971.
[21] D.Y. Coudreuse, G. Roel, M.C. Betist, O. Destree, H.C. Korswagen, Science 312 (2006) 921.
[22] S. Pfeiffer, S. Ricardo, J.B. Manneville, C. Alexandre, J.P. Vincent, Curr. Biol. 12 (2002) 957.
[23] K. Bartscherer, M. Boutros, EMBO Rep. 9 (2008) 977.
[24] J. Papkoff, B. Schryver, Mol. Cell. Biol. 10 (1990) 2723.
[25] B.D. Smolich, J.A. McMahon, A.P. McMahon, J. Papkoff, Mol. Biol. Cell 4 (1993) 1267.
[26] V. Greco, M. Hannus, S. Eaton, Cell 106 (2001) 633.
[27] D. Panakova, H. Sprong, E. Marois, C. Thiele, S. Eaton, Nature 435 (2005) 58.
[28] F. Cong, L. Schweizer, H. Varmus, Development 131 (2004) 5103.
[29] J. Kitajewski, J.O. Mason, H.E. Varmus, Mol. Cell. Biol. 12 (1992) 784.
[30] G.S. Coombs, J. Yu, C.A. Canning, C.A. Veltri, T.M. Covey, J.K. Cheong, V. Utomo, N. Banerjee, Z.H. Zhang, R.C. Jadulco, G.P. Concepcion, T.S. Bugni, M.K. Harper, I. Mihalek, C.M. Jones, C.M. Ireland, D.M. Virshup, J. Cell Sci. 123 (2010) 3357.
[31] T. Valenta, J. Lukas, V. Korinek, Nucleic Acids Res. 31 (2003) 2369.
[32] J.C. Hsieh, L. Kodjabachian, M.L. Rebbert, A. Rattner, P.M. Smallwood, C.H. Samos, R. Nusse, I.B. Dawid, J. Nathans, Nature 398 (1999) 431.
[33] S.F. Jue, R.S. Bradley, J.A. Rudnicki, H.E. Varmus, A.M. Brown, Mol. Cell. Biol. 12 (1992) 321.
[34] L. Doubravska, S. Simova, L. Cermak, T. Valenta, V. Korinek, L. Andera, Apoptosis 13 (2008) 573.
[35] Q. Xu, Y. Wang, A. Dabdoub, P.M. Smallwood, J. Williams, C. Woods, M.W. Kelley, L. Jiang, W. Tasman, K. Zhang, J. Nathans, Cell 116 (2004) 883.
[36] T. Valenta, J. Lukas, L. Doubravska, B. Fafilek, V. Korinek, EMBO J. 25 (2006) 2326.
[37] U.K. Laemmli, Nature 227 (1970) 680.
[38] J. Lukas, P. Mazna, T. Valenta, L. Doubravska, V. Pospichalova, M. Vojtechova, B. Fafilek, R. Ivanek, J. Plachy, J. Novak, V. Korinek, Nucleic Acids Res. 37 (2009) 3007.
[39] M. Bar-Peled, N.V. Raikhel, Anal. Biochem. 241 (1996) 140.
[40] P.D. Nieuwkoop, Acta Biotheor. 17 (1967) 151.
[41] M. Kuhl, S. Finnemann, O. Binder, D. Wedlich, Mech. Dev. 54 (1996) 71.
[42] J. Vandesompele, K. De Preter, F. Pattyn, B. Poppe, N. Van Roy, A. De Paepe, F. Speleman, Genome Biol. 3 (2002) RESEARCH0034.

[43] V. Korinek, N. Barker, P.J. Morin, D. van Wichen, R. de Weger, K.W. Kinzler, B. Vogelstein, H. Clevers, Science 275 (1997) 1784.
[44] A. Kaykas, R.T. Moon, BMC Cell Biol. 5 (2004) 16.
[45] D. Wessel, U.I. Flugge, Anal. Biochem. 138 (1984) 141.
[46] M.T. Veeman, D.C. Slusarski, A. Kaykas, S.H. Louie, R.T. Moon, Curr. Biol. 13 (2003) 680.
[47] D. Lingwood, K. Simons, Science 327 (2010) 46.
[48] J. Papkoff, Mol. Cell. Biol. 9 (1989) 3377.
[49] T. Kadowaki, E. Wilder, J. Klingensmith, K. Zachary, N. Perrimon, Genes Dev. 10 (1996) 3116.
[50] K. Tanaka, K. Okabayashi, M. Asashima, N. Perrimon, T. Kadowaki, Eur. J. Biochem. 267 (2000) 4300.
[51] U. Lorenz, Immunol. Rev. 228 (2009) 342.
[52] G.H. Baeg, X. Lin, N. Khare, S. Baumgartner, N. Perrimon, Development 128 (2001) 87.
[53] S. Neumann, D.Y. Coudreuse, D.R. van der Westhuyzen, E.R. Eckhardt, H.C. Korswagen, G. Schmitz, H. Sprong, Traffic 10 (2009) 334.
[54] N.T. Morrell, P. Leucht, L. Zhao, J.B. Kim, D. ten Berge, K. Ponnusamy, A.L. Carre, H. Dudek, M. Zachlederova, M. McElhaney, S. Brunton, J. Gunzner, M. Callow, P. Polakis, M. Costa, X.M. Zhang, J.A. Helms, R. Nusse, PLoS ONE 3 (2008) e2930.
[55] J.F. Bazan, F.J. de Sauvage, Cell 138 (2009) 1055.
[56] M. Ikeya, S.M. Lee, J.E. Johnson, A.P. McMahon, S. Takada, Nature 389 (1997) 966.

Supplementary Figures

Supplementary Figure S1 Comparison of expression levels of ectopic Wnt1 and Wnt3a mRNAs in Rat2 cells

qRT-PCR analysis of total RNA isolated from Rat2 fibroblasts transduced with retroviral constructs expressing wild-type or mutant Wnt1 or Wnt3a ligands. The abundance of corresponding mRNA is given as the average CT values after normalizing to the *Ubb* levels.

Supplementary Figure S2 Non-acylated and non-N-glycosylated Wnt1 and Wnt3a are secreted

(**A**) Laser scanning confocal microscopy images of HeLa cells transfected with the indicated Wnt1-expression constructs grown overnight on coverslips. To visualize extracellular Wnt1, living cells were incubated with fresh culture medium containing antigen-purified anti-Wnt1 polyclonal antiserum (30 min at 37°C). Cells were then washed, fixed in paraformaldehyde and treated with Triton X-100. The retained rabbit immunoglobulins were directly stained using the ALEXA 488 dye conjugated to a goat anti-rabbit antibody. Subsequently, the specimens were carefully rinsed with PBS and incubated with the same anti-Wnt1 primary antibody. The final staining was performed with ALEXA 594 conjugated to a goat anti-rabbit antibody. The merged images (d, h, l, p, t) were generated by an overlay of the corresponding scans gained in the green input channel detecting extracellular or endocytosed Wnt/immunoglobulin complexes [panels (b, f, j, n, r)], red input channel (c, g, k, o, s) detecting mainly intracellular and partly extracellular [see e.g. the panel (l)] Wnt and blue channel capturing the DAPI nuclear stain (a, e, i, m, q). Boxed areas in (d), (h), (l), (p) and (t) are magnified in (d'), (h'), (l'), (p'), and (t'), respectively. (**B**) HeLa cells were transfected with Wnt3a constructs and processed as in (A) using antigen-purified anti-Wnt3 polyclonal

antiserum. (**C**) Laser scanning confocal microscopy images of L cells transfected with the indicated Wnt1-expression constructs. The cells were processed as in (A); greyscale images are presented only. Boxed areas in (b), (e), (h), (k) and (o) are magnified in (b'), (e'), (h'), (k'), and (o'), respectively. Bar, 10 μm.

Supplementary Figure S3 The absence of acyl adducts does not influence Wnt1 targeting to lipid rafts

Density gradients of the membrane fractions isolated from Rat2 cells stably expressing wild-type Wnt1 or mutant non-acylated Wnt1(S224A). Six fractions were taken from top (T) to bottom (B) of sucrose gradient and subjected to immunoblotting (IB) with the antibody as indicated.

Supplementary Figure S4 All secreted variants of Wnt1 or Wnt3a interact with the Frizzled receptor and Lrp co-receptor

Co-immunoprecipitation of EGFP-tagged mouse Frizzled 4 (Fz4-EGFP) and Flag-tagged mouse Lrp5 (Lrp5-Flag) with different Wnt1 and Wnt3a proteins. Cell lysates prepared from HEK 293 cells transfected with constructs as indicated were precipitated using anti-Wnt1 or anti-Wnt3a rabbit polyclonal antibodies. Precipitated Wnt proteins were detected using the appropriate chicken anti-Wnt antisera. Anti-Flag or anti-EGFP monoclonal antibodies were used to detect Lrp5 and Fz8, respectively. In lanes denoted "input", ten percent of the total lysate used for one immunoprecipitation were loaded. Notice negligible association of Lrp5 or Fz8 with intracellular ΔNWnt3a and ΔNWnt1 proteins. IB, immunoblotting; IP, immunoprecipitation.

Supplementary Figure S5 The N-glycosylation status of Wnt1 and Wnt3a in Xenopus cells

Xenopus A6 cells were lipofected with the indicated Wnt-expression constructs. Transfected cells were processed as described in the legend to Fig. 1B.

Supplementary Figure S1

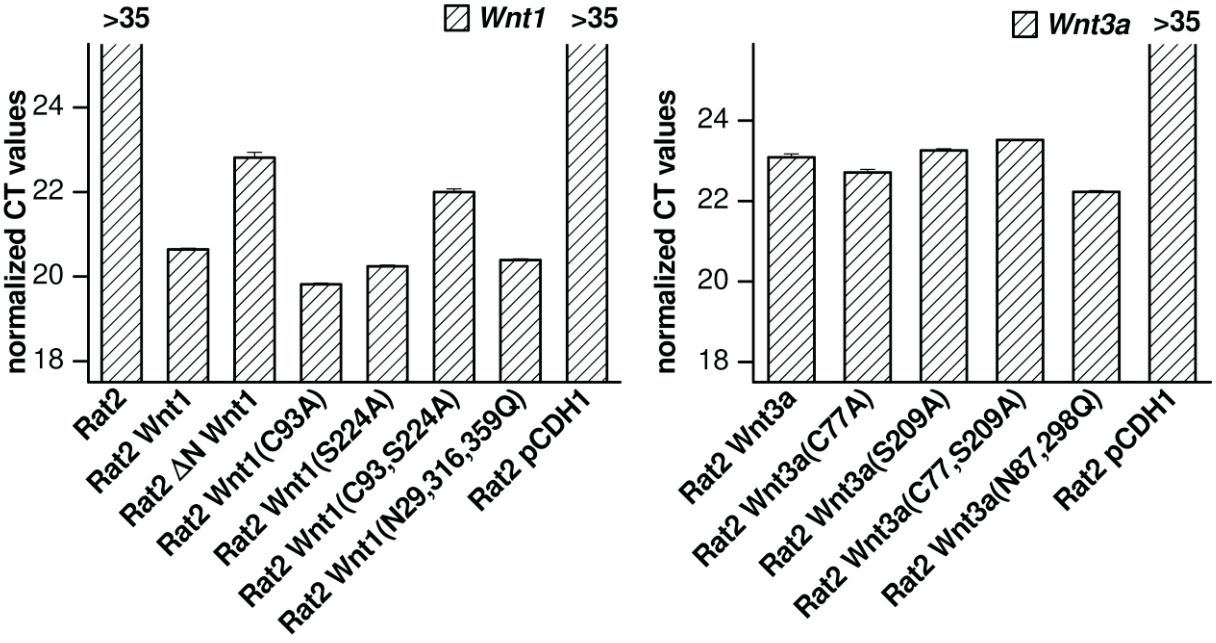

Supplementary Figure S2

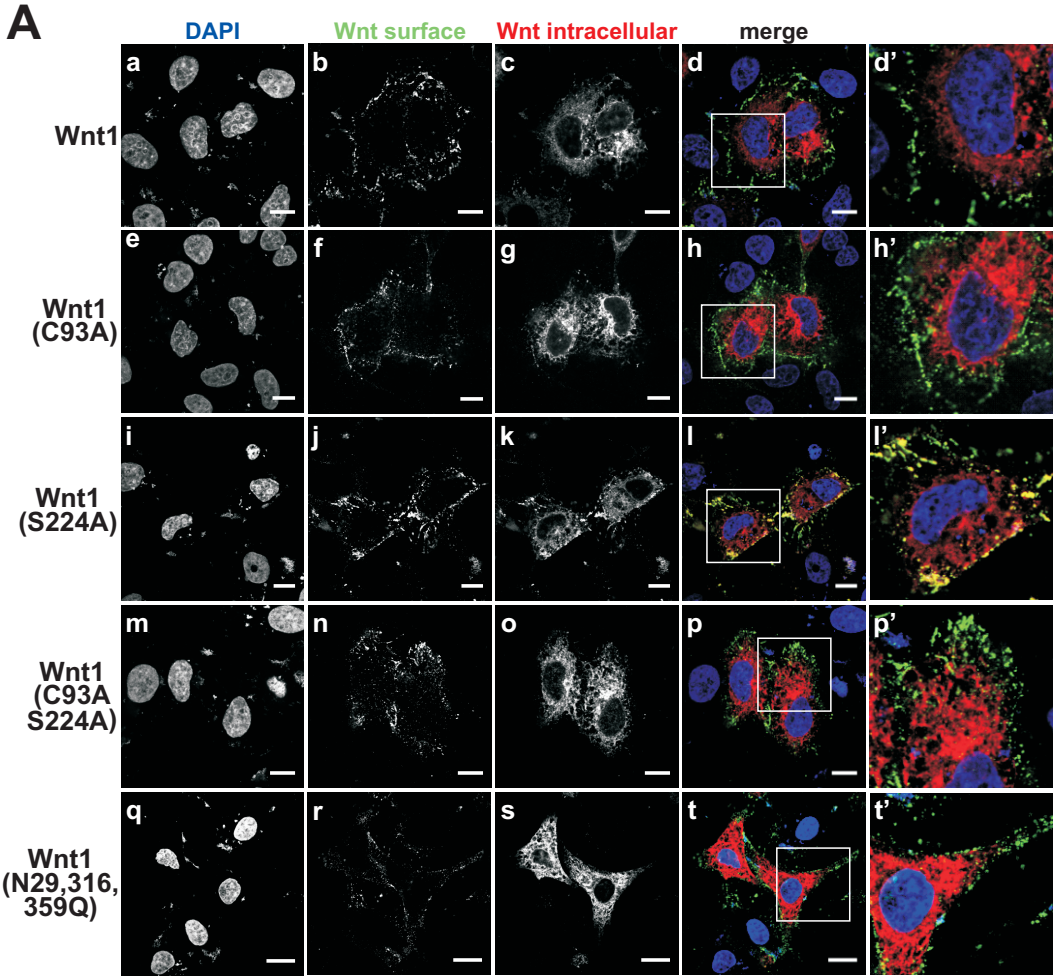

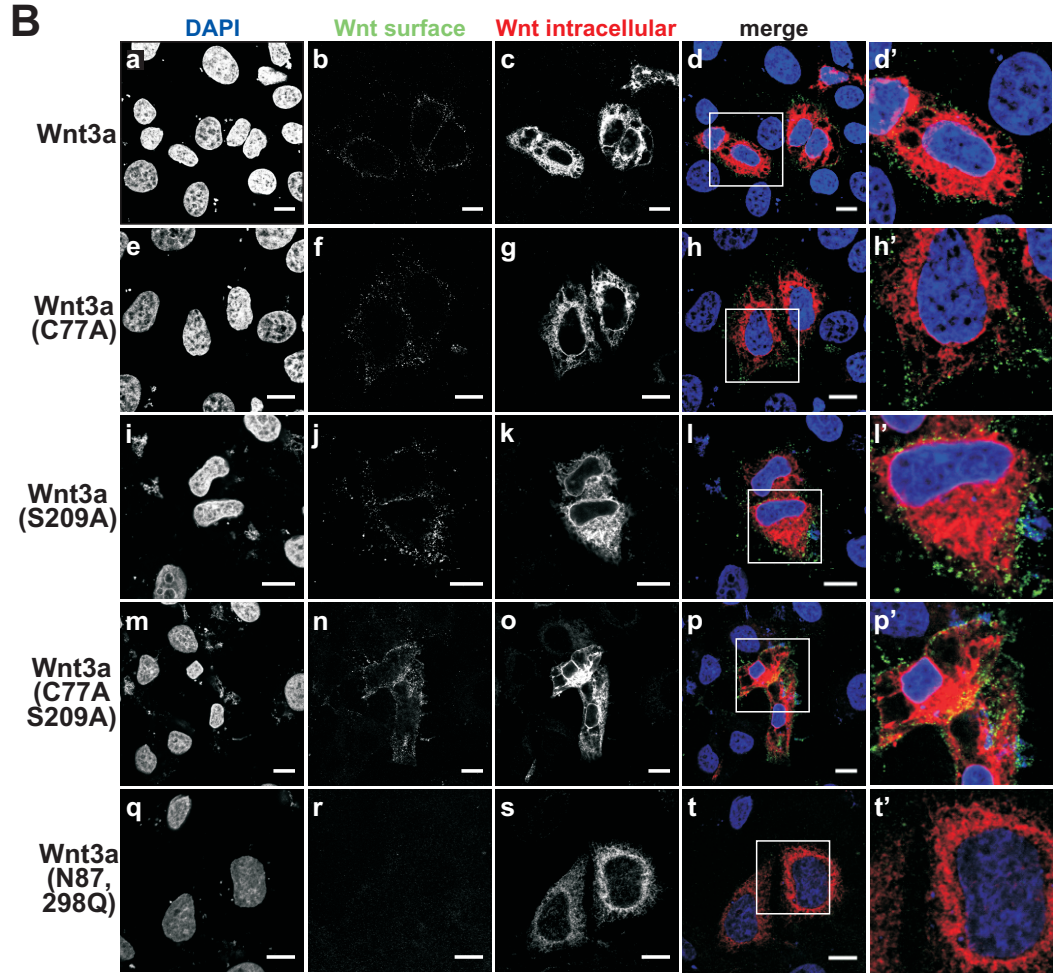

Supplementary Figure S2

C

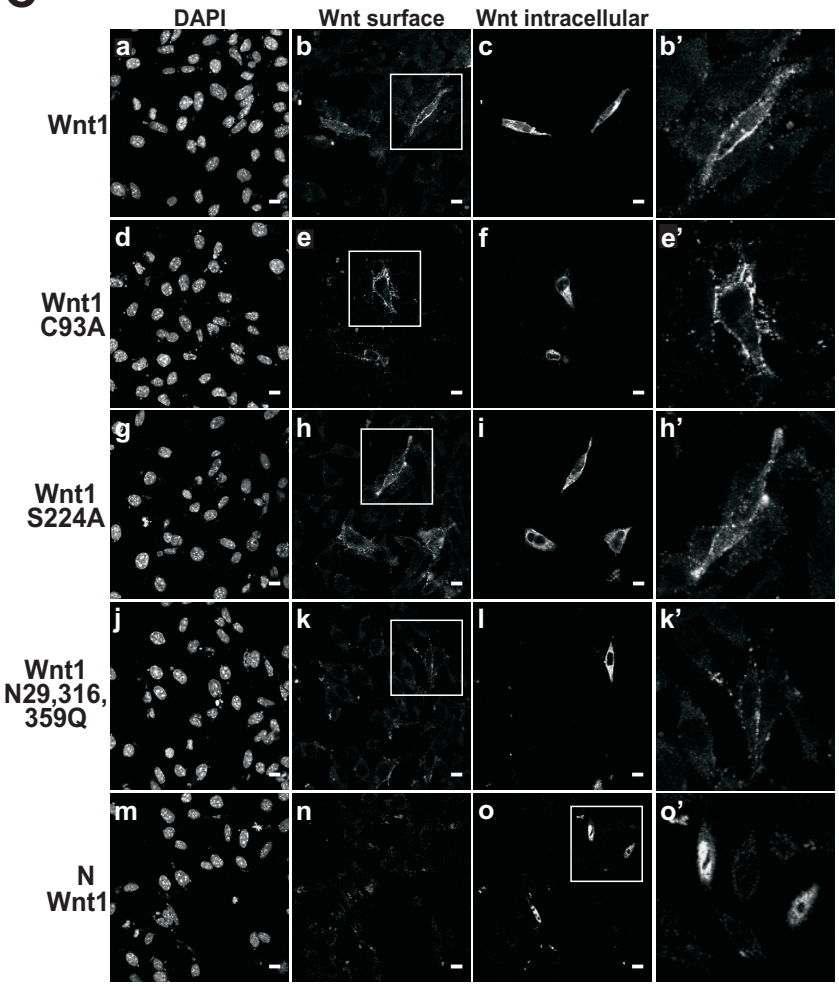

Supplementary Figure S3

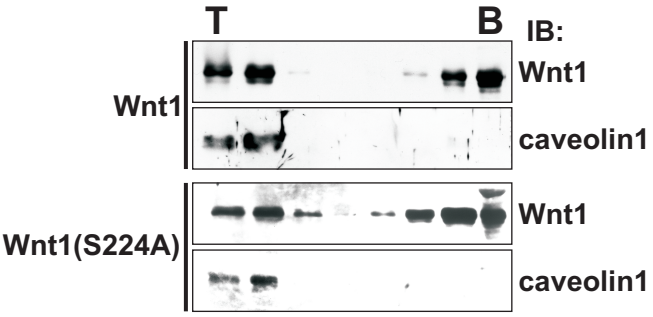

Supplementary Figure S4

Wnt1 wt	+	–	–	–	–	–
N	–	+	–	–	–	–
C93A	–	–	+	–	–	–
S224A	–	–	–	+	–	–
C93A,S224A	–	–	–	–	+	–
N29,316,359Q	–	–	–	–	–	+
Lrp5-Flag	+	+	+	+	+	+
Fz4-EGFP	+	+	+	+	+	+

Wnt3a wt	+	–	–	–	–	–
N	–	+	–	–	–	–
C77A	–	–	+	–	–	–
S209A	–	–	–	+	–	–
C77A,S209A	–	–	–	–	+	–
N87,298Q	–	–	–	–	–	+
Lrp5-Flag	+	+	+	+	+	+
Fz4-EGFP	+	+	+	+	+	+

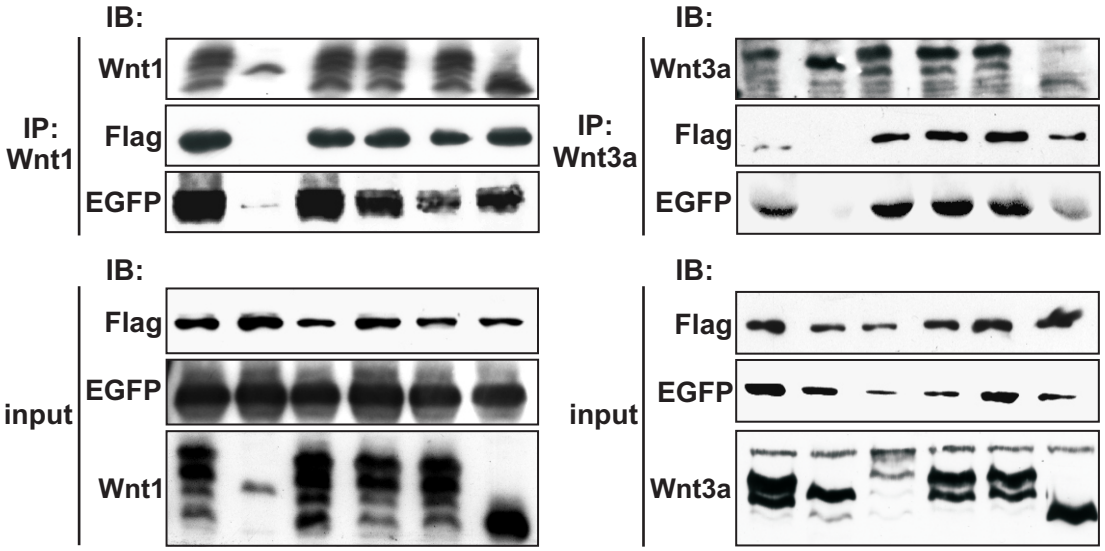

Supplementary Figure S5

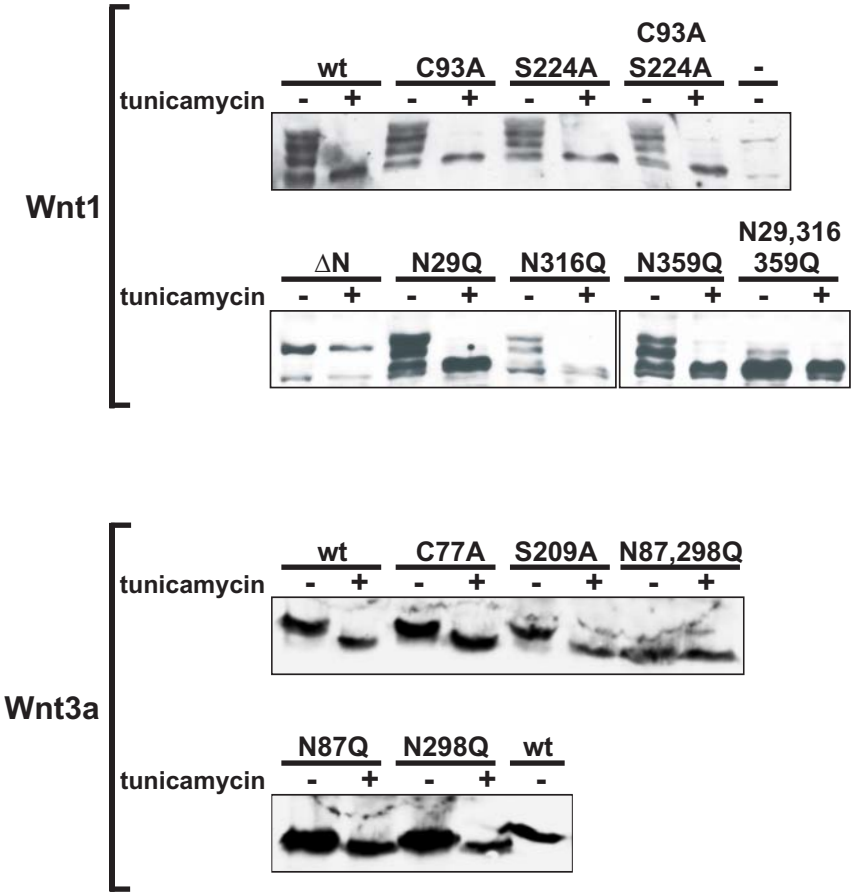

Generation of two modified mouse alleles of the Hic1 tumor suppressor gene

Transcription factor *HIC1* was previously identified in our laboratory as a protein interacting with the TCF4/β-catenin complex[191]. It has been defined that HIC1 and restrain TCF4/β-catenin proteins from the Wnt-responsive promoters and thus attenuates the Wnt signaling output[191].

HIC1 was named according to the fact, that it resides in a CpG island and its promoter is frequently epigenetically silenced in human tumors. Data from mice have firmly established *Hic1* as a tumor suppressor gene which deficiency leads to gender specific cancer development[263]. Complete ablation of *Hic1* results in prenatal mortality, probably due to severe developmental defects of the head and limbs[264]. The phenotypes emphasize the biological importance of *Hic1*, but the embryonic lethality limits the use of *Hic1*-defficient mice for further studies and calls for generation of the *Hic1* conditional knock-out allele.

The present article describes generation of two new strains dedicated to study the role of Hic1 and relation of this protein to the Wnt pathway *in vivo*.

The first mouse strain, the $Hic1^{flox}$ mice, harbors a conditional *Hic1* null allele with the coding region folxed by two loxP sites. When are these animals crossed to animals expressing Cre recombinase, large portion of *Hic1* coding DNA is excised in Cre-expressing cells. This enables to inactivate the gene in selected tissues.

The second mouse strain harbors a gene encoding a monomeric variant of enhanced green fluorescent protein, citrine, instead of major coding part of *Hic1*. The $Hic1^{cit/+}$ mice are viable and fertile and allow tracing *Hic1* expression either by citrine fluorescence or by anti-citrine antibody. Moreover, $Hic1^{cit}$ is genetically a null allele; therefore $Hic1^{cit/cit}$ mice display the same embryonic lethal phenotype as observed in $Hic1^{-/-}$ and represent also useful tools to study the molecular mechanisms behind the embryonic lethality. Additionally, this knock-in allele is a convenient alternative marker of *Hic1* expression since there are no good antibodies recognizing Hic1. We used this surrogate marker and anti-GFP antibody to study the expression pattern of *Hic1* during embryonic development previously revealed by *in situ* hybridization[265]. Moreover, we report that $Hic1^{cit}$ is strongly expressed in the spongiotrophoblast layer in placenta, predominantly in glycogen trophoblast cells and trophoblast giant cells.

My contribution to this work: I performed the *in-situ* hybridization. The results were used in Figures 3 and 4.

TECHNOLOGY REPORT

Generation of Two Modified Mouse Alleles of the Hic1 Tumor Suppressor Gene

Vendula Pospichalova,[1] Jolana Tureckova,[1] Bohumil Fafilek,[1] Martina Vojtechova,[1] Michaela Krausova,[1] Jan Lukas,[1] Eva Sloncova,[1] Sylvia Takacova,[2] Vladimir Divoky,[2] Dominique Leprince,[3] Jiri Plachy,[1] and Vladimir Korinek[1]*

[1]Department of Cell and Developmental Biology, Institute of Molecular Genetics, Academy of Sciences of the Czech Republic, 142 20 Prague 4, Czech Republic

[2]Department of Biology, Faculty of Medicine, Palacky University, 77515 Olomouc, Czech Republic

[3]CNRS UMR 8161, Institut de Biologie de Lille, Université Lille Nord de France, Institut Pasteur de Lille, IFR 142, 59017 Lille Cedex, France

Received 3 December 2010; Revised 10 January 2011; Accepted 12 January 2011

Summary: *HIC1* (*hypermethylated in cancer 1*) is a tumor suppressor gene located on chromosome 17p13.3, a region frequently hypermethylated or deleted in human neoplasias. In mouse, *Hic1* is essential for embryonic development and exerts an antitumor role in adult animals. Since *Hic1*-deficient mice die perinatally, we generated a conditional *Hic1* null allele by flanking the *Hic1*-coding region by *lox*P sites. When crossed to animals expressing Cre recombinase in a cell-specific manner, the *Hic1* conditional mice will provide new insights into the function of Hic1 in developing and mature tissues. Additionally, we used gene targeting to replace sequence-encoding amino acids 186–893 of Hic1 by citrine fluorescent protein cDNA. We demonstrate that the distribution of Hic1-citrine fusion polypeptide corresponds to the expression pattern of wild-type *Hic1*. Consequently, Hic1-citrine "reporter" mice can be used to monitor the activity of the *Hic1* locus using citrine fluorescence. genesis 49:142–151, 2011. **© 2011 Wiley-Liss, Inc.**

Key words: hypermethylated in cancer 1; Hic1 tumor suppressor; gene targeting; a conditional null allele; citrine reporter mice; placenta

RESULTS AND DISCUSSION

The *Hic1* gene encodes an evolutionarily conserved transcriptional repressor containing the BTB/POZ (Broad complex, Tramtrack, and Bric à brac/Pox viruses and Zinc finger) domain at the N-terminus and the C-terminal DNA-binding region that includes five Krüppel-like C2H2 zinc fingers (Wales et al., 1995). The loss of human *HIC1* expression was observed in leukemia and tumors of colon, lung, brain, breast, and prostate [reviewed in (Fleuriel et al., 2009)]. Homozygous disruption of *Hic1* impairs development and results in embryonic and perinatal lethality (Carter et al., 2000). The mutant embryos exhibit various defects including limb abnormalities and craniofacial malformations. Heterozygous $Hic1^{+/-}$ mice developed an age- and gender-dependent spectrum of malignant tumors with a predominance of epithelial cancers in males (75%) and lymphomas and sarcomas (80%) in females (Chen *et al.*, 2003). Further analysis of the $Hic1^{+/-}$ mice revealed that in cancer tissue, the promoter region of the nontargeted *Hic1* allele was hypermethylated at the CpG islands. This promoter modification led to transcriptional silencing and induced formation of *Hic1*-negative tumors. These data point to the important functions of *Hic1* during embryogenesis and in mature tissues.

*Correspondence to: Vladimir Korinek, Institute of Molecular Genetics AS CR, Videnska 1083, 142 20 Prague 4, Czech Republic.
E-mail: korinek@img.cas.cz

Contract grant sponsor: Grant Agency of the Czech Republic, Contract grant numbers: 204/07/1567; 204/09/H058, Contract grant sponsor: Grant Agency of Charles University in Prague, Contract grant number: 43-251027, Contract grant sponsor: Academy of Sciences of the Czech Republic, Contract grant number: AV0Z50520514
Published online 20 January 2011 in
Wiley Online Library (wileyonlinelibrary.com).
DOI: 10.1002/dvg.20719

To assess the role of *Hic1* in adult mice, we used gene targeting in mouse embryonic stem (ES) cells to produce a conditional *Hic1* null allele. Furthermore, we performed an "in frame" insertion of the *citrine* gene encoding a monomeric variant of enhanced yellow fluorescent protein into the *Hic1* locus. In these Hic1-citrine reporter animals, the sequence encoding the central CtBP-interacting domain and the C-terminal zinc finger was replaced by *citrine* cDNA. Consequently, transcription from the *Hic1* locus in various cells or tissues can be easily followed by tracking citrine fluorescence or by immunodetection of the citrine protein. The latter fact is important, because, to our knowledge, no Hic1-specific antibody working on histological specimens is currently commercially available. Moreover, citrine-positive cells can be isolated by fluorescence-activated cell sorting (FACS) and used for subsequent analyses.

The *Hic1* gene spans 4.2 kb on mouse chromosome 11 and consists of two exons and one intron. We inserted the first *loxP* site into the intron and the second *loxP* site into the 3′ untranslated region (UTR) in exon 2 (Fig. 1a). This arrangement allows Cre-mediated deletion of the translated part of exon 2, which yields a nonfunctional gene (Carter et al., 2000). Mouse hybrid v6.5 ES cells (Rideout *et al.*, 2000) were electroporated with the linearized Hic1-floxNeo targeting vector (Fig 1a). Clones surviving selection were screened by Southern blotting for homologous recombination at both 5′ and 3′ regions of the *Hic1* locus (Fig. 1b). Cells of clones with appropriate integration were karyotyped. ES cells of chromosomally stable clones were injected into C57BL/6 blastocysts. We obtained one female and ten male chimeras. Breeding of three highly chimeric males to C57BL/6 females yielded germline transmission, and $Hic1^{floxNeo}$ heterozygous mice were identified by Southern blotting and PCR genotyping (Fig. 1c).

The targeting construct includes yeast *FLP* recombinase (*FLPe*) driven by the promoter of the *Ace* gene. This part of the construct should drive testis-specific "self-excision" of the selection cassette flanked by the FRT sites. However, we noted that the cassette was not removed from the genome of offspring of chimeric males, possibly due to insufficient levels of FLPe expression. Of note, French and colleagues encountered an identical problem using a construct based on the same targeting vector (French *et al.*, 2007). To circumvent any possible influence of the cassette on transcription of the "floxed" (i.e., flanked by *lox*P sites) *Hic1* gene or neighboring loci, we mated $Hic1^{floxNeo/+}$ heterozygotes to *ACTB-FLPe* transgenic mice expressing FLPe from the ubiquitously active regulatory region of the human *β-ACTIN* gene (Rodriguez *et al.*, 2000). Moreover, to verify the functionality of the *lox*P sites, we intercrossed $Hic1^{flox/+}$ with *ZP3-Cre* hemizygous females, which produce Cre recombinase in oocytes (Shafi *et al.*, 2000). Cre-mediated excision of the floxed sequence occurred in all pups carrying the $Hic1^{flox}$ allele, and *ZP3-Cre* transgene and $Hic1^{delEx2/+}$ mice were generated (Fig. 1d).

Subsequently, mating of $Hic1^{delEx2/+}$ F1 hybrids was performed. As expected, no $Hic1^{delEx2/delEx2}$ animals were present among pups at weaning age. Next, embryos at various developmental stages were harvested from 19 matings. PCR genotyping showed a complete absence of $Hic1^{delEx2/delEx2}$ embryos at embryonic day (E) 10.5 and at later stages. On the other hand, apparently normal $Hic1^{delEx2/delEx2}$ animals were detected at E8.5 [of 89 embryos collected at different stages, 52 were $Hic1^{+/+}$, 34 $Hic1^{delEx2/+}$, and 3 embryos (from two litters isolated at E8.5) were $Hic1^{delEx2/delEx2}$]. As we observed an increased frequency of resorbed embryos during matings, we presume that $Hic1^{delEx2/delEx2}$ mice die in utero at approximately E9.5. Interestingly, Carter and colleagues previously targeted a similar region of *Hic1* using a "standard" knockout experiment and reported that replacement of exon 2 with β-galactosidase and a neomycin resistance expression cassette produced a null allele (Carter et al., 2000). Nevertheless, these *Hic1*-deficient embryos displayed diverse gross developmental defects and died throughout the second half of embryonic development. Interestingly, the mammalian genome contains hypermethylated in cancer 2 (*Hic2*), a gene related to *Hic1* (Deltour et al., 2001). We speculate that there is redundancy between the two genes in some tissues. Given that we used ES cells of other origin than those used by Carter and colleagues; we suggest that the genetic background-related differences in the expression patterns of *Hic1* and/or *Hic2* might account for the observed discrepancy in phenotypes of *Hic1*-deficient mice.

We crossed $Hic1^{flox/flox}$ mice, which were viable and fertile, and isolated mouse embryonic fibroblasts (MEFs) from E14.5 $Hic1^{flox/flox}$ embryos and performed excision of floxed exon 2 *in vitro* by lentiviral transduction of Cre recombinase. Transduced cells were just briefly selected for puromycin resistance; therefore, the PCR genotyping revealed that exon 2 was not deleted in all cells in the culture (data not shown). However, the level of *Hic1* mRNA was dramatically reduced in Cre-producing fibroblasts and not in MEFs infected with control "empty" lentivirus. Moreover, decreased *Hic1* expression was accompanied by substantial reduction in the Hic1 protein level, indicating that we undoubtedly obtained a *Hic1* null allele (Fig. 1e). Recently, several genes repressed by Hic1 have been identified in a number of independent screens. All the screens used ectopic Hic1 overexpression in otherwise Hic1 negative cells. We tested the expression of *Sirt1* and *ephrin-A1*, which were originally cloned as genes whose expression was upregulated in

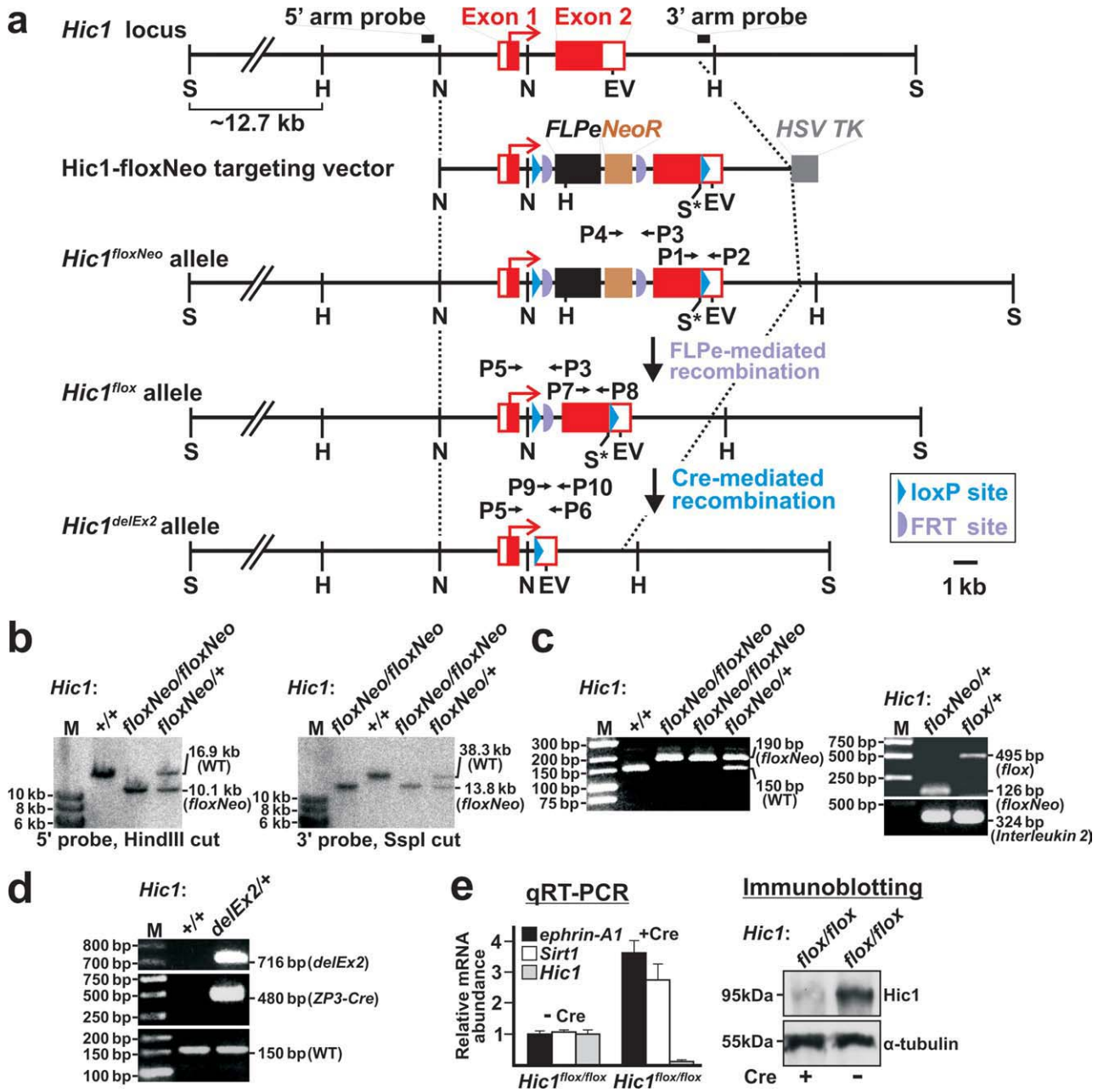

FIG. 1. Generation of mice harboring a *Hic1* conditional null allele. (**a**) The targeting strategy for conditional deletion of the major part of the second exon of the *Hic1* gene using the Hic1-floxNeo targeting vector in mouse ES cells. Exons are depicted by red boxes; coding sequences are filled. Recombination of the targeting vector with the *Hic1* locus resulted in the introduction of an *FLPe-NeoR* cassette, flanked by FRT sites (violet semicircles), into the first intron of the *Hic1* gene. The targeting leaves two *lox*P sites (blue triangles) surrounding the cassette and exon 2. The construct includes the *herpes simplex virus thymidine kinase* (*HSV TK*) gene for selection against clones with randomly integrated vector. FLPe-mediated recombination removed the selection cassette and generated the *flox* allele. The *delEx2* allele can be produced from either the *floxNeo* or *flox* allele by Cre-mediated recombination. Relevant restriction enzyme sites and positions of probes used for Southern blotting are indicated. (**b**) The Southern blot analysis of ES cell clone DNA detecting the homologous recombination at the 5′-(left) or 3′-end (right) of the *Hic1* gene. (**c**) PCR genotyping of mice with the wild-type (WT) or modified *Hic1* alleles. Left, the result of PCR using primers P1 and P2 spanning the *Hic1* 3′ UTR. Right, the excision of the *FLPe-NeoR* cassette was determined by multiplex PCR with primers P3, P4, and P5 (see Fig. 1a and Materials and Methods section). The quality of individual DNA isolations was verified using primers for the *Interleukin 2* gene. (**d**) Cre-mediated deletion of exon 2 of the *Hic1* gene in mice. The excision of *Hic1* genomic sequences was monitored by PCR using primers P5 and P6 spanning the genomic region located between the *lox*P sites (upper panel). The presence of the *Zp3-Cre* transgene in $Hic1^{delEx2/+}$ mice was verified by a primer set generating a 480 bp product (middle panel). The remaining WT allele (bottom panel) was detected as described in (c). (**e**) Left, the expression of the putative Hic1-regulated genes, *ephrin-A1* and *Sirt1*, is relieved in *Hic1*-deficient cells. Quantitative "real-time" RT-PCR (qRT-PCR) analysis of total RNA isolated from $Hic1^{flox/flox}$ MEFs transduced either with a lentiviral vector encoding Cre recombinase or with "empty" lentivirus. The abundance of corresponding mRNA is given as the average cycle threshold (Ct) values and the corresponding standard deviations (SD) after normalizing to the *Ubb* levels. The expression level of the genes in MEFs transduced with the empty vector was set to one. Right, representative Western blotting of cell lysates of Cre-expressing or control MEFs. Equal loading was confirmed by immunoblotting using an anti-α-tubulin antibody. H, HindIII; EV, EcoRV; N, NotI; S, SspI; M, molecular weight markers. The asterisk marks the SspI site newly introduced into genomic DNA. For the sake of clarity, the size of exons and expression cassettes in Figures 1a and 2a does not completely correspond to the scale indicated in the right bottom corner of the schemes.

Hic1-deficient MEFs (Chen *et al.*, 2005; Zhang *et al.*, 2010). As shown in Figure 1e, transcription of *Sirt1* and *ephrin-A1* was induced upon depletion of *Hic1*, thus confirming the previous results. In summary, mice carrying the $Hic1^{flox}$ allele can be crossed to various Cre deletor mice and used to study the role of Hic1 tumor suppressor in adult tissues.

The knock-in of *citrine* into the *Hic1* locus was generated similarly to the $Hic1^{floxNeo}$ allele with several modifications. In the Hic1-citNeo targeting vector, the coding region of exon 2 was replaced by *citrine* sequence using internal NarI and EcoRV restriction sites (Fig. 2a). The targeting leads to the production of the Hic1-citrine fusion polypeptide that includes 185 N-terminal amino acids of Hic1 fused to full-length citrine protein. Furthermore, *lox*P sites were removed from the backbone of the vector by PCR-based mutagenesis. The Hic1-citNeo construct was transfected by electroporation into v6.5 ES cells, and cells of one correctly targeted clone (Fig. 2b) with standard karyotype were injected into C57BL/6 blastocysts. One chimeric male and two females were obtained and mated to C57BL/6 mice. Germline transmission of the $Hic1^{citNeo}$ allele was achieved from the male and one female chimera. Finally, $Hic1^{cit/+}$ mice were generated by crossing $Hic1^{citNeo/+}$ animals to *ACTB-FLPe* mice. Because the $Hic1^{cit}$ is a null *Hic1* allele, $Hic1^{cit/cit}$ mice displayed the same embryonic lethal phenotype as observed in $Hic1^{delEx2/delEx2}$ mice [65 embryos from 11 litters were collected with following genotypes: 29 $Hic1^{+/+}$, 34 $Hic1^{cit/+}$, and 2 $Hic1^{cit/cit}$ (stages E8.5 and E10.5)].

According to our prediction, the production of Hic1-citrine from the *Hic1* locus should be easily traceable by citrine fluorescence or by citrine-specific antibodies. Indeed, Hic1-citrine was detected in MEFs derived from $Hic1^{cit/+}$ embryos by FACS and by immunoblotting (Fig. 2c). This indicates that cells derived from $Hic1^{cit/+}$ mice can be isolated according to the levels of citrine fluorescence and used in subsequent experiments. Interestingly, Hic1-citrine was found not only in the cytoplasm, but also in the cell nucleus (Fig. 4f,i), although the Hic1 N-terminus does not contain the consensus sequence of the nuclear localization signal. Importantly, *Hic1-citrine* mRNA in embryos and adult tissues showed a similar expression pattern as WT *Hic1* (Fig. 2d). Furthermore, in subsequent tests, we noticed an agreement between the localization of Hic1-citrine protein detected by immunohistochemical staining and the tissue distribution of *Hic1* mRNA obtained previously by in situ hybridization (Grimm *et al.*, 1999). The onset of detectable Hic1-citrine fluorescence was at E10.5 and was noted in the somite derivatives and in limb buds, where it persisted throughout subsequent developmental stages (Fig. 3a–g). From E11.5, the signal retained the segmented pattern, but moreover appeared in the craniofacial and nasal area (Fig. 3b,d,f,g). Immunohistochemical localization of Hic1-citrine was mainly observed in mesenchyme adjacent to cartilagenous condensations of the skeletal system (Fig. 3m,q,y). Prominent anti-Hic1-citrine staining was also observed in mesenchyme surrounding the spinal cord (Fig. 3s), spinal and peripheral nerves (Fig. 3m,n,s,t,z), gut epithelium (Fig. 3p), and epithelial budding of the nose and salivary glands (Fig. 3k,u). Additionally, Hic1-citrine was noted in the pancreas (Fig. 3o), metanephric kidney (Fig. 3aa), developing muscles (Fig. 3v–x), and in the region of trigeminal ganglion (Fig. 3v). In agreement with the results of the quantitative real-time PCR (qRT-PCR) analysis, *Hic1-citrine* was strongly expressed in placenta at E10.5 and subsequent developmental stages (Figs. 2d, 3g, and 4). The Hic1-citrine was produced predominantly in the spongiotrophoblast layer, and the highest levels were detected in glycogen trophoblast cells (GTCs) and polyploid trophoblast giant cells (TGCs) (Fig. 4f,g,i,j) although some TGCs were apparently negative for Hic1-citrine (inset in Fig. 4f). Finally, we performed control *in situ* hybridization of *Hic1* mRNA using specimens prepared from WT mice and observed a virtually identical pattern as seen for Hic1-citrine (Figs. 3w′,aa′ and 4c,d). In summary, although we cannot exclude that the stability of *Hic1-citrine* mRNA (and protein) may differ from WT *Hic1* in some tissues, our data indicate that Hic1-citrine produced from the knock-in *Hic1* allele can be used as a convenient alternative marker of Hic1 expression.

MATERIALS AND METHODS

Gene Targeting and Generation of $Hic1^{floxNeo}$ and $Hic1^{citrineNeo}$ Mice

DNA containing the *Hic1* locus was isolated from two genomic clones of a 129/SvJ bacteriophage lambda DASH II library (Stratagene). The clones were identified by plaque hybridization using human *HIC1* cDNA as a probe. DNA including two *Hic1* exons was cloned into the vector pEASY-FLIRT (Casola, 2004). The construct Hic1-floxNeo contained a *lox*P-*FRT-FLPe-NeoR-FRT* cassette in the intron, with a second *lox*P site inserted in the 3′ UTR of the *Hic1* gene. In spite of this arrangement, the distance of the *lox*P sites still remained considerable, 2630 bps. Therefore, an SspI site was newly introduced into genomic DNA just upstream of the distal *lox*P site. This site-enabled discrimination of ES cells that underwent homologous recombination in the region downstream or upstream of the 3′ UTR *lox*P site (Fig. 1a). To generate the Hic1-citNeo targeting construct, both *lox*P sites were removed from the pEASY-FLIRT vector by PCR mutagenesis. Subsequently, the major part of the coding sequence of the second exon was replaced by *citrine* cDNA [(Glebov and Nichols, 2004); a gift of K. Drbal] using internal NarI and EcoRV

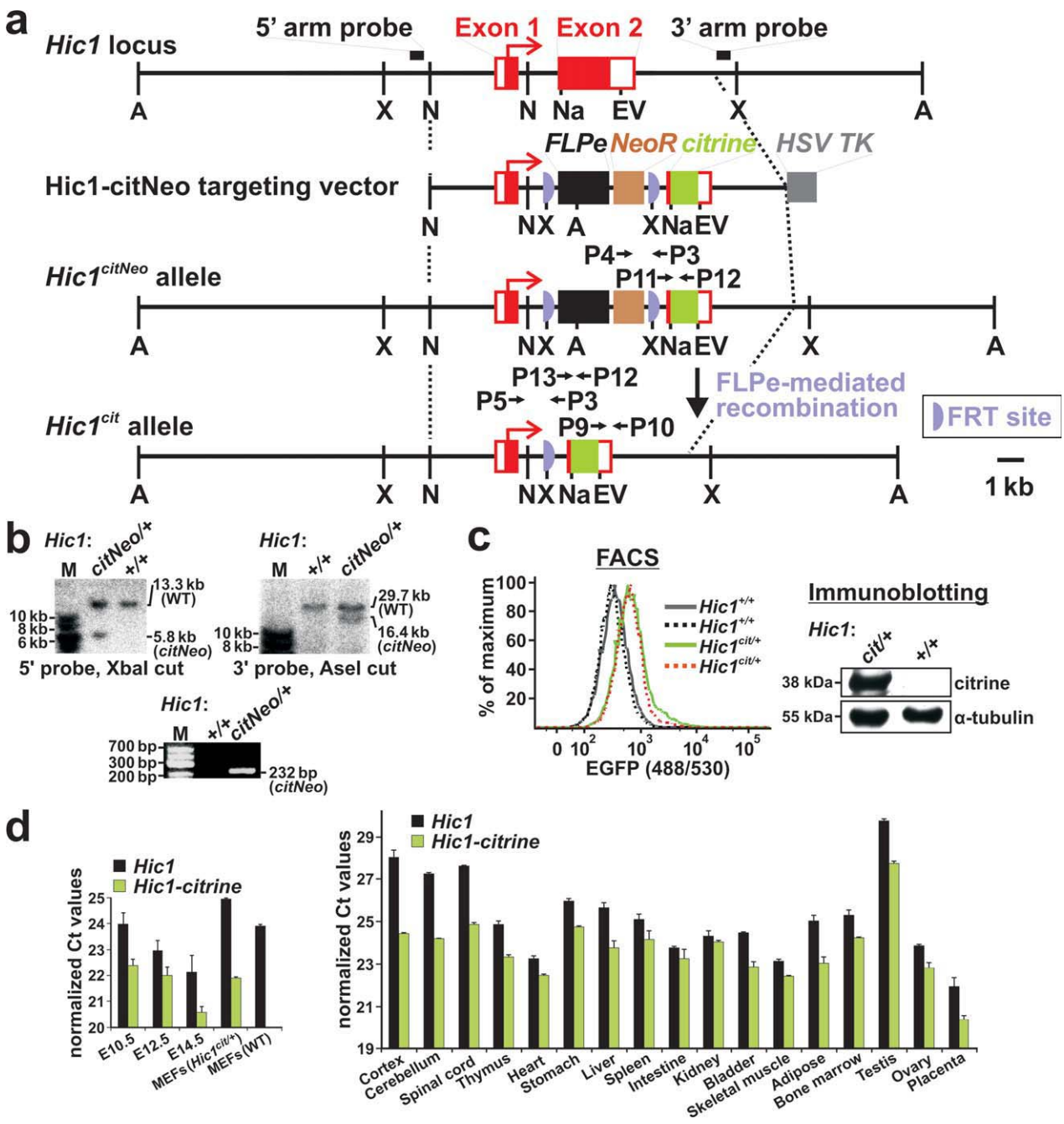

FIG. 2. Generation of *Hic1* reporter mice. (**a**) The strategy for the replacement of the major part of the *Hic1*-coding sequence with *citrine fluorescent protein* cDNA. Gene targeting in mouse ES cells generated a *citNeo* null allele in which the *citrine* gene is fused "in frame" into nucleotide 42 of the second exon of the *Hic1* gene replacing the coding sequence. The targeting left two FRT sites surrounding an *FLPe-NeoR* cassette. FLPe-mediated recombination removed the selection cassette and generated the *cit* allele. (**b**) Top, Southern blot analysis of targeted ES cell clones. Bottom, PCR genotyping of mice with the WT or *citNeo* allele using primers detecting *Hic1-citrine* cDNA. The deletion of the resistance cassette was detected using primers P3, P4, and P5 (see also Fig. 1c). (**c**) Left, FACS analysis of citrine fluorescence in MEFs isolated from two $Hic1^{cit/+}$ and two control $Hic1^{+/+}$ embryos at E14.5. Right, immunoblotting of Hic1-citrine fusion protein present in lysates of $Hic1^{cit/+}$ MEFs isolated from E14.5 embryos. (**d**) The expression pattern of the *Hic1-citrine* gene in mouse embryos and adult tissues. Results of qRT-PCR analyses performed with *citrine* primers (P13 ad P12) and *Hic1*-specific primers (P9 and P10) on cDNA generated from mouse embryos, adult mouse tissues, and from MEFs (obtained at E14.5). The expression levels of *Hic1* and *Hic1*-citrine mRNA are presented as average Ct values and corresponding SDs after normalization to the levels of *Ubb* cDNA. A, AseI; EV, EcoRV; N, NotI; Na, NarI; X, XbaI; M, molecular weight markers.

restriction sites. Hybrid [C57BL/6(F) × 129/Sv(M)] v6.5 ES cells (Open Biosystems) were grown on a feeder layer of MEFs (Stem Cell Technologies) treated with mitomycin C (Sigma; 2 h, final concentration 10 μg/ml). ES cells were cultured in Glutamax Dulbecco's modified Eagle's medium (Gibco) supplemented with 15% FBS (Hyclone; ES cells tested), 2 mM L-glutamine, 1 mM sodium pyruvate, 1× nonessential amino acids, 0.1 mM β-mercaptoethanol, and penicillin/streptomycin (100 UI; all chemicals were purchased from Gibco). One milliliter of conditioned media obtained from COS-7 cells stably expressing mouse leukemia inhibitory factor was added to the final volume of 500 ml. About 1×10^7 ES cells were transfected by electroporation (Gene Pulser II system, Bio-Rad Laboratories; settings: 230 V, 500 μF) with 20 μg of ClaI-linearized targeting constructs. Colonies surviving G418 (Gibco; 350 μg/ml active compound) and gancyclovir (Sigma; 2.5 μM) were picked, expanded in fresh culture dishes, and screened for homologous recombination by Southern blotting. Cells of clones with appropriate targeting were karyotyped, and the functionality of *lox*P and FRT sites was tested in transient transfections using Cre or FLPe recombinase-producing expression constructs. One clone of each targeting construct was injected into blastocysts of superovulated C57BL/6 females. The blastocyst injections were performed using the services of the Karolinska Center for Transgene Technologies (Stockholm, Sweden). Chimeric mice were bred to C57BL/6 animals. Germline transmission of the targeted alleles was verified by Southern blot hybridization. All regulated procedures were carried out under Project License IMG 9/2006.

PCR Genotyping

Genotyping was performed using lysates prepared from a tip of a mouse tail or a piece of embryo. Samples were digested in 0.5 ml of lysis buffer [10 mM Tris–HCl pH 8.0, 100 mM NaCl, 25 mM EDTA pH 8.0, 0.5% SDS (w/v), 0.1 mg/ml Proteinase K (Fermentas)] for 12 h at 56°C. Digested samples were centrifuged (14,000*g*; 10 min) and supernatants were precipitated with ethanol. Dry DNA samples were dissolved in TE buffer (10 mM Tris–HCl pH 8.0, 1 mM EDTA, pH 8.0) and used (1 of 100 of isolated genomic DNA) for PCR with 2× PCR Master Mix (Fermentas). The strategy used to genotype various *Hic1* alleles is described in Figures 1a and 2a. The amplification of the WT allele using primers P1 (5′-CCCCACCTTTCTACACCTCA-3′) and P2 (5′-GAGAGG CAGGGTTCTCCTTT-3′) generated a 150 bp product. The *lox*P site insertion into the *Hic1* locus yielded a larger, 190 bp DNA fragment. The excision of the *FLPe-NeoR* cassette was determined by multiplex PCR with primers P3 (5′-GGTTAGCCGTCGACGAAGTTCCTAT-3′), P4 (5′-GTGGGCTCTATGGCTTCTGA-3′), and P5 (5′-CTCCTGCCCCGATATAACGC-3′). The *floxNeo* allele gave a 126 bp fragment; the length of the PCR product amplified from the *flox* allele is 495 bp. PCR using primers P5 and P6 (5′-TGAGGAACTTCACATTAT CAGTCC-3′) indicated the excision of *Hic1* genomic sequences (a 716 bp fragment). The *Hic1-citrine* reporter mice were genotyped by PCR reaction with primers P11 (5′-GATGGAGGCGCCTATGGTGA-3′) and P12 (5′-GGCGAAGCACATCAGGCCGT-3′), which generated a 232 bp fragment. *ZP3-Cre* [C57BL/6J, Tg (Zp3-cre)1Gwh] and *ACTB-FLPe* transgenic mice [B6.Cg-Tg (ACTFLPe)9205 Dym/J; both strains were purchased from The Jackson Laboratory] were genotyped using primers FZP3Cre (5′-GCGGTCTGGCAGTAAAAACTA TC-3′) and RZP3Cre (5′-GTGAAACAGCATTGCTGTC ACTT-3′; PCR is yielding the fragment size of 480 bp); FACTFLPe (5′-CACTGATATTGTAAGTAGTTTGC-3′) and RACTFLPe (5′-CTAGTGCGAAGTAGTGATCAGG-3′; fragment size 725 bp). The quality of DNA isolations was tested by PCR using primers specific for the *Interleukin 2* gene; FIl2 (5′-CTAGGCCACAGAATTGAAAGATCT-3′), RIl2 (5′-GTAGGTGGAAATTCTAGCATCATCC-3′; a 324 bp fragment). All PCR reactions were performed using the following cycling conditions with 1M betaine (final concentration; Sigma) as a supplement: initial denaturation (98°C, 3 min), amplification (37 cycles at 98°C for 30 s, 55°C for 30 s, and 72°C for 45 s), and final extension (72°C for 5 min).

Lentiviral Transductions

The construct encoding Cre recombinase (*Cre* cDNA was kindly provided by C.L. Cepko via Addgene) was generated in the mammalian lentiviral vector, pCDH1 (System Biosciences). Lentiviruses were prepared using the Trans-Lentiviral Packaging System (Open Biosystems). HEK 293 FT cells used for packaging lentiviral stocks were purchased from Invitrogen. Transient transfections of the pCDH1-Cre construct were performed using Fugene HD (Roche Applied Science). MEFs generated from E14.5 embryos according to the standard procedure (Larabell *et al.*, 1997) were transduced with the recombinant lentiviruses and selected without subcloning using puromycin (Alexis; 2 μg/ml).

RNA Purification and qRT-PCR

Total RNAs were isolated from embryos, adult tissues, or MEFs using the Trizol reagent (Invitrogen). A detailed description of the quantitative real-time PCR (qRT-PCR) procedure was given previously (Lukas *et al.*, 2009). All primers were calculated using the Primer 3 computer service at http://biotools.umassmed.edu/bioapps/primer3_www.cgi. Two housekeeping genes, β-*actin* (*Actb*) and *Ubiquitin b* (*Ubb*), were used as internal control genes to standardize the quality of different cDNA preparations (Vandesompele *et al.*, 2002). cDNAs

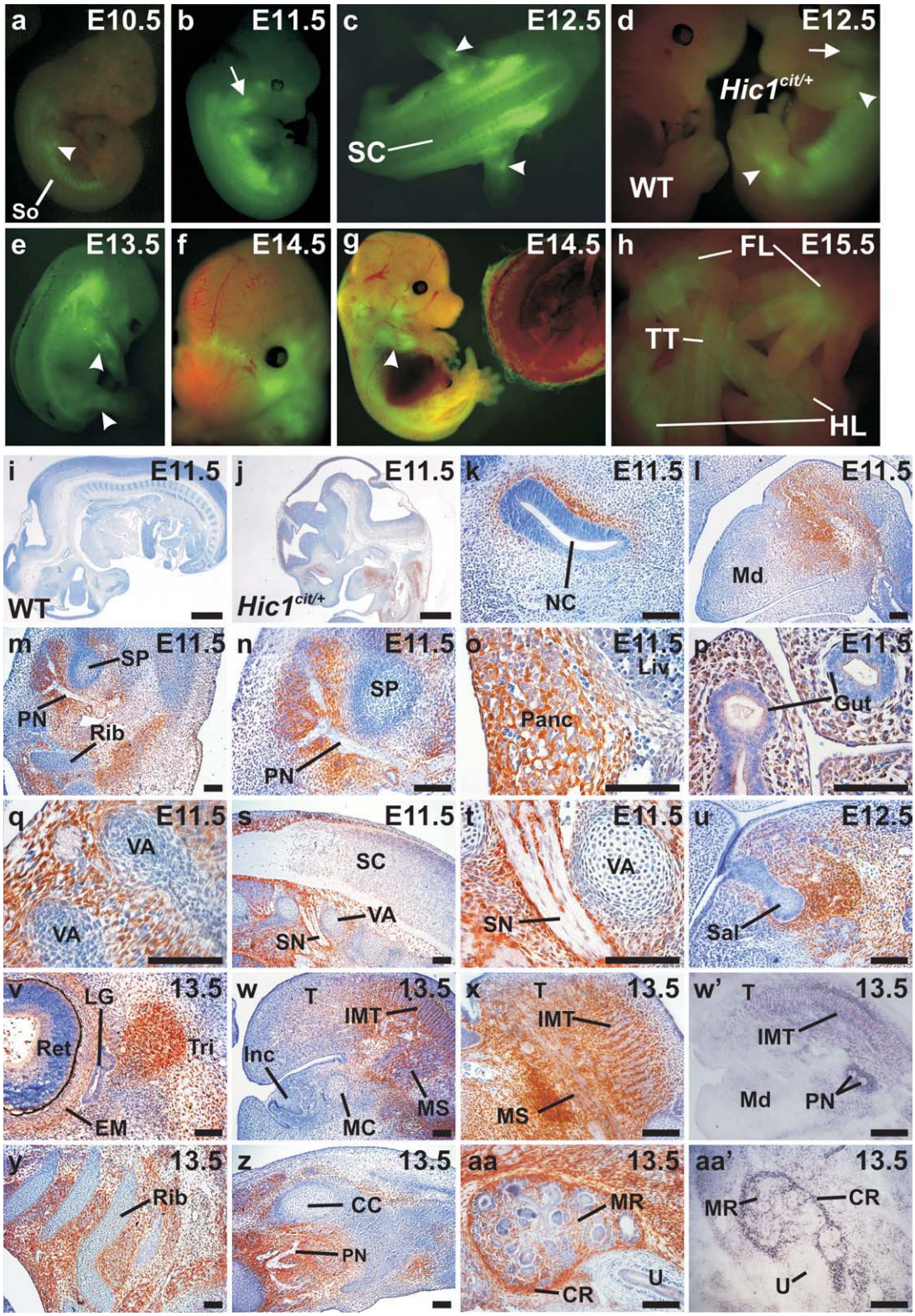
a E10.5
So
b E11.5
c E12.5
SC
d E12.5
Hic1cit/+
WT
e E13.5
f E14.5
g E14.5
h E15.5
FL
TT
HL
i E11.5
WT
j E11.5
Hic1cit/+
k E11.5
NC
l E11.5
Md
m E11.5
SP
PN
Rib
n E11.5
SP
PN
o E11.5
Liv
Panc
p E11.5
Gut
q E11.5
VA
VA
s E11.5
SC
VA
SN
t E11.5
VA
SN
u E12.5
Sal
v 13.5
LG
Ret
Tri
EM
w 13.5
T
IMT
Inc
MS
MC
x 13.5
T
IMT
MS
w' 13.5
T
IMT
Md
PN
y 13.5
Rib
z 13.5
CC
PN
aa 13.5
MR
CR
U
aa' 13.5
MR
CR
U

FIG. 3

were produced from three independent RNA isolations using animals or MEFs (of the corresponding genotype) derived from the same litter. Samples containing all components except reverse transcriptase were prepared in parallel and used as negative controls. The PCR reactions were performed in triplicate for each primer set in Light Cycler 480 (Roche Applied Science). Data were analyzed using LightCycler 480 Software 1.5 and normalized to *Actb* or *Ubb* levels. Because both normalizations produced similar results, only the data set obtained by normalization to *Ubb* is presented. Two primer sets were used to detect *Hic1* expression. Primers P7 (5′-CAACCTGTACGTGTGCATCC-3′) and P8 (5′-ACGTGTGCATTCAGCTGTTC-3′) were derived from the sequence deleted in the *delEx2* allele; primers P9 (5′-GTCTCTGCTTCCGAGGTGTC-3′) and P10 (5′-CAGCTAAAGTTGGGCTCAGG-3′) primed on the distal part of the *Hic1* 3′ UTR, which is presumably present in mRNAs produced from both the WT and *delEx2* alleles (see Fig. 1a and the PCR Genotyping section). Both primer sets showed substantial decrease in *Hic1* mRNA levels in Cre-transduced $Hic1^{loxP/loxP}$ MEFs. This indicated that mRNA expressed from the *delEx2* locus is unstable; only the results obtained with the P9 and P10 primers are shown (Fig. 1e). *Citrine* cDNA was detected by two combinations of primers: P11 and P12 or P13 (5′-GCGAGGGCGATGCCACCTAC-3′) and P12 (Fig. 2a). The following primers were used; *Actb*, FActb (5′-GATCTGGCACCACACCTTCT-3′), RActb (5′-GGGGTGT TGAAGGTCTCAAA-3′); *ephrin-A1*, Fephrin-A1 (5′-ACC GTGGAGAAGCCTGTGGGA-3′), Rephrin-A1 (5′-CCTC CTCACGGAACTTGGGATTTGAAC-3′); *Sirt1*, FSirt1 (5′-C GGAGGGCCAGAGAGGCAGT-3′), RSirt1 (5′-CTCTTG CGGAGCGGCTCGTC-3′); *Ubb*, FUbb (5′-ATGTGAAG GCCAAGATCCAG-3′), RUbb (5′-TAATAGCCACCCCTCA GACG-3′).

Antibodies and Western Blotting

cDNAs encoding N-terminally His-tagged human HIC1 (aa 154-396) and citrine (full-length polypeptide) were subcloned into the pET28b vector (Novagen). Recombinant proteins were purified from bacterial [*E. coli*, strain BL-21 (DE3)] cell lysates by TALON affinity resins (Clontech) and used for immunizing rabbits or chickens. Immunoglobulins present in the resulting rabbit antisera were purified using Melon Gel IgG Purification Kit (Pierce) according to the manufacturer's instructions. The following commercially available mouse monoclonal antibodies were used: anti-α-tubulin (TU-01; Exbio) and anti-GFP (JL8; Clontech). MEFs grown in 10-cm culture dishes to 90% confluence were washed twice in ice-cold phosphate-buffered saline (PBS) and harvested by scraping the surface of the dish in Laemmli sample buffer (Laemmli, 1970) and immunoblotted. A detailed protocol describing the immunoblotting procedure can be found elsewhere (Lukas *et al.*, 2009). Peroxidase-conjugated anti-chicken, anti-mouse, or anti-rabbit secondary antibodies were purchased from Sigma.

Flow Cytometry and Fluorescent Microscopy

Freshly isolated MEFs were washed twice with PBS. The citrine production in living cells (negatively stained with Hoechst 33258) was analyzed by an LSRII flow cytometer (BD Biosciences). For fluorescent microscopy,

FIG. 3. Tracing Hic1-citrine expression during embryonic development (**a–h**) The knock-in of the *citrine* gene into the *Hic1* locus allows tracing Hic1-citrine expression in the intact embryos. Citrine fluorescence was first detected at stage E10.5 in the putative somite derivatives and limb buds [arrowhead in (a)]. From the twelfth embryonic day and in later stages, the signal is retained in body segments, limb buds, and limbs [arrowheads in panels (c, d, e, and g)], but moreover, supervenes in the craniofacial and nasal area (b–g), where it includes the presumptive maxillary/mandibular components of the first branchial arch [arrows in (b and d)]. Fluorescent signal was also observed in the placenta (g). At E15.5, the expression was clearly visible in digits of both fore- and hindlimbs (**h**). (**i–aa**) Immunohistochemical detection of Hic1-citrine in paraffin-embedded sections of mouse embryos at E11.5, E12.5, and E13.5. All embryos were cut parasagitally except for (z), which shows a transversal section of the forelimb. The sections were stained with a rabbit anti-citrine polyclonal antibody (visualized as brownish precipitate of DAB substrate) and counterstained with hematoxylin nuclear stain (blue). The specimen in panel (i) was derived from WT mice to confirm the specificity of the staining; the remaining samples were prepared from $Hic1^{cit/+}$ embryos. For comparison, the images in (w′) and (aa′) depict the localization of *Hic1* mRNA using in situ hybridization of *Hic1* antisense riboprobes on the frozen sections of WT embryos. Corresponding immunohistochemical staining is shown in (w) and (aa), respectively. Panel (j) depicts the whole rostral part of $Hic1^{cit/+}$ embryo at lower magnification to illustrate the strength and localization of the positive signal. Microphotographs in (m), (s), and (w) are shown in more detail in (n), (t), and (x), respectively. Through all developmental stages tested, Hic1-citrine expression was observed in mesenchyme adjacent to precartilage or cartilage condensations of the skeletal system. These included the mandibular component of the first branchial arch (l and w), anlages of the ribs and vertebrae (m, q, and y), and the precartilage primordia of the developing limbs (z). Anti-Hic1-citrine staining was also detected in mesenchyme surrounding the spinal cord and spinal and peripheral nerves (m, n, s, t, and z) and epithelial buds, for example of the nose and salivary glands (k and u). Prominent staining for Hic1-citrine was noted in the pancreas (o), metanephric kidney (aa), and in mesenchyme facing the gut epithelium (p). Hic1-citrine was produced in developing tongue muscles (l, w, and x), in the presumptive eyelid muscle and the area of trigeminal ganglion (v). CC, cartilageous condensations; CR, cortical region of metanephros; EM, eyelid muscle; FL, forelimb, HL, hindlimb; Gut, lumen of the gut; IMT, intrinsic muscle of the tongue; Inc, incisor; LG, ductus of the lacrimal gland; Liv, liver; MC, Meckel's cartilage; Md, mandibular component of the first pharyngeal arch; MR, medullar region of metanephros; MS, precursor of median fibrous septum of the tongue; NC, nasal cavity; Panc, pancreas; PN, peripheral nerves; Ret, retina; Rib, rib anlage; Sal, salivary gland; SC, spinal cord; SN, spinal nerve; So, somites; SP, shoulder primordium; T, tongue; TT, tip of the tail; Tri, trigeminal ganglium; U, ureter; VA, vertebrate anlage. Bars represent 0.5 mm in (i and j) and 0.1 mm in (k–aa′).

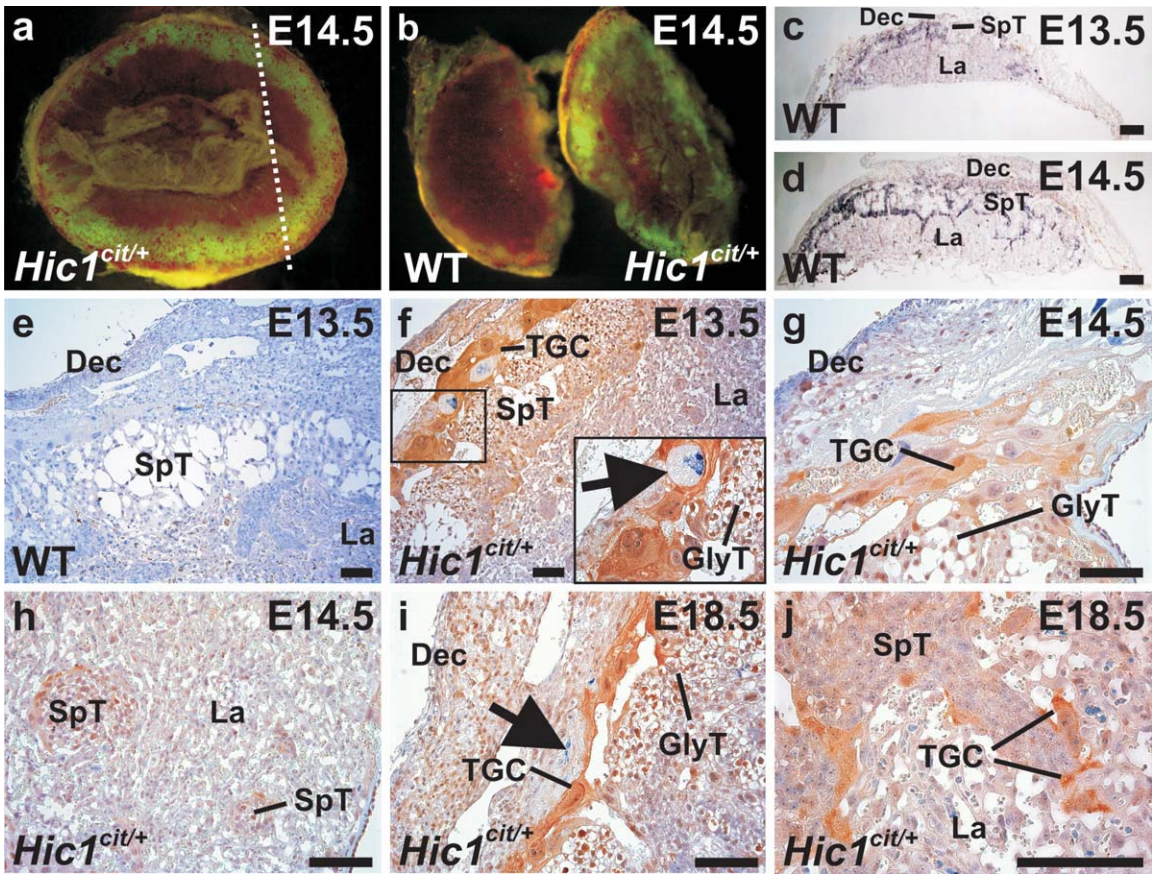

FIG. 4. Hic1-citrine is strongly expressed in spongiotrophoblast of the placenta. Fluorescent microphotographs of the whole placenta obtained from the *Hic1*$^{cit/+}$ mouse embryos at E14.5 (**a**) and of two placental tips cut from WT and *Hic1*$^{cit/+}$ animals of the same developmental stage (**b**). Pictures were taken from the fetal side; the cutting plane in (b) is shown in (a). (**c** and **d**) Detection of *Hic1* mRNA in spongiotrophoblast (SpT) using in situ hybridization of *Hic1* antisense riboprobes on the radial frozen sections of the *Hic1*$^{+/+}$ placenta at E13.5 and E14.5. (**e–j**) Immunodetection of Hic1-citrine protein in radial paraffin sections of placenta at mid- and late gestation. The sections were oriented with their maternal (decidual) part to the top left corner and the fetal side at the bottom right corner. Pictures were taken from the middle part of the placenta except in (g), where a more lateral part is shown; (h) depicts the labyrinth in close proximity to the fetus. The detail of the "contact zone" between SpT and the labyrinth is shown in (j). All sections were stained with a rabbit anti-citrine polyclonal antibody and counterstained with hematoxylin. The specimen in (e) was derived from WT mice to confirm the specificity of the staining, the remaining samples were taken from *Hic1*$^{cit/+}$ embryos. Nuclear and cytoplasmic Hic1-citrine were detected in all parts of the placenta with prominent staining in the SpT layer and in SpT cells invading the deciduum (g and i). Especially strong staining was observed in glycogen trophoblast (GlyT) cells and trophoblasts giant cells [(TGC); (f–j)] at various locations, although we noted that some TGC were negative for Hic1-citrine [arrow in the inset in (f) and in (i)]. Dec, deciduum; GlyT, glycogen trophoblast cells; La, the labyrinth layer; TGC, trophoblasts giant cells; SpT, spongiotrophoblast. Bar in (c and d) represents 0.5 mm, in other images 0.1 mm.

embryos were harvested in cold PBS and directly photographed using an SZX10 stereomicroscope (Olympus).

Immunohistochemical Staining

Approximately 30 *Hic1*$^{+/+}$ and an equivalent number of *Hic1*$^{cit/+}$ embryos were fixed (including placentae) in 4% (v/v) formaldehyde-PBS, embedded in paraffin, and sectioned (6 μm). For immunohistochemical analyses, dewaxed sections were treated with 0.75% H_2O_2 in methanol for 20 min. The slides were then immersed in citrate buffer (10 mM, pH 6.0) and incubated for 20 min at 98°C in a steam bath. Slides were washed in PBS and incubated with 5% goat nonimmune serum (Jackson ImmunoResearch) for 20 min at RT to block nonspecific binding. The purified rabbit anti-citrine antibody served as primary antibody. The antibody was visualized with goat anti-rabbit biotinylated antiserum (Molecular Probes) and streptavidin/biotin/horseradish peroxidase (HRP) detection system (DAKO). HRP was detected using H_2O_2 and diaminobenzidine (Fluka) substrate; tissue was counterstained with hematoxylin.

RNA Probes and *In Situ* Hybridization

A DNA fragment encompassing the nucleotides 2300–3616 in the second exon of the mouse *Hic1* gene (numbering corresponds to *Hic1* sequence accession No. NM_010430.2) was subcloned into pBluescript SK II (Stratagene). The construct was linearized, and digox-

igenin-labeled antisense RNA and control sense probes were generated from the template using the DIG RNA Labeling Kit (Roche Applied Science). Dissected embryos and placentae were embedded in O.C.T. medium (Tissue-Tek). Ten micron sections were cut and mounted on Super Frost Plus slides (Electron Microscopy Sciences). Sections were postfixed in 4% (w/v) paraformaldehyde in PBS (4°C, 10 min), acetylated for 10 min (acetic anhydride, 0.25%; Sigma), and hybridized with digoxigenin-labeled probes overnight at 62°C. *In situ* hybridization was carried out as described previously (Machon et al., 2002).

ACKNOWLEDGMENTS

We thank Karel Drbal for cDNA encoding citrine; we are grateful to Tomas Stopka for *ZP3-Cre* and *ACTB-FLPe* transgenic mice used in the study. We further thank Jan Ove Bratteng, Johannes Wilbertz, and Stephan Teglund for blastocyst injections and breeding of the chimeric mice; Thomas O'Hearn and Sarka Takacova for critically reading the manuscript.

LITERATURE CITED

Carter MG, Johns MA, Zeng X, Zhou L, Zink MC, Mankowski JL, Donovan DM, Baylin SB. 2000. Mice deficient in the candidate tumor suppressor gene Hic1 exhibit developmental defects of structures affected in the Miller-Dieker syndrome. Hum Mol Genet 9:413–419.

Casola S. 2004. Conditional gene mutagenesis in B-lineage cells. Methods Mol Biol 271:91–109.

Chen WY, Wang DH, Yen RC, Luo J, Gu W, Baylin SB. 2005. Tumor suppressor HIC1 directly regulates SIRT1 to modulate p53-dependent DNA-damage responses. Cell 123:437–448.

Chen WY, Zeng X, Carter MG, Morrell CN, Chiu Yen RW, Esteller M, Watkins DN, Herman JG, Mankowski JL, Baylin SB. 2003. Heterozygous disruption of Hic1 predisposes mice to a gender-dependent spectrum of malignant tumors. Nat Genet 33:197–202.

Deltour S, Pinte S, Guerardel C, Leprince D. 2001. Characterization of HRG22, a human homologue of the putative tumor suppressor gene HIC1. Biochem Biophys Res Commun 287:427–434.

Fleuriel C, Touka M, Boulay G, Guerardel C, Rood BR, Leprince D. 2009. *HIC1* (hypermethylated in cancer 1) epigenetic silencing in tumors. Int J Biochem Cell Biol 41:26–33.

French CA, Groszer M, Preece C, Coupe AM, Rajewsky K, Fisher SE. 2007. Generation of mice with a conditional Foxp2 null allele. Genesis 45:440–446.

Glebov OO, Nichols BJ. 2004. Lipid raft proteins have a random distribution during localized activation of the T-cell receptor. Nat Cell Biol 6:238–243.

Grimm C, Sporle R, Schmid TE, Adler ID, Adamski J, Schughart K, Graw J. 1999. Isolation and embryonic expression of the novel mouse gene Hic1, the homologue of HIC1, a candidate gene for the Miller-Dieker syndrome. Hum Mol Genet 8:697–710.

Laemmli UK. 1970. Cleavage of structural proteins during the assembly of the head of bacteriophage T4. Nature 227:680–685.

Larabell CA, Torres M, Rowning BA, Yost C, Miller JR, Wu M, Kimelman D, Moon RT. 1997. Establishment of the dorso-ventral axis in *Xenopus embryos* is presaged by early asymmetries in beta-catenin that are modulated by the Wnt signaling pathway. J Cell Biol 136:1123–1136.

Lukas J, Mazna P, Valenta T, Doubravska L, Pospichalova V, Vojtechova M, Fafilek B, Ivanek R, Plachy J, Novak J, Korinek V. 2009. Dazap2 modulates transcription driven by the Wnt effector TCF-4. Nucleic Acids Res 37:3007–3020.

Machon O, van den Bout CJ, Backman M, Rosok O, Caubit X, Fromm SH, Geronimo B, Krauss S. 2002. Forebrain-specific promoter/enhancer D6 derived from the mouse Dach1 gene controls expression in neural stem cells. Neuroscience 112:951–966.

Rideout WM III, Wakayama T, Wutz A, Eggan K, Jackson-Grusby L, Dausman J, Yanagimachi R, Jaenisch R. 2000. Generation of mice from wild-type and targeted ES cells by nuclear cloning. Nat Genet 24:109–110.

Rodriguez CI, Buchholz F, Galloway J, Sequerra R, Kasper J, Ayala R, Stewart AF, Dymecki SM. 2000. High-efficiency deleter mice show that FLPe is an alternative to Cre-loxP. Nat Genet 25:139–140.

Shafi R, Iyer SP, Ellies LG, O'Donnell N, Marek KW, Chui D, Hart GW, Marth JD. 2000. The O-GlcNAc transferase gene resides on the X chromosome and is essential for embryonic stem cell viability and mouse ontogeny. Proc Natl Acad Sci USA 97:5735–5739.

Vandesompele J, De Preter K, Pattyn F, Poppe B, Van Roy N, De Paepe A, Speleman F. 2002. Accurate normalization of real-time quantitative RT-PCR data by geometric averaging of multiple internal control genes. Genome Biol 3:RESEARCH0034.

Wales MM, Biel MA, el Deiry W, Nelkin BD, Issa JP, Cavenee WK, Kuerbitz SJ, Baylin SB. 1995. p53 activates expression of HIC-1, a new candidate tumour suppressor gene on 17p13.3. Nat Med 1:570–577.

Zhang W, Zeng X, Briggs KJ, Beaty R, Simons B, Chiu Yen RW, Tyler MA, Tsai HC, Ye Y, Gesell GS, Herman JG, Baylin SB, Watkins DN. 2010. A potential tumor suppressor role for Hic1 in breast cancer through transcriptional repression of ephrin-A1. Oncogene 29:2467–2476.

DAZAP2 modulates transcription driven by the Wnt effector TCF4

In search for new interacting partners of TCF4, we identified Dazap2 (Deleted in Azoospermia Associated Protein 2). *Dazap2* encodes a small ubiquitously expressed protein with high a content of prolines[266]. Dazap2 is likely a very important protein, considering its extremely high DNA and protein sequence conservation in the evolution, with only 1 aa (of total 168 aas) difference between mouse and human proteins, and the number of identified binding partners[267].

In our study, we identified Dazap2 as a direct binding partner to all TCF/LEF family members potentiating the Wnt/β-catenin driven transcription. Dazap2 knockdown decreases binding of TCF4 to the promoters of the Wnt-signaling target genes. The activity of the Wnt/β-catenin dependent reporters positively correlated with the amounts of Dazap2 in cells. Interestingly, endogenous Dazap2 protein shows a mostly cytoplasmic distribution which changes to nuclear upon ectopic *TCF4* expression. This indicates that TCF4 translocates/retains Dazap2 into/in the nucleus in a dose-dependent manner.

My contribution to this work: I generated the constructs which were used to obtain the data depicted in Figure 2 and Supplementary Figures 2 and 3.

Nucleic Acids Research Advance Access published March 20, 2009

Nucleic Acids Research, 2009, 1–14
doi:10.1093/nar/gkp179

Dazap2 modulates transcription driven by the Wnt effector TCF-4

Jan Lukas, Petr Mazna, Tomas Valenta, Lenka Doubravska, Vendula Pospichalova, Martina Vojtechova, Bohumil Fafilek, Robert Ivanek, Jiri Plachy, Jakub Novak and Vladimir Korinek*

Institute of Molecular Genetics, Academy of Sciences of the Czech Republic, Videnska 1083, 142 20 Prague 4, Czech Republic

Received 10 February 2009; Revised 27 February 2009; Accepted 4 March 2009

ABSTRACT

A major outcome of the canonical Wnt/β-catenin-signalling pathway is the transcriptional activation of a specific set of target genes. A typical feature of the transcriptional response induced by Wnt signalling is the involvement of Tcf/Lef factors that function in the nucleus as the principal mediators of signalling. Vertebrate Tcf/Lef proteins perform two well-characterized functions: in association with β-catenin they activate gene expression, and in the absence of Wnt ligands they bind TLE/Groucho proteins to act as transcriptional repressors. Although the general characteristics of Tcf/Lef factors are well understood, the mechanisms that control their specific roles in various cellular backgrounds are much less defined. In this report we reveal that the evolutionary conserved Dazap2 protein functions as a TCF-4 interacting partner. We demonstrate that a short region proximal to the TCF-4 HMG box mediates the interaction and that all Tcf/Lef family members associate with Dazap2. Interestingly, knockdown of Dazap2 not only reduced the activity of Wnt signalling as measured by Tcf/β-catenin reporters but additionally altered the expression of Wnt-signalling target genes. Finally, chromatin immunoprecipitation studies indicate that Dazap2 modulates the affinity of TCF-4 for its DNA-recognition motif.

INTRODUCTION

The Wnt-signalling pathway is essential during different developmental processes for determining cell fate. In addition, aberrant activation of this pathway has been implicated in cellular transformation and cancer [see some recent reviews (1–3)]. Transcription factors of the Tcf/Lef family are important downstream effectors of the so-called canonical Wnt/β-catenin-signalling pathway. In vertebrates the family consists of four members: Tcf-1, Tcf-3, Tcf-4 and Lef-1 (4). All vertebrate Tcf/Lef proteins (further referred to as Tcfs) contain virtually identical DNA-binding domains, a high mobility group (HMG) box, and a highly conserved β-catenin-interacting region. In the absence of the Wnt signal, Tcf/Lef factors interact with Transducin-like enhancer of split (TLE)/Groucho co-repressors to mediate the transcriptional repression of Tcf-bound genes (5–7). Alternatively, upon initiation of Wnt signalling the constitutive degradation of β-catenin is inhibited allowing this protein to accumulate both in the cytoplasm and nucleus, with the nuclear form able to displace TLE/Groucho co-repressors from Tcfs (8). Since β-catenin contains a strong transactivation domain, Tcf/β-catenin heterocomplexes function as transcriptional activators of specific Wnt-responsive genes such as *c-myc* (9), *Cyclin D1* (10,11), *Axin2* (12) and *CD44* (13). For a more comprehensive survey on Wnt signalling, please refer to the Wnt signalling home page at http://www.stanford.edu/%7ernusse/wntwindow.html.

Although the general function of Tcfs as transcriptional repressors or co-activators is well understood, their specific roles in Wnt signalling or cell physiology are much less defined. Besides β-catenin and TLE/Groucho co-repressors several other proteins associate with the HMG box of Tcfs. Such factors include proteins containing the I-mfa domain that mask the DNA-interacting region of Tcf-3, thereby preventing Tcf-3/β-catenin heterodimers from activating transcription (14). Likewise, RUNX3 forms a ternary complex with β-catenin and Tcfs to attenuate the transactivation potential of Tcf/β-catenin complexes by decreasing their DNA-binding activity (15).

Expression of mouse *Tcf*/*Lef* genes during embryogenesis and in adult tissues often overlaps. Nevertheless, gene-targeting experiments have demonstrated that individual Tcf members control their own cell biological

*To whom correspondence should be addressed. Tel: +4202 4106 3146; Fax: +4202 4447 2282; Email: korinek@img.cas.cz

programs (16–19). This observation implies that throughout evolution the functions originally executed by a single Tcf polypeptide have been distributed in more complex organisms among several family members. A plausible explanation for the functional diversity among Tcfs would be their selective interaction with distinct partners as the amino-acid sequences outside the highly conserved DNA- and β-catenin-binding domains are less homologous. Indeed, it has been reported that LEF-1 activates some promoters together with ALY, a nuclear protein that specifically binds LEF-1 and AML-1 (20). Additionally, LEF-1 cooperates with the Microphthalmia-associated transcription factor (MITF) to activate the expression of melanocyte-specific genes (21). Interestingly, although the activity of LEF-1 is suppressed by association with PIASy (a nuclear matrix-associated SUMO E3 ligase), this interaction results in increased TCF-4-regulated transcription (22,23). Two Tcf/Lef family members, Tcf-3 and Tcf-4, contain binding motifs for C-terminal-binding proteins (CtBPs) at their C-termini (24–26). As CtBPs operate as short-distance transcriptional repressors, interaction with such factors strengthens the repressive potential of these Tcfs in the absence of Wnt signalling (27). Besides CtBP, TCF-4 also binds the Hypermethylated in cancer 1 (HIC1) tumour suppressor. This interaction leads to the recruitment of TCF-4 into nuclear 'speckles' called HIC1 bodies. Upon association with HIC1, TCF-4 is unable to bind Wnt-responsive gene promoters. Thus, HIC1 functions as a nuclear TCF-4-specific Wnt pathway inhibitor (27). Finally, to add another layer of complexity to the regulation of Wnt target genes it has also been demonstrated that alternative promoters and/or alternative splicing of Tcf/Lef mRNAs occurs (28,29). A mechanism by which distinct Lef/Tcf isoforms may acquire individual properties is illustrated by their interaction with Hic-5 (hydrogen peroxide-induced clone 5). Hic-5 has been shown to bind a highly conserved and alternatively spliced exon of Lef/Tcf proteins and this results in the formation of a Lef/Tcf subtype-specific repressive complex that prevents target gene activation (30).

Mammalian Dazap2, also known as Proline codon-rich transcript, brain expressed (Prtb), was originally isolated in a mouse gene trap screen as a transcript expressed in the inner ear (31). This gene encodes a small 17 kDa protein that is highly conserved throughout evolution. The protein does not share significant sequence homology with any protein family and its most notable feature is a high content of prolines (17%) and several potential Src homology 2 (SH2)- and SH3-binding motifs (32). The *Dazap2* gene is broadly expressed during mouse embryonic development and in adult mouse and human tissues (31,33–35). Interestingly, *Dazap2* mRNA and protein are frequently down-regulated in multiple myeloma patients (36) whilst *Dazap2* mRNA is known to increase in adhering mouse osteoblasts or in rat astrocytes grown in high ammonia or hypo-osmotic conditions (37). In humans, Dazap2 interacts with RNA-binding testes-specific proteins DAZ and DAZL1 (35). In addition, Dazap2 also binds the Sox6 transcription factor to regulate L-type Ca^{++} channel α_{1c} expression during cardiac myocyte development (33). Recently, Kim and colleagues (38) described the interaction of Dazap2 with the Eukaryotic initiation factor 4G (eIF4G) which is essential for the formation of discrete cytoplasmic foci, named stress granules (SGs). SGs are formed upon translation inhibition and contain translation initiation factors and 40S ribosomal subunits (34,38). Finally, the protein level of Dazap2 is regulated by its interaction with NEDD4, an E3 ubiquitin ligase (39). Taken together, the aforementioned data indicate that Dazap2 functions in diverse roles in cell biology and physiology.

In this study we have used a yeast two-hybrid screen to identify Dazap2 as a TCF-4 interacting partner. Furthermore, we show that a short region proximal to the TCF-4 HMG box mediates this interaction. Interestingly, although this region is only partially conserved among Tcfs, all Tcf/Lef family members associate with Dazap2 in mammalian cells. Upon interaction with TCF-4 the subcellular distribution of Dazap2 is dramatically shifted from the cytoplasm into the nucleus. Upon knockdown of *Dazap2* a reduction in the activity of Tcf/β-catenin reporters was observed along with the expression of several Wnt-signalling target genes. Chromatin immunoprecipitation experiments performed in cells with down-regulated Dazap2 expression revealed a remarkable decrease in TCF-4 binding to Tcf-responsive elements in the promoters of genes tested. We propose that Dazap2 modulates the affinity of Tcfs to their recognition motifs.

MATERIALS AND METHODS

Plasmid constructs

Constructs encoding proteins fused at the N-terminus to EGFP were prepared using the pEGFP-C vector (Clontech); plasmids encoding Myc-tagged proteins were generated using the pK-Myc vector (26) and plasmids expressing Flag-tagged polypeptides were constructed in the vector pFlag-CMV-5a (Sigma). cDNAs encoding human *TCF-4* (GenBank accession number NM_030756), human *TCF-1* (NM_003202), and mouse *Lef-1* (NM_010703) were described previously (26,40,41). Full-length cDNA encoding human *TCF-3* (NM_031283) was purchased from Open Biosystems whilst the cDNA encoding human *β-catenin* (NM_205081) was kindly provided by B. Vogelstein (The Johns Hopkins Kimmel Cancer Center); cDNA encoding the full-length human DAZAP2 protein (NP_055579) was cloned by RT–PCR using template mRNA isolated from DLD-1 cells. PCR amplification steps were performed with Phusion High-Fidelity DNA Polymerase (Finnzymes). Mouse cDNA encoding *Wnt-1* [a gift from M.van Dijk (University Hospital Utrecht)] was subcloned into the mammalian expression vector pXJ41 (kindly provided by L. Andera, IMG, Prague, Czech Republic). Mouse cDNA encoding *Grg4* [a TLE/Groucho repressor (NM_011600)] was kindly provided by Z. Kozmik (IMG). Human *TAB1* (U49928), mouse *Tak1* (D76446) and mouse *Nlk* (NM_008702) cDNAs were obtained from T. Ishitani (Nagoya University). PCR-derived constructs were verified by sequencing; details of plasmid constructs are available on request.

Yeast two-hybrid screen

The cDNA encoding the N-terminal part of TCF-4 lacking the β-catenin-interacting domain [amino acids (aa) 31–333] was subcloned into the vector pGBKT7 (Clontech) and introduced into yeast AH109 cells by the standard lithium acetate transformation protocol. Expression of the TCF-4 fragment and GAL-4 DNA-binding domain (DBD) bait protein was tested in cell lysates by immunoblotting using anti-Myc and anti-TCF-4 monoclonal antibodies. A pre-transformed mouse 17-day embryo Matchmaker cDNA library amplified in the yeast strain Y187 (Clontech) was used for the screen according to the manufacturer's instructions. The 'library' and 'bait' cells were first mated in liquid cultures before subsequent plating on selective agar plates. After incubation at 30°C for 7–10 days, clones of growing cells were picked and streaked onto fresh selective plates and subjected to β-galactosidase filter lift assays. Plasmids isolated from positive clones were transformed into the yeast strain Y187 and their specificity tested by mini-mating with AH109 yeast cells that expressed the GAL-4 DBD or GAL-4 DBD-Lamin fusion proteins as bait. Clones that specifically interacted with the GAL-4 DBD-TCF-4 bait were sequenced. For the interaction domain mapping experiment cDNAs encoding corresponding fragments of TCF-4 (see legend to Figure 1 for details) were subcloned into the pGBKT7 vector and the resulting constructs were transformed into AH109 yeast cells. Individual yeast clones were mated with Y187 cells containing the Dazap2 prey and the growth of diploid yeast was tested on agar plates under selective conditions.

Cell lines, transfections, retrovirus production and infection

Human embryonic kidney (HEK) 293, human HeLa, DLD-1 and U2OS cells and mouse Wnt3a-producing L cells were purchased from ATCC. Mouse C57MG cells were kindly provided by R. Nusse and K. Willert (Stanford University). HEK 293 FT cells used for production of retroviral stocks were obtained from Invitrogen. pSuperTOPFLASH HEK 293 (STF 293) cells containing the integrated variant of the Wnt/β-catenin-responsive luciferase reporter pSuperTOPFLASH (42) were a kind gift from Q. Xu and J. Nathans (Johns Hopkins University). Cell lines were maintained in Dulbecco's modified Eagle's medium (DMEM) supplemented with 10% fetal bovine serum (Hyclone) and antibiotics. Cells in cultures were regularly checked for the presence of mycoplasma and only mycoplasma-free cells were used in experiments. Transfections of human cells were performed using the Lipofectamine RNAiMAX [small inhibitory RNAs (siRNA) transfections] or Lipofectamine 2000 reagent (plasmid or combined plasmid and siRNAs transfections). Both reagents were purchased from Invitrogen. C57MG cells were transfected using Fugene HD (Roche). Retroviral stocks were produced as described previously (26). Lentiviral stocks were prepared using the Trans-Lentiviral Packaging System (Open Biosystems) according to the manufacturer's protocol. Retroviral (or lentiviral) infections have been described previously (26); puromycin (Alexis; final concentration 5 μg/ml) resistant cells were selected without subcloning for 10 days and used in subsequent experiments.

GST interaction assays

Constructs expressing Glutathione S-transferase (GST)-TCF-4 fusion proteins were prepared using the pET-42b vector (Novagen). GST-TCF-4 (full-length), GST-TCF-4-N-term (aa 1–333), GST-TCF-C-term (aa 333–596), GST-TCF-4 (aa 1–214), GST-TCF-4 (aa 1–228), GST-TCF-4 (aa 214–310), GST-TCF-4 (aa 228–310) and GST-β-catenin (full-length) fusion proteins were expressed in the BL21 (DE3) strain of *Escherichia coli*. The mouse Dazap2 and human TCF-4 proteins were produced *in vitro* using the Quick TNT Coupled Reticulocyte System (Promega). A detailed protocol describing GST pull-down assays was reported previously (26).

Antibodies, co-immunoprecipitation and western blotting

Antiserum to Dazap2 was produced by immunization of rabbits or hens with a bacterially expressed mouse full-length polypeptide. An anti-β-catenin rabbit polyclonal antibody was produced by immunization with a bacterially expressed C-terminal fragment (aa 585–781) derived from the human polypeptide; an anti-β-catenin mouse monoclonal antibody was prepared in collaboration with Exbio Praha (Czech Republic) using standard techniques from the splenocytes of mice immunized with a bacterially produced β-catenin fragment. The anti-TCF-4 monoclonal and anti-TCF-4 and anti-EGFP rabbit polyclonal antibodies were reported previously (27). The following commercially available mouse monoclonal antibodies were used: anti-Myc 9E10 (Roche), anti-Flag M2 (Sigma), anti-Flag (Exbio), anti-α-tubulin TU-01 (Exbio). A detailed protocol describing the immunoblotting procedure can be found in the Supplementary Data.

Immunofluorescent microscopy

For immunofluorescence studies, Dazap2 polyclonal antibodies were purified by affinity chromatography using the GST-Dazap2 antigen coupled to glutathione Sepharose 4B (Amersham Pharmacia Biotech) (43). The purified antibodies were subsequently stored at 4°C in PBS supplemented with 1% BSA [(w/v), Sigma, molecular biology grade]. Monoclonal antibodies were used as hybridoma cell culture supernatants without dilution. Cells grown on coverslips were fixed (when cells were transfected prior to staining, the fixation was performed 18 h after transfection) in cold methanol (−20°C, 5 min) followed by a brief incubation in acetone (−20°C, 30 s). Alternatively, fixation was performed for 10 min at room temperature using a 4% (v/v) solution of paraformaldehyde (Electron Microscopy Sciences) diluted in PBS before cells were subsequently permeabilized with 0.2% (v/v) Triton X-100 (Sigma; room temperature, 15 min) diluted in PBS. After washing with PBS, cells were pre-incubated in 1% BSA (Fraction V; Sigma) for 20 min at room temperature. The cells were then stained with primary GST-Dazap2-purified polyclonal antibodies (5 μg/ml in PBS) or with an anti-TCF-4 monoclonal antibody (undiluted hybridoma culture supernatant; room

temperature, 60 min). The samples were washed three times with PBS, and consecutively incubated with a relevant fluorescently labelled secondary antibody. The ALEXA 488 dye conjugated to goat anti-chicken or goat anti-rabbit antibodies and ALEXA 594 conjugated to a goat anti-mouse antibody (dilution 1:500; Molecular Probes) were used. To pre-block the Dazap2 antibody, antigen-purified antibodies (20 μg/ml) were incubated with the bacterially expressed Dazap2 or EGFP (negative control) proteins (overnight at 4°C; the concentration of recombinant protein in each sample was 50 μg/ml), before being diluted in PBS (final concentration 5 μg of the antibody per ml) and used for staining. Finally, the samples were washed three times in PBS, incubated with DAPI nuclear stain (Molecular Probes; 1 min, room temperature, final concentration 1 μM), washed and mounted in MOWIOL (Calbiochem). Immunofluorescence was visualized using a confocal laser scanning microscope (TCS SP5; Leica). The system was carefully tested for overlaps between individual optical channels and the microscopic images were taken separately for each fluorescence channel using the sequential scanning mode.

RNA purification and real-time quantitative RT–PCR (qRT–PCR)

Standard procedures were used for RNA purification and reverse transcription. Briefly, total RNAs were isolated from cells using the Trizol reagent (Invitrogen); random or oligo dT-primed cDNA was prepared in a 20 μl reaction from 1 μg of total RNA using Superscript II RNAseH$^-$ reverse transcriptase (Invitrogen). cDNAs were produced from at least two independent RNA isolations and the PCR reactions were performed in triplicate for each primer set. Two percent of the resulting cDNA was used for one quantitative PCR reaction. Control reactions (containing corresponding aliquots from cDNA synthesis reactions that were performed without reverse transcriptase; minus RT controls) were run in parallel duplicates. PCR reactions were run using the LightCycler 480 Real-Time PCR System (Roche). Typically, a 5 μl reaction mixture contained 2.5 μl of LightCycler 480 SYBR Green I Master mix (Roche), 0.5 μl of primers (final concentration 0.5 μM) and cDNA diluted in 2 μl of deionized water. Crossing-threshold (CT) values were calculated by LightCycler® 480 Software (Roche) using the second-derivative maximum algorithm. The specificity of each PCR product was analysed using the in-built melting curve analysis tool for each DNA product identified; additionally, some selected PCR products were verified by sequencing. All primers were calculated using Primer 3 computer services at http://frodo.wi.mit.edu/. Two housekeeping genes, *β-actin* and *ubiquitin C* (*Ubc*) were used as internal control genes to standardize the quality of different cDNA preparations (44). Primer sequences are listed in Supplementary Data.

Wnt3a purification

Recombinant mouse Wnt3a ligand was isolated from the culture medium of Wnt3a-producing L cells according to a detailed protocol published on the Internet (http://www.stanford.edu/%7ernusse/assays/W3aPurif.htm). The activity of individual batches of purified Wnt3a protein were tested using Wnt3a-stimulated and control (Wnt3a storage buffer added only) STF 293 cells and luciferase assays.

Knockdown of Dazap2

For gene knockdowns of human *DAZAP2*, four duplex siRNAs were purchased from Dharmacon. The target sequences (on the plus DNA strand) were as follows: #1 5′-GGA GCC AAC GUC CUC GUA A-3′, #2 5′-CAC CAU GUC AGC CGC AUU U-3′, #3 5′-UCA GAG CUC UAU CGU CCG A-3′, #4 5′-CUU CAU GGG UGG UUC AGA U-3′. Control EGFP siRNA (Dharmacon) target sequence was: 5′-GCG ACG TAA ACG GCC ACA AGT TC-3′. Cells transfected with duplex siRNAs at a concentration of 30 nM were grown for 24–72 h before further analysis. To generate a stable knockdown of *Dazap2* in mouse C57MG cells, the cells were transduced with retroviruses (purchased from Open Biosystems) that express *Dazap2* shRNA (shRNA #1 code: TRCN0000085966, shRNA #2 code: TRCN0000085965). Non-silencing lentiviral shRNAmir (pGIPZ; Open Biosystems) were used as a control. The constructs were packaged and transduced into the target cells as described by the manufacturer. The cells were selected without subcloning using appropriate antibiotics before they were used for further analysis.

Reporter gene assays and Wnt stimulation

To assay TCF-mediated transcription, firefly luciferase pTOPFLASH and pFOPFLASH reporters containing either three copies of the optimal Tcf motif GATCAAAGG or three copies of a mutant motif GGCCAAAGG, respectively were used (45). Additionally, *Cyclin D1* reporter constructs containing one copy of the Tcf-interacting motif (designated 163CD1LUC) or its mutated variant (163mtLefCD1LUC) (10) (a gift from A. Ben-Ze'ev, The Weizmann Institute of Science) and the *Axin2* promoter reporter (46) (a gift from F. Costantini, Columbia University Medical Center) were used. Reporter gene assays were performed as described previously (26). Briefly, cells were seeded into 24-well plates ($\sim 10^5$ cells per well, depending on the cell type) and transfected 2 h later with a Lipofectamine mixture containing 100 ng *Renilla* pRL-SV40 plasmid (Promega) as an internal control, 500 ng luciferase reporter plasmid, and up to 1 μg of the particular expression vector. The total amount of DNA was kept constant by adding empty expression vector where necessary. For transfection into STF 293 cells (containing an integrated TCF-dependent reporter pSuperTOPFLASH) (42,47), a mixture that included 50 ng *Renilla* plasmid and up to 1.5 μg of a specific expression or stuffer vector was prepared. Two independent systems were utilized to activate Wnt signalling: (i) co-transfection of cells with a *Wnt1*-expressing plasmid. Cells were analysed 24 h post-transfection; (ii) stimulation of cells with purified recombinant Wnt3a ligand. Cells were transfected with corresponding constructs and 15 h post-transfection recombinant Wnt3a (only the vehicle

was used in control experiments) was added and the cells cultured for additional 16 h before their harvest and lysis. The activity of firefly and *Renilla* luciferase in cell lysates were determined using the Dual luciferase system (Promega) and a single tube luminometer Sirius (Berthold). All reporter gene assays were done in triplicate. Reporter gene activities shown are average values plus standard deviations calculated from at least three independent experiments after normalization against the activity of *Renilla* luciferase.

Chromatin immunoprecipitation (ChIP)

For ChIP experiments, STF 293 cells were grown in 10-cm culture dishes and transfected either with siRNA #2 targeting *Dazap2* or control siRNA (non-silencing siRNA set; Dharmacon). Two days later the cells were transferred into 15-cm culture dishes and subsequently stimulated with Wnt3a or Wnt3a storage buffer alone for 16 h. The cells were fixed directly in the dishes using formaldehyde [1% (v/v); Sigma] then harvested and subjected to ChIP analysis according to Kirmizis (48). Usually, chromatin isolated from cells grown in one 15-cm culture dish was used for immunoprecipitation with one specific antibody. Rabbit anti-Dazap2, TCF-4 and β-catenin polyclonal antibodies were used for ChIP; the negative control experiments were performed with a rabbit anti-EGFP polyclonal antibody. The amount of precipitated DNA was analysed using the LightCycler 480 Real-Time PCR System (Roche) in an analogous manner to real-time qRT–PCR. Half a percent of decrosslinked and purified (by phenol extraction) input chromatin (chromatin that was not subjected to ChIP) was analysed in control PCR reactions. The primers used for the PCR amplification are listed in the Supplementary Data.

RESULTS

Dazap2, a small evolutionary conserved protein, interacts with the TCF-4 N-terminus

It is well known that the function of the nuclear effectors of Wnt signalling, the Tcf/Lef transcription factors, can be modulated by various interacting partners. As such, we decided to perform a yeast two-hybrid screen (Y2H) to search for novel TCF-interacting proteins. An N-terminal part of human TCF-4 protein (aa 31–333) was used as bait. This truncated protein lacks its very N-terminus that encodes the main β-catenin-interacting domain (8,49) as well as the C-terminal DNA-binding HMG box (Figure 1A). From a cDNA library collected from a Day 17 mouse embryo we obtained seven yeast colonies (out of $\sim 5 \times 10^7$ diploid yeast cells) growing in selective broths. Of these clones only one encoded a protein that specifically interacted with the TCF-4 bait and not the Gal-4 DNA-binding domain (DBD) alone, Gal-4 DBD-Lamin and Gal-4 DBD-p53 fusion proteins or with the C-terminal part of TCF-4 used as bait in our previous study (26) (Figure 1A and data not shown). The resulting plasmid DNA isolated from the yeast cells encoded a full-length 168 aa polypeptide described previously as Proline codon-rich transcript, brain expressed (Prtb) or

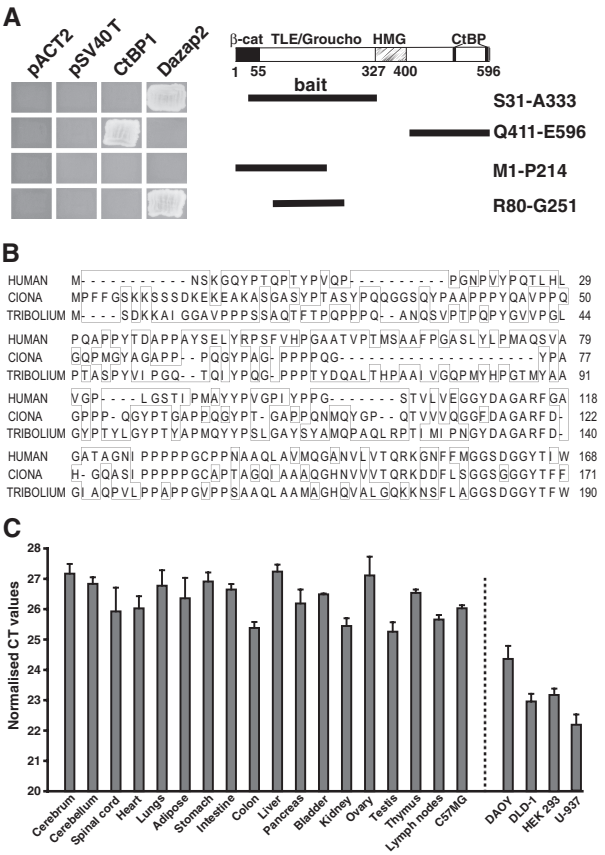

Figure 1. Interaction between Dazap2 and TCF-4 in a yeast two-hybrid screen. (**A**) Deletion mutants of human TCF-4 (schematically represented on the right as thick black lines) were tested in an Y2H mini-mating assay for interaction with full-length mouse Dazap2. The left panel shows the growth of clones of yeast cells on selective agar plates. The yeast cells contain plasmids as indicated above and express TCF-4 deletion mutants that are depicted on the right. None of the TCF-4 proteins binds to the separate GAL4 activation domain (AD) encoded by 'empty' library vector pACT2 or to the fusion protein GAL4 AD-SV40 T large antigen (pSV40 T). β-cat, β-catenin interaction domain; TLE/Groucho, TLE/Groucho-binding domain; CtBP, CtBP-binding sites; HMG, DNA-binding domain. (**B**) Amino-acid comparison of human, sea squirt (*Ciona*) and red flour beetle (*Tribolium*) Dazap2. Protein sequences were aligned by the ClustalV program. The amino-acid differences are boxed. GenBank accession numbers: *Homo sapiens*, NP_055579; *Tribolium castaneum*, XP_973572; *Ciona intestinalis*, NM_001032667. (**C**) The *Dazap2* gene is broadly expressed in tissues and cell lines. Results of qRT–PCR analyses performed with Dazap2-specific primers on cDNA generated from adult mouse tissues, mouse mammary epithelium C57MG cells, human medulloblastoma DAOY, human embryonic kidney HEK 293, human adenocarcinoma DLD-1 and human lymphoma U-937 cells. The reactions were performed in triplicate. The results shown are from one representative experiment from a total of two. The expression levels of *Dazap2* mRNA in the indicated tissues or cell lines are presented as average CT values and the corresponding standard deviations (SD) after normalization to the levels of *β-actin* cDNA.

DAZ-associated protein 2 (Dazap2) (31,35). Although Dazap2 does not share significant homology with any known protein family, Dazap2 orthologues isolated from various species display remarkable sequence similarity (there is only one amino acid change between human and mouse proteins), especially within the C-terminal half (Figure 1B and Supplementary Figure 1). To determine

the expression pattern of *Dazap2* mRNA in adult mouse tissues and several different cell lines we performed quantitative real-time RT–PCR analysis (qRT–PCR), which revealed virtually ubiquitous expression (Figure 1C). We further delineated the minimal region in TCF-4 required for association with Dazap2. We generated several deletions in the TCF-4 bait used for the primary screen and tested their ability to interact with full-length Dazap2 via Y2H. As shown in Figure 1A, truncated bait containing aa 80–251 was able to bind Dazap2, however, a protein spanning aa 1–214 could not. Taken together, these results reveal that the relatively short sequence in TCF-4 spanning aa 214–251 is essential for the interaction.

All Tcf/Lef family members associate with Dazap2 in mammalian cells

Direct binding between Dazap2 and TCF-4 was evaluated *in vitro* by pull-down assays that utilized bacterially expressed GST-tagged TCF-4 and *in vitro* translated Dazap2. Dazap2 associated both with full-length GST-TCF-4 and with the truncated TCF-4 N-terminal fragment. No interaction was detected between Dazap2 and GST alone or with the C-terminal part of TCF-4 (TCF-4-C-term) that encompassed the DNA-binding HMG box domain (Figure 2A and data not shown). Furthermore, we performed a detailed mapping of the putative interaction domains in both proteins using pull-down assays. In agreement with Y2H the Dazap2-binding region was mapped to aa 214–228 in the TCF-4 N-terminus (Figure 2A). On the other hand, any truncation of Dazap2 abolished its association with TCF-4 (Supplementary Figure 2 and data not shown), indicating that non-adjacent parts of the Dazap2 polypeptide participate in the interaction interface. The interaction of Dazap2 with TCF-4 was further confirmed in mammalian cells using co-immunoprecipitations. Experiments involving HEK 293 cells double-transfected with constructs expressing Dazap2-Flag and TCF-4-Myc demonstrated that Flag-tagged Dazap2 could be co-isolated with Myc-tagged TCF-4 when an anti-Myc monoclonal antibody was used for precipitation; conversely, Myc-tagged TCF-4 was present in the anti-Flag precipitates (Figure 2B). The interaction of these two proteins is specific since parallel single-transfection assays did not reveal any binding of Dazap2 and TCF-4 to the anti-Myc- or anti-Flag-tag antibodies, respectively (Figure 2B). In addition, we analysed the ability of endogenous TCF-4 and Dazap2 to interact by performing co-immunoprecipitation assays with rabbit polyclonal antibodies raised against these polypeptides. Analysis of a variety of cell types (DLD-1, HEK 293, C57MG) by co-immunoprecipitation using the anti-Dazap2 or anti-TCF-4 antibodies confirmed our earlier observations and demonstrated that endogenous Dazap2 and TCF-4 do associate. Negative control reactions using an anti-EGFP rabbit polyclonal antibody failed to pull down any proteins again confirming that the interaction is specific (Figure 2C and data not shown). The human colon adenocarcinoma cell line, DLD-1 harbours a mutation in the tumour suppressor

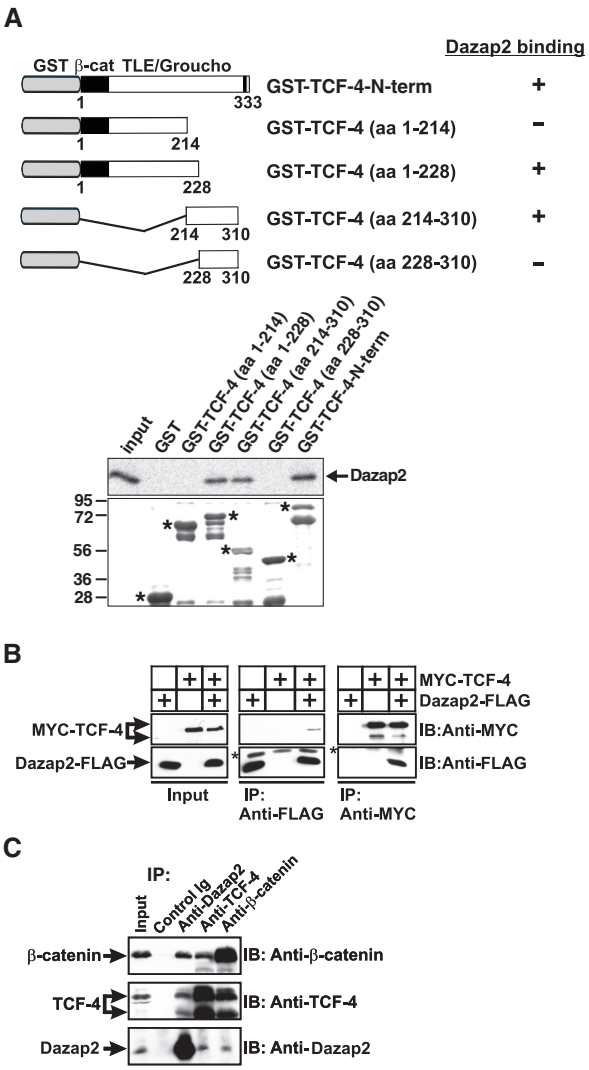

Figure 2. Association between Dazap2 and TCF-4 *in vitro* and in mammalian cells. (**A**) Interaction of Dazap2 with TCF-4 in GST pull-down assays. The top panel represents a schematic diagram of the TCF-4 proteins used in the *in vitro* pull-down assays. The bottom panel displays the pull-down assay results between the different bacterially expressed GST fusion TCF-4 proteins and *in vitro* translated [^{35}S]-labelled Dazap2. Ten percent of the total reaction was loaded in the lane denoted 'Input'. Under the autoradiograph is a Coomassie Blue-stained gel that shows the amount of GST-tagged TCF-4 proteins used in the experiment. The putative intact forms of the recombinant proteins are labelled by asterisks; the faster migrating bands result from a partial degradation of the corresponding GST fusion proteins. Molecular weight markers in kDa are indicated on the left. (**B**) Co-immunoprecipitation of FLAG-tagged Dazap2 and MYC-tagged TCF-4. Cell lysates prepared from HEK 293 cells transfected with constructs as indicated were precipitated using anti-MYC and anti-FLAG monoclonal antibodies. The asterisks indicate the light chains of immunoglobulins used in the experiments. (**C**) Endogenous complexes of Dazap2, TCF-4 and β-catenin in human cells. Lysates prepared from DLD-1 cells were subjected to immunoprecipitation with anti-Dazap2, anti-TCF-4, anti-β-catenin or anti-EGFP (Control Ig) rabbit polyclonal antibodies. Blots were probed by either anti-TCF-4, anti-β-catenin mouse monoclonal or anti-Dazap2 chicken polyclonal antibodies. In lanes denoted 'Input', 10% of the total lysate used for one immunoprecipitation was loaded; IP, immunoprecipitation; IB, immunoblotting.

APC that results in the accumulation of nuclear TCF-4/β-catenin complexes. Interestingly, Dazap2 was present in the precipitates obtained by incubating DLD-1 cell lysates with an anti-β-catenin antibody and similarly, β-catenin was isolated using an anti-Dazap2 antibody (Figure 2C). Since we did not detect any association between Dazap2 and β-catenin in GST pull-down assays (Supplementary Figure 3) we conclude that these proteins do not interact directly but are instead brought to one heterocomplex via association with their common partner, the TCF-4 factor. We also noted that the endogenous TCF-4 protein extracted from various mammalian cells migrates in the denaturing gels as a double band representing polypeptides of the apparent molecular weight 65 and 85 kDa, respectively (Figures 2C, 5A, 6A and data not shown). Interestingly, both these bands showed immunoreactivity with various monoclonal antibodies recognizing different epitopes in TCF-4 (data not shown). Moreover, ectopic expression of TCF-4 generated two different protein forms similar to their endogenously produced counterparts (Figure 2B and Supplementary Figure 5). As the expression of the both putative TCF-4 proteins was specifically down-regulated by *TCF-4* shRNA (Supplementary Figure 4) and the predicted M_w of TCF-4 is 65.3 kDa, we concluded that the slower migrating and mostly more prominent band represents the TFC-4 polypeptide, possibly modified by sumoylation (23).

To visualize the subcellular distribution of endogenous DAZAP2 protein we selected the human lymphoma U-937 cell line as it exhibits a relatively high level of *DAZAP2* mRNA expression (Figure 1C). Analysis of Dazap2-stained cells by confocal microscopy revealed a predominantly cytoplasmic distribution with some additional nuclear staining (diffuse or in distinct dots or 'puncta') (Figure 3A). The staining of putative Dazap2 protein was specific as both polyclonal antisera showed a virtually identical subcellular distribution. Moreover, the observed reactivity was completely abolished by pre-incubation of the primary antibodies with Dazap2 (and not with control EGFP) recombinant protein (Figure 3A and data not shown). Finally, we tested the co-localization of ectopically expressed TCF-4 and Dazap2 (either EGFP- or Myc-tagged) in HeLa cells. In single-transfected cells expressing either TCF-4 or Dazap2, TCF-4 was clearly nuclear whilst Dazap2 (visualized by either EGFP or Myc antibodies) displayed a primarily cytoplasmic and partly nuclear localization. When both proteins were co-expressed, Dazap2 was sequestered to the nucleus in a dose-dependent manner unlike the control EGFP-only protein, which remained uniformly distributed between the cytoplasm and nucleus irrespective of the presence or absence of the TCF-4 factor (Figure 3B and data not shown). Altogether, the data reported here indicate that Dazap2 interacts directly with TCF-4 and that this interaction results in its subcellular redistribution to the nucleus.

As the essential region in TCF-4 required for binding to Dazap2 displays some sequence homology with the corresponding sequences in other Tcf/Lef family members (Figure 4A), we decided to further analyse whether Dazap2 can interact with additional Tcf/Lef proteins.

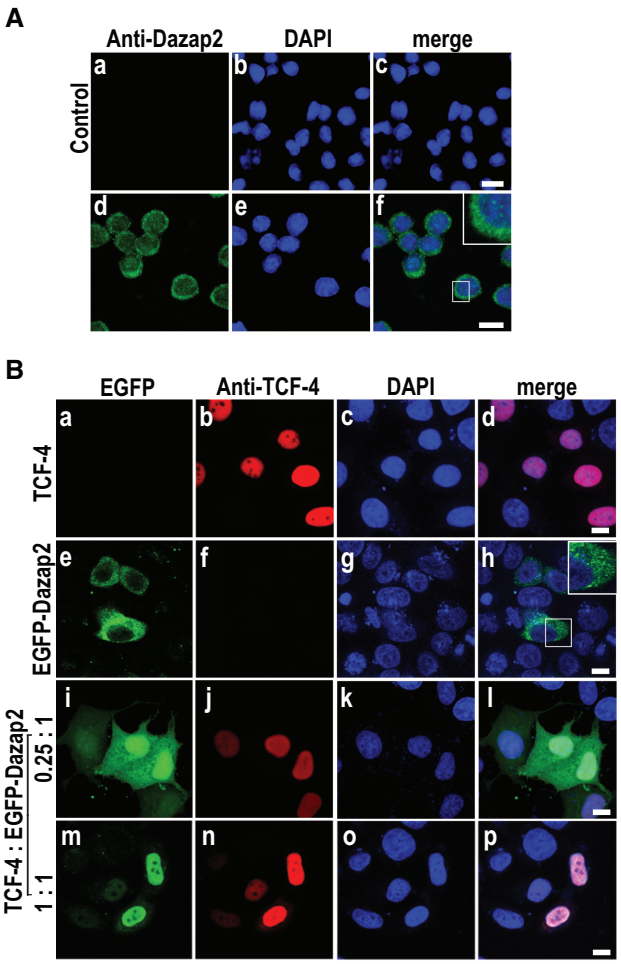

Figure 3. TCF-4 translocates Dazap2 into the nucleus. (**A**) Endogenous Dazap2 protein shows a mostly cytoplasmic distribution in human cells. Laser scanning confocal micrographs of U-937 cells stained with an antigen-purified chicken anti-Dazap2 polyclonal antibody. The merged images (c) and (f) were generated by an overlay of endogenous Dazap2 captured in the green channel and the DAPI nuclear stain captured in the blue channel. The first row, labelled 'Control', shows the cells stained with the primary antibody pre-blocked with Dazap2 recombinant protein as described in the 'Materials and methods' section; inset in (f) shows a magnified image as indicated. Bar, 10 μm. (**B**) Nuclear co-localization of ectopically expressed EGFP-Dazap2 and TCF-4 proteins. Laser scanning confocal microscopy images of HeLa cells transfected with constructs (as indicated on the left) and subsequently stained with the mouse anti-TCF-4 monoclonal antibody. The images (i, j, k, l) show cells transfected with TCF-4 and EGFP-Dazap2 constructs at a ratio 0.25 (TCF-4) to 1 (EGFP-Dazap2); the images (m, n, o, p) were obtained at a ratio 1 to 1. The merged images (d, h, l, p) were generated by an overlay of the corresponding images gained either in the green input channel detecting EGFP-Dazap2, red input channel detecting TCF-4 or blue channel to detect the DAPI nuclear stain. Inset in (h) shows a magnified image as indicated. Bar: 10 μm.

Constructs expressing Myc-tagged TCF-1, -3, -4, Lef-1 and Flag-tagged Dazap2 were either single- or double-transfected into HEK 293 cells and their ability to interact was tested by co-immunoprecipitation using anti-Myc or anti-Flag antibodies as described above. All TCF/Lef proteins analysed were isolated from cell lysates containing Flag-Dazap2 using the anti-Flag antibody.

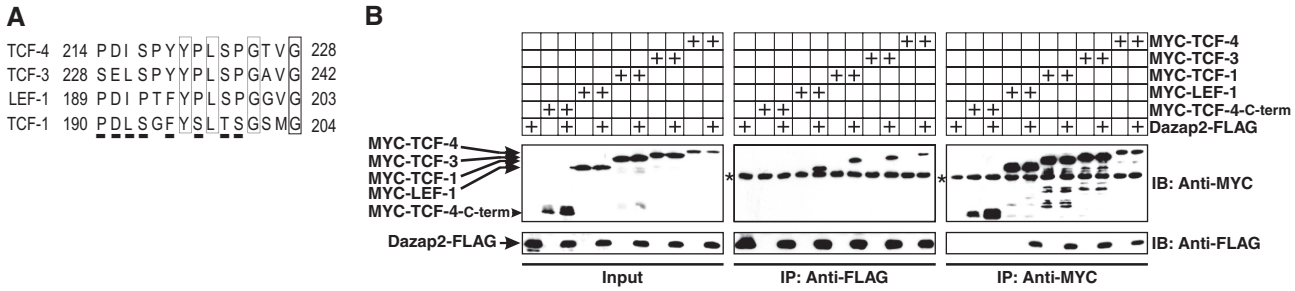

Figure 4. Dazap2 interacts with all members of the Tcf/Lef family. (**A**) The region of TCF-4 required for interaction with Dazap2 as identified by GST pull-down assays (aa 214–228) is partly conserved in other Tcf/Lef family members. The corresponding sequences of the human proteins were aligned using the ClustalV program. Fully conserved amino-acid residues are boxed whilst amino-acid residues with similar biochemical properties are underlined. GenBank accession numbers: TCF-4, NP_110383; TCF-3, NP_112573; LEF-1, NP_057353; TCF-1, NP_003193. (**B**) Co-immunoprecipitation of Dazap2-FLAG and MYC-tagged TCF/LEF transcription factors in human HEK 293 cells transfected with various Tcf expression constructs as indicated. Co-immunoprecipitation of TCF/LEF proteins using an anti-FLAG antibody is also shown. In the gel denoted 'Input', 10% of total lysates was loaded. The asterisks indicate the heavy chains of immunoglobulins used in the experiments.

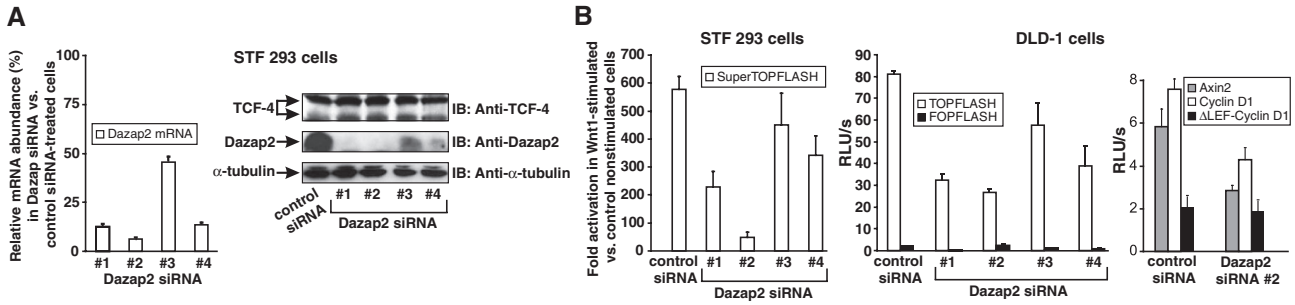

Figure 5. The activity of the Wnt/β-catenin-dependent reporters positively correlates with the amounts of Dazap2 in the cells. (**A**) HEK 293 cells containing the integrated reporter pSuperTOPFLASH (STF 293 cells) were transfected with four different *Dazap2*-specific siRNAs marked 1 to 4 or with control siRNA (*EGFP*-specific) and the changes in the levels of *Dazap2* mRNA or protein were tested 24 h post transfection. The left panel shows the results obtained by qRT–PCR analysis. The relative abundance of *Dazap2* mRNA in *Dazap2* siRNA- versus control siRNA-transfected cells (the level of *Dazap2* mRNA in control cells was set to 100%) was derived from the average CT values after normalizing to the levels of *β-ACTIN* cDNA. Data from two independent experiments performed in triplicate were combined in the graph. SDs (standard deviations) are shown by error bars. The right panel shows western blots of whole cell extracts prepared from STF 293 cells treated with siRNAs as indicated. Blots were probed with anti-Dazap2, anti-TCF-4 or anti-α-tubulin (as an internal control) antibodies. (**B**) Results of the reporter gene assays in human cells. STF 293 and DLD-1 adenocarcinoma cells were transfected with *Dazap2* or control siRNAs. To stimulate the integrated pSuperTOPFLASH in STF 293 cells the siRNA transfection mixtures additionally contained a *Wnt1*-expression construct; mixtures including an empty vector were used in control transfections. DLD-1 cells were co-transfected with siRNA and the Tcf/β-catenin-responsive reporter pTOPFLASH or pFOPFLASH as a negative control. After 24 h, cells were harvested and luciferase (firefly) activities were determined in the lysates. The histograms represent mean values of triplicate experiments with SDs. The reporter activity in unstimulated (empty vector) STF 293 cells was arbitrarily set to 1. For DLD-1 cells the average luciferase light units per second (RLU/s) are given; the values were corrected for the efficiency of transfection using the internal control *Renilla* luciferase expression plasmid. The results of one representative experiment from two in total are shown.

Reciprocally, Dazap2 was similarly pulled down from cells co-expressing Myc-tagged TCF/Lef proteins with the anti-Myc antibody (Figure 4B). In agreement with previous results Dazap2 did not co-immunoprecipitate with the C-terminal part of TCF-4 (TCF-4-C-term) lacking the Dazap2-interaction domain (Figure 4B). Since the short stretch of amino acids mediating the Dazap2 binding is in close proximity to a region which is alternatively spliced in most of Tcf/Lef family members (alternative splicing involves exon IVa in Tcf-1, exon VI in Lef-1 and exon VIII in Tcf-4) (50–52), we generated a TCF-4 variant lacking exon VIII and tested its ability to bind Dazap2 in GST pull-down and co-immunoprecipitation assays. As this variant associated with Dazap2 to the same extent as the non-spliced form (Supplementary Figure 5), the assays further confirmed the importance of the already defined interaction motif.

Dazap2 knockdown decreases Wnt/β-catenin-mediated transcription

To examine whether Dazap2 overexpression has any effect on Wnt-mediated transcription we co-transfected a TCF/β-catenin-responsive luciferase reporter, pTOPFLASH or its mutated variant, pFOPFLASH into HEK 293 cells in conjunction with a Dazap2 expression construct. The cells were subsequently stimulated by recombinant Wnt3a and the luciferase activities were determined from cell lysates. The ectopic expression of Dazap2 displayed neither an inhibitory nor stimulatory effect on Wnt signalling. Furthermore, analyses of Wnt-regulated transcription in DLD-1 cells that should exhibit constitutive Wnt signalling or U2OS cells that are activated by the Wnt3a ligand were not affected by *Dazap2* overexpression (data not shown). Finally, RNA interference (RNAi) was used to

down-regulate the expression of *Dazap2* and the resulting Tcf/β-catenin-dependent transcription was analysed. First, we utilized four distinct siRNA duplexes and tested their efficiency towards *Dazap2* mRNA using qRT–PCR and western blotting. As shown in Figure 5A, all four siRNAs reduced the levels of *Dazap2* mRNA and protein to different extents, with siRNA #1 and #2 showing the highest efficiency (as compared to the control EGFP siRNA). Subsequently, we introduced by lipofection the siRNAs into cells containing the genome-integrated variant of the pTOPFLASH reporter, pSuper TOPFLASH [the resultant cells were termed pSuper TOPFLASH (STF) 293]. To stimulate Wnt signalling the cells were co-transfected with a *Wnt1* expression construct. Twenty-four hours post-transfection the cells were harvested, cell lysates prepared and luciferase activities measured. In a parallel analogous experiment, DLD-1 cells were co-transfected with siRNA duplexes and a DNA mixture containing the pTOPFLASH or pFOPFLASH (negative control) reporter in addition to a *Renilla* luciferase-expressing plasmid that acted as an internal control. The next day cells were harvested and processed as described for STF 293 cells. Surprisingly, Tcf-driven transcription measured from the integrated or ectopic reporter pTOPFLASH was substantially reduced in the *Dazap2* siRNA-treated cells. Of importance, the extent of signalling reduction corresponded to the efficiency of the *Dazap2* knockdown as documented for the individual *Dazap2*-specific siRNAs (Figure 5B). Virtually identical results were obtained with Wnt-stimulated U2OS cells (data not shown). Furthermore, Dazap2 protein knockdown also negatively affected the transcription of two additional well-defined Tcf/β-catenin-dependent reporter constructs that contained either a 5-kb promoter region of the *Axin2* (46) gene or a 163-nt long enhancer element proximal to the transcription start of the *Cyclin D1* gene (10) (Figure 5B). Importantly, when a single Tcf/Lef-binding site in the *Cyclin D1* reporter was mutated, the resulting plasmid (designated as ΔLEF-Cyclin D1) not only lost its responsiveness to Wnt signalling but its basal expression did not change in cells treated with *Dazap2* or control siRNA (Figure 5B). To ensure the two *Dazap2*-specific siRNAs used did not induce any non-specific 'off-target' effects, two lentiviral constructs containing shRNA against mouse *Dazap2* were purchased and introduced into mouse mammary epithelium C57MG cells. Since both shRNAs showed a similar efficiency to down-regulate *Dazap2* expression (Figure 6A) and the Wnt stimulation had no effect on Dazap2 expression (Figure 6A and B), the polyclonal cell cultures were mixed and luciferase reporter assays performed. As expected, the cells with down-regulated *Dazap2* displayed a decrease in Wnt-stimulated transcription as compared to control cells containing non-silencing shRNAs (generated in parallel experiments) (Figure 6C). Therefore, these experiments confirm our previous results obtained from transient transfection assays performed in human cells.

To analyse whether *Dazap2* knockdown has any effect on the transcription of endogenous Wnt-signalling target genes, C57MG cells expressing *Dazap2* or control shRNAs were stimulated with Wnt3a ligand and the

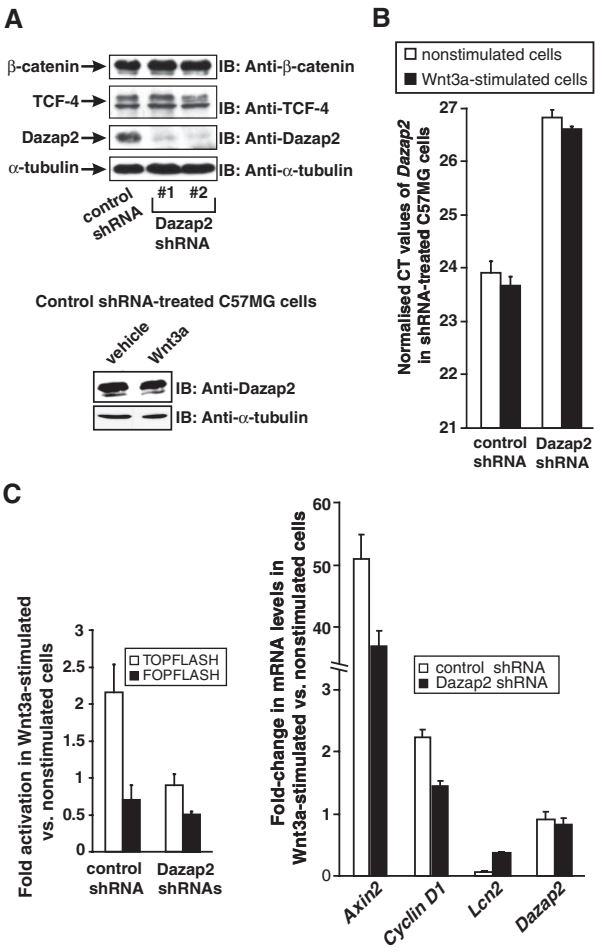

Figure 6. Down-regulation of *Dazap2* reduces the responsiveness of C57MG cells to Wnt3a stimulation. (**A**) The top panel shows a series of western blots from whole cell extracts prepared from mammary gland epithelium C57MG cells transduced with retroviral vectors expressing either a non-silencing control shRNA or two different *Dazap2* shRNAs. Prior to harvesting, cells were stimulated with Wnt3a ligand for 16 h. The blots were probed with antibodies as indicated. The bottom panel shows the western blot of whole cell extracts prepared from non-silencing control shRNA-treated cells incubated with Wnt3a or vehicle for 16 h. (**B**) The relative abundance of *Dazap2* mRNA in control or *Dazap2* shRNAs-expressing (a mixed culture of cells containing *Dazap2* shRNA 1 and 2 was used) cells as measured by qRT–PCR. The cells were cultured without activation or stimulated with Wnt3a for 16 h. The expression of the *Dazap2* gene is indicated by average CT values obtained by qRT–PCR assay on the corresponding mRNA after normalization to the levels of *β-actin* cDNA. (**C**) The left panel depicts control or *Dazap2* shRNA #1 and #2-producing C57MG cells that were transfected with the indicated reporters. Twenty-four hours post-transfection, cells were either stimulated with Wnt3a ligand or grown without stimulation. After additional 16 h, the cells were harvested and luciferase activities were determined in lysates. These activities were corrected for the efficiency of transfection by determining the luciferase/*Renilla* ratio. Values in unstimulated cells were arbitrarily set to 1. Transfections were done in triplicates and the results from one experiment out of two in total are presented with SDs. The right panel shows cDNAs prepared from Wnt3a-treated or control cells expressing non-silencing or *Dazap2* shRNAs analysed by qRT–PCR. The relative abundance of the indicated mRNAs in given cells (the levels of the tested mRNAs in unstimulated cells was set to 1) was derived from the average CT values after normalizing to the levels of *β-actin* cDNA. Data shown are from one representative experiment from a total of two.

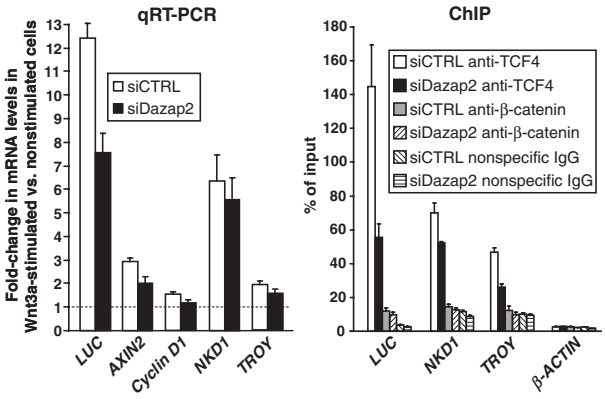

Figure 7. *Dazap2* knockdown decreases binding of TCF-4 to the promoters of the Wnt-signalling target genes. STF 293 cells were transfected with *Dazap2* siRNA #2 (siDazap2) or control siRNA (siCTRL). After a 2-day expansion the cells were transferred to large culture dishes and stimulated with either Wnt3a ligand or Wnt3a storage buffer only. After 16 h, the cells were harvested and used for mRNA isolation and cDNA preparation. Alternatively, the cells were fixed directly in the dishes and utilized for chromatin immunoprecipitation (ChIP). The left panel shows the results from qRT–PCR analysis. The relative abundance of the indicated mRNAs in Wnt3a-stimulated versus control cells was derived from the average CT values after normalizing to the levels of *β-ACTIN* cDNA. The right panel shows the ChIP analysis of chromatin isolated from STF 293 cells transfected with control or *Dazap2* siRNA #2 duplexes. Only results for Wnt3a-stimulated cells are shown. The diagram represents the relative amounts of the respective DNA element pulled-down by the indicated antibodies. The amount of input non-immunoprecipitated DNA (evaluated separately for each primer set) was arbitrarily set to 100%. Data from one representative experiment from two in total are given.

expression of several putative Tcf/β-catenin targets was assessed by qRT–PCR. As shown in Figure 6C, *Dazap2* down-regulation resulted in the lower stimulation of the *Cyclin D1* and *Axin2* genes by Wnt3a than observed in control shRNA-producing cells. Interestingly, the reduced level of Dazap2 protein partly relieved the Wnt-mediated repression of the *lipocalin 2* (*Lcn2*) gene (Figure 6C). Additionally, we performed qRT–PCR analysis in STF 293 cells transiently transfected with control or *Dazap2* siRNA. As described above, STF 293 cells contain a stably integrated luciferase reporter that is under the control of eight Tcf/Lef-binding sites. This endogenous reporter, which we named *Luciferase* (*LUC*), was activated at the mRNA level up to 13-fold upon stimulation with Wnt3a for 16 h (Figure 7). In agreement with the reporter gene assays, *Dazap2* knockdown resulted in an approximately forty percent reduction in transcription of this gene after treatment with Wnt3a. A similar although less robust decrease in Wnt-activated expression was observed in several other Wnt-signalling target genes including *AXIN2*, *CYCLIN D1*, *naked cuticle homologue 1* (*NKD1*; 53,54) and *tumor necrosis factor receptor superfamily, member 19* [(*TNFRSF19*), known also as *TROY*; (55,56) (Figure 7)]. To clarify the possible mechanism behind Dazap2 function we wanted to perform ChIP analysis. Since we did not succeed to perform ChIP on the promoters of the *Axin2* and *Cyclin D1* genes in any mouse or human cells (including C57MG and STF 293 cells) we extended our analysis to the TCF-responsive enhancers of the *Luciferase*, *NKD1* and *TROY* genes. We did not observe ChIP using our anti-Dazap2 antibody and furthermore, we only detected a limited pull-down of the *Luciferase* transgene (the most extensively up-regulated gene in the assay) by the anti-β-catenin antibody. Instead we used our anti-TCF-4 antibody to immunoprecipitate DNA elements that spanned the promoter regions of the tested genes (Figure 7). Interestingly, reduction of Dazap2 lowered the binding of TCF-4 to the promoters of these Wnt-signalling target genes. To verify the ChIP results, two control experiments were carried out. First, we performed ChIP with a non-specific antibody (rabbit anti-EGFP). Second, we used an anti-TCF-4 antibody in an attempt to immunoprecipitate irrelevant chromosomal DNA that concealed the open reading frames of the *β-ACTIN* or *LUC* genes. In these experiments we never noted any effect of the cellular levels of Dazap2 on the quantity of precipitated DNA (Figure 7 and data not shown). As *Dazap2* knockdown did not alter the amount of TCF-4 and β-catenin in the cell (Figures 5A, 6A and data not shown) these results imply that the Dazap2/TCF-4 interaction might influence the efficiency of TCF-4 binding to the promoters of the genes regulated by the canonical Wnt-signalling pathway.

DISCUSSION

In this report we provide evidence for an association between the nuclear Wnt-signalling pathway effectors, Tcf/Lef proteins, and a small evolutionary conserved protein Dazap2. Dazap2 was isolated in a Y2H screen that utilized the N-terminal part of the TCF-4 factor as bait. Although the Dazap2-interacting domain in TCF-4 is only partially preserved in other Tcf/Lef proteins, co-immunoprecipitation assays carried out in mammalian cells clearly demonstrated that all Tcf/Lef family members bind to Dazap2 with similar affinities (Figure 4B). We further delineated a short region in TCF-4 spanning aa 214–228 as the interaction domain essential for Dazap2 binding (Figure 2A). Interestingly, the homologous region in all Tcfs contains amino acids that are not identical but display similar biochemical properties (Figure 4A). This might indicate a common structural basis for the association of Tcf/Lef proteins with Dazap2.

Dazap2 was originally identified as a transcript expressed in the mouse inner ear with its expression further observed in the embryonic heart and developing and adult mouse brain (31). This report is in stark contrast to our finding that illustrates ubiquitous expression of *Dazap2* mRNA in various mouse tissues (Figure 1C). Nevertheless, our data are in agreement with northern blot analyses that indicate broad expression of the *Dazap2* gene in different human and mouse tissues and cell lines (32–34). The most remarkable feature of Dazap2 is the conservation of its DNA and protein sequence throughout evolution. The identity between human and mouse protein orthologues is virtually 100% (there is only one aa change from 168 aa in total) (Supplementary Figure 1) and human Dazap2 aligns well, especially at the C-terminus, with the putative Dazap2 proteins identified in the invertebrates *Ciona*

intestinalis and *Tribolium castaneum* (Figure 1B). Given that Dazap2 was identified as a binding partner of many cellular proteins (57), the necessity to preserve these interactions might possibly explain the low mutational rate of the Dazap2 sequence throughout evolution. With respect to the high sequence homology of Dazap2 in various species it is rather striking that *Dazap2* mutant mice do not display any remarkable phenotype and are born and bred as their wild-type littermates (31). The *Dazap2*$^{-/-}$ mice were generated from ES cells via gene trap technology. Although we cannot exclude that the modified *Dazap2* locus still produces an intact protein, the insertion site of the reporter gene just several nucleotides downstream of the putative translation start site and a complete absence of *Dazap2* mRNA expression indicate that the mutant animals are really *Dazap2* null. There are two possibilities that might explain an absence of phenotype in *Dazap2*$^{-/-}$ mice. First, the phenotype may be very subtle and/or the mice have to be challenged in some way to display any phenotype and second, there is another *Dazap2* homologue in the mouse genome that can functionally replace the damaged gene. Indeed, a sequence database search in the mouse genome revealed a *Dazap2* pseudogene localized on chromosome 4 and one gene similar to *Dazap2* on chromosome 13. This *Dazap2-like* gene comprises several exons and introns and encodes a putative 168 aa polypeptide that is highly homologous to Dazap2 (Supplementary Figure 6). Therefore, we speculate that these genes are redundant and *Dazap2-like* can compensate for the absence of the *Dazap2* gene. Interestingly, we have not been able to detect the expression of the Dazap2-like product in any of the cell lines tested (data not shown). Thus, to settle this matter definitively, the possible redundancy of these two genes should be tested directly in the *Dazap2* mutant animals. Another noticeable feature of the Dazap2 protein is its subcellular localization. Several authors have used confocal or fluorescent microscopy to visualize ectopically expressed Dazap2 as a wild-type untagged protein or as a variant fused to different tags (mostly N-terminal EGFP). These authors described the subcellular distribution of Dazap2 as diffuse in the cytoplasm and nucleus (32,36), in nuclear puncta (39) or in the nucleus and cytoplasmic SG bodies (38). These experiments were predominantly performed in HeLa cells. Interestingly, we noted in HeLa (and Cos-7) cells that both tagged or untagged Dazap2 principally localizes in the cytoplasm and partly in the nucleus but this distribution can differ in a limited fraction of the cells possibly as a consequence of the cell cycle. Nevertheless, Dazap2 was efficiently translocated to the nuclei (or retained in the nuclei) in cells expressing TCF-4, thus further confirming the interaction between Dazap2 and TCF-4 (Figure 3B).

To assess the biological significance of the association between Dazap2 and Tcfs, we first ectopically expressed Dazap2 together with three different Tcf/β-catenin-responsive reporters in various cells. The cells were further stimulated with purified Wnt3a ligand and the activities of the reporters were determined in lysates. Surprisingly, we never observed changes in the transcriptional activity of the reporters depending on the increased levels of Dazap2. Subsequently, we utilized RNAi technology to test the influence of *Dazap2* knockdown on Wnt-dependent transcription. In cells with reduced levels of *Dazap2* mRNA and protein the activities of the Tcf/β-catenin reporters were significantly decreased and the extent of reduction correlated well with the ability of each particular siRNA to down-regulate *Dazap2* (Figure 5A and B). The observed results were not related to the non-specific 'off-target' effects of the siRNA duplexes used since control non-silencing siRNA did not show any impact on the transcriptional activity of the tested constructs. Additionally, similar effects on Wnt signalling were observed in cells stably expressing *Dazap2* shRNAs (Figure 6C). Importantly, we also demonstrated by qRT–PCR that *Dazap2* knockdown also negatively influenced the transcriptional activation of endogenous Wnt-signalling target genes, although to a lesser extent than observed for the reporter genes (Figures 6C and 7). There are several possibilities that could explain the partial discrepancy between the results obtained from the reporter gene assays and the qRT–PCR analysis of endogenous genes. First, the transcriptional regulation of the reporter genes is less complex than that of the endogenous promoters and possibly more dependent on the activity of the Wnt pathway. Second, in the transient siRNA transfections we noted fast 'exhaustion' of *Dazap2* siRNA followed by rapid return of *Dazap2* mRNA and protein to the original levels (data not shown). This in fact could be responsible for the less pronounced effects of *Dazap2* knockdown especially in experiments where prolonged treatment with *Dazap2* siRNA was needed (Figure 7). Finally, the reporters used in the study encode a 'standard' luciferase protein that is quite stable and accumulates in the cells. This presumably would also explain the differences between luminometric measurements and the qRT–PCR analysis.

A possible explanation for the negative impact of *Dazap2* down-regulation on Wnt-stimulated transcription is that Dazap2 is a stabilizing component of TCF-4/β-catenin heterocomplexes (Figure 2C). To evaluate this possibility we tried to examine whether reduced levels of Dazap2 could disrupt these complexes. However, co-immunoprecipitation experiments from shRNA-producing cells did not reveal any difference in the amounts of β-catenin pulled down by TCF-4 in cells with normal or decreased *Dazap2* expression (data not shown). We also excluded the possibility that Dazap2 is important for the production or stability of TCF-4 or β-catenin which could have accounted for the decrease in transcriptional activation from the reporters as *Dazap2* knockdown did not influence the expression of either of these Wnt-signalling effectors (Figures 5A, 6A and data not shown). The Dazap2 interacting domain in Tcfs partly overlaps with a region that *in vivo* is bound by TLE/Groucho proteins (5,6,8). Therefore, we tested the hypothesis that Dazap2 binding might block the association of Tcfs with these co-repressors and would in turn increase the activating function of the Tcf/Lef transcription factors. We transfected pTOPFLASH into control siRNA- or *Dazap2* siRNA-treated HEK 293 cells together with Grg4, a mouse TLE/Groucho homologue.

The cells were subsequently stimulated with Wnt3a, harvested and reporter activities measured in cell lysates. In a parallel experiment, control siRNA- or *Dazap2* siRNA-treated cells were lipofected with pTOPFLASH and cDNA encoding either a negative regulator of Wnt signalling, nemo-like kinase (NLK) alone or in combination with its upstream activating kinases TAB1 and TAK1. The TAB/TAK/NLK cascade is a downstream component of a negative feed-back loop that is activated by Wnt signalling (58). Active NLK phosphorylates Tcfs and importantly, this phosphorylation prevents the binding of Tcf/β-catenin complexes to DNA and consequently leads to Tcf ubiquitylation and degradation (59–61). Interestingly, the NLK phosphorylation sites in Tcfs are located just proximal to the region indispensable for Dazap2 binding (59). Intriguingly, Winkel and colleagues (62) recently reported that Dazap2 (referred to as PRTB) interacts with TAK1 kinase and enhances its enzymatic activity. Nevertheless, we did not observe any of the repressive effects of Grg4 or NLK on Wnt signalling (using the ectopic or integrated reporter) and thus we did not notice any enhancement of this repression in cells with reduced *Dazap2* expression. Based on these observations we excluded the possibility that Dazap2 functions as a blocker of the negative functions of TLE/Groucho and NLK. Finally, we performed a ChIP experiment utilizing chromatin isolated from STF 293 cells with *DAZAP2* down-regulated. The assay revealed a remarkable decrease in the association of TCF-4 to the Tcf-responsive sites in the promoters of Wnt-signalling target genes (Figure 7). These data imply that the Tcf/Lef interacting partner Dazap2 can modulate *in vivo* the affinity of Tcfs for their recognition motifs. Interestingly, in mouse mammary gland epithelium C57MG cells, decreased levels of Dazap2 partly relieved the repression on the *Lcn2* gene mediated by Wnt3a treatment (Figure 6C). As the repressive effect of active Wnt signalling on *Lcn2* does not depend on the direct binding of Tcf/β-catenin complexes to the *Lcn2* promoter (63), this result suggests that Dazap2 levels might modulate the complex output of the Wnt-signalling pathway. To prove this hypothesis, we tested the expression of genes that respond differentially to the Wnt signal in C57MG cells, *Stromelysin-1* (*Sl-1*/*Mmp3*) and *mesothelin* (*Msln*) (64). However, qRT–PCR analysis revealed that the transcription of these two genes depends on the plating density of cells in culture rather than specifically on Wnt signalling (P.M. and V.K., unpublished data). Nevertheless, preliminary cDNA microarray data obtained from mRNAs isolated from Wnt-stimulated C57MG cells expressing *Dazap2*-specific or control shRNAs indicate that indeed, both the activating and also the inhibitory function of Tcf/Lef proteins might be influenced by the amounts of Dazap2 (P.M., R.I. and V.K., unpublished data).

SUPPLEMENTARY DATA

Supplementary Data are available at NAR Online.

ACKNOWLEDGEMENTS

We thank L. Andera, A. Ben-Ze'ev, F. Costantini, T. Ishitani, Z. Kozmik, M.van Dijk and B. Vogelstein for vectors, plasmid constructs and reporters. We are grateful to J. Nathans, R. Nusse, K. Willert and Q. Xu for cell lines used in the study. We further thank A. Corlett and S. Takacova for critically reading the manuscript.

FUNDING

Grant Agency of the Czech Republic [grant number 204/07/1567]; qChIP/chip06 project from the Ministry of Education, Youth and Sports of the Czech Republic [B06077]; Institutional grant from the Academy of Sciences of the Czech Republic [AV0Z50520514] to the Institute of Molecular Genetics. Funding for open access charge: Grant Agency of the Czech Republic and the Ministry of Education, Youth and Sports of the Czech Republic.

Conflict of interest statement. None declared.

REFERENCES

1. Huang,H. and He,X. (2008) Wnt/beta-catenin signaling: new (and old) players and new insights. *Curr. Opin. Cell Biol.*, **20**, 119–125.
2. Polakis,P. (2007) The many ways of Wnt in cancer. *Curr. Opin. Genet. Dev.*, **17**, 45–51.
3. Reya,T. and Clevers,H. (2005) Wnt signalling in stem cells and cancer. *Nature*, **434**, 843–850.
4. Clevers,H. and van de Wetering,M. (1997) TCF/LEF factor earn their wings. *Trends Genet.*, **13**, 485–489.
5. Roose,J., Molenaar,M., Peterson,J., Hurenkamp,J., Brantjes,H., Moerer,P., van de Wetering,M., Destree,O. and Clevers,H. (1998) The Xenopus Wnt effector XTcf-3 interacts with Groucho-related transcriptional repressors. *Nature*, **395**, 608–612.
6. Brantjes,H., Roose,J., van de Wetering,M. and Clevers,H. (2001) All Tcf HMG box transcription factors interact with Groucho-related co- repressors. *Nucleic Acids Res.*, **29**, 1410–1419.
7. Levanon,D., Goldstein,R.E., Bernstein,Y., Tang,H., Goldenberg,D., Stifani,S., Paroush,Z. and Groner,Y. (1998) Transcriptional repression by AML1 and LEF-1 is mediated by the TLE/Groucho corepressors. *Proc. Natl Acad. Sci. USA*, **95**, 11590–11595.
8. Daniels,D.L. and Weis,W.I. (2005) Beta-catenin directly displaces Groucho/TLE repressors from Tcf/Lef in Wnt-mediated transcription activation. *Nat. Struct. Mol. Biol.*, **12**, 364–371.
9. He,T.C., Sparks,A.B., Rago,C., Hermeking,H., Zawel,L., da Costa,L.T., Morin,P.J., Vogelstein,B. and Kinzler,K.W. (1998) Identification of c-MYC as a target of the APC pathway. *Science*, **281**, 1509–1512.
10. Shtutman,M., Zhurinsky,J., Simcha,I., Albanese,C., D'Amico,M., Pestell,R. and Ben-Ze'ev,A. (1999) The cyclin D1 gene is a target of the beta-catenin/LEF-1 pathway. *Proc. Natl Acad. Sci. USA*, **96**, 5522–5527.
11. Tetsu,O. and McCormick,F. (1999) Beta-catenin regulates expression of cyclin D1 in colon carcinoma cells. *Nature*, **398**, 422–426.
12. Lustig,B., Jerchow,B., Sachs,M., Weiler,S., Pietsch,T., Karsten,U., van de Wetering,M., Clevers,H., Schlag,P.M., Birchmeier,W. *et al.* (2002) Negative feedback loop of Wnt signaling through upregulation of conductin/axin2 in colorectal and liver tumors. *Mol. Cell Biol.*, **22**, 1184–1193.
13. Wielenga,V.J., Smits,R., Korinek,V., Smit,L., Kielman,M., Fodde,R., Clevers,H. and Pals,S.T. (1999) Expression of CD44 in

Apc and Tcf mutant mice implies regulation by the WNT pathway. *Am. J. Pathol.*, **154**, 515–523.
14. Snider,L., Thirlwell,H., Miller,J.R., Moon,R.T., Groudine,M. and Tapscott,S.J. (2001) Inhibition of Tcf3 binding by I-mfa domain proteins. *Mol. Cell Biol.*, **21**, 1866–1873.
15. Ito,K., Lim,A.C., Salto-Tellez,M., Motoda,L., Osato,M., Chuang,L.S., Lee,C.W., Voon,D.C., Koo,J.K., Wang,H. *et al.* (2008) RUNX3 attenuates beta-catenin/T cell factors in intestinal tumorigenesis. *Cancer Cell*, **14**, 226–237.
16. Korinek,V., Barker,N., Moerer,P., van Donselaar,E., Huls,G., Peters,P.J. and Clevers,H. (1998) Depletion of epithelial stem-cell compartments in the small intestine of mice lacking Tcf-4. *Nat. Genet.*, **19**, 379–383.
17. Nguyen,H., Rendl,M. and Fuchs,E. (2006) Tcf3 governs stem cell features and represses cell fate determination in skin. *Cell*, **127**, 171–183.
18. van Genderen,C., Okamura,R.M., Farinas,I., Quo,R.G., Parslow,T.G., Bruhn,L. and Grosschedl,R. (1994) Development of several organs that require inductive epithelial- mesenchymal interactions is impaired in LEF-1-deficient mice. *Genes Dev.*, **8**, 2691–2703.
19. Verbeek,S., Izon,D., Hofhuis,F., Robanus-Maandag,E., te Riele,H., van de Wetering,M., Oosterwegel,M., Wilson,A., MacDonald,H.R. and Clevers,H. (1995) An HMG-box-containing T-cell factor required for thymocyte differentiation. *Nature*, **374**, 70–74.
20. Bruhn,L., Munnerlyn,A. and Grosschedl,R. (1997) ALY, a context-dependent coactivator of LEF-1 and AML-1, is required for TCRalpha enhancer function. *Genes Dev.*, **11**, 640–653.
21. Yasumoto,K., Takeda,K., Saito,H., Watanabe,K., Takahashi,K. and Shibahara,S. (2002) Microphthalmia-associated transcription factor interacts with LEF-1, a mediator of Wnt signaling. *EMBO J.*, **21**, 2703–2714.
22. Sachdev,S., Bruhn,L., Sieber,H., Pichler,A., Melchior,F. and Grosschedl,R. (2001) PIASy, a nuclear matrix-associated SUMO E3 ligase, represses LEF1 activity by sequestration into nuclear bodies. *Genes Dev.*, **15**, 3088–3103.
23. Yamamoto,H., Ihara,M., Matsuura,Y. and Kikuchi,A. (2003) Sumoylation is involved in beta-catenin-dependent activation of Tcf-4. *EMBO J.*, **22**, 2047–2059.
24. Brannon,M., Gomperts,M., Sumoy,L., Moon,R.T. and Kimelman,D. (1997) A beta-catenin/XTcf-3 complex binds to the siamois promoter to regulate dorsal axis specification in Xenopus. *Genes Dev.*, **11**, 2359–2370.
25. Cuilliere-Dartigues,P., El-Bchiri,J., Krimi,A., Buhard,O., Fontanges,P., Flejou,J.F., Hamelin,R. and Duval,A. (2006) TCF-4 isoforms absent in TCF-4 mutated MSI-H colorectal cancer cells colocalize with nuclear CtBP and repress TCF-4-mediated transcription. *Oncogene*, **25**, 4441–4448.
26. Valenta,T., Lukas,J. and Korinek,V. (2003) HMG box transcription factor TCF-4's interaction with CtBP1 controls the expression of the Wnt target Axin2/Conductin in human embryonic kidney cells. *Nucleic Acids Res.*, **31**, 2369–2380.
27. Valenta,T., Lukas,J., Doubravska,L., Fafilek,B. and Korinek,V. (2006) HIC1 attenuates Wnt signaling by recruitment of TCF-4 and beta-catenin to the nuclear bodies. *EMBO J.*, **25**, 2326–2337.
28. Hecht,A. and Stemmler,M.P. (2003) Identification of a promoter-specific transcriptional activation domain at the C terminus of the Wnt effector protein T-cell factor 4. *J. Biol. Chem.*, **278**, 3776–3785.
29. Arce,L., Yokoyama,N.N. and Waterman,M.L. (2006) Diversity of LEF/TCF action in development and disease. *Oncogene*, **25**, 7492–7504.
30. Ghogomu,S.M., van Venrooy,S., Ritthaler,M., Wedlich,D. and Gradl,D. (2006) HIC-5 is a novel repressor of lymphoid enhancer factor/T-cell factor-driven transcription. *J. Biol. Chem.*, **281**, 1755–1764.
31. Yang,W. and Mansour,S.L. (1999) Expression and genetic analysis of prtb, a gene that encodes a highly conserved proline-rich protein expressed in the brain. *Dev. Dyn.*, **215**, 108–116.
32. Shi,Y., Luo,S., Peng,J., Huang,C., Tan,D. and Hu,W. (2004) The structure, expression and function prediction of DAZAP2, a down-regulated gene in multiple myeloma. *Genomics Proteomics Bioinformatics*, **2**, 47–54.
33. Cohen-Barak,O., Yi,Z., Hagiwara,N., Monzen,K., Komuro,I. and Brilliant,M.H. (2003) Sox6 regulation of cardiac myocyte development. *Nucleic Acids Res.*, **31**, 5941–5948.
34. Sommerfeldt,D.W., Zhi,J., Rubin,C.T. and Hadjiargyrou,M. (2002) Proline-rich transcript of the brain (prtb) is a serum-responsive gene in osteoblasts and upregulated during adhesion. *J. Cell Biochem.*, **84**, 301–308.
35. Tsui,S., Dai,T., Roettger,S., Schempp,W., Salido,E.C. and Yen,P.H. (2000) Identification of two novel proteins that interact with germ-cell-specific RNA-binding proteins DAZ and DAZL1. *Genomics*, **65**, 266–273.
36. Shi,Y.W., Shen,R., Ren,W., Tang,L.J., Tan,D.R. and Hu,W.X. (2007) Molecular features and expression of DAZAP2 in human multiple myeloma. *Chin. Med. J.*, **120**, 1659–1665.
37. Warskulat,U., Kreuels,S., Muller,H.W. and Haussinger,D. (2001) Identification of osmosensitive and ammonia-regulated genes in rat astrocytes by Northern blotting and differential display reverse transcriptase-polymerase chain reaction. *J. Hepatol.*, **35**, 358–366.
38. Kim,J.E., Ryu,I., Kim,W.J., Song,O.K., Ryu,J., Kwon,M.Y., Kim,J.H. and Jang,S.K. (2008) Proline-rich transcript in brain protein induces stress granule formation. *Mol. Cell Biol.*, **28**, 803–813.
39. Hamilton,M.H., Tcherepanova,I., Huibregtse,J.M. and McDonnell,D.P. (2001) Nuclear import/export of hRPF1/Nedd4 regulates the ubiquitin-dependent degradation of its nuclear substrates. *J. Biol. Chem.*, **276**, 26324–26331.
40. Korinek,V., Barker,N., Morin,P.J., van Wichen,D., de Weger,R., Kinzler,K.W., Vogelstein,B. and Clevers,H. (1997) Constitutive transcriptional activation by a beta-catenin-Tcf complex in APC-/- colon carcinoma. *Science*, **275**, 1784–1787.
41. van de Wetering,M., Oosterwegel,M., Dooijes,D. and Clevers,H. (1991) Identification and cloning of TCF-1, a T lymphocyte-specific transcription factor containing a sequence-specific HMG box. *EMBO J.*, **10**, 123–132.
42. Xu,Q., Wang,Y., Dabdoub,A., Smallwood,P.M., Williams,J., Woods,C., Kelley,M.W., Jiang,L., Tasman,W., Zhang,K. *et al.* (2004) Vascular development in the retina and inner ear: control by Norrin and Frizzled-4, a high-affinity ligand-receptor pair. *Cell*, **116**, 883–895.
43. Bar-Peled,M. and Raikhel,N.V. (1996) A method for isolation and purification of specific antibodies to a protein fused to the GST. *Anal. Biochem.*, **241**, 140–142.
44. Vandesompele,J., De Preter,K., Pattyn,F., Poppe,B., Van Roy,N., De Paepe,A. and Speleman,F. (2002) Accurate normalization of real-time quantitative RT-PCR data by geometric averaging of multiple internal control genes. *Genome Biol.*, **3**, 1–12.
45. Korinek,V., Barker,N., Morin,P.J., van Wichen,D., de Weger,R., Kinzler,K.W., Vogelstein,B. and Clevers,H. (1997) Constitutive transcriptional activation by a beta-catenin-Tcf complex in APC-/- colon carcinoma [see comments]. *Science*, **275**, 1784–1787.
46. Jho,E.H., Zhang,T., Domon,C., Joo,C.K., Freund,J.N. and Costantini,F. (2002) Wnt/beta-catenin/Tcf signaling induces the transcription of Axin2, a negative regulator of the signaling pathway. *Mol. Cell Biol.*, **22**, 1172–1183.
47. Kaykas,A. and Moon,R.T. (2004) A plasmid-based system for expressing small interfering RNA libraries in mammalian cells. *BMC Cell Biol.*, **5**, 16.
48. Kirmizis,A., Bartley,S.M., Kuzmichev,A., Margueron,R., Reinberg,D., Green,R. and Farnham,P.J. (2004) Silencing of human polycomb target genes is associated with methylation of histone H3 Lys 27. *Genes Dev.*, **18**, 1592–1605.
49. Molenaar,M., van de Wetering,M., Oosterwegel,M., Peterson-Maduro,J., Godsave,S., Korinek,V., Roose,J., Destree,O. and Clevers,H. (1996) XTcf-3 transcription factor mediates beta-catenin-induced axis formation in Xenopus embryos. *Cell*, **86**, 391–399.
50. Gradl,D., Konig,A. and Wedlich,D. (2002) Functional diversity of Xenopus lymphoid enhancer factor/T-cell factor transcription factors relies on combinations of activating and repressing elements. *J. Biol. Chem.*, **277**, 14159–14171.
51. Pukrop,T., Gradl,D., Henningfeld,K.A., Knochel,W., Wedlich,D. and Kuhl,M. (2001) Identification of two regulatory elements within the high mobility group box transcription factor XTCF-4. *J. Biol. Chem.*, **276**, 8968–8978.

52. Van de Wetering,M., Castrop,J., Korinek,V. and Clevers,H. (1996) Extensive alternative splicing and dual promoter usage generate Tcf-1 protein isoforms with differential transcription control properties. *Mol. Cell Biol.*, **16**, 745–752.
53. Koch,A., Waha,A., Hartmann,W., Hrychyk,A., Schuller,U., Wharton,K.A. Jr, Fuchs,S.Y., von Schweinitz,D. and Pietsch,T. (2005) Elevated expression of Wnt antagonists is a common event in hepatoblastomas. *Clin Cancer Res.*, **11**, 4295–4304.
54. Zhang,S., Cagatay,T., Amanai,M., Zhang,M., Kline,J., Castrillon,D.H., Ashfaq,R., Oz,O.K. and Wharton,K.A. Jr (2007) Viable mice with compound mutations in the Wnt/Dvl pathway antagonists nkd1 and nkd2. *Mol. Cell Biol.*, **27**, 4454–4464.
55. Buttitta,L., Tanaka,T.S., Chen,A.E., Ko,M.S. and Fan,C.M. (2003) Microarray analysis of somitogenesis reveals novel targets of different WNT signaling pathways in the somitic mesoderm. *Dev. Biol.*, **258**, 91–104.
56. Phesse,T.J., Parry,L., Reed,K.R., Ewan,K.B., Dale,T.C., Sansom,O.J. and Clarke,A.R. (2008) Deficiency of Mbd2 attenuates Wnt signaling. *Mol. Cell Biol.*, **28**, 6094–6103.
57. Rual,J.F., Venkatesan,K., Hao,T., Hirozane-Kishikawa,T., Dricot,A., Li,N., Berriz,G.F., Gibbons,F.D., Dreze,M., Ayivi-Guedehoussou,N. *et al.* (2005) Towards a proteome-scale map of the human protein-protein interaction network. *Nature*, **437**, 1173–1178.
58. Smit,L., Baas,A., Kuipers,J., Korswagen,H., van de Wetering,M. and Clevers,H. (2004) Wnt activates the Tak1/Nemo-like kinase pathway. *J. Biol. Chem.*, **279**, 17232–17240.
59. Ishitani,T., Ninomiya-Tsuji,J. and Matsumoto,K. (2003) Regulation of lymphoid enhancer factor 1/T-cell factor by mitogen-activated protein kinase-related Nemo-like kinase-dependent phosphorylation in Wnt/beta-catenin signaling. *Mol. Cell Biol.*, **23**, 1379–1389.
60. Ishitani,T., Ninomiya-Tsuji,J., Nagai,S., Nishita,M., Meneghini,M., Barker,N., Waterman,M., Bowerman,B., Clevers,H., Shibuya,H. *et al.* (1999) The TAK1-NLK-MAPK-related pathway antagonizes signalling between beta- catenin and transcription factor TCF. *Nature*, **399**, 798–802.
61. Yamada,M., Ohnishi,J., Ohkawara,B., Iemura,S., Satoh,K., Hyodo-Miura,J., Kawachi,K., Natsume,T. and Shibuya,H. (2006) NARF, an nemo-like kinase (NLK)-associated ring finger protein regulates the ubiquitylation and degradation of T cell factor/lymphoid enhancer factor (TCF/LEF). *J. Biol. Chem.*, **281**, 20749–20760.
62. Winkel,A., Stricker,S., Tylzanowski,P., Seiffart,V., Mundlos,S., Gross,G. and Hoffmann,A. (2008) Wnt-ligand-dependent interaction of TAK1 (TGF-beta-activated kinase-1) with the receptor tyrosine kinase Ror2 modulates canonical Wnt-signalling. *Cell Signal.*, **20**, 2134–2144.
63. Ziegler,S., Rohrs,S., Tickenbrock,L., Langerak,A., Chu,S.T., Feldmann,I., Jakubowski,N. and Muller,O. (2007) Lipocalin 24p3 is regulated by the Wnt pathway independent of regulation by iron. *Cancer Genet. Cytogenet.*, **174**, 16–23.
64. Prieve,M.G. and Moon,R.T. (2003) Stromelysin-1 and mesothelin are differentially regulated by Wnt-5a and Wnt-1 in C57mg mouse mammary epithelial cells. *BMC Dev. Biol.*, **3**, 1–10.

Supplementary data

Supplementary Materials and Methods

Coimmunoprecipitation and western blotting

To obtain whole cell lysates, human or mouse cells were incubated in lysis buffer [50 mM Tris, pH 7.8, 400 mM NaCl, 0.5% (v/v) Triton X-100] supplemented with Complete (EDTA free) protease inhibitor cocktail (Roche) for 30 min at 4°C (rotating platform). The lysates were cleared by centrifugation (14 000 x g, 15 min, 4°C) and used for coimmunoprecipitation with an appropriate antibody coupled to protein A/G Sepharose beads (Amersham Pharmacia Biotech). For one assay 20-30 micro litres of beads loaded with 1 μg of purified (on protein A Sepharose) monoclonal antibody were used; alternatively, beads were loaded with 10 μl of unpurified antiserum. After elution (SDS sample buffer) the precipitates were separated by SDS PAGE and transferred onto polyvinylidene fluoride membranes (Millipore). The membranes were blocked with 5% (w/v) non-fat milk in PBS containing 0.05% (v/v) Tween-20 (Sigma) and incubated with specific primary antibodies at a final concentration of 1 μg/ml (the unpurified chicken anti-Dazap2 antiserum was diluted 500 times). After several washes with PBS/Tween the blots were incubated with the appropriate peroxidase-conjugated anti-rabbit (BioRad), anti-mouse (BioRad) or anti-chicken secondary antibodies (Sigma) diluted according to the manufacturer's recommendation. The proteins were visualised with an enhanced chemiluminescence system (Pierce).

qRT-PCR analysis

Primers for the following human and mouse genes were used (first primer is derived from the plus and the second primer from the minus DNA strand): human *AXIN2* (*hAXIN2*), 5'-TGA GGT CCA CGG AAA CTG TTG ACA GT-3', 5'-CCC TCC CGC GAA TTG AGT GTG A-3'; mouse *Axin2* (*mAxin2*), 5'-TAG GCG GAA TGA AGA TGG AC-3', 5'-CTG GTC ACC CAA CAA GGA GT-3'; *hCYCLIN D1*, 5'-CCA TCC AGT GGAGGT TTG TC-3', 5'-AGC GTA TCG TAG GAG TGG GA-3'; *mCyclin D1*, 5'-AGT GCG TGC AGA AGG AGA TT-3', 5'-CTC TTC GCA CTT CTG CTC CT-3'; *Dazap2* (priming on both human and mouse cDNAs), 5'-ACC CTA TAC CGA TGC TCC AC-3', 5'-CAG AGA GGC TCC AGG AAA TG-3'; *hTROY*, 5'-CTA TGG GGA GGA TGC ACA GT-3', 5'-TCT CCA CAA GGC ACA CAC TC-3'; *hNKD1*, 5'-CGC CGG GAT AGA AAA CTA CA-3', 5'-GCA TTG AGC TGA

CAC GAA AA-3'; *mLcn2*, 5'-GCC CAG GAC TCA ACT CAG AA-3', 5'-GAC CAG GAT GGA GGT GAC AT-3'; *firefly luciferase* (*LUC*), 5'-TCA AAG AGG CGA ACT GTG TG-3', 5'-CGC TTC CGG ATT GTT TAC AT-3'; *hβ-ACTIN*, 5'-ATG GCC ACG GCT GCT TCC AGC-3', 5'-GGG TGT AAC GCA ACT AAG TCA T-3'; *mβ-Actin*, 5'-GAT CTG GCA CCA CAC CTT CT-3', 5'-GGG GTG TTG AAG GTC TCA AA-3'; *hUBIQUITIN C* (*UBC*), 5'-GCT TTG TTG GGT GAG CTT GT-3', 5'-TCA CGA AGA TCT GCA TTT TGA-3'; *mUbc* (*Ubc*), 5'-ATG TGA AGG CCA AGA TCC AG-3', 5'-TAA TAG CCA CCC CTC AGA CG-3'.

Primers for ChIP

Primers derived from the Tcf/Lef-dependent enhancer of the integrated pSuperTOPFLASH reporter [designed as the *Luciferase* gene (*LUC*)], sense: 5'-AGT GCA GGT GCC AGA ACA TT-3' and reverse 5'-AAC AGT ACC GGA ATG CCA AG-3'; control region downstream this enhancer (*CTRL1*), sense: 5'-ATC CAT CTT GCT CCA ACA CC-3' and reverse 5'-TCG CGG TTG TTA CTT GAC TG-3'; *NKD1* promoter, 5'-GAC CTC CCC AGA CAA AAC AA-3', 5'-TCA GCC AGT CTC TGG GAT CT-3'; *TROY*, 5'-TTT CAT CTC CCT GCT CGT CT-3', 5'-TGC GAA AAA TGC AGT GAA AG-3'; *β*-ACTIN (open reading frame), 5'-ATG GCC ACG GCT GCT TCC AGC-3', 5'-GGG TGT AAC GCA ACT AAG TCA T-3'.

Supplementary Figure Legends

Supplementary Figure 1 Evolutionary conservation of the vertebrate Dazap2 proteins

Protein sequences were aligned using the ClustalV program. The amino acid residues that differ from the "consensus" (defined by at least three proteins species matching for a given position) are boxed. GenBank accession numbers: *Homo sapiens*, NP_055579; *Mus musculus*, NP_036003; *Danio rerio*, NP_956087; *Xenopus laevis*, NP_001086003; *Tribolium castaneum*, XP_973572; *Ciona intestinalis*, NM_001032667. The sequence of chicken (*Gallus gallus*) Dazap2 was assembled from three independent ESTs: BB630813, BY097208, CJ065215.

Supplementary Figure 2 The truncation of Dazap2 disrupts its binding to TCF-4

The pull-down assay results between the bacterially expressed GST fusion TCF-4 N-terminus and different variants of the *in vitro* translated [^{35}S]-labelled Dazap2 protein. Ten percent of the total reaction was loaded in the lane denoted "Input". A Coomassie Blue-stained gel under the autoradiograph shows the amount of GST-tagged TCF-4 protein and GST (control) used in the individual pull-downs. The putative intact form of the fusion protein is labelled by an asterisk; the faster migrating bands result from a partial degradation of the recombinant polypeptide. Molecular weight markers in kDa are indicated on the left.

Supplementary Figure 3 Association of Dazap2 with β-catenin is indirect and mediated by TCF-4

Dazap2, the full-length TCF-4 protein and its truncated variant lacking the main β-catenin interaction domain (TCF-ΔN; used as a negative control) were produced *in vitro* using the Quick TNT Coupled Reticulocyte System (Promega). Two separate TNT reactions were set up to produce both [^{35}S]-labelled (total volume 10 μl) and non-labelled TCF-4 (50 μl) proteins. One half (5 μl) of the labelling reaction was mixed with corresponding non-labelled protein and pre-incubated with GST-β-catenin bound to Glutathione Sepharose 4 for 1 hour at 4°C. The excess of the unbound TCF-4 proteins was washed off three times with GST binding buffer. Then, [^{35}S]-labelled Dazap2 was added to the mixture and incubated for 1 hour at 4°C. The beads were collected by centrifugation and washed three times in GST binding buffer. Bound proteins were eluted, separated by SDS-PAGE and analysed by autoradiography. Both autoradiograph (top) and Coomassie-stained gel (bottom) are shown. In the lane denoted "Input" one tenth of *in vitro* produced Dazap2 was loaded. To estimate the translational efficiency of the individual TCF-4 constructs, a second half of the reaction containing labelled TCF-4 polypeptide was loaded in the line denoted "Transl". Note that Dazap2 was specifically retained on GST-β-catenin only when the latter was preincubated with the full-length TCF-4 protein. On the contrary, Dazap2 was not detectable when incubated with GST-β-catenin-bound beads either alone or in combination with the N-terminally truncated TCF-4 variant.

Supplementary Figure 4 The TCF-4 protein is produced in mammalian cells in two different forms

Results of western blotting of the cell extracts prepared from DLD-1 cells stably transduced with lentiviral vectors expressing either *TCF-4* or a control non-silencing shRNA (purchased

from Open Biosystems). The blots were probed with the anti-TCF-4 and anti-α-tubulin (a loading control) monoclonal antibody. Molecular weight markers in kDa are indicated on the left.

Supplementary Figure 5 The TCF-4 protein lacking exon VIII retains its ability to bind Dazap2

Left, pull-down assays between [^{35}S]-labelled Dazap2 and the GST fusion proteins containing the complete TCF-4 N-terminal part (GST-TCF-4-N-term; aa 1-333) or its variant lacking the amino acids encoded by exon VIII (GST-TCF-4-N-term Δ exon VIII). Ten percent of the total reaction was loaded in the lane denoted "Input". A Coomassie Blue-stained gel under the autoradiograph shows the amount of the GST-tagged TCF-4 protein used in the experiment; the putative intact forms of the recombinant proteins are labelled by asterisks. (**B**) Co-immunoprecipitation of FLAG-tagged Dazap2 and MYC-tagged TCF-4 full-length (MYC-TCF-4) or a variant lacking the amino acids encoded by exon VIII (MYC-TCF-4 Δ exon VIII). Cell lysates prepared from HEK 293 cells transfected with constructs as indicated were precipitated using anti-MYC and anti-FLAG monoclonal antibodies. In lanes denoted "Input", ten percent of the total lysate used for one immunoprecipitation were loaded; IP, immunoprecipitation; IB, immunoblotting.

Supplementary Figure 6 The mouse genome contains two homologous Dazap2 proteins

Alignment of Dazap2 (NP_036003) derived from the gene on chromosome 15 with the putative Dazap2-like protein (XP_001473666) encoded on chromosome 13. The sequences were aligned using the ClustalV program. The amino acid residues that differ are boxed.

Supplementary Figure 1

```
HUMAN     MNSKGQYPTQPTYPVQPPGNP-VYPQTLHLP-QAPPYTDAPPAYSELYRP  48
MOUSE     MNSKGQYPTQPTYPVQPPGNP-VYPQTLHLP-QAPPYTDAPPAYSELYRP  48
CHICKEN   MNGKGQYPTQPPYPVQSAANPPVYPQTVPLP-QPPPYTDAPPAYSELYRP  49
XENOPUS   MNNKGQYPSAPAYPTQAPNSQSVYPPTMHLP-QAPSYTDAPPAYSELYRA  49
DANIO     MNNKGSYPQQAVYPQQSTA--PVYPPAMQVPAQVSQYPDAPPPYSEVYQP  48

HUMAN     SFV--HPGAATVPTMSAAFPGASLYLPM-AQSVAVGPLGSTIPMAYYPVG  95
MOUSE     SFV--HPGAATVPTMSAAFPGASLYLPM-AQSVAVGPLGSTIPMAYYPVG  95
CHICKEN   SFV--PLGAATVPTMSAAYPGASVFLPV-AQSVAVGPIGSSVPMAYYPVG  96
XENOPUS   AYM--QQAAANMSALSAHYPSTSMYLPM-AQPMQVAQMSSQVPMAYYPIG  96
DANIO     RYMAPPPAPGQMPQMTSAYPGTQMYMPMHAQTVPMGAMASSVPMAYYPMG  98

HUMAN     PIYPPGSTVLVEGGYDAGARFGAGATAGNIPPPPPGCPPNAAQLAVMQGA  145
MOUSE     PIYPPGSAVLVEGGYDAGARFGAGATAGNIPPPPPGCPPNAAQLAVMQGA  145
CHICKEN   PVYPPGSTVLVEGGFDAGARFGAGGTAS-IPPPPPGCPPNAAQLAVMQGA  145
XENOPUS   PVYPPGSTVLVDGGYDAGARFGVGNSPS-VPPPPTGCPPNAAQLAAMQGA  145
DANIO     PVYPPGSTVMVDGGFDAGARFGPG-TGSSIPPPPPGHLPNAAQMAAMQGA  147

HUMAN     NVLVTQRKGNFFMGGSDGGYTIW                             168
MOUSE     NVLVTQRKGNFFMGGSDGGYTIW                             168
CHICKEN   NVLVTQRKGNFFLGGSDGGYTI                              167
XENOPUS   NVLVTQRKGNYFMGGSDGGYTIW                             168
DANIO     NVVMTQRKGNFFMGGSSGGYTIW                             170
```

Supplementary Figure 2

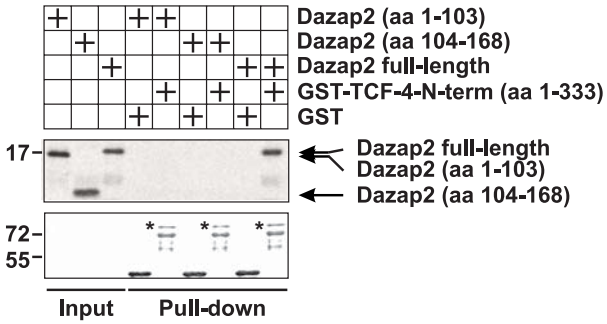

Supplementary Figure 3

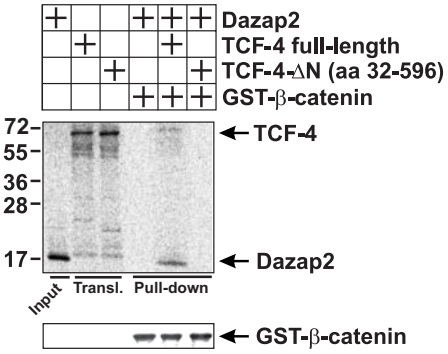

Supplementary Figure 4

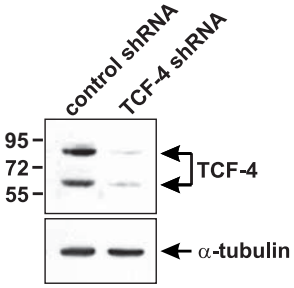

Supplementary Figure 5

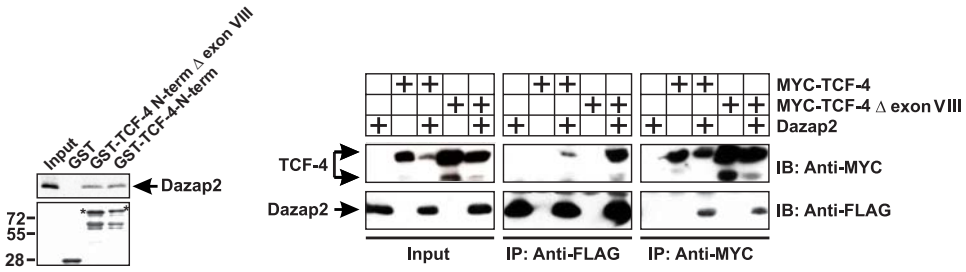

Supplementary Figure 6

```
Dazap2       MNSKG-QYPTQPTYPVQPPGNPVYPQTLHLPQAPPYTDAPPAYSELYRPS  49
Dazap2- like MNSKGGQYPTQPTYPVQPPGNPVYPQTLHLPQAPPYTDAPPAYSELYRPS  50

Dazap2       FVHPGAATVPTMSAAFPGASLYLPMAQSVAVGPLGSTIPMAYYPVGPIYP  99
Dazap2-like  FVHPGAATVPTMSAAFPGASLYLPMAQSVAVGPLGSTIPMAYYAVGPNYS 100

Dazap2       PGSAVLVEGGYDAGARFGAGATAGNIPPPPPGCPPNAAQLAVMQGANVLV 149
Dazap2-like  PGSAVLVEGGHDAGARFGAGATAGNIPPPPPGCPPNTAQLAVMQGANVPV 150

Dazap2       TQRKGNFFMGGSDGGYTIW                                 168
Dazap2-like  TQLKGNFFMGGT-GGYTMW                                 168
```

Discussion

The thesis presents several diverse ways of the Wnt pathway modulation. One of the modulations described in the first publication is represented by a molecule of TROY, a member of the tumor necrosis factor receptor family. We found *TROY* is a target gene of the Wnt pathway and it is expressed in human colorectal cancer cells and in mouse tumors. Previously, *Troy* has been detected as a Wnt/β-catenin target gene by microarray profiling but no data suggested TROY role in Wnt signaling regulation[249, 261]. Moreover, we detected *Troy* transcripts in fast-cycling $Lrg5^+$ stem cells, whereas originally Troy expression was confined to the adult central nervous system, the developing hair follicle and embryonic skin[268]. Interestingly, elevated expression of *Troy* was detected only in all tested types of mouse intestinal tumors but we did not detect increased *TROY* expression in human sporadic colorectal cancer. Moreover, TROY expression in 35 premalignant polyps of human colon was even lower than in healthy tissue. We tested whether the downregulation of *TROY* expression could be explained by promoter methylation but we did not find any significant increase in CpG dinucleotide methylations in any of the tested samples. Therefore, we concluded that *TROY* expression in heterogeneous samples of human colorectal cancer is probably regulated by complex mechanism which does not include transcriptional silencing promoted by methylation. Repression of TROY expression by CCAAT-enhancer-binding proteins (C/EBPs) α and δ has been already described[269]. Moreover, *TROY* promoter contains c-JUN, GATA-1 and OCT-1 binding sites. This suggests that *TROY* expression may be attenuated by those factors, which were shown previously to repress transcription[270-272].

Since expression of both genes, *Lgr5* and *Troy*, is confined to one type of ISCs and is regulated by Wnt signaling and Ascl2[247], it is strange that only *LGR5* expression was related to prognosis prediction in colorectal cancer patients[273]. Yet, prognostic significance of LGR5 expression in these malignancies is controversial[274]. In addition, LGR5, has been proposed as a marker of colorectal cancer stem cells[260] and glioblastoma[275]. TROY has been also pronounced as a marker of glioblastoma[276], suggesting there might be a link between *TROY* and *LGR5* expression also in cancerous tissues. Our analysis failed to reveal any significant correlation between *LGR5* expression and tumor stage/patient prognosis. Therefore, it is possible that our library of human colorectal tumors was too small to reveal any correlation. Nevertheless, decreased expression of *TROY* in non-malignant intestinal polyps might have some significance since decreased expression of Wnt target genes, as those which are known negative regulators of the pathway like AXIN2 and APCDD1, have been related to poor prognosis[277].

TROY was described as an interacting partner for Nogo-66 receptor 1 (NgR1) and such as a coactivator of RhoA signaling[278]. Moreover, in glial tumor or HEK293 cells, TROY participates in the Rac1 and JNK pathways, respectively[276, 279].Recently, a study of Hashimoto and colleagues revealed that the cytokine lymphotoxin-α (LTα) binds to Troy and triggers NFκB signaling[280].

However, we have failed to repeat these experiments. Instead, we followed the study defining TROY as an interacting partner to NgR1. Since LGR5 belongs to the same protein family as NgR1, we tested the hypothesis that TROY might interact with LGR5 as well. We found TROY interacts with LGR5 and inhibits canonical Wnt signaling, although the mechanism of TROY action is uncertain. Recently, LGR-interacting zinc and ring finger (ZNRF) 3 and ring finger (RNF) 43 transmembrane ubiquitin ligases were identified as negative regulators of Wnt signaling[281, 282]. These related proteins decrease the stability of the Wnt receptor Fz through ubiquitin-mediated degradation. TROY has been found to interact with tumor necrosis factor receptor associated factor (TRAF) 6[283, 284], an E3 ubiquitin ligase otherwise involved in the NFκB signaling[285]. It is thus possible, that mechanism of TROY action involves ubiquitination mediated by TRAF6, although this hypothesis requires further testing.

Strikingly, Troy deficient mice display relatively subtle and survival-compatible phenotype[280, 286] which would argue for Troy redundancy. Partial redundancy between Troy and homologous protein Edar has already been suggested[268]. However, Edar expression was not observed in CBC cells (unpublished data), which rules out the possible Wnt-related role of Edar in the gut. It is thus more likely that lack of Troy, at least in the gut of *Troy*$^{-/-}$ mice, is not compensated by a single molecule but rather by some unknown signaling mechanism. This regulation is probably somehow eliminated in crypts grown outside the intestinal mesenchyme, i.e. in the case of organoid culture. This may explain why Troy deficiency was manifested only in the organoid culture.

The aim of the second study was to define the relationship between post-translational modification and the signaling activities of Wnt proteins. We demonstrated that for Wnt activity in mammalian cells, the acylation is absolutely essential contrary to glycosylation, which is not absolutely required. These results are in concordance with previous observations that Wnt glycosylation is dispensable for its function[27, 28]. Moreover, our data suggest that N-glycosylation precedes and conditions Wnts for efficient acylation because N-glycosylation-deficient Wnts displayed apparently reduced acyl content. Additionally, our experiments revealed differences in autocrine stimulation induced by glycosylation deficient Wnt1 and Wnt3a. Whereas signaling mediated by sugar-deficient Wnt3a was impaired, as compared to wild-type protein, Wnt1 without sugar modification was able to signal as wild-type Wnt1. Because both ligands were tested in the same cell line, Wnt signal was perceived by the same set of receptors. Thus, N-glycosylation may determine the affinity of Wnt ligands for various Fz receptors.

Acylation of Wnt molecules was initially described for mouse Wnt3a, which is modified on two residues: a conserved cysteine residue labeled with palmitic acid via a thioester[19] and a conserved serine residue linked via an oxyester to a palmitoleic acid[262]. Our data not only confirmed these findings but further enhance them by revealing that palmitoleoylation on serine occurs first followed by cysteine palmitoylation. However, in contrast to previous study[262], our

results demonstrate that for intracellular transport to the cellular surface, fatty acid modification is not essential. The discrepancy can be explained by technical differences between assays – whereas the other group did not observe Wnt3a with mutated serine in cell conditioned media and detected retained overexpressed protein in the endoplasmatic reticulum, we search specifically for a presence of Wnt proteins at the cellular surface. Concerning the function of the cysteine palmitoylation, our observations support recent finding, which suggested that palmitate moiety mediates interaction of Wnt with lipoprotein particles and thus release of Wnt3a to culture media[287]. As for the serine palmitoleoylation, recently published report revealing crystal structure of Xenopus Wnt8 in complex with a Fz CRD firmly confirmed the necessity of this modification for Wnt-Fz interaction[26]. However, the same study also showed that only the conserved serine residue is lipidated. This result disclose obvious dissimilarity between various Wnts, suggesting that knowledge of structure of one ligand/receptor complex, although highly valuable, cannot fully cover the complexity of Wnt ligands. Just to illustrate the complexity of Wnt ligand family, Wnt5a and Wnt11 are intracellularly formed into a hetero-oligomer, which showed higher signaling activity than either individual Wnt and was required for Xenopus axis formation[288].

The third publication documents generation of two modified alleles of mouse tumor suppressor gene *Hic1*. The work was based on a previous result of our laboratory which revealed a crosstalk of HIC1 and the canonical Wnt signaling pathway[191]. We have found that HIC1 physically interacts with the TCF4/β-catenin complex and restrain these proteins from the Wnt-responsive promoters and thus attenuates Wnt signaling output[191]. Efficient sequestration of TCF4 and β-catenin to HIC1 bodies is dependent on TCF4 interacting protein CtBP1 and the intact BTB/POZ oligomerization domain of HIC1[191]. Moreover, HIC1 also interacts with some other proteins of the Wnt signaling cascade like APC and likely Dvl3 (unpublished data).

Since $Hic1^{-/-}$ mice are embryonically lethal, we generated conditional *Hic1* allele to study role of Hic1 in canonical Wnt signaling *in vivo*. Recent publication reporting genetic interaction between *Hic1* and the Wnt pathway in the intestinal tumors later justified our approach[289]. The study describes accelerated formation of the gastrointestinal tumors in $Apc^{+/\Delta 716}Hic1^{+/-}$ double heterozygote mice which carry a truncating mutation (Δ716) in one allele of the *Apc* gene and one null allele of *Hic1*. Additionally, the absence of Hic1 protein in tumor tissue was accompanied by the increased expression of genes which are directly repressed by Hic1 and which are known to promote tumorigenesis e.g. *Sirt1* and *Sox9*[289].

With use of these generated mice strains, we confirmed synergistic effect of *Hic1* with *Apc* in prevention of colorectal carcinogenesis (unpublished results). Mice with conditionally deleted *Hic1* together with mutant *Apc* developed bigger intestinal tumors than mice with only mutated *Apc*. Moreover, *Hic1* deficient intestinal epithelia displayed elevated expression of Wnt target genes *Lgr5*, *Ascl2*, and *Sp5* (unpublished results). These data indicate that Hic1 may directly attenuate Wnt signaling in the intestinal epithelium and intestinal tumors which potentially

confirms the previously obtained *in vitro* data[191]. Other unpublished results indicate that short term deletion of *Hic1* in the intestinal epithelium augments goblet cell number, at the expense of enteroendocrine cells, and increases and mispositions expression of Paneth cells markers. Long term deletion next led to formation of dysplastic villi and preneoplastic lesions which were infiltrated with proinflamatory leukocytes. These data rather implicate a Wnt-signaling unrelated role of Hic1 in the intestinal epithelia homeostasis.

In the fourth report, we provided evidence for an association between TCF proteins and a small evolutionary conserved protein Dazap2. Dazap2 was originally identified as a transcript expressed in the mouse inner ear, in the embryonic heart and in both developing and adult mouse brain[290]. However, we found Dazap2 to be ubiquitously expressed in various mouse tissues, concordantly with other groups[291, 292] . Ubiquitous expression of Dazap2 together with its highly conserved evolutionarily homology suggests general importance of Dazap2 of yet unknown significance.

Dazap2 was identified as a binding partner of many cellular proteins[267] and since in our hands Dazap2 bind to all Wnt nuclear effector of TCF/LEF family with similar affinities, it can be concluded it has a role in canonical Wnt signaling as well. Moreover, RNAi knock-down of Dazap2 resulted in reduced activities in Tcf/β-catenin reporter and these reductions correlated with the ability of each siRNA to downregulate Dazap2 mRNA level. Additionally, Dazap2 was identified as an important player in FGF induced neural patterning[293] and in Ror2 mediated activation of the Wnt pathway[294]. However, in contrast to our study the last publication proposed cytoplasmic function of Dazap2. We always observed cytoplasmic distribution of Dazap2, which changed to nuclear upon ectopic expression of TCF4. Together, these studies indicate Dazap2 involvement in many cellular processes, cytoplasmic as well as nuclear, and suggest it is a rather important protein. Moreover, our microarray data from *Dazap2* targeting shRNA treated cells indicated that both the activating as well as inhibitory functions of TCFs might be influenced by Dazap2 amounts (unpublished results).

Strikingly, the Dazap2$^{-/-}$ mice lack any obvious phenotype[290], which could be explained by redundancy with some other genes. Indeed, a sequence database search in the mouse genome revealed a Dazap2 pseudogene localized on chromosome 4 and one gene similar to Dazap2 on chromosome 13. Function of proteins like Dazap2 may be considered important as there are homologous proteins to provide backup of Dazap2-functionality.

Conclusions

We identified new ways of Wnt pathway modulation that enhance the knowledge about the regulation of this important signaling cascade. The results, presented in four independent publications, can be summed up as follows:

1. We have identified *TROY*, a gene encoding a membrane protein from the tumor necrosis factor receptor superfamily as a genuine target of the Wnt/β-catenin pathway in the intestinal context. In our study, we utilized lineage tracing experiments to show that Troy represents – next to Lgr5 – another marker specific for the fast-cycling ISCs. We proved that Troy creates a regulatory feedback loop by interacting with Lgr5 to limit the level of canonical Wnt signaling in the intestinal stem cells.

2. We provided an evidence for the sequence of glycosylation and acylation of the mouse Wnt1 and Wnt3a. First, N-glycosylation occurs, then palmitoleoylation on serine which conditions and precedes the cysteine palmitoylation. These lipid adducts are necessary for interaction of Wnt proteins with the extracellular matrix, which is related to their ability to induce Wnt signaling.

3. We generated two modified alleles of *Hic1* tumor suppressor gene. A conditional *Hic1* null allele uses Cre/loxP system that can overcome the embryonic lethality of *Hic1*$^{-/-}$ mice, and *Hic1-citrine* 'reporter' strain expresses a reliable surrogate marker of Hic1 locus activity thus allowing tracking the *Hic1* expressing cells.

4. We have identified the interaction between TCF4 and a small and evolutionarily conserved protein Dazap2. The meaning of this interaction is to positively modulate TCF4 affinity for its specific DNA sequence, as concluded from negative impact on Wnt/β-catenin stimulated transcription after Dazap2 knock-down.

References

1. Sonis S, Haddad R, Posner M, et al. Gene expression changes in peripheral blood cells provide insight into the biological mechanisms associated with regimen-related toxicities in patients being treated for head and neck cancers. Oral Oncol 2007;43:289-300.
2. Cadigan KM, Nusse R. Wnt signaling: a common theme in animal development. Genes Dev 1997;11:3286-305.
3. Wodarz A, Nusse R. Mechanisms of Wnt signaling in development. Annu Rev Cell Dev Biol 1998;14:59-88.
4. Hobmayer B, Rentzsch F, Kuhn K, et al. WNT signalling molecules act in axis formation in the diploblastic metazoan Hydra. Nature 2000;407:186-9.
5. Peifer M, Polakis P. Wnt signaling in oncogenesis and embryogenesis--a look outside the nucleus. Science 2000;287:1606-9.
6. Logan CY, Nusse R. The Wnt signaling pathway in development and disease. Annu Rev Cell Dev Biol 2004;20:781-810.
7. Clevers H, Nusse R. Wnt/beta-catenin signaling and disease. Cell 2012;149:1192-205.
8. Polakis P. Wnt signaling and cancer. Genes Dev 2000;14:1837-51.
9. Park M, Shen K. WNTs in synapse formation and neuronal circuitry. EMBO J 2012;31:2697-704.
10. Lustig B, Jerchow B, Sachs M, et al. Negative feedback loop of Wnt signaling through upregulation of conductin/axin2 in colorectal and liver tumors. Mol Cell Biol 2002;22:1184-93.
11. Jho EH, Zhang T, Domon C, et al. Wnt/beta-catenin/Tcf signaling induces the transcription of Axin2, a negative regulator of the signaling pathway. Mol Cell Biol 2002;22:1172-83.
12. Yan D, Wiesmann M, Rohan M, et al. Elevated expression of axin2 and hnkd mRNA provides evidence that Wnt/beta -catenin signaling is activated in human colon tumors. Proc Natl Acad Sci U S A 2001;98:14973-8.
13. He TC, Sparks AB, Rago C, et al. Identification of c-MYC as a target of the APC pathway. Science 1998;281:1509-12.
14. Barker N, van Es JH, Kuipers J, et al. Identification of stem cells in small intestine and colon by marker gene Lgr5. Nature 2007;449:1003-7.
15. Nusse R, Varmus HE. Many tumors induced by the mouse mammary tumor virus contain a provirus integrated in the same region of the host genome. Cell 1982;31:99-109.
16. Sharma RP, Chopra VL. Effect of the Wingless (wg1) mutation on wing and haltere development in Drosophila melanogaster. Dev Biol 1976;48:461-5.
17. Port F, Basler K. Wnt trafficking: new insights into Wnt maturation, secretion and spreading. Traffic 2010;11:1265-71.
18. Miller JR. The Wnts. Genome Biol 2002;3:REVIEWS3001.
19. Willert K, Brown JD, Danenberg E, et al. Wnt proteins are lipid-modified and can act as stem cell growth factors. Nature 2003;423:448-52.
20. Tanaka K, Kitagawa Y, Kadowaki T. Drosophila segment polarity gene product porcupine stimulates the posttranslational N-glycosylation of wingless in the endoplasmic reticulum. J Biol Chem 2002;277:12816-23.
21. Kurayoshi M, Yamamoto H, Izumi S, et al. Post-translational palmitoylation and glycosylation of Wnt-5a are necessary for its signalling. Biochem J 2007;402:515-23.
22. Bradley RS, Brown AM. The proto-oncogene int-1 encodes a secreted protein associated with the extracellular matrix. EMBO J 1990;9:1569-75.
23. Kadowaki T, Wilder E, Klingensmith J, et al. The segment polarity gene porcupine encodes a putative multitransmembrane protein involved in Wingless processing. Genes Dev 1996;10:3116-28.

24. Caricasole A, Ferraro T, Rimland JM, et al. Molecular cloning and initial characterization of the MG61/PORC gene, the human homologue of the Drosophila segment polarity gene Porcupine. Gene 2002;288:147-57.
25. Franch-Marro X, Wendler F, Griffith J, et al. In vivo role of lipid adducts on Wingless. J Cell Sci 2008;121:1587-92.
26. Janda CY, Waghray D, Levin AM, et al. Structural basis of Wnt recognition by Frizzled. Science 2012;337:59-64.
27. Mason JO, Kitajewski J, Varmus HE. Mutational analysis of mouse Wnt-1 identifies two temperature-sensitive alleles and attributes of Wnt-1 protein essential for transformation of a mammary cell line. Mol Biol Cell 1992;3:521-33.
28. Komekado H, Yamamoto H, Chiba T, et al. Glycosylation and palmitoylation of Wnt-3a are coupled to produce an active form of Wnt-3a. Genes Cells 2007;12:521-34.
29. Panakova D, Sprong H, Marois E, et al. Lipoprotein particles are required for Hedgehog and Wingless signalling. Nature 2005;435:58-65.
30. Zecca M, Basler K, Struhl G. Direct and long-range action of a wingless morphogen gradient. Cell 1996;87:833-44.
31. van den Heuvel M, Nusse R, Johnston P, et al. Distribution of the wingless gene product in Drosophila embryos: a protein involved in cell-cell communication. Cell 1989;59:739-49.
32. Korkut C, Ataman B, Ramachandran P, et al. Trans-synaptic transmission of vesicular Wnt signals through Evi/Wntless. Cell 2009;139:393-404.
33. Strand M, Micchelli CA. Quiescent gastric stem cells maintain the adult Drosophila stomach. Proc Natl Acad Sci U S A 2011;108:17696-701.
34. Sato T, van Es JH, Snippert HJ, et al. Paneth cells constitute the niche for Lgr5 stem cells in intestinal crypts. Nature 2010;469:415-8.
35. Banziger C, Soldini D, Schutt C, et al. Wntless, a conserved membrane protein dedicated to the secretion of Wnt proteins from signaling cells. Cell 2006;125:509-22.
36. Bartscherer K, Pelte N, Ingelfinger D, et al. Secretion of Wnt ligands requires Evi, a conserved transmembrane protein. Cell 2006;125:523-33.
37. Goodman RM, Thombre S, Firtina Z, et al. Sprinter: a novel transmembrane protein required for Wg secretion and signaling. Development 2006;133:4901-11.
38. Pan CL, Baum PD, Gu M, et al. C. elegans AP-2 and retromer control Wnt signaling by regulating mig-14/Wntless. Dev Cell 2008;14:132-9.
39. Bolognesi R, Farzana L, Fischer TD, et al. Multiple Wnt genes are required for segmentation in the short-germ embryo of Tribolium castaneum. Curr Biol 2008;18:1624-9.
40. Ching W, Hang HC, Nusse R. Lipid-independent secretion of a Drosophila Wnt protein. J Biol Chem 2008;283:17092-8.
41. Belenkaya TY, Wu Y, Tang X, et al. The retromer complex influences Wnt secretion by recycling wntless from endosomes to the trans-Golgi network. Dev Cell 2008;14:120-31.
42. Port F, Kuster M, Herr P, et al. Wingless secretion promotes and requires retromer-dependent cycling of Wntless. Nat Cell Biol 2008;10:178-85.
43. Reichsman F, Smith L, Cumberledge S. Glycosaminoglycans can modulate extracellular localization of the wingless protein and promote signal transduction. J Cell Biol 1996;135:819-27.
44. Malanchi I, Santamaria-Martinez A, Susanto E, et al. Interactions between cancer stem cells and their niche govern metastatic colonization. Nature 2012;481:85-9.
45. Lin K, Wang S, Julius MA, et al. The cysteine-rich frizzled domain of Frzb-1 is required and sufficient for modulation of Wnt signaling. Proc Natl Acad Sci U S A 1997;94:11196-200.
46. Mii Y, Taira M. Secreted Wnt "inhibitors" are not just inhibitors: regulation of extracellular Wnt by secreted Frizzled-related proteins. Dev Growth Differ 2011;53:911-23.
47. Hsieh JC, Kodjabachian L, Rebbert ML, et al. A new secreted protein that binds to Wnt proteins and inhibits their activities. Nature 1999;398:431-6.

48. Malinauskas T, Aricescu AR, Lu W, et al. Modular mechanism of Wnt signaling inhibition by Wnt inhibitory factor 1. Nat Struct Mol Biol 2011;18:886-93.
49. Zhang X, Abreu JG, Yokota C, et al. Tiki1 is required for head formation via Wnt cleavage-oxidation and inactivation. Cell 2012;149:1565-77.
50. Pinson KI, Brennan J, Monkley S, et al. An LDL-receptor-related protein mediates Wnt signalling in mice. Nature 2000;407:535-8.
51. Tamai K, Semenov M, Kato Y, et al. LDL-receptor-related proteins in Wnt signal transduction. Nature 2000;407:530-5.
52. Schulte G, Bryja V. The Frizzled family of unconventional G-protein-coupled receptors. Trends Pharmacol Sci 2007;28:518-25.
53. Bhanot P, Brink M, Samos CH, et al. A new member of the frizzled family from Drosophila functions as a Wingless receptor. Nature 1996;382:225-30.
54. Dann CE, Hsieh JC, Rattner A, et al. Insights into Wnt binding and signalling from the structures of two Frizzled cysteine-rich domains. Nature 2001;412:86-90.
55. Wehrli M, Dougan ST, Caldwell K, et al. arrow encodes an LDL-receptor-related protein essential for Wingless signalling. Nature 2000;407:527-30.
56. Semenov MV, Tamai K, Brott BK, et al. Head inducer Dickkopf-1 is a ligand for Wnt coreceptor LRP6. Curr Biol 2001;11:951-61.
57. Mao B, Wu W, Li Y, et al. LDL-receptor-related protein 6 is a receptor for Dickkopf proteins. Nature 2001;411:321-5.
58. He X, Semenov M, Tamai K, et al. LDL receptor-related proteins 5 and 6 in Wnt/beta-catenin signaling: arrows point the way. Development 2004;131:1663-77.
59. Gong Y, Bourhis E, Chiu C, et al. Wnt isoform-specific interactions with coreceptor specify inhibition or potentiation of signaling by LRP6 antibodies. PLoS One 2010;5:e12682.
60. Tamai K, Zeng X, Liu C, et al. A mechanism for Wnt coreceptor activation. Mol Cell 2004;13:149-56.
61. Mao J, Wang J, Liu B, et al. Low-density lipoprotein receptor-related protein-5 binds to Axin and regulates the canonical Wnt signaling pathway. Mol Cell 2001;7:801-9.
62. Zeng X, Tamai K, Doble B, et al. A dual-kinase mechanism for Wnt co-receptor phosphorylation and activation. Nature 2005;438:873-7.
63. Davidson G, Wu W, Shen J, et al. Casein kinase 1 gamma couples Wnt receptor activation to cytoplasmic signal transduction. Nature 2005;438:867-72.
64. Cong F, Schweizer L, Varmus H. Wnt signals across the plasma membrane to activate the beta-catenin pathway by forming oligomers containing its receptors, Frizzled and LRP. Development 2004;131:5103-15.
65. Bilic J, Huang YL, Davidson G, et al. Wnt induces LRP6 signalosomes and promotes dishevelled-dependent LRP6 phosphorylation. Science 2007;316:1619-22.
66. Gao C, Chen YG. Dishevelled: The hub of Wnt signaling. Cell Signal 2010;22:717-27.
67. Chen W, ten Berge D, Brown J, et al. Dishevelled 2 recruits beta-arrestin 2 to mediate Wnt5A-stimulated endocytosis of Frizzled 4. Science 2003;301:1391-4.
68. Fiedler M, Mendoza-Topaz C, Rutherford TJ, et al. Dishevelled interacts with the DIX domain polymerization interface of Axin to interfere with its function in down-regulating beta-catenin. Proc Natl Acad Sci U S A 2011;108:1937-42.
69. Schwarz-Romond T, Metcalfe C, Bienz M. Dynamic recruitment of axin by Dishevelled protein assemblies. J Cell Sci 2007;120:2402-12.
70. Semenov M, Tamai K, He X. SOST is a ligand for LRP5/LRP6 and a Wnt signaling inhibitor. J Biol Chem 2005;280:26770-5.
71. Gonzalez-Sancho JM, Aguilera O, Garcia JM, et al. The Wnt antagonist DICKKOPF-1 gene is a downstream target of beta-catenin/TCF and is downregulated in human colon cancer. Oncogene 2005;24:1098-103.
72. Semenov MV, Zhang X, He X. DKK1 antagonizes Wnt signaling without promotion of LRP6 internalization and degradation. J Biol Chem 2008;283:21427-32.

73. Ellwanger K, Saito H, Clement-Lacroix P, et al. Targeted disruption of the Wnt regulator Kremen induces limb defects and high bone density. Mol Cell Biol 2008;28:4875-82.
74. Green JL, Kuntz SG, Sternberg PW. Ror receptor tyrosine kinases: orphans no more. Trends Cell Biol 2008;18:536-44.
75. Peradziryi H, Kaplan NA, Podleschny M, et al. PTK7/Otk interacts with Wnts and inhibits canonical Wnt signalling. EMBO J 2011;30:3729-40.
76. van Amerongen R, Nusse R. Towards an integrated view of Wnt signaling in development. Development 2009;136:3205-14.
77. Xu Q, Wang Y, Dabdoub A, et al. Vascular development in the retina and inner ear: control by Norrin and Frizzled-4, a high-affinity ligand-receptor pair. Cell 2004;116:883-95.
78. Richter M, Gottanka J, May CA, et al. Retinal vasculature changes in Norrie disease mice. Invest Ophthalmol Vis Sci 1998;39:2450-7.
79. Wang Y, Huso D, Cahill H, et al. Progressive cerebellar, auditory, and esophageal dysfunction caused by targeted disruption of the frizzled-4 gene. J Neurosci 2001;21:4761-71.
80. Kato M, Patel MS, Levasseur R, et al. Cbfa1-independent decrease in osteoblast proliferation, osteopenia, and persistent embryonic eye vascularization in mice deficient in Lrp5, a Wnt coreceptor. J Cell Biol 2002;157:303-14.
81. Xia CH, Liu H, Cheung D, et al. A model for familial exudative vitreoretinopathy caused by LRP5 mutations. Hum Mol Genet 2008;17:1605-12.
82. Kim KA, Kakitani M, Zhao J, et al. Mitogenic influence of human R-spondin1 on the intestinal epithelium. Science 2005;309:1256-9.
83. Kazanskaya O, Glinka A, del Barco Barrantes I, et al. R-Spondin2 is a secreted activator of Wnt/beta-catenin signaling and is required for Xenopus myogenesis. Dev Cell 2004;7:525-34.
84. Sato T, Vries RG, Snippert HJ, et al. Single Lgr5 stem cells build crypt-villus structures in vitro without a mesenchymal niche. Nature 2009;459:262-5.
85. Parr BA, Shea MJ, Vassileva G, et al. Mouse Wnt genes exhibit discrete domains of expression in the early embryonic CNS and limb buds. Development 1993;119:247-61.
86. Echelard Y, Vassileva G, McMahon AP. Cis-acting regulatory sequences governing Wnt-1 expression in the developing mouse CNS. Development 1994;120:2213-24.
87. Yoshida M, Suda Y, Matsuo I, et al. Emx1 and Emx2 functions in development of dorsal telencephalon. Development 1997;124:101-11.
88. Nam JS, Turcotte TJ, Yoon JK. Dynamic expression of R-spondin family genes in mouse development. Gene Expr Patterns 2007;7:306-12.
89. Yamada W, Nagao K, Horikoshi K, et al. Craniofacial malformation in R-spondin2 knockout mice. Biochem Biophys Res Commun 2009;381:453-8.
90. Bell SM, Schreiner CM, Wert SE, et al. R-spondin 2 is required for normal laryngeal-tracheal, lung and limb morphogenesis. Development 2008;135:1049-58.
91. de Lau W, Barker N, Low TY, et al. Lgr5 homologues associate with Wnt receptors and mediate R-spondin signalling. Nature 2011;476:293-7.
92. Carmon KS, Gong X, Lin Q, et al. R-spondins function as ligands of the orphan receptors LGR4 and LGR5 to regulate Wnt/beta-catenin signaling. Proc Natl Acad Sci U S A 2011;108:11452-7.
93. Glinka A, Dolde C, Kirsch N, et al. LGR4 and LGR5 are R-spondin receptors mediating Wnt/beta-catenin and Wnt/PCP signalling. EMBO Rep 2011;12:1055-61.
94. Van Schoore G, Mendive F, Pochet R, et al. Expression pattern of the orphan receptor LGR4/GPR48 gene in the mouse. Histochem Cell Biol 2005;124:35-50.
95. Mazerbourg S, Bouley DM, Sudo S, et al. Leucine-rich repeat-containing, G protein-coupled receptor 4 null mice exhibit intrauterine growth retardation associated with embryonic and perinatal lethality. Mol Endocrinol 2004;18:2241-54.

96. Song H, Luo J, Luo W, et al. Inactivation of G-protein-coupled receptor 48 (Gpr48/Lgr4) impairs definitive erythropoiesis at midgestation through down-regulation of the ATF4 signaling pathway. J Biol Chem 2008;283:36687-97.
97. Weng J, Luo J, Cheng X, et al. Deletion of G protein-coupled receptor 48 leads to ocular anterior segment dysgenesis (ASD) through down-regulation of Pitx2. Proc Natl Acad Sci U S A 2008;105:6081-6.
98. Barker N, Huch M, Kujala P, et al. Lgr5(+ve) stem cells drive self-renewal in the stomach and build long-lived gastric units in vitro. Cell Stem Cell 2010;6:25-36.
99. Barker N, Ridgway RA, van Es JH, et al. Crypt stem cells as the cells-of-origin of intestinal cancer. Nature 2009;457:608-11.
100. Jaks V, Barker N, Kasper M, et al. Lgr5 marks cycling, yet long-lived, hair follicle stem cells. Nat Genet 2008;40:1291-9.
101. Snippert HJ, Haegebarth A, Kasper M, et al. Lgr6 marks stem cells in the hair follicle that generate all cell lineages of the skin. Science 2010;327:1385-9.
102. Kinzler KW, Vogelstein B. Lessons from hereditary colorectal cancer. Cell 1996;87:159-70.
103. Korinek V, Barker N, Morin PJ, et al. Constitutive transcriptional activation by a beta-catenin-Tcf complex in APC-/- colon carcinoma. Science 1997;275:1784-7.
104. Morin PJ, Sparks AB, Korinek V, et al. Activation of beta-catenin-Tcf signaling in colon cancer by mutations in beta-catenin or APC. Science 1997;275:1787-90.
105. Rubinfeld B, Albert I, Porfiri E, et al. Loss of beta-catenin regulation by the APC tumor suppressor protein correlates with loss of structure due to common somatic mutations of the gene. Cancer Res 1997;57:4624-30.
106. Liu W, Dong X, Mai M, et al. Mutations in AXIN2 cause colorectal cancer with defective mismatch repair by activating beta-catenin/TCF signalling. Nat Genet 2000;26:146-7.
107. Ikeda S, Kishida S, Yamamoto H, et al. Axin, a negative regulator of the Wnt signaling pathway, forms a complex with GSK-3beta and beta-catenin and promotes GSK-3beta-dependent phosphorylation of beta-catenin. Embo J 1998;17:1371-84.
108. Kishida S, Yamamoto H, Ikeda S, et al. Axin, a negative regulator of the wnt signaling pathway, directly interacts with adenomatous polyposis coli and regulates the stabilization of beta-catenin. J Biol Chem 1998;273:10823-6.
109. Liu C, Li Y, Semenov M, et al. Control of beta-catenin phosphorylation/degradation by a dual-kinase mechanism. Cell 2002;108:837-47.
110. Sakanaka C, Weiss JB, Williams LT. Bridging of beta-catenin and glycogen synthase kinase-3beta by axin and inhibition of beta-catenin-mediated transcription. Proc Natl Acad Sci U S A 1998;95:3020-3.
111. Major MB, Camp ND, Berndt JD, et al. Wilms tumor suppressor WTX negatively regulates WNT/beta-catenin signaling. Science 2007;316:1043-6.
112. Tanneberger K, Pfister AS, Brauburger K, et al. Amer1/WTX couples Wnt-induced formation of PtdIns(4,5)P2 to LRP6 phosphorylation. EMBO J 2011;30:1433-43.
113. Luo W, Peterson A, Garcia BA, et al. Protein phosphatase 1 regulates assembly and function of the beta-catenin degradation complex. EMBO J 2007;26:1511-21.
114. Su Y, Fu C, Ishikawa S, et al. APC is essential for targeting phosphorylated beta-catenin to the SCFbeta-TrCP ubiquitin ligase. Mol Cell 2008;32:652-61.
115. Henderson BR, Fagotto F. The ins and outs of APC and beta-catenin nuclear transport. EMBO Rep 2002;3:834-9.
116. Sierra J, Yoshida T, Joazeiro CA, et al. The APC tumor suppressor counteracts beta-catenin activation and H3K4 methylation at Wnt target genes. Genes Dev 2006;20:586-600.
117. Barth AI, Nathke IS, Nelson WJ. Cadherins, catenins and APC protein: interplay between cytoskeletal complexes and signaling pathways. Curr Opin Cell Biol 1997;9:683-90.

118. Wen Y, Eng CH, Schmoranzer J, et al. EB1 and APC bind to mDia to stabilize microtubules downstream of Rho and promote cell migration. Nat Cell Biol 2004;6:820-30.
119. Wang Y, Coffey RJ, Osheroff N, et al. Topoisomerase IIalpha binding domains of adenomatous polyposis coli influence cell cycle progression and aneuploidy. PLoS One 2010;5:e9994.
120. Chen T, Yang I, Irby R, et al. Regulation of caspase expression and apoptosis by adenomatous polyposis coli. Cancer Res 2003;63:4368-74.
121. Brocardo MG, Borowiec JA, Henderson BR. Adenomatous polyposis coli protein regulates the cellular response to DNA replication stress. Int J Biochem Cell Biol 2011;43:1354-64.
122. Tanneberger K, Pfister AS, Kriz V, et al. Structural and functional characterization of the Wnt inhibitor APC membrane recruitment 1 (Amer1). J Biol Chem 2011;286:19204-14.
123. Aberle H, Bauer A, Stappert J, et al. beta-catenin is a target for the ubiquitin-proteasome pathway. Embo J 1997;16:3797-804.
124. Li VS, Ng SS, Boersema PJ, et al. Wnt signaling through inhibition of beta-catenin degradation in an intact Axin1 complex. Cell 2012;149:1245-56.
125. Ozawa M, Baribault H, Kemler R. The cytoplasmic domain of the cell adhesion molecule uvomorulin associates with three independent proteins structurally related in different species. EMBO J 1989;8:1711-7.
126. Graham TA, Weaver C, Mao F, et al. Crystal structure of a beta-catenin/Tcf complex. Cell 2000;103:885-96.
127. Huber AH, Nelson WJ, Weis WI. Three-dimensional structure of the armadillo repeat region of beta- catenin. Cell 1997;90:871-82.
128. Eklof Spink K, Fridman SG, Weis WI. Molecular mechanisms of beta-catenin recognition by adenomatous polyposis coli revealed by the structure of an APC-beta-catenin complex. EMBO J 2001;20:6203-12.
129. Huber AH, Weis WI. The structure of the beta-catenin/E-cadherin complex and the molecular basis of diverse ligand recognition by beta-catenin. Cell 2001;105:391-402.
130. Poy F, Lepourcelet M, Shivdasani RA, et al. Structure of a human Tcf4-beta-catenin complex. Nat Struct Biol 2001;8:1053-7.
131. Valenta T, Hausmann G, Basler K. The many faces and functions of beta-catenin. EMBO J 2012;31:2714-36.
132. Valenta T, Gay M, Steiner S, et al. Probing transcription-specific outputs of beta-catenin in vivo. Genes Dev 2012;25:2631-43.
133. Huelsken J, Vogel R, Brinkmann V, et al. Requirement for beta-catenin in anterior-posterior axis formation in mice. J Cell Biol 2000;148:567-78.
134. Grigoryan T, Wend P, Klaus A, et al. Deciphering the function of canonical Wnt signals in development and disease: conditional loss- and gain-of-function mutations of beta-catenin in mice. Genes Dev 2008;22:2308-41.
135. Korswagen HC, Herman MA, Clevers HC. Distinct beta-catenins mediate adhesion and signalling functions in C. elegans. Nature 2000;406:527-32.
136. Huang P, Senga T, Hamaguchi M. A novel role of phospho-beta-catenin in microtubule regrowth at centrosome. Oncogene 2007;26:4357-71.
137. Hadjihannas MV, Bruckner M, Behrens J. Conductin/axin2 and Wnt signalling regulates centrosome cohesion. EMBO Rep 2010;11:317-24.
138. Piedra J, Miravet S, Castano J, et al. p120 Catenin-associated Fer and Fyn tyrosine kinases regulate beta-catenin Tyr-142 phosphorylation and beta-catenin-alpha-catenin Interaction. Mol Cell Biol 2003;23:2287-97.
139. Brembeck FH, Schwarz-Romond T, Bakkers J, et al. Essential role of BCL9-2 in the switch between beta-catenin's adhesive and transcriptional functions. Genes Dev 2004;18:2225-30.

140. Bustos VH, Ferrarese A, Venerando A, et al. The first armadillo repeat is involved in the recognition and regulation of beta-catenin phosphorylation by protein kinase CK1. Proc Natl Acad Sci U S A 2006;103:19725-30.
141. Piedra J, Martinez D, Castano J, et al. Regulation of beta-catenin structure and activity by tyrosine phosphorylation. J Biol Chem 2001;276:20436-43.
142. van Veelen W, Le NH, Helvensteijn W, et al. beta-catenin tyrosine 654 phosphorylation increases Wnt signalling and intestinal tumorigenesis. Gut 2011;60:1204-12.
143. Roura S, Miravet S, Piedra J, et al. Regulation of E-cadherin/Catenin association by tyrosine phosphorylation. J Biol Chem 1999;274:36734-40.
144. Taurin S, Sandbo N, Qin Y, et al. Phosphorylation of beta-catenin by cyclic AMP-dependent protein kinase. J Biol Chem 2006;281:9971-6.
145. Wu X, Tu X, Joeng KS, et al. Rac1 activation controls nuclear localization of beta-catenin during canonical Wnt signaling. Cell 2008;133:340-53.
146. Stadeli R, Hoffmans R, Basler K. Transcription under the control of nuclear Arm/beta-catenin. Curr Biol 2006;16:R378-85.
147. Yokoya F, Imamoto N, Tachibana T, et al. beta-catenin can be transported into the nucleus in a Ran-unassisted manner. Mol Biol Cell 1999;10:1119-31.
148. Fagotto F, Gluck U, Gumbiner BM. Nuclear localization signal-independent and importin/karyopherin- independent nuclear import of beta-catenin. Curr Biol 1998;8:181-90.
149. Shitashige M, Satow R, Honda K, et al. Regulation of Wnt signaling by the nuclear pore complex. Gastroenterology 2008;134:1961-71, 1971 e1-4.
150. Sharma M, Jamieson C, Johnson M, et al. Specific armadillo repeat sequences facilitate beta-catenin nuclear transport in live cells via direct binding to nucleoporins Nup62, Nup153, and RanBP2/Nup358. J Biol Chem 2012;287:819-31.
151. Zhang N, Wei P, Gong A, et al. FoxM1 promotes beta-catenin nuclear localization and controls Wnt target-gene expression and glioma tumorigenesis. Cancer Cell 2011;20:427-42.
152. van de Wetering M, Cavallo R, Dooijes D, et al. Armadillo coactivates transcription driven by the product of the Drosophila segment polarity gene dTCF. Cell 1997;88:789-99.
153. Mosimann C, Hausmann G, Basler K. Parafibromin/Hyrax activates Wnt/Wg target gene transcription by direct association with beta-catenin/Armadillo. Cell 2006;125:327-41.
154. Wolf D, Rodova M, Miska EA, et al. Acetylation of beta-catenin by CREB-binding protein (CBP). J Biol Chem 2002;277:25562-7.
155. Levy L, Wei Y, Labalette C, et al. Acetylation of beta-catenin by p300 regulates beta-catenin-Tcf4 interaction. Mol Cell Biol 2004;24:3404-14.
156. Xing Y, Takemaru K, Liu J, et al. Crystal structure of a full-length beta-catenin. Structure 2008;16:478-87.
157. Kaidi A, Williams AC, Paraskeva C. Interaction between beta-catenin and HIF-1 promotes cellular adaptation to hypoxia. Nat Cell Biol 2007;9:210-7.
158. Pawlowski JE, Ertel JR, Allen MP, et al. Liganded androgen receptor interaction with beta-catenin: nuclear co-localization and modulation of transcriptional activity in neuronal cells. J Biol Chem 2002;277:20702-10.
159. Mulholland DJ, Read JT, Rennie PS, et al. Functional localization and competition between the androgen receptor and T-cell factor for nuclear beta-catenin: a means for inhibition of the Tcf signaling axis. Oncogene 2003;22:5602-13.
160. Essers MA, de Vries-Smits LM, Barker N, et al. Functional interaction between beta-catenin and FOXO in oxidative stress signaling. Science 2005;308:1181-4.
161. Arce L, Yokoyama NN, Waterman ML. Diversity of LEF/TCF action in development and disease. Oncogene 2006;25:7492-504.
162. van Beest M, Dooijes D, van De Wetering M, et al. Sequence-specific high mobility group box factors recognize 10-12-base pair minor groove motifs. J Biol Chem 2000;275:27266-73.

163. Archbold HC, Yang YX, Chen L, et al. How do they do Wnt they do?: regulation of transcription by the Wnt/beta-catenin pathway. Acta Physiol (Oxf) 2012;204:74-109.
164. Mao CD, Byers SW. Cell-context dependent TCF/LEF expression and function: alternative tales of repression, de-repression and activation potentials. Crit Rev Eukaryot Gene Expr 2011;21:207-36.
165. Atcha FA, Syed A, Wu B, et al. A unique DNA binding domain converts T-cell factors into strong Wnt effectors. Mol Cell Biol 2007;27:8352-63.
166. Chang MV, Chang JL, Gangopadhyay A, et al. Activation of wingless targets requires bipartite recognition of DNA by TCF. Curr Biol 2008;18:1877-81.
167. Weise A, Bruser K, Elfert S, et al. Alternative splicing of Tcf7l2 transcripts generates protein variants with differential promoter-binding and transcriptional activation properties at Wnt/{beta}-catenin targets. Nucleic Acids Res 2009.
168. Van de Wetering M, Castrop J, Korinek V, et al. Extensive alternative splicing and dual promoter usage generate Tcf-1 protein isoforms with differential transcription control properties. Mol Cell Biol 1996;16:745-52.
169. Wallmen B, Schrempp M, Hecht A. Intrinsic properties of Tcf1 and Tcf4 splice variants determine cell-type-specific Wnt/beta-catenin target gene expression. Nucleic Acids Res 2012.
170. Wray J, Kalkan T, Gomez-Lopez S, et al. Inhibition of glycogen synthase kinase-3 alleviates Tcf3 repression of the pluripotency network and increases embryonic stem cell resistance to differentiation. Nat Cell Biol 2011;13:838-45.
171. Yi F, Pereira L, Hoffman JA, et al. Opposing effects of Tcf3 and Tcf1 control Wnt stimulation of embryonic stem cell self-renewal. Nat Cell Biol 2011;13:762-70.
172. Verbeek S, Izon D, Hofhuis F, et al. An HMG-box-containing T-cell factor required for thymocyte differentiation. Nature 1995;374:70-4.
173. van Genderen C, Okamura RM, Farinas I, et al. Development of several organs that require inductive epithelial- mesenchymal interactions is impaired in LEF-1-deficient mice. Genes Dev 1994;8:2691-703.
174. Galceran J, Farinas I, Depew MJ, et al. Wnt3a-/--like phenotype and limb deficiency in Lef1(-/-)Tcf1(-/-) mice. Genes Dev 1999;13:709-17.
175. DasGupta R, Fuchs E. Multiple roles for activated LEF/TCF transcription complexes during hair follicle development and differentiation. Development 1999;126:4557-68.
176. Maretto S, Cordenonsi M, Dupont S, et al. Mapping Wnt/beta-catenin signaling during mouse development and in colorectal tumors. Proc Natl Acad Sci U S A 2003;100:3299-304.
177. Cavallo RA, Cox RT, Moline MM, et al. Drosophila Tcf and Groucho interact to repress Wingless signalling activity. Nature 1998;395:604-8.
178. Roose J, Molenaar M, Peterson J, et al. The Xenopus Wnt effector XTcf-3 interacts with Groucho-related transcriptional repressors. Nature 1998;395:608-12.
179. Daniels DL, Weis WI. Beta-catenin directly displaces Groucho/TLE repressors from Tcf/Lef in Wnt-mediated transcription activation. Nat Struct Mol Biol 2005;12:364-71.
180. MacDonald BT, Tamai K, He X. Wnt/beta-catenin signaling: components, mechanisms, and diseases. Dev Cell 2009;17:9-26.
181. Phillips BT, Kimble J. A new look at TCF and beta-catenin through the lens of a divergent C. elegans Wnt pathway. Dev Cell 2009;17:27-34.
182. Hoppler S, Kavanagh CL. Wnt signalling: variety at the core. J Cell Sci 2007;120:385-93.
183. Hikasa H, Ezan J, Itoh K, et al. Regulation of TCF3 by Wnt-dependent phosphorylation during vertebrate axis specification. Dev Cell 2010;19:521-32.
184. Lee W, Swarup S, Chen J, et al. Homeodomain-interacting protein kinases (Hipks) promote Wnt/Wg signaling through stabilization of beta-catenin/Arm and stimulation of target gene expression. Development 2009;136:241-51.
185. Hikasa H, Sokol SY. Phosphorylation of TCF proteins by homeodomain-interacting protein kinase 2. J Biol Chem 2011;286:12093-100.

186. Mahmoudi T, Li VS, Ng SS, et al. The kinase TNIK is an essential activator of Wnt target genes. Embo J 2009;28:3329-40.
187. Sachdev S, Bruhn L, Sieber H, et al. PIASy, a nuclear matrix-associated SUMO E3 ligase, represses LEF1 activity by sequestration into nuclear bodies. Genes Dev 2001;15:3088-103.
188. Ihara M, Yamamoto H, Kikuchi A. SUMO-1 modification of PIASy, an E3 ligase, is necessary for PIASy-dependent activation of Tcf-4. Mol Cell Biol 2005;25:3506-18.
189. Yamamoto H, Ihara M, Matsuura Y, et al. Sumoylation is involved in beta-catenin-dependent activation of Tcf-4. Embo J 2003;22:2047-59.
190. Daniels DL, Weis WI. ICAT inhibits beta-catenin binding to Tcf/Lef-family transcription factors and the general coactivator p300 using independent structural modules. Mol Cell 2002;10:573-84.
191. Valenta T, Lukas J, Doubravska L, et al. HIC1 attenuates Wnt signaling by recruitment of TCF-4 and beta-catenin to the nuclear bodies. Embo J 2006;25:2326-37.
192. Kramps T, Peter O, Brunner E, et al. Wnt/wingless signaling requires BCL9/legless-mediated recruitment of pygopus to the nuclear beta-catenin-TCF complex. Cell 2002;109:47-60.
193. Parker DS, Jemison J, Cadigan KM. Pygopus, a nuclear PHD-finger protein required for Wingless signaling in Drosophila. Development 2002;129:2565-76.
194. Thompson B, Townsley F, Rosin-Arbesfeld R, et al. A new nuclear component of the Wnt signalling pathway. Nat Cell Biol 2002;4:367-73.
195. Brack AS, Murphy-Seiler F, Hanifi J, et al. BCL9 is an essential component of canonical Wnt signaling that mediates the differentiation of myogenic progenitors during muscle regeneration. Dev Biol 2009;335:93-105.
196. Schwab KR, Patterson LT, Hartman HA, et al. Pygo1 and Pygo2 roles in Wnt signaling in mammalian kidney development. BMC Biol 2007;5:15.
197. Jamora C, DasGupta R, Kocieniewski P, et al. Links between signal transduction, transcription and adhesion in epithelial bud development. Nature 2003;422:317-22.
198. Delmas V, Beermann F, Martinozzi S, et al. Beta-catenin induces immortalization of melanocytes by suppressing p16INK4a expression and cooperates with N-Ras in melanoma development. Genes Dev 2007;21:2923-35.
199. Blauwkamp TA, Chang MV, Cadigan KM. Novel TCF-binding sites specify transcriptional repression by Wnt signalling. EMBO J 2008;27:1436-46.
200. Myant K, Sansom OJ. Wnt/Myc interactions in intestinal cancer: partners in crime. Exp Cell Res 2012;317:2725-31.
201. Dang CV, O'Donnell KA, Zeller KI, et al. The c-Myc target gene network. Semin Cancer Biol 2006;16:253-64.
202. Zeller KI, Zhao X, Lee CW, et al. Global mapping of c-Myc binding sites and target gene networks in human B cells. Proc Natl Acad Sci U S A 2006;103:17834-9.
203. Sansom OJ, Meniel VS, Muncan V, et al. Myc deletion rescues Apc deficiency in the small intestine. Nature 2007;446:676-9.
204. Vlad A, Rohrs S, Klein-Hitpass L, et al. The first five years of the Wnt targetome. Cell Signal 2008;20:795-802.
205. Bottomly D, Kyler SL, McWeeney SK, et al. Identification of {beta}-catenin binding regions in colon cancer cells using ChIP-Seq. Nucleic Acids Res 2010;38:5735-45.
206. Liu P, Wakamiya M, Shea MJ, et al. Requirement for Wnt3 in vertebrate axis formation. Nat Genet 1999;22:361-5.
207. Liu C, Kato Y, Zhang Z, et al. beta-Trcp couples beta-catenin phosphorylation-degradation and regulates Xenopus axis formation. Proc Natl Acad Sci U S A 1999;96:6273-8.
208. Ikeya M, Lee SM, Johnson JE, et al. Wnt signalling required for expansion of neural crest and CNS progenitors. Nature 1997;389:966-70.

209. Yoshikawa Y, Fujimori T, McMahon AP, et al. Evidence that absence of Wnt-3a signaling promotes neuralization instead of paraxial mesoderm development in the mouse. Dev Biol 1997;183:234-42.
210. Snippert HJ, Clevers H. Tracking adult stem cells. EMBO Rep 2011;12:113-22.
211. Luis TC, Ichii M, Brugman MH, et al. Wnt signaling strength regulates normal hematopoiesis and its deregulation is involved in leukemia development. Leukemia 2012;26:414-21.
212. Tompkins KA. Wnt proteins in mineralized tissue development and homeostasis. Connect Tissue Res 2011;52:448-58.
213. Yokota H, Leong DJ, Sun HB. Mechanical loading: bone remodeling and cartilage maintenance. Curr Osteoporos Rep 2011;9:237-42.
214. Tang QQ, Lane MD. Adipogenesis: from stem cell to adipocyte. Annu Rev Biochem 2012;81:715-36.
215. Benhamouche S, Decaens T, Godard C, et al. Apc tumor suppressor gene is the "zonation-keeper" of mouse liver. Dev Cell 2006;10:759-70.
216. Losick VP, Morris LX, Fox DT, et al. Drosophila stem cell niches: a decade of discovery suggests a unified view of stem cell regulation. Dev Cell 2011;21:159-71.
217. Pinto D, Clevers H. Wnt, stem cells and cancer in the intestine. Biol Cell 2005;97:185-96.
218. Barker N, Clevers H. Leucine-rich repeat-containing G-protein-coupled receptors as markers of adult stem cells. Gastroenterology 2010;138:1681-96.
219. Barker N, Clevers H. Tracking down the stem cells of the intestine: strategies to identify adult stem cells. Gastroenterology 2007;133:1755-60.
220. van Amerongen R, Bowman AN, Nusse R. Developmental Stage and Time Dictate the Fate of Wnt/beta-Catenin-Responsive Stem Cells in the Mammary Gland. Cell Stem Cell 2012.
221. Blanpain C, Fuchs E. Epidermal homeostasis: a balancing act of stem cells in the skin. Nat Rev Mol Cell Biol 2009;10:207-17.
222. Blanpain C, Horsley V, Fuchs E. Epithelial stem cells: turning over new leaves. Cell 2007;128:445-58.
223. Haegebarth A, Clevers H. Wnt signaling, lgr5, and stem cells in the intestine and skin. Am J Pathol 2009;174:715-21.
224. Andl T, Reddy ST, Gaddapara T, et al. WNT signals are required for the initiation of hair follicle development. Dev Cell 2002;2:643-53.
225. Gat U, DasGupta R, Degenstein L, et al. De Novo hair follicle morphogenesis and hair tumors in mice expressing a truncated beta-catenin in skin. Cell 1998;95:605-14.
226. Zeng YA, Nusse R. Wnt proteins are self-renewal factors for mammary stem cells and promote their long-term expansion in culture. Cell Stem Cell 2010;6:568-77.
227. ten Berge D, Kurek D, Blauwkamp T, et al. Embryonic stem cells require Wnt proteins to prevent differentiation to epiblast stem cells. Nat Cell Biol 2011;13:1070-5.
228. Li J, Chen B. Oct4 was a novel target of Wnt signaling pathway. Mol Cell Biochem 2012;362:233-40.
229. Pereira L, Yi F, Merrill BJ. Repression of Nanog gene transcription by Tcf3 limits embryonic stem cell self-renewal. Molecular and cellular biology 2006;26:7479-91.
230. Sato N, Meijer L, Skaltsounis L, et al. Maintenance of pluripotency in human and mouse embryonic stem cells through activation of Wnt signaling by a pharmacological GSK-3-specific inhibitor. Nat Med 2004;10:55-63.
231. Sperger JM, Chen X, Draper JS, et al. Gene expression patterns in human embryonic stem cells and human pluripotent germ cell tumors. Proc Natl Acad Sci U S A 2003;100:13350-5.
232. Heath JK. Transcriptional networks and signaling pathways that govern vertebrate intestinal development. Curr Top Dev Biol 2010;90:159-92.
233. Korinek V, Barker N, Moerer P, et al. Depletion of epithelial stem-cell compartments in the small intestine of mice lacking Tcf-4. Nat Genet 1998;19:379-83.

234. Half E, Bercovich D, Rozen P. Familial adenomatous polyposis. Orphanet J Rare Dis 2009;4:22.
235. van Es JH, Jay P, Gregorieff A, et al. Wnt signalling induces maturation of Paneth cells in intestinal crypts. Nat Cell Biol 2005;7:381-6.
236. Gregorieff A, Pinto D, Begthel H, et al. Expression pattern of Wnt signaling components in the adult intestine. Gastroenterology 2005;129:626-38.
237. Sangiorgi E, Capecchi MR. Bmi1 is expressed in vivo in intestinal stem cells. Nature genetics 2008;40:915-20.
238. Montgomery RK, Carlone DL, Richmond CA, et al. Mouse telomerase reverse transcriptase (mTert) expression marks slowly cycling intestinal stem cells. Proc Natl Acad Sci U S A 2011;108:179-84.
239. Takeda N, Jain R, LeBoeuf MR, et al. Interconversion between intestinal stem cell populations in distinct niches. Science 2011;334:1420-4.
240. He XC, Zhang J, Tong WG, et al. BMP signaling inhibits intestinal stem cell self-renewal through suppression of Wnt-beta-catenin signaling. Nat Genet 2004;36:1117-21.
241. He XC, Yin T, Grindley JC, et al. PTEN-deficient intestinal stem cells initiate intestinal polyposis. Nat Genet 2007;39:189-98.
242. Yan KS, Chia LA, Li X, et al. The intestinal stem cell markers Bmi1 and Lgr5 identify two functionally distinct populations. Proc Natl Acad Sci U S A 2012;109:466-71.
243. Tian H, Biehs B, Warming S, et al. A reserve stem cell population in small intestine renders Lgr5-positive cells dispensable. Nature 2011;478:255-9.
244. Greco V, Guo S. Compartmentalized organization: a common and required feature of stem cell niches? Development 2010;137:1586-94.
245. Li L, Clevers H. Coexistence of quiescent and active adult stem cells in mammals. Science 2010;327:542-5.
246. Reya T, Clevers H. Wnt signalling in stem cells and cancer. Nature 2005;434:843-50.
247. van der Flier LG, van Gijn ME, Hatzis P, et al. Transcription factor achaete scute-like 2 controls intestinal stem cell fate. Cell 2009;136:903-12.
248. Farin HF, van Es JH, Clevers H. Redundant Sources of Wnt Regulate Intestinal Stem Cells and Promote Formation of Paneth Cells. Gastroenterology 2012.
249. Sato T, van Es JH, Snippert HJ, et al. Paneth cells constitute the niche for Lgr5 stem cells in intestinal crypts. Nature 2011;469:415-8.
250. Kim TH, Escudero S, Shivdasani RA. Intact function of Lgr5 receptor-expressing intestinal stem cells in the absence of Paneth cells. Proc Natl Acad Sci U S A 2012;109:3932-7.
251. Reya T, Morrison SJ, Clarke MF, et al. Stem cells, cancer, and cancer stem cells. Nature 2001;414:105-11.
252. Eaves CJ. Cancer stem cells: Here, there, everywhere? Nature 2008;456:581-2.
253. Borovski T, De Sousa EMF, Vermeulen L, et al. Cancer stem cell niche: the place to be. Cancer Res 2011;71:634-9.
254. Hanahan D, Weinberg RA. Hallmarks of cancer: the next generation. Cell 2011;144:646-74.
255. Loeb LA, Loeb KR, Anderson JP. Multiple mutations and cancer. Proc Natl Acad Sci U S A 2003;100:776-81.
256. Sabates-Bellver J, Van der Flier LG, de Palo M, et al. Transcriptome profile of human colorectal adenomas. Mol Cancer Res 2007;5:1263-75.
257. Jubb AM, Chalasani S, Frantz GD, et al. Achaete-scute like 2 (ascl2) is a target of Wnt signalling and is upregulated in intestinal neoplasia. Oncogene 2006;25:3445-57.
258. Vermeulen L, De Sousa EMF, van der Heijden M, et al. Wnt activity defines colon cancer stem cells and is regulated by the microenvironment. Nat Cell Biol 2010;12:468-76.
259. Stange DE, Engel F, Longerich T, et al. Expression of an ASCL2 related stem cell signature and IGF2 in colorectal cancer liver metastases with 11p15.5 gain. Gut 2010;59:1236-44.

260. Kemper K, Prasetyanti PR, de Lau W, et al. Monoclonal Antibodies Against Lgr5 Identify Human Colorectal Cancer Stem Cells. Stem Cells 2012.
261. Buttitta L, Tanaka TS, Chen AE, et al. Microarray analysis of somitogenesis reveals novel targets of different WNT signaling pathways in the somitic mesoderm. Dev Biol 2003;258:91-104.
262. Takada R, Satomi Y, Kurata T, et al. Monounsaturated fatty acid modification of Wnt protein: its role in Wnt secretion. Dev Cell 2006;11:791-801.
263. Chen WY, Zeng X, Carter MG, et al. Heterozygous disruption of Hic1 predisposes mice to a gender-dependent spectrum of malignant tumors. Nat Genet 2003;33:197-202.
264. Carter MG, Johns MA, Zeng X, et al. Mice deficient in the candidate tumor suppressor gene Hic1 exhibit developmental defects of structures affected in the Miller-Dieker syndrome. Hum Mol Genet 2000;9:413-9.
265. Grimm C, Sporle R, Schmid TE, et al. Isolation and embryonic expression of the novel mouse gene Hic1, the homologue of HIC1, a candidate gene for the Miller-Dieker syndrome. Hum Mol Genet 1999;8:697-710.
266. Tsui S, Dai T, Roettger S, et al. Identification of two novel proteins that interact with germ-cell-specific RNA-binding proteins DAZ and DAZL1. Genomics 2000;65:266-73.
267. Rual JF, Venkatesan K, Hao T, et al. Towards a proteome-scale map of the human protein-protein interaction network. Nature 2005;437:1173-8.
268. Kojima T, Morikawa Y, Copeland NG, et al. TROY, a newly identified member of the tumor necrosis factor receptor superfamily, exhibits a homology with Edar and is expressed in embryonic skin and hair follicles. The Journal of biological chemistry 2000;275:20742-7.
269. Qiu W, Hu Y, Andersen TE, et al. Tumor necrosis factor receptor superfamily member 19 (TNFRSF19) regulates differentiation fate of human mesenchymal (stromal) stem cells through canonical Wnt signaling and C/EBP. J Biol Chem 2010;285:14438-49.
270. Hsu W, Kerppola TK, Chen PL, et al. Fos and Jun repress transcription activation by NF-IL6 through association at the basic zipper region. Mol Cell Biol 1994;14:268-76.
271. Weiss MJ, Orkin SH. GATA transcription factors: key regulators of hematopoiesis. Exp Hematol 1995;23:99-107.
272. Schwachtgen JL, Remacle JE, Janel N, et al. Oct-1 is involved in the transcriptional repression of the von willebrand factor gene promoter. Blood 1998;92:1247-58.
273. Saigusa S, Inoue Y, Tanaka K, et al. Clinical significance of LGR5 and CD44 expression in locally advanced rectal cancer after preoperative chemoradiotherapy. Int J Oncol 2012;41:1643-52.
274. Ziskin JL, Dunlap D, Yaylaoglu M, et al. In situ validation of an intestinal stem cell signature in colorectal cancer. Gut 2012.
275. Nakata S, Campos B, Bageritz J, et al. LGR5 is a Marker of Poor Prognosis in Glioblastoma and is Required for Survival of Brain Cancer Stem-Like Cells. Brain Pathol 2012.
276. Paulino VM, Yang Z, Kloss J, et al. TROY (TNFRSF19) is overexpressed in advanced glial tumors and promotes glioblastoma cell invasion via Pyk2-Rac1 signaling. Mol Cancer Res 2010;8:1558-67.
277. de Sousa EMF, Colak S, Buikhuisen J, et al. Methylation of cancer-stem-cell-associated Wnt target genes predicts poor prognosis in colorectal cancer patients. Cell Stem Cell 2011;9:476-85.
278. Shao Z, Browning JL, Lee X, et al. TAJ/TROY, an orphan TNF receptor family member, binds Nogo-66 receptor 1 and regulates axonal regeneration. Neuron 2005;45:353-9.
279. Eby MT, Jasmin A, Kumar A, et al. TAJ, a novel member of the tumor necrosis factor receptor family, activates the c-Jun N-terminal kinase pathway and mediates caspase-independent cell death. The Journal of biological chemistry 2000;275:15336-42.
280. Hashimoto T, Schlessinger D, Cui CY. Troy binding to lymphotoxin-alpha activates NF kappa B mediated transcription. Cell cycle (Georgetown, Tex 2008;7:106-11.

281. Koo BK, Spit M, Jordens I, et al. Tumour suppressor RNF43 is a stem-cell E3 ligase that induces endocytosis of Wnt receptors. Nature 2012;488:665-9.
282. Hao HX, Xie Y, Zhang Y, et al. ZNRF3 promotes Wnt receptor turnover in an R-spondin-sensitive manner. Nature 2012;485:195-200.
283. Naito A, Yoshida H, Nishioka E, et al. TRAF6-deficient mice display hypohidrotic ectodermal dysplasia. Proc Natl Acad Sci U S A 2002;99:8766-71.
284. Ohazama A, Courtney JM, Tucker AS, et al. Traf6 is essential for murine tooth cusp morphogenesis. Dev Dyn 2004;229:131-5.
285. Wu H, Arron JR. TRAF6, a molecular bridge spanning adaptive immunity, innate immunity and osteoimmunology. Bioessays 2003;25:1096-105.
286. Pispa J, Pummila M, Barker PA, et al. Edar and Troy signalling pathways act redundantly to regulate initiation of hair follicle development. Hum Mol Genet 2008;17:3380-91.
287. Neumann S, Coudreuse DY, van der Westhuyzen DR, et al. Mammalian Wnt3a is released on lipoprotein particles. Traffic 2009;10:334-43.
288. Cha SW, Tadjuidje E, White J, et al. Wnt11/5a complex formation caused by tyrosine sulfation increases canonical signaling activity. Curr Biol 2009;19:1573-80.
289. Mohammad HP, Zhang W, Prevas HS, et al. Loss of a single Hic1 allele accelerates polyp formation in Apc(Delta716) mice. Oncogene.
290. Yang W, Mansour SL. Expression and genetic analysis of prtb, a gene that encodes a highly conserved proline-rich protein expressed in the brain. Dev Dyn 1999;215:108-16.
291. Shi Y, Luo S, Peng J, et al. The structure, expression and function prediction of DAZAP2, a down-regulated gene in multiple myeloma. Genomics Proteomics Bioinformatics 2004;2:47-54.
292. Sommerfeldt DW, Zhi J, Rubin CT, et al. Proline-rich transcript of the brain (prtb) is a serum-responsive gene in osteoblasts and upregulated during adhesion. J Cell Biochem 2002;84:301-8.
293. Roche DD, Liu KJ, Harland RM, et al. Dazap2 is required for FGF-mediated posterior neural patterning, independent of Wnt and Cdx function. Dev Biol 2009;333:26-36.
294. Winkel A, Stricker S, Tylzanowski P, et al. Wnt-ligand-dependent interaction of TAK1 (TGF-beta-activated kinase-1) with the receptor tyrosine kinase Ror2 modulates canonical Wnt-signalling. Cell Signal 2008;20:2134-44.